





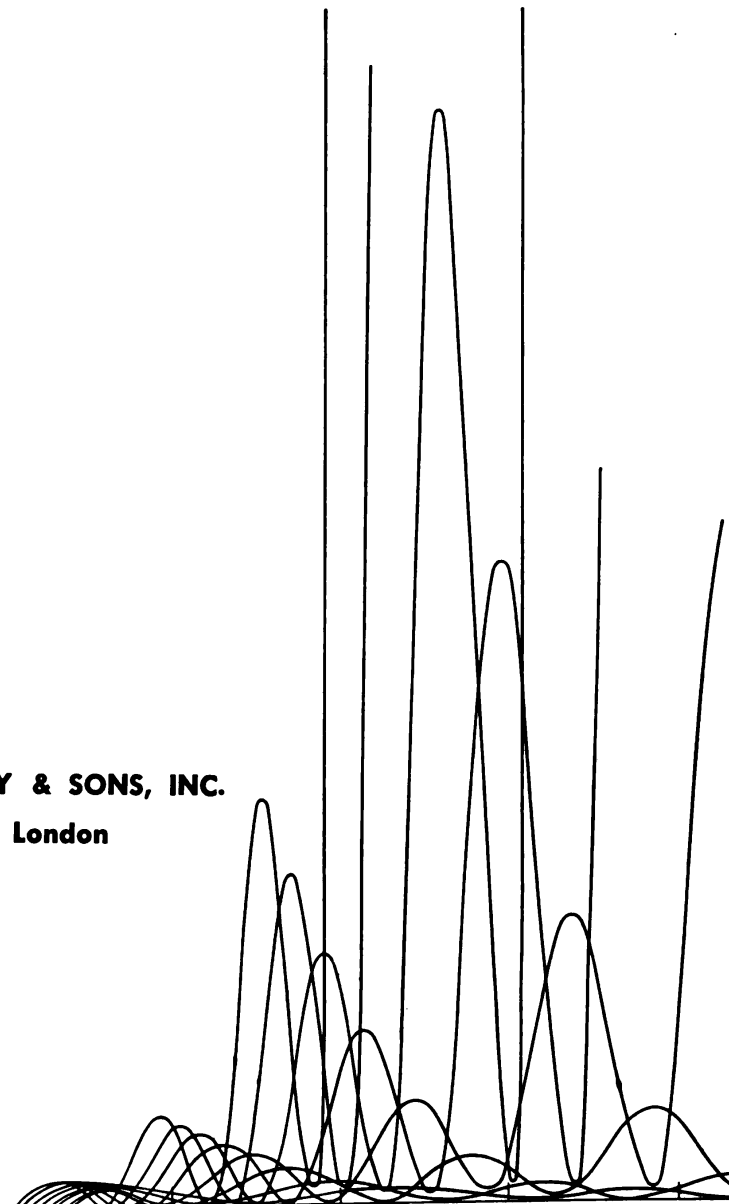
# Coupled mode and parametric electronics

**WILLIAM H. LOISELL**

**Member of the Technical Staff, Bell Telephone Laboratories, Inc.**

# Coupled mode and parametric electronics

**JOHN WILEY & SONS, INC.**  
**New York • London**



Phoenix  
TK  
7870  
• L87

**Copyright © 1960 by John Wiley & Sons, Inc.**

All rights reserved. This book or any part thereof must not be reproduced in any form without the written permission of the publisher.

**Library of Congress Catalog Card Number: 60-15555**

**Printed in the United States of America**

87-373328

TO

**MY WIFE** for her devotion  
**MY CHILDREN** for their affection  
**C. F. QUATE** for motivation  
**J. S. COOK** for stimulation



# Foreword

There is scarcely a branch of modern science whose theory does not depend intimately on the concept of wave motion with its related concepts of impedance, power flow, modes, and coupling. The theory of coupled modes, therefore, provides a unifying viewpoint to many seemingly unrelated physical problems.

The application of the concept of coupled modes to traveling wave tubes, backward wave oscillators, parametric amplifiers, and related devices makes a story with aspects as fascinating as many of the better-known adventures in science. Use of the coupled mode theory has come about gradually through the contributions of many people and has provided scientific adventure of high order. Most of these devices and a great part of the understanding of their behavior were obtained without benefit of coupled modes, but it remained for these principles to provide a common ground for their understanding.

More than thirty years ago L. Tonks and I. Langmuir provided the first evidence that electron-beam phenomena could be described in terms of waves. W. C. Hahn and S. Ramo later used electron waves to explain much of the behavior of klystrons. However, in attacking every new electron-beam problem, it was natural to start with the basic physics of an electron fluid. R. Kompfner, in the invention of the traveling wave tube, considered an electron fluid interacting with a moving wave. Although he found a series solution to the problem, which was very useful and powerful, it largely lost track of the wave nature of the phenomena. J. R. Pierce also solved the traveling wave tube problem by starting from the basic physics of an electron fluid, but his solutions involved four waves. The coupled modes were implicit in Pierce's analysis and were recognized as such, but the possibilities were not yet fully appreciated.

As the traveling wave tube art progressed, the wave character of the electron stream became better appreciated. W. E. Matthews showed that most of the traveling wave tube characteristics could be obtained from a purely coupled mode approach. Experiments showed by means of a mechanical model that waves on a moving medium, not necessarily electrons, were responsible for the growing waves, and L. J. Chu, with his kinetic-power theorem for electron beams, provided an important missing link. Since then there have been many individual contributions which have put the coupled mode approach to electron-beam devices on a firmer footing.

Perhaps the greatest impetus to the development of a complete coupled mode theory as we see it in this book has been the recently revived interest in parametric amplification. Introduced back in the nineteenth century by Faraday and Lord Raleigh, the parametric (i.e., variable reactance) interaction actually predates the vacuum tube. Indeed, the early interest faded because of the competition of the vacuum tube as an amplifier and modulator. New interest was generated a decade ago by the realization that this method of amplification had low noise properties surpassing conventional vacuum tubes. The parametric amplifier inherently uses coupled circuits, but, despite this, the work until recently has ignored the convenience of coupled mode theory. Whether the circuit is distributed or lumped or whether it uses varactor diodes, ferrites, electron beams, ferroelectrics, superconducting materials, or who knows what next, the theoretical work on these devices is greatly simplified when the nature of the modes is recognized and the approach is made through the coupling of these modes rather than the coupling of circuits or currents.

Today the powerful unified approach of coupled mode theory makes the earlier analyses almost obsolete, and in microwave tubes and distributed amplifiers and parametric devices, as in other branches of physics and engineering, coupled mode theory provides a straightforward logical approach to the understanding of the phenomena and to the design of structures. In exchange for the fascination and adventure of the historical approach to a new art, it provides the beauty and unity of a natural logical mathematical approach.

C. C. CUTLER

*Bell Telephone Laboratories  
August 1960*

# Preface

There is a threefold purpose in writing this book. The first is to give an introduction to the theory of coupled modes and to show how the use of the theory simplifies the study of coupled systems. The second is to present a unified theory of traveling wave tubes, backward wave oscillators, and similar microwave devices from this common point of view. The third is to treat, from the same fundamental approach, the theory of parametric amplifiers, oscillators, and frequency converters.

A book devoted to the theory of coupled modes should consider the subject from a general viewpoint so that it can be applied in any field. However, examples of its application are necessarily limited by space, and a simplified theory is presented with a view to the examples chosen. It would be interesting to apply the theory to the multimode waveguide, the telegraphist's equations, problems in solid-state physics, and to show the relation to quantum mechanics. However, it seems sufficient in this book to restrict the examples to electron-beam tubes, parametric amplifiers, and related devices.

The application of the concept to the traveling wave tube and related electron-beam devices is natural because it was in connection with this field that I found the opportunity for the development of these concepts, as applied to modes on moving systems, and also because this field is badly in need of such a unified mathematical treatment. The application to parametric amplifiers stands out as a subject of very immediate interest, the development of which has depended strongly upon this approach. It is believed that neither of these subjects is adequately treated in these terms elsewhere in the literature.

The book has been written so that a first-year graduate student or a senior in electrical engineering who has had a course in Maxwell field theory and has reached a reasonable mathematical maturity should be

able to read it. Although largely mathematical in nature, the book contains no very difficult mathematics, and the more tedious sections have been relegated to the appendices. It is expected that a study of the book should give a solid background in the theory of beam-type microwave tubes (traveling wave tubes, backward wave oscillators, Kompfner dip conditions, and the like) and parametric amplifiers as well as a good working knowledge of coupled mode systems in general.

I am particularly indebted to Dr. C. F. Quate of the Sandia Corporation who encouraged me to write this book and who made extensive suggestions on the manuscript. Some of the material presented is an outgrowth of research on tapered directional couplers and space-charge wave parametric amplifiers in collaboration with Mr. J. S. Cook, with whom I had useful discussions during the preparation of the manuscript. I am also indebted to Dr. H. G. Unger who reviewed the entire manuscript and made extensive suggestions. Other colleagues at Bell Laboratories who have read various chapters and have given valuable criticism are Mr. C. C. Cutler, Dr. A. H. Dayem, Mr. R. S. Engelbrecht, Dr. E. I. Gordon, Dr. J. W. Kluver, Dr. R. Kompfner, Mr. W. W. Mumford, Dr. K. M. Poole, Dr. P. K. Tien, Dr. M. Uenohara, and Dr. L. R. Walker. I also wish to thank Dr. A. Ashkin for permission to use some of his unpublished experimental results on space-charge wave parametric amplifiers and Dr. H. Heffner of Stanford University who very kindly supplied me with some of the bibliography on parametric devices presented in Chapter 4. Miss N. M. Morris of our Library Staff also helped immeasurably in the preparation of the bibliography. I have enjoyed as well a very helpful discussion with Dr. H. A. Haus of Massachusetts Institute of Technology regarding his work on coupled mode theory. Mrs. E. Jenkins, Mrs. B. J. Dojchak, Mrs. B. Haisch, and Miss R. Rohbacker did a magnificent job in typing the manuscript throughout its many revisions.

I should also like to thank Bell Telephone Laboratories for allowing me to write this book.

WILLIAM H. LOUISELL

*Bell Telephone Laboratories  
August 1960*

# Contents

<b>CHAPTER</b>	<b>PAGE</b>
<b>1. THEORY OF COUPLED MODES</b>	<b>1</b>
<b>Part I. Coupling of Modes of Vibration, 3</b>	
1.1. SIMPLE LINEAR OSCILLATOR, 3	
1.2. Two COUPLED LINEAR OSCILLATORS, 7	
Coupled Mode Form of Equations of Motion, 8	
Normal Mode Frequencies for the Coupled System, 10	
Energy Conservation, 10	
1.3. Two WEAKLY COUPLED OSCILLATORS, 11	
1.4. DIRECT APPROACH TO COUPLED MODE THEORY, 12	
Coupled Mode Approximation, 12	
Boundary Conditions. Transfer Factor Defined, 13	
1.5. GENERAL APPROACH TO COUPLED MODE THEORY, 15	
General Equations, 15	
Energy Conservation, 16	
Evaluation of the Coupling Coefficients, 17	
<b>Part II. Coupling of Modes of Propagation, 18</b>	
1.6. SINGLE UNIFORM TRANSMISSION LINE, 19	
Transmission Line Equations, 20	
Normal Mode Form, 21	
Phase and Group Velocity, 23	
Boundary Conditions. Power Flow in Lossless Line, 23	
1.7. GENERAL APPROACH TO COUPLING OF TWO LOSSLESS MODES OF PROPAGATION, 25	
Equations in Coupled Mode Form, 25	
Power Conservation, 25	
Normal Mode Propagation Constants, 26	
1.8. THE DIRECTIONAL COUPLER. ACTIVE AND PASSIVE MODE COUPLING, 26	

CONTENTS

CHAPTER

PAGE

A Codirectional Coupler. Passive Mode Coupling, 27	
A Contradirectional Coupler. Active Mode Coupling, 30	
1.9. SUMMARY, 32	
Bibliography, 33	

**2. SOME NORMAL MODES ON ELECTRON BEAMS 35**

2.1. FUNDAMENTAL EQUATIONS GOVERNING WAVE PROPAGATION ON ELECTRON BEAMS, 35	
2.2. SMALL SIGNAL APPROXIMATION, 37	
2.3. SMALL SIGNAL POYNTING THEOREM, 38	
2.4. SPACE-CHARGE WAVES IN A ONE-DIMENSIONAL ELECTRON BEAM IN A DRIFT REGION, 39	
Simplifying Assumptions, 39	
Space-Charge Wave Equations, 40	
Normal Mode Form, 41	
Electromechanical Nature of the Waves, 43	
Kinetic Power Flow in Space-Charge Waves, 44	
Mode Excitation, 47	
2.5. SPACE-CHARGE WAVES IN A FINITE CYLINDRICAL BEAM IN A DRIFT REGION, 47	
2.6. THE FAST AND SLOW CYCLOTRON NORMAL MODES, 51	
Simplifying Assumptions, 51	
Cyclotron Wave Equations (Normal Mode Form), 52	
Nature of the Modes, 54	
Remarks, 59	
2.7. THE SYNCHRONOUS NORMAL MODES, 60	
2.8. REMARKS, 64	
Bibliography, 65	

**3. SPACE-CHARGE WAVES COUPLED TO SLOW WAVE CIRCUITS 67**

3.1. THE MODEL, 67	
The Helix as a Slow Wave Circuit, 67	
Beam Coupled to Circuit, 70	
Coupled Mode Form of Beam-Circuit Equations, 72	
3.2. THE CHU KINETIC POWER THEOREM, 74	
3.3. THE TRAVELING WAVE TUBE, 75	
Coupling of Forward Circuit Mode and Slow Space-Charge Mode, 75	
TWT Transfer Factors. Weak Coupling Approximation, 75	
TWT Solutions, Large QC, Circuit and Slow Modes	
Synchronous. Gain, 76	
General TWT Case, 78	

CONTENTS	xii
CHAPTER	PAGE
3.4. THE KOMPFNER DIP. (DIRECTIONAL COUPLER), 80 Coupling of Forward Circuit Mode and Fast Space-Charge Mode, 80 General Case, Small QC, 82	
3.5. THE BACKWARD WAVE AMPLIFIER AND OSCILLATOR, 84	
3.6. REMARKS, 89 Bibliography, 90	
<b>4. PARAMETRIC COUPLING PRINCIPLE FOR LUMPED CIRCUITS 92</b>	
4.1. MECHANISM OF ENERGY TRANSFER, 93	
4.2. DIRECT COUPLED MODE APPROACH TO THE DEGENERATE PARAMETRIC OSCILLATOR, 93 Weak Coupling Approximation, 96 Initial Conditions, 98 Energy Considerations. The Manley-Rowe Relations, 99	
4.3. THE GENERAL COUPLED MODE APPROACH FOR NON- DEGENERATE PARAMETRICALLY COUPLED ELEMENTS, 100 General Equations, 100 Consequences of Manley-Rowe Relations, 101 Evaluation of the Mutual Coupling Coefficients, 102 Initial Conditions, 103 Phase of the "Pump" Relative to the Charge, 103	
4.4. THE MANLEY-ROWE RELATIONS, 104	
4.5. THE THREE-FREQUENCY PARAMETRIC AMPLIFIER. GAIN, 109	
4.6. NOISE FIGURE OF PARAMETRIC AMPLIFIERS, 115	
4.7. THE FREQUENCY CONVERTER, 118	
4.8. REMARKS, 120	
4.9. BRIEF HISTORY OF THE PARAMETRIC AMPLIFIER, 121 Bibliography, 121	
<b>5. PARAMETRIC COUPLING PRINCIPLE FOR DISTRIBUTED     CIRCUITS 131</b>	
5.1. DISTRIBUTED PARAMETRIC AMPLIFIER. GENERAL COUPLED MODE THEORY, 132	
5.2. DISTRIBUTED FREQUENCY CONVERTER, 137	
5.3. GENERAL COUPLED MODE THEORY WHEN MANY MODES ARE COUPLED, 137 Linearized Time-Invariant Systems, 138 Linearized System with Time-Varying Parameters, 139	
5.4. A FOUR-FREQUENCY TRAVELING WAVE PARAMETRIC AMPLIFIER (PUMP FREQUENCY LOWER THAN SIGNAL FREQUENCY), 140	

CHAPTER

PAGE

5.5. NOISE FIGURE OF DISTRIBUTED PARAMETRIC AMPLIFIERS,	142
5.6. REMARKS,	146
Bibliography,	146

<b>6. SEMICONDUCTOR DIODE PARAMETRIC AMPLIFIERS</b>	<b>148</b>
---	------------

6.1. THE P-N JUNCTION DIODE AS A VARIABLE CAPACITANCE ELEMENT,	149
6.2. DIODE AMPLIFIER GAIN,	154
6.3. DIODE NOISE CONSIDERATIONS,	154
6.4. EXPERIMENTAL RESULTS FOR LUMPED CIRCUITS,	160
6.5. EXPERIMENTAL RESULTS FOR DISTRIBUTED CIRCUITS,	163
6.6. REMARKS,	166
Bibliography,	166

<b>7. PARAMETRIC AMPLIFICATION OF FAST SPACE-CHARGE WAVES</b>	<b>168</b>
---	------------

7.1. THE FAST SPACE-CHARGE WAVE PARAMETRIC AMPLIFIER,	169
Coupled Mode Form of Equations,	169
The Coupling Coefficients. Manley-Rowe Relations,	171
Boundary Conditions. Gain Threshold,	171
Validity of the Weak Coupling Approximation,	174
The Frequency Converter,	175
7.2. EXPERIMENTAL RESULTS,	176
7.3. EFFECT OF HIGHER IDLER FREQUENCIES ON GAIN,	180
7.4. REMARKS,	186
Bibliography,	188

<b>8. FAST CYCLOTRON MODE PARAMETRIC AMPLIFIER</b>	<b>190</b>
--	------------

8.1. SLOW WAVE CIRCUIT COUPLED TO CYCLOTRON AND SYNCHRONOUS MODES,	190
Coupled Mode Equations,	191
Power Theorem,	193
Fast Cyclotron Wave Coupler,	194
8.2. PARAMETRIC COUPLING PRINCIPLE APPLIED TO FAST CYCLOTRON WAVE,	195
The Pump Field,	196
Equations of Motion in the Pump Region,	197
Boundary Conditions. Gain,	199
Manley-Rowe Relations,	199
8.3. DESCRIPTION OF ADLER TUBE. EXPERIMENTAL RESULTS,	200

CONTENTS	xv
CHAPTER	PAGE
8.4. CROSSED FIELD VERSION, 202	
Bibliography, 202	
<b>9. FERRITE PARAMETRIC AMPLIFIERS</b>	<b>203</b>
9.1. THE MAGNETIZATION EQUATIONS OF MOTION, 204	
Equations of Motion, 205	
The Uniform Precession Mode, 207	
9.2. PARAMETRIC COUPLING MECHANISM, 209	
9.3. THREE MODES OF OPERATION, 212	
9.4. THEORY OF ELECTROMAGNETIC OPERATION, 213	
Landau-Lifshitz Equation, 214	
The Pump Magnetization, 214	
Parametric Coupling, 216	
9.5. EXPERIMENTAL RESULTS, 220	
9.6. TRAVELING WAVE VERSION, 220	
9.7. FERROMAGNETIC FREQUENCY CONVERTER, 223	
9.8. CONCLUSIONS, 225	
Bibliography, 225	
<b>Appendix A Coaxial Cable as a Transmission Line</b>	<b>227</b>
<b>Appendix B Space-Charge Waves in a Cylindrical Beam</b>	<b>231</b>
<b>Appendix C General Method of Finding the Normal Mode Form</b>	<b>235</b>
<b>Appendix D Normal Mode Form for the Synchronous Modes</b>	<b>238</b>
<b>Appendix E Coupled Mode Form of Beam-Circuit Equations</b>	<b>240</b>
<b>Appendix F The Chu Kinetic Power Theorem</b>	<b>241</b>
<b>Appendix G Matrix Representation of TWT Power Series Solutions</b>	<b>244</b>
<b>Appendix H Evaluation of Mutual Coupling Coefficients</b>	<b>246</b>
<b>Appendix I Effect of Loss on Coupled Mode Theory</b>	<b>248</b>
<b>Appendix J Evaluation of Space-Charge Mutual Coupling Coefficients</b>	<b>250</b>
<b>Appendix K Coupled Mode Equations for Circuit-Cyclotron System</b>	<b>256</b>
<b>Appendix L Equations of Motion for Beam in Quadrupolar Pump Field</b>	<b>261</b>
<b>Index</b>	<b>265</b>



## Chapter 1

# Theory of coupled modes

The concept of mutual coupling in oscillating and propagating systems provides an extremely useful and versatile tool in understanding and solving many types of problems. A few examples which may be cited are coupled mechanical oscillators, coupled electric circuits, molecular vibrations in solids, acoustic waves, directional couplers, wave filters, and microwave amplifiers, such as traveling wave tubes, backward wave amplifiers, and parametric amplifiers. The purpose of this book is to teach a common approximate method of treating such problems by applying it to several interesting examples in microwave electronics. This approximate method is called the method of coupled modes.

Conceptually, the coupled mode approach is quite simple. A complicated coupled system is first divided up into a number of isolated parts or elements. The equations of motion for the isolated elements are then solved exactly, and the solutions are expressed in terms of the "normal modes" of the element. The original complex coupled system is then assumed to be made up of the isolated elements weakly coupled together. The coupling perturbs the state of motion of each element slightly, and the motion of the original coupled system is described by this perturbation on the motion of the isolated elements.\*

An example may help clarify several points. Consider two waveguides weakly coupled by a series of small holes in a common wall between them. It is desired to find the waves that propagate in such a coupled system. The system is first divided into two isolated or uncoupled waveguides. Each guide is an element in the sense intended in the pre-

\* The reader who is familiar with quantum mechanics will easily recognize the "method of coupled modes" as a special case of perturbation theory. However, this theory is more general than is needed in this book, and a very simplified version is given. No attempt is made to make the theory mathematically rigorous, for it is felt that the complications this would entail are not justified in a book of this nature.

ceding paragraph. The waves that can propagate in each element are then found. It is well known that if no restriction is made on frequency waves can propagate in an infinite number of ways along each guide. For each wave configuration that can propagate in the forward direction there is a corresponding one that can propagate in the backward direction. These waves are called the "normal modes" of the element. They represent independent solutions of the wave equation. For simplicity, assume that only the lowest order forward and backward mode in each guide exists. The original coupled system is now visualized as being composed of the four original modes, two in each element, which are weakly coupled by the perturbing action of the holes in the guides. The coupling will slightly alter the field distributions of the original waves.

It should be obvious that the elements must be weakly coupled if the method is to offer any real advantage. If this is not a valid approximation, the solutions for the coupled system will be sufficiently different from the uncoupled solutions that a knowledge of the solutions for the isolated elements will not be useful.

When the elements are weakly coupled, it can usually be argued from physical considerations that some of the modes of the isolated elements will play little part in the coupling mechanism. In this case these modes can be neglected with subsequent simplification of the original problem. To see how this might work, consider again the example of the two coupled waveguides. A little reflection should convince us that the forward modes in each guide would, in general, couple much more effectively to one another than to the backward modes when the elements are weakly coupled. Therefore, the problem can be greatly simplified by neglecting the backward modes in the analysis. By the technique of considering a weakly coupled system in terms of separate elements, a greater physical understanding of the coupling mechanism can be obtained in addition to the analytical simplification.

This chapter is restricted to the study of coupled systems composed of only two elements. Specifically, two coupled simple pendula and two coupled transmission lines are treated. This restriction allows the method of coupled modes to be demonstrated without undue mathematical complication, although the method can be applied when more elements are coupled. Since the problem can be solved exactly when only two simple elements are coupled, the exact solutions may be used to test the validity of the approximate coupled mode solutions. In later chapters these approximations are used to treat traveling wave tubes, parametric amplifiers, and other devices, and it is important to know their range of applicability.

It may appear that the simple cases discussed in this chapter are more labored than necessary. However, there are many mathematical and physical features that can be demonstrated for the simple case that might be obscured if they were presented in sections dealing with specific devices. It is therefore felt that a thorough treatment of the pendula and transmission lines is justified.

## Part I

### COUPLING OF MODES OF VIBRATION

#### 1.1 Simple Linear Oscillator

The theory of coupling of modes of vibration begins with a study of the simplest element that can be used as a building block of complicated vibrating systems, the simple linear oscillator. The purpose of this section is to express the equations of motion in a particularly useful form for future work.

In classical mechanics there are three formulations of the equations of motion<sup>1</sup> commonly used: (1) the Newtonian, (2) the Hamiltonian, and (3) the Lagrangian. In various problems one of these forms may prove simpler than another. For example, in the analysis of mechanical structures, such as bridges, the Newtonian form is applied. In quantum mechanics the Hamiltonian form proves to be the most appropriate, whereas in quantum electrodynamics the Lagrangian form is used. Although all three are given for the simple linear oscillator, no prior knowledge of them is necessary.

There is still another form of the equations of motion, closely related to the Hamiltonian, which is called the *normal mode form* and which proves very useful in the theory of coupled modes. It will now be derived for the simple oscillator.

The simple pendulum and the simple *LC* circuit (Figure 1.1) will be considered in parallel in the development of the normal mode form of the equations of motion. The language of mechanics will be used, merely as a convenience, although the meaning when applied to the *LC* circuit should be obvious.

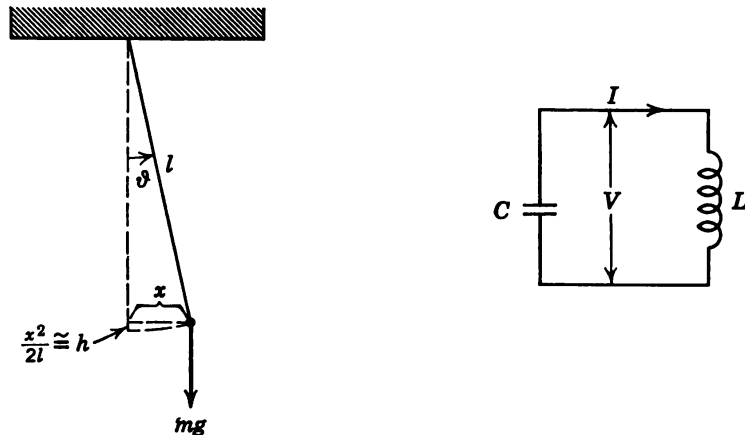


Figure 1.1 Coordinates for the simple oscillator.

The Hamiltonian form of the equations of motion<sup>1</sup> for the simple oscillator is given by

$$\left. \begin{array}{l} m \frac{dv}{dt} = -m \frac{g}{l} x \\ \frac{dx}{dt} = v \end{array} \right| \quad \left. \begin{array}{l} \frac{dI}{dt} = -\frac{1}{L} V \\ \frac{dV}{dt} = \frac{1}{C} I \end{array} \right| \quad \begin{array}{l} (a) \\ (b) \end{array} \quad \begin{array}{l} (c) \\ (d) \end{array} \quad (1.1)$$

where  $m$  is the mass of the pendulum bob,  $g$  is the acceleration of gravity,  $l$  is the length of the pendulum, and  $x$  is the *small* displacement of the pendulum bob as shown in Figure 1.1. The symbols in the  $LC$  circuit case have their usual meaning.

The Hamiltonian form consists of two coupled first-order differential equations. The displacement is coupled to the velocity in Eq. 1.1a, and the velocity is coupled to the displacement in Eq. 1.1b. The coupling coefficient is  $-g/l$  in the first case and  $+1$  in the second. The difference in sign is important. When the signs are different, the solutions will be periodic; if they are the same, solutions will be growing and decaying exponentials.

The kinetic energy of the oscillator is given by  $T(v) = mv^2/2$ , and the potential energy is  $V(x) = mgx^2/2l$ . Energy for the oscillator will be periodically converted from potential to kinetic and vice versa. When the pendulum is at its maximum excursion, the velocity is zero and all the energy will be potential. When the displacement goes through zero, all the energy will be kinetic. It is characteristic of oscillating systems that two forms of energy are available and that there will be a periodic interchange of energy between the two forms. In the  $LC$  circuit the

energy is in the form of magnetic energy stored in the magnetic field around the inductance ( $LI^2/2$ ) and electric energy stored in the electric field between the condenser plates ( $CV^2/2$ ). Since the signs of the coupling coefficients in Eqs. 1.1c and d are opposite, it follows that the system will oscillate with energy periodically exchanged between the electric and magnetic fields. The Hamiltonian form brings out the coupling explicitly between the two variables used to describe the system.

The Lagrangian form of the equations of motion in this simple case can be found by substituting Eq. 1.1b into Eq. 1.1a. This results in

$$\left. \begin{array}{l} \frac{d^2x}{dt^2} = -\frac{g}{l}x \quad (a) \\ \frac{dx}{dt} = v \quad (b) \end{array} \right| \quad \left. \begin{array}{l} \frac{d^2V}{dt^2} = -\frac{1}{LC}V \quad (c) \\ \frac{dV}{dt} = \frac{1}{C}I \quad (d) \end{array} \right. \quad (1.2)$$

Equation 1.2a will also be recognized as the Newtonian form of the equations of motion. It, of course, is the most familiar and is frequently used to find the motion of a simple oscillator. It is a decoupled second-order differential equation. The solution involves two arbitrary constants of integration that are usually evaluated in terms of the initial displacement and initial velocity. Therefore, Eqs. 1.2a and 1.2b must both be used to express the arbitrary constants in terms of the initial displacement and velocity.

The simple oscillator can be equally well described by two *decoupled* first-order differential equations. This is the *normal mode form* of the equations of motion. It is desirable, since it is usually easier to solve first-order differential equations than second-order or coupled first-order equations. One way to derive this form is to find linear combinations of the Hamiltonian equations that will decouple them. In this simple case multiply both sides of Eq. 1.1b by an arbitrary constant  $Y$  and add to Eq. 1.1a. This yields

$$\frac{d}{dt}(v + Yx) = Y\left(v - \frac{g}{lY}x\right) \quad \left| \quad \frac{d}{dt}(I + YV) = \frac{Y}{C}\left(I - \frac{C}{LY}V\right) \quad (1.3)\right.$$

Now if  $Y$  is chosen to be

$$\left. \begin{array}{l} Y = \pm j\omega \quad (a) \\ \omega = +\sqrt{\frac{g}{l}} \quad (b) \end{array} \right| \quad \left. \begin{array}{l} Y = \pm j\sqrt{\frac{C}{L}} \\ \equiv \pm j\omega C \quad (c) \\ \omega = +\frac{1}{\sqrt{LC}} \quad (d) \end{array} \right. \quad (1.4)$$

where

then Eq. 1.3 can be written

$$\begin{aligned} \left( \frac{d}{dt} - j\omega \right) a &= 0 \\ \left( \frac{d}{dt} + j\omega \right) a^* &= 0 \end{aligned} \quad (1.5)$$

where

$$\begin{array}{l|l} a = \frac{1}{2}\sqrt{m}(v + j\omega x) & a = \frac{1}{2}\sqrt{L}(I + j\omega CV) \\ a^* = \frac{1}{2}\sqrt{m}(v - j\omega x) & a^* = \frac{1}{2}\sqrt{L}(I - j\omega CV) \end{array} \quad (1.6)$$

The reason for the choice of normalization constants,  $\frac{1}{2}\sqrt{m}$  and  $\frac{1}{2}\sqrt{L}$ , will become apparent shortly.

Equations 1.5 are the two first-order decoupled equations that were sought. They are said to be the *normal mode form* of the equations of motion \* and describe the oscillator equally as well as Eqs. 1.1 or 1.2. The quantities  $a(t)$  and  $a^*(t)$  are called the *normal mode amplitudes* or simply the *normal modes of the oscillating element*. They are made up of a linear combination of a real velocity,  $v(t)$ , and a real displacement,  $x(t)$ , and can be visualized as two counterrotating vectors of constant length. The magnitudes of these vectors are normalized (by choosing the constants in Eqs. 1.6 to be  $\frac{1}{2}\sqrt{m}$  and  $\frac{1}{2}\sqrt{L}$ ), so that the sum of their squares gives the total energy stored in the system. That is,

$$\begin{array}{l|l} E = \frac{m}{2}[v^2(t) + \omega^2x^2(t)] & E = \frac{1}{2}[CV^2(t) + LI^2(t)] \\ = |a(t)|^2 + |a^*(t)|^2 & = |a(t)|^2 + |a^*(t)|^2 \end{array} \quad (1.7)$$

That the correct normalization has been chosen may be verified by direct substitution of  $a$  and  $a^*$  from Eqs. 1.6. Furthermore,  $|a|^2$  and  $|a^*|^2$  represent the energy stored in the  $a$  and  $a^*$  modes, respectively. Since  $v$  and  $x$  are real,  $|a|^2 = |a^*|^2$  and equal amounts of energy are stored in the two modes.

The solutions of the normal mode equations (1.5) are

$$\begin{aligned} a(t) &= a(0)e^{j\omega t} = \frac{1}{2}\sqrt{m}[v(t) + j\omega x(t)] \\ a^*(t) &= a^*(0)e^{-j\omega t} = \frac{1}{2}\sqrt{m}[v(t) - j\omega x(t)] \end{aligned} \quad (1.8)$$

\* This form is sometimes called the wave or diagonal representation in conventional operator algebra.

where  $a(0)$  and  $a^*(0)$  are constants of integration. It follows from Eqs. 1.8 that

$$a(0) = \frac{1}{2}\sqrt{m} [v(0) + j\omega x(0)] = \sqrt{\frac{1}{2}E} \exp \left[ j \tan^{-1} \frac{\omega x(0)}{v(0)} \right]$$

where  $E$  is the total energy given by Eqs. 1.7. Therefore, it is seen that two arbitrary constants must be given to specify the motion completely.

Although it may seem artificial to call  $a$  and  $a^*$  different normal modes, this mode division offers the advantage of visualizing  $v + j\omega x$  and  $v - j\omega x$  as two counterrotating vectors. When two oscillators are weakly coupled, it appears quite plausible that modes that rotate in the same sense will couple more effectively than modes that rotate in opposite senses. Therefore, dividing modes up in this fashion will aid in understanding and simplifying more involved coupled systems.

## 1.2 Two Coupled Linear Oscillators

In this section the equations of motion of two coupled oscillators are solved exactly, in order that approximate solutions given in the next three sections may be compared to check their range of validity.

Consider the two simple coupled pendula shown in Figure 1.2. The pendula are of length  $l_1$  and  $l_2$ , respectively, and the bobs on each of mass  $m$  are connected by a weightless spring whose spring constant is  $k$ . The amplitudes of oscillation are assumed small and are designated by  $x_1$  and  $x_2$ , respectively, as shown in the figure. Both pendula swing in a common plane.

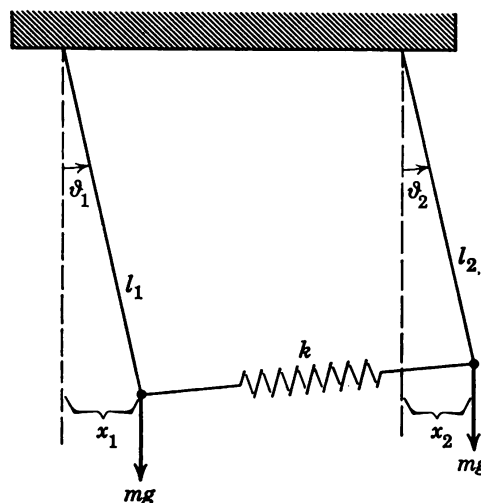


**Figure 1.2** Coordinates for system of two coupled elements.

The kinetic and potential energies for small displacements are, respectively,

$$T = \frac{m}{2} (v_1^2 + v_2^2) \quad (1.9)$$

$$V \cong \frac{m}{2} \left( \frac{g}{l_1} x_1^2 + \frac{g}{l_2} x_2^2 \right) + \frac{k}{2} (x_1 - x_2)^2$$

where  $g$  is the acceleration due to gravity. The first two terms in the potential energy are the gravitational potential energies of the two bobs, whereas the term proportional to  $k$  is the energy due to the coupling. When  $x_1 = x_2$ , the spring energy is zero, since the spring is not assumed to be under tension when the two bobs are at rest. As  $x_1 - x_2$  increases, the tension increases and so does the stored potential energy in the spring.

It is easy to show either from the Hamiltonian or by analyzing the forces on each bob that the Hamiltonian form of the equations of motion is given by

$$\frac{dv_1}{dt} = -\omega_1^2 x_1 + \frac{k}{m} (x_2 - x_1) \quad (a)$$

$$\frac{dx_1}{dt} = v_1 \quad (b)$$

$$\frac{dv_2}{dt} = -\omega_2^2 x_2 + \frac{k}{m} (x_1 - x_2) \quad (c)$$

$$\frac{dx_2}{dt} = v_2 \quad (d)$$

where

$$\omega_{1,2}^2 = \frac{g}{l_{1,2}} \quad (1.11)$$

The terms  $g/l_{1,2}$  represent the gravitational restoring forces, and  $\pm k(x_1 - x_2)$  represent the spring restoring forces.

**Coupled mode form of equations of motion.** The equations of motion (1.10) can be solved exactly as they stand. However, for future work, it is especially useful to put these equations in what is called a coupled mode form. This is made up of linear combinations of the coupled equations of motion such that when the mutual coupling coefficient  $k$  goes to zero the resulting equations are in the normal mode form of the two isolated (uncoupled) elements. This will become clear

by carrying out the required procedure on Eqs. 1.10. Multiply Eq. 1.10b by  $\pm j\omega_1$  and add to Eq. 1.10a. Similarly, multiply Eq. 1.10d by  $\pm j\omega_2$  and add to Eq. 1.10c. Define the mode amplitudes as

$$\begin{aligned} a_1 &= \frac{1}{2}\sqrt{m}(v_1 + j\omega_1 x_1) \\ a_2 &= \frac{1}{2}\sqrt{m}(v_2 + j\omega_2 x_2) \end{aligned} \quad (1.12)$$

and the indicated linear combinations of Eqs. 1.10 can be written as

$$\begin{aligned} \frac{da_1}{dt} &= c_{11}a_1 + c_{12}a_2 + c_{13}a_1^* + c_{14}a_2^* & (a) \\ \frac{da_2}{dt} &= c_{21}a_1 + c_{22}a_2 + c_{23}a_1^* + c_{24}a_2^* & (b) \\ \frac{da_1^*}{dt} &= c_{31}a_1 + c_{32}a_2 + c_{33}a_1^* + c_{34}a_2^* & (c) \\ \frac{da_2^*}{dt} &= c_{41}a_1 + c_{42}a_2 + c_{43}a_1^* + c_{44}a_2^* & (d) \end{aligned} \quad (1.13)$$

where

$$\begin{aligned} c_{11} &= -c_{33} = j\omega_1 \left(1 + \frac{k}{2m\omega_1^2}\right) \\ c_{22} &= -c_{44} = j\omega_2 \left(1 + \frac{k}{2m\omega_2^2}\right) \\ c_{13} &= c_{21} = -c_{23} = -c_{31} = c_{41} = -c_{43} = -j \frac{k}{2m\omega_1} \\ c_{12} &= -c_{14} = c_{24} = c_{32} = -c_{34} = -c_{42} = -j \frac{k}{2m\omega_2} \end{aligned} \quad (1.14)$$

No approximations have been made beyond the original small amplitude assumption.

When the mutual coupling  $k$  is zero, these equations reduce to the normal mode form of the two isolated pendula (Eqs. 1.5). Therefore, they satisfy the requirements for a coupled mode form as defined above. The name *coupled mode form* has been chosen, since the  $a_1$ ,  $a_1^*$ ,  $a_2$ , and  $a_2^*$  normal modes of the isolated elements (pendula) are coupled by the mutual coupling coefficient  $k$ . The  $c_{ij}$ 's are called the *mode coupling coefficients*. In this form it is seen that  $k$  couples all four isolated modes. The usefulness of the apparently complicated form of the equations will

become obvious when approximations are made in later sections. For example, it will be shown that the unstarred modes will be little affected by the starred modes, since they are rotating in opposite directions. This will allow considerable simplification. However, the present form will show precisely the validity of this assumption.

**Normal mode frequencies for the coupled system.** It has already been noted that the equations of motion for the simple problem of two coupled pendula can be solved exactly. In order to find these exact solutions by the standard technique, assume solutions of the form  $a_1(t) = a_1(0)e^{i\omega t}$ ,  $a_1^*(t) = a_1^*(0)e^{i\omega t}$ ,  $a_2(t) = a_2(0)e^{i\omega t}$ , and  $a_2^*(t) = a_2^*(0)e^{i\omega t}$ . Substitute these solutions in Eqs. 1.13. This yields a set of four homogeneous algebraic equations for the four constants  $a_1(0)$ ,  $a_2(0)$ , and their conjugates. In order to have nontrivial solutions, recall that the determinant of the coefficients must vanish. This requirement leads to an equation that  $\omega$  must satisfy. This equation is called the *secular* or *determinantal* equation. The roots of the secular equation in this case are easily found to be  $\omega = \pm\omega_a$  and  $\omega = \pm\omega_b$ , where

$$\omega_{a,b} = \left[ \frac{\omega_1^2 + \omega_2^2}{2} + \frac{k}{m} \pm \sqrt{\left( \frac{\omega_1^2 - \omega_2^2}{2} \right)^2 + \left( \frac{k}{m} \right)^2} \right]^{\frac{1}{2}} \quad (1.15)$$

These are the frequencies of the normal modes of the coupled system. They play the same role for the coupled system that  $\pm\omega_1$  and  $\pm\omega_2$  play for the uncoupled oscillators.

**Energy conservation.** It is next of interest to evaluate the total energy of the coupled pendula in terms of the *coupled mode amplitudes*,  $a_1$  and  $a_2$  and their conjugates, using no approximations. The exact expression can be used to show the validity of the weak coupling approximation, which is given in Section 1.3.

The total energy of the two coupled pendula (Eqs. 1.9) is

$$E = \frac{m}{2} \left( v_1^2 + \omega_1^2 x_1^2 + v_2^2 + \omega_2^2 x_2^2 + \frac{k}{m} (x_1 - x_2)^2 \right) \quad (1.16)$$

where the  $\omega_{1,2}^2$  are defined by Eq. 1.11. Now solve Eqs. 1.12 for  $v_{1,2}$  and  $x_{1,2}$  in terms of  $a_1$  and  $a_2$ ; substitute these equations in Eq. 1.16, and it follows that

$$E = |a_1|^2 + |a_1^*|^2 + |a_2|^2 + |a_2^*|^2 - \frac{k}{2m} \left( \frac{a_1 - a_1^*}{\omega_1} - \frac{a_2 - a_2^*}{\omega_2} \right)^2 \quad (1.17)$$

The first four terms represent the energy contained in the two pendula when they are uncoupled or isolated from one another ( $k = 0$ ), and the last expression represents the energy associated with the coupling mechanism.

Except for applying boundary conditions, the exact problem of the two coupled pendula has now been solved. It is next of interest to assume that the coupling is weak and to see how this simplifies the problem.

### 1.3 Two Weakly Coupled Oscillators

The two coupled pendula considered in Section 1.2 are said to be weakly coupled when the energy associated with the coupling is small compared with the gravitational potential energy of either pendulum. Mathematically, this approximation means that

$$\frac{k}{2m} \ll \omega_{1,2}^2 \quad (1.18)$$

where  $\omega_{1,2}^2 = g/l_{1,2}$ . It follows from Eq. 1.17 that the energy is then given approximately by

$$E \cong |a_1|^2 + |a_1^*|^2 + |a_2|^2 + |a_2^*|^2 \quad (1.19)$$

Another assumption is implicit in stating that the energy is given approximately by the energy of the mode amplitudes of the foregoing isolated elements, viz.,

$$\omega_1^2 \cong \omega_2^2 \quad (1.20)$$

For if  $\omega_1^2 \gg \omega_2^2$  and both pendula have the same angular amplitudes ( $\theta \cong x_1/l_1 = x_2/l_2$ ), it follows that  $\omega_1^2 x_1^2 = \omega_2^2 x_2^2 l_1/l_2 \ll \omega_2^2 x_2^2$ , since  $l_1 \ll l_2$ . In this case the energy is given approximately by  $|a_2|^2 + |a_2^*|^2$  only. Therefore, interest will be centered on cases in which the two pendula are approximately the same length, since the effect of the coupling will be great only under this assumption. Stated more physically, little energy will be transferred back and forth between the two pendula unless they are approximately equal in length. The assumption  $\omega_1^2 \cong \omega_2^2$  is called the *large transfer factor assumption*, since a large fraction of the energy will be periodically transferred between the two pendula.

Under the weak coupling assumption (Eq. 1.18), the exact frequencies of the normal modes (Eqs. 1.15) can be written approximately as

$$\omega_{a,b} \cong \frac{\omega_1 + \omega_2}{2} + \frac{k}{2m\sqrt{\omega_1\omega_2}} \pm \sqrt{\left(\frac{\omega_1 - \omega_2}{2}\right)^2 + \left(\frac{k}{2m\sqrt{\omega_1\omega_2}}\right)^2} \quad (1.21a)$$

since  $\omega_1 \cong \omega_2$ . When  $\omega_1 = \omega_2$ , these normal mode frequencies reduce to

$$\begin{aligned}\omega_a &\cong \omega_1 \left( 1 + \frac{k}{m\omega_1^2} \right) \\ \omega_b &\cong \omega_1\end{aligned}\tag{1.21b}$$

Section 1.4 demonstrates how these approximate results on the energy and frequency can be obtained directly from the coupled mode form of the equations.

#### 1.4 Direct Approach to Coupled Mode Theory

**Coupled mode approximation.** In the direct approach to coupled mode theory it is argued that the starred modes are only slightly affected by the unstarred modes, since these modes are represented by counter-rotating vectors. Accordingly, the coupled mode approximation neglects all coupling terms between the starred and unstarred modes in Eqs. 1.13. It will be shown that this approximation is equivalent to the weak coupling approximation of Section 1.3 when the pendula are of approximately the same length ( $k/m \ll \omega_{1,2}^2$  and  $\omega_1^2 \cong \omega_2^2$ ).

Neglect all coupling terms to the complex conjugate modes in Eqs. 1.13. They then reduce to

$$\begin{aligned}\frac{da_1}{dt} &= c_{11}a_1 + c_{12}a_2 & (a) \\ \frac{da_2}{dt} &= c_{21}a_1 + c_{22}a_2 & (b)\end{aligned}\tag{1.22}$$

with two similar equations involving  $a_1^*$  and  $a_2^*$ . The coupling coefficients are given by Eqs. 1.14.

Now the solutions of these equations are of the form  $e^{j\omega t}$ , and  $\omega$  is given by

$$\omega_{a,b} \cong \left[ \frac{\omega_1 + \omega_2}{2} + \frac{k}{2m\sqrt{\omega_1\omega_2}} \pm \sqrt{\left(\frac{\omega_1 - \omega_2}{2}\right)^2 + \left(\frac{k}{2m\sqrt{\omega_1\omega_2}}\right)^2} \right]\tag{1.23}$$

since  $\omega_1 \cong \omega_2$ . The solutions for the conjugate modes are similarly found to be  $-\omega_a$  and  $-\omega_b$ . It is therefore clear, by comparing with Eq. 1.21a, that the frequencies obtained by neglecting the conjugate modes when  $\omega_1 \cong \omega_2$  are identical with those obtained from the weak coupling approximation when  $\omega_1 \cong \omega_2$ .

In order to make the equivalence of the approximations even more convincing, multiply Eq. 1.22a by  $a_1^*$ , Eq. 1.22b by  $a_2^*$ , the complex conjugate of Eq. 1.22a by  $a_1$ , and the complex conjugate of Eq. 1.22b by  $a_2$  and add both sides of the resulting equations. Then, by utilizing Eqs. 1.14, the following equation is obtained

$$\frac{d}{dt} (|a_1|^2 + |a_2|^2) = (c_{12} + c_{21}^*)a_1^*a_2 + \text{c.c.} \quad (1.24)$$

where c.c. means complex conjugate. Since  $\omega_1 \cong \omega_2$ , it follows from Eqs. 1.14 that  $c_{12} \cong -c_{21}^*$ . Therefore, from Eq. 1.24 it follows that

$$|a_1|^2 + |a_2|^2 \cong \text{constant} \quad (1.25a)$$

Similar manipulation with the conjugate modes shows that

$$|a_1^*|^2 + |a_2^*|^2 \cong \text{constant} \quad (1.25b)$$

so that the total energy is given approximately by Eq. 1.19.

**Boundary conditions. Transfer factor defined.** It has just been shown that the weak coupling approximation is equivalent to neglecting the coupling between the counterrotating modes. It is now of interest to show that for a given coupling strength,  $k$ , a maximum amount of energy will be exchanged periodically between the two pendula when  $\omega_1^2 \cong \omega_2^2$ . To show this, boundary conditions must be applied.

The general solution of Eqs. 1.22 is

$$a_1(t) = d_1 e^{j\omega_a t} + d_2 e^{j\omega_b t}$$

where  $d_1$  and  $d_2$  are constants of integration to be determined in terms of the initial conditions. From Eq. 1.22a and the foregoing expression for  $a_1$  it follows that

$$a_2(t) = \frac{1}{c_{12}} [(j\omega_a - c_{11})d_1 e^{j\omega_a t} + (j\omega_b - c_{11})d_2 e^{j\omega_b t}]$$

Assume that at  $t = 0$  pendulum 2 is at rest, so that  $x_2(0) = v_2(0) = 0$  and, by Eqs. 1.12,  $a_2(0) = 0$ . Assume that pendulum 1 has an initial nonzero velocity,  $v_1(0)$ , but no initial displacement,  $x_1(0) = 0$ . Therefore, from Eqs. 1.12  $a_1(0) = \frac{1}{2}\sqrt{m}v_1(0)$ . Now let  $t = 0$  in the two foregoing equations and solve for  $d_1$  and  $d_2$  in terms of  $a_1(0)$ . Substitute these values of  $d_1$  and  $d_2$  into the equations, and after simplification it follows that

$$\begin{aligned} |a_1(t)|^2 &= |a_1(0)|^2 [1 - F_{12} \sin^2 \Omega t] \\ |a_2(t)|^2 &= |a_1(0)|^2 F_{12} \sin^2 \Omega t \end{aligned} \quad (1.26)$$

where

$$\Omega = \sqrt{\left(\frac{\omega_1 - \omega_2}{2}\right)^2 + \left(\frac{k}{2m\sqrt{\omega_1\omega_2}}\right)^2} \quad (1.27)$$

and

$$F_{12} = \left[ 1 + \left(\frac{\omega_1 - \omega_2}{2}\right)^2 \left(\frac{2m}{k}\right)^2 \omega_1\omega_2 \right]^{-1}$$

The total energy in pendulum 1 is approximately  $E_1 = |a_1|^2 + |a_1^*|^2 \equiv 2|a_1|^2$ , with a similar expression for the energy in pendulum 2. Sketches of  $|a_1(t)|^2/|a_1(0)|^2$  and  $|a_2(t)|^2/|a_1(0)|^2$  are shown in Figure 1.3. They are the normalized energies contained in the two pendula.

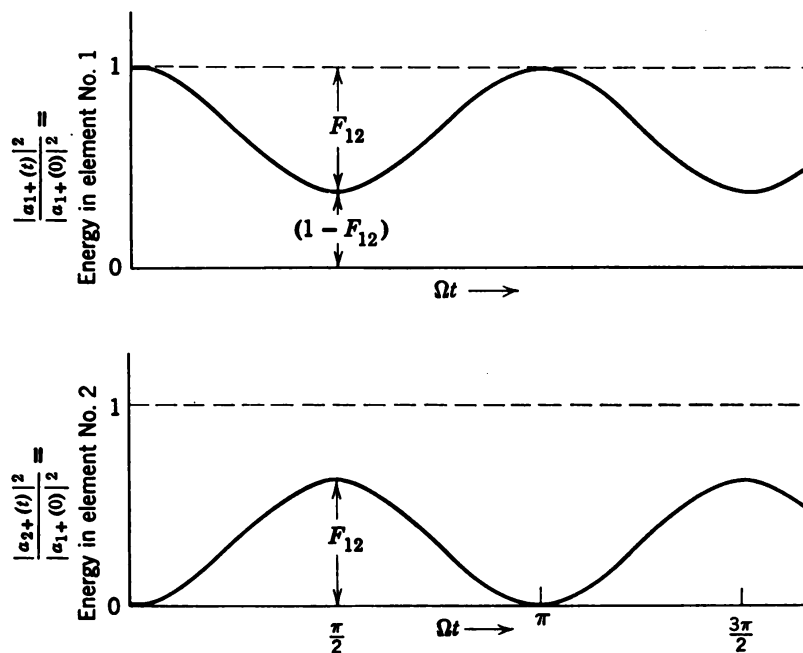


**Figure 1.3** Energy division for two coupled pendula of different lengths as a function of time. (From Cook, Reference 28.)

The initial energy in element 1 is periodically transferred to element 2. The quantity  $F_{12}$  determines the maximum fraction of the energy transferred, as may be seen in the figure. If  $|F_{12}| = 1$ , which occurs if  $\omega_1 = \omega_2$ , then all the energy is interchanged periodically, but if  $|F_{12}| \ll 1$  very little energy is transferred between the modes.  $F_{12}$  is called the *transfer factor* between the  $a_1$ - and  $a_2$ - modes.<sup>2,3</sup>

The foregoing observations suggest that a transfer factor can be defined for any two modes, and the relative magnitudes of these factors for different modes can be used to decide the relative importance of various

modes. Accordingly, define the transfer factor between modes  $i$  and  $j$  by

$$F_{ij} = \left[ 1 + \left( \frac{c_{ii} - c_{jj}}{2} \right)^2 \frac{1}{c_{ij}c_{ji}} \right]^{-1} \quad (1.28)$$

If, for example,  $|F_{ij}| \approx 1$ , coupling must be retained, but if  $|F_{ij}| \ll 1$  the modes are little affected by one another. It has already been shown that  $|F_{12}| = 1$  if  $\omega_1 = \omega_2$ . (See Eqs. 1.27.) It is easy to show that\*  $|F_{12^*}| \ll 1$  if  $k/m \ll \omega_1^2$ . Therefore, in the present case the foregoing criteria lead to the weak coupling or coupled mode approximations in a consistent manner.

It is not known how valid the transfer factor criteria will be when many modes are coupled. It will be shown to be applicable for the theory of the traveling wave tube in which four modes are coupled, and it is believed that it will give a first approximation for neglecting modes in more complex problems. However, the physical meaning of  $F_{ij}$  will be different in such cases.

### 1.5 General Approach to Coupled Mode Theory

The following more general approach to coupled mode theory has been made by Pierce.<sup>4</sup>

**General equations.** Consider a linear system with two unattenuated normal modes of vibration. Assume that the two modes are continuously coupled in a linear manner. Let  $a_1$  and  $a_2$  measure the complex amplitudes of the two normal modes before coupling. They are normalized so that  $2|a_1|^2$  and  $2|a_2|^2$  represent the energy associated with normal modes  $a_1$  and  $a_2$ , respectively. The system is represented schematically in Figure 1.4.

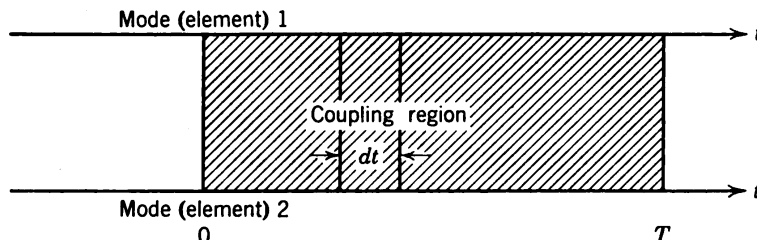


Figure 1.4 Symbolic representation of two coupled lossless modes of vibration.

Let  $\omega_1 dt$  represent the phase shift mode  $a_1$  experiences in time  $dt$ , and let  $\omega_2 dt$  represent the phase shift of mode  $a_2$ , both in the absence of coupling. Because of the coupling, some of the energy in mode  $a_2$  is

\*  $2^*$  refers to the  $a_2^*$ -mode.

transferred to mode  $a_1$  and some of the energy in mode  $a_1$  is transferred to mode  $a_2$ . Let  $c_{12}$  be the mutual coupling coefficient per unit time for mode  $a_2$  to  $a_1$ , and let  $c_{21}$  be the mutual coupling coefficient per unit time for mode  $a_1$  to  $a_2$ . Assume that the self-coupling coefficients  $c_{11} \cong j\omega_1$  and  $c_{22} \cong j\omega_2$  and that  $c_{12}, c_{21} \ll \omega_1, \omega_2$ . This states that the elements are weakly coupled. Under these conditions the coupled mode equations can be written

$$\begin{aligned}\frac{da_1}{dt} &= j\omega_1 a_1 + c_{12} a_2 & (a) \\ \frac{da_2}{dt} &= j\omega_2 a_2 + c_{21} a_1 & (b)\end{aligned}\quad (1.29)$$

The phase of  $a_1$  relative to  $a_2$  is arbitrary.

It should be noted that these equations apply to an arbitrary system, since the values of the mutual coupling coefficients are undetermined. If they are applied to the coupled oscillators, the  $c_{12}$  and  $c_{21}$  would turn out to be given by direct comparison<sup>5</sup> with Eqs. 1.14 and 1.22. However, another method for evaluating the coupling coefficients due to Haus<sup>6</sup> is given below.

**Energy conservation.** The coupling coefficients  $c_{12}$  and  $c_{21}$  must be related if energy is to be conserved, regardless of the particular system under consideration.

Recall that the mode amplitudes were defined so that the total energy of the coupled system is given approximately by

$$W = 2[|a_1(t)|^2 + |a_2(t)|^2] \quad (1.30)$$

under the weak coupling approximation. If energy is to be conserved, therefore, it is clear that

$$\frac{dW}{dt} = 0 \quad (1.31)$$

Now differentiate  $W$  given in Eq. 1.30 with respect to  $t$ , use Eqs. 1.29 and the complex conjugates of these equations to simplify, and it will be found that

$$\frac{d}{dt}(|a_1|^2 + |a_2|^2) = [(c_{12} + c_{21}^*)a_1^*a_2 + (c_{12}^* + c_{21})a_1a_2^*] = 0 \quad (1.32)$$

For strict energy conservation, this expression must be identically true for all time. Since the phases of  $a_1$  and  $a_2$  are arbitrary,  $dW/dt = 0$  if and only if

$$c_{12} = -c_{21}^* \quad (1.33)$$

It will be recognized from the work in Section 1.4 that this relation will be approximately true only if  $\omega_1 \cong \omega_2$ .

**Evaluation of the coupling coefficients.**<sup>6</sup> The coupling coefficients can be evaluated only when a particular coupled system is considered. It has already been mentioned that the coupling coefficients can be evaluated by comparing with the exact equations. Two coupled pendula will now be used to illustrate an alternative method which involves a consideration of the power transferred from one element to the other.

The power transferred to element 1 by the force of element 2 is given by \*

$$P_{21} = f_{21}v_1 = k(x_2 - x_1)v_1 \quad (1.34)$$

where  $f_{21}$  is the force exerted on element 1 by element 2,  $v_1$  is the velocity of element 1,  $(x_2 - x_1)$  is the relative displacement of pendulum 2 with respect to 1, and  $k$  is the spring constant. This power transferred to element 1 must just equal the time rate of change of the energy stored in element 1. If

$$a_{1,2} = \frac{1}{2}\sqrt{m}(v_{1,2} + j\omega_1 x_{1,2}) \quad (1.35)$$

and  $v_{1,2} = dx_{1,2}/dt$ , it, therefore, follows that

$$\frac{d}{dt}(2|a_1|^2) = k(x_2 - x_1)v_1 \quad (1.36a)$$

Now, to first order,  $x_1$  and  $v_1$  are correlated so that  $kx_1v_1$  averaged over each cycle of oscillation of pendulum 1 is approximately zero.  $x_2$  and  $v_1$ , on the other hand, are essentially independent, and Eq. 1.36a can be written

$$\frac{d}{dt}(2|a_1|^2) \cong kx_2v_1 \quad (1.36b)$$

By using Eq. 1.29a and its complex conjugate, the left side of Eq. 1.36b can be written

$$\frac{d}{dt}(2|a_1|^2) = 2(c_{12}a_1^*a_2 + c_{12}^*a_1a_2^*) \quad (1.37)$$

so that by Eqs. 1.36b and 1.37

$$c_{12}a_1^*a_2 + c_{12}^*a_1a_2^* = \frac{k}{2}x_2v_1 \quad (1.38)$$

\* From the definition of work,  $dW = \mathbf{f} \cdot d\mathbf{s}$ , where  $\mathbf{f}$  is a force moving through a distance  $d\mathbf{s}$ . Furthermore, power is defined by  $\mathbf{f} \cdot (d\mathbf{s}/dt) = \mathbf{f} \cdot \mathbf{v}$  since  $\mathbf{v} = d\mathbf{s}/dt$ .

A similar argument for the energy transferred to element 2 shows that

$$c_{21}a_1a_2^* + c_{21}^*a_1^*a_2 = \frac{k}{2}x_1v_2 \quad (1.39)$$

Now subtract Eq. 1.39 from Eq. 1.38, use Eqs. 1.33 and 1.35, and if  $\omega_1^2 \cong \omega_2^2$  it follows that

$$c_{12}a_1^*a_2 + c_{12}^*a_1a_2^* = -j\frac{k}{2m\sqrt{\omega_1\omega_2}}(a_1^*a_2 - a_1a_2^*) \quad (1.40)$$

It therefore follows by identifying coefficients that

$$c_{12} = -j\frac{k}{2m\sqrt{\omega_1\omega_2}} = -c_{21}^* \quad (1.41)$$

which agrees with Eq. 1.14.

The direct and general approaches to the coupled mode approximation have been presented for coupled oscillating elements. The general approach has been extended by Haus<sup>7</sup> to include systems that are more strongly coupled. Unfortunately, the method is more complicated and is omitted in the present work.

## Part II

### COUPLING OF MODES OF PROPAGATION

So far, the theory of coupled modes has been applied only to coupled oscillating elements. It can be applied equally well to coupled elements that propagate waves, such as waveguides or transmission lines. Insofar as they take the same form, the coupled mode equations for propagating modes are analogous to those for oscillating modes. Distance in propagating structures plays the role of time in oscillating elements, whereas the propagation constant plays the role of frequency. The dual of energy in the oscillator is power in the transmission line. However, it will be shown that there are four normal modes associated with the line because of the presence of both forward and backward propagating waves. In order to establish this duality, a single uniform lossless transmission line will be considered to put the equations in normal mode form, just as was done for the simple oscillator in Section 1.1.

### 1.6 Single Uniform Transmission Line

In the theory of coupled modes of vibrating systems the simple oscillator was taken as the simplest element to use to form more complicated coupled systems. In the theory of coupled modes of propagation the role of the oscillator is played by a simple transmission line. It will be assumed that the reader is familiar with the theory of transmission lines. However, the equations for the equivalent circuit for a transmission line<sup>8-11</sup> will be derived, and they will be cast in normal mode form. The analogy with the simple oscillator will then become apparent.

Figure 1.5a shows one example of a transmission line made up of two parallel wires in a dielectric. The voltage between the two lines is given by

$$V = \int_1^2 \mathbf{E} \cdot d\mathbf{s} \quad (1.42)$$

where  $\mathbf{E}$  is the electric field of the propagating wave in the dielectric medium. The integration may be carried from conductor 1 to conductor 2, as shown in the figure. The current carried by the conductor is evaluated by Ampère's law

$$I = \oint \mathbf{H} \cdot d\mathbf{s} \quad (1.43)$$

where  $\mathbf{H}$  is the magnetic field and the path of integration may be around the surface of the conductor in a transverse plane.

Figure 1.5b shows a typical electric and magnetic field configuration around the conductors.

The average electromagnetic power flow in a direction parallel to the wires is found by integrating Poynting's vector across a transverse plane. This power flow is given by

$$P_z = \frac{1}{2} \operatorname{Re}(VI^*) = \iint \frac{1}{2} \operatorname{Re}(\mathbf{E} \times \mathbf{H}^*) \cdot \mathbf{e}_3 dx dy \quad (1.44)$$

where  $\mathbf{e}_3$  is a unit vector in the direction of propagation. The integration extends over the entire plane in this case.

Figure 1.5c shows the equivalent circuit for the line with loss. It is represented by a series inductance per unit length,  $L$ , a series resistance per unit length,  $R$ , which is due to the loss in the line, a shunt capacitance, and a shunt susceptance per unit length,  $C$  and  $G$ , respectively. The shunt susceptance is due to the losses in the dielectric. In order to determine the equivalent circuit parameters in terms of the geometry and dielectric properties of the actual line, Maxwell's equations must be

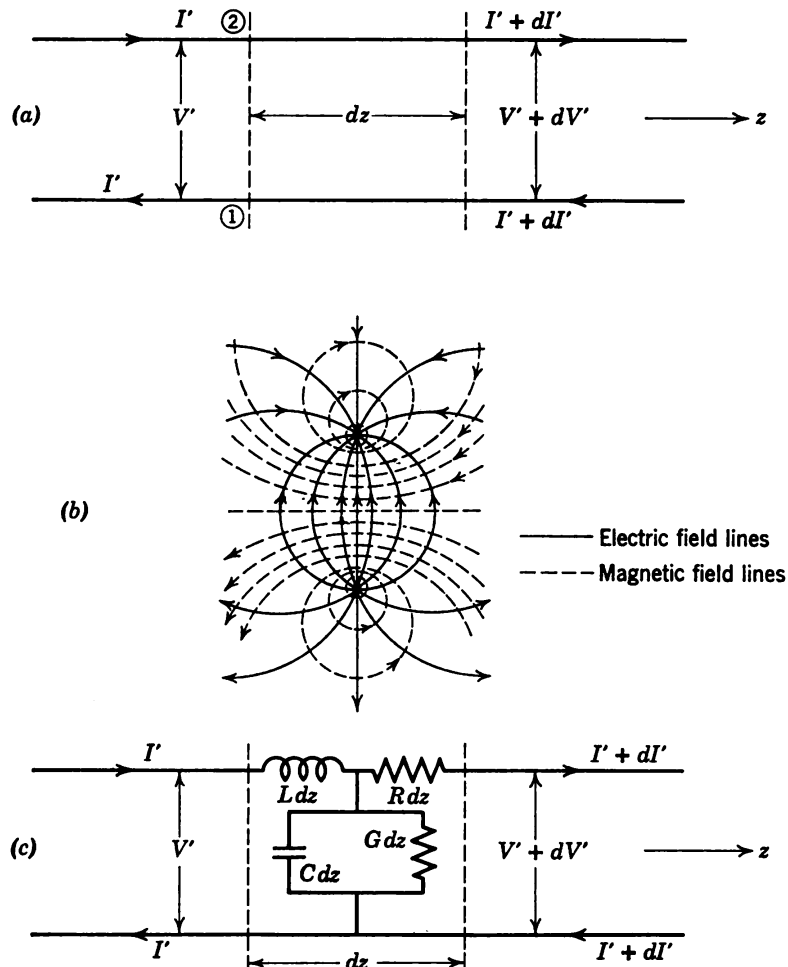


**Figure 1.5** Transmission line: (a) symbolic representation of line; (b) field distribution at a cross section of two-wire transmission line; (c) equivalent circuit of line. (From Sarbacker and Edson, Reference 9.)

solved. This procedure is carried out for a coaxial cable in Appendix A for review purposes.

In the work that follows the equivalent circuit will be used. This equivalent circuit can be used to represent a large class of actual circuits.<sup>10</sup>

**Transmission line equations.** Consider now an element of length  $dz$  of the equivalent circuit of Figure 1.5c. In this length the voltage will drop by virtue of the series resistance and the inductance and is given by

$$dV = -\frac{\partial V}{\partial z} dz = R dz I + L dz \frac{dI}{dt}$$

Further, the current will *decrease* by the action of the shunt capacitance and conductance and is given by

$$dI = -\frac{\partial I}{\partial z} dz = G dz V + C dz \frac{\partial V}{\partial t}$$

Since position and time are independent variables, the partial derivatives must be used. These are the transmission line equations with loss.  $R$ ,  $G$ ,  $L$ , and  $C$  are given per unit length.

Neglect loss, and these equations reduce to

$$\begin{aligned} \frac{\partial V}{\partial z}(z, t) &= -L \frac{\partial I}{\partial t}(z, t) & (a) \\ \frac{\partial I}{\partial z}(z, t) &= -C \frac{\partial V}{\partial t}(z, t) & (b) \end{aligned} \quad (1.45)$$

**Normal mode form.** Equations 1.45 may be called the “Hamiltonian” form of the transmission line equations by analogy with Eqs. 1.1. They show that the voltage and current are coupled, which allows for interchange of electric and magnetic energy as a wave propagates down the line. They are more complicated than the  $LC$  lumped circuit equations, since both distance and time are involved.

In order to put Eqs. 1.45 in normal mode form, the same procedure is used as in Eq. 1.3. Let

$$b_{\pm}(z, t) = \frac{1}{2} \frac{1}{\sqrt{Z_0}} [V(z, t) \pm Z_0 I(z, t)] \quad (1.46a)$$

where  $V(z, t)$  and  $I(z, t)$  are taken as real quantities and

$$Z_0 = +\sqrt{\frac{L}{C}} \quad (1.47)$$

is the characteristic impedance of the line. These mode amplitudes are normalized so that the square of their amplitudes represents the power carried by the mode. Then, by multiplying Eq. 1.45b by  $Z_0$  and adding and subtracting from Eq. 1.45a, it follows that

$$\frac{\partial b_{\pm}}{\partial z} = \mp \sqrt{LC} \frac{\partial b_{\pm}}{\partial t} \quad (1.48)$$

In order to take advantage of complex notation, let

$$b_{\pm}(z, t) = a_{\pm}(z)e^{j\omega t} + a_{\pm}^*(z)e^{-j\omega t}$$

and

$$\begin{aligned} V(z, t) &= \operatorname{Re} V(z)e^{j\omega t} \\ I(z, t) &= \operatorname{Re} I(z)e^{j\omega t} \end{aligned} \quad (1.46b)$$

where  $a_{\pm}$ ,  $V(z)$ , and  $I(z)$  are complex quantities and

$$a_{\pm}(z) = \frac{1}{4\sqrt{Z_0}} [V(z) \pm Z_0 I(z)] \quad (1.46c)$$

In terms of the complex  $V(z)$  and  $I(z)$ , Eqs. 1.45a and b can be written

$$\begin{aligned} \frac{dV}{dz} &= -j\omega LI & (c) \\ \frac{dI}{dz} &= -j\omega CV & (d) \end{aligned} \quad (1.45)$$

together with the conjugate equations.

Substitute Eq. 1.46c into Eqs. 1.45c and d, and it follows that the *normal mode form* of the transmission line equations is

$$\left. \begin{aligned} \left( \frac{d}{dz} + j\beta \right) a_+(z) &= 0 & \left( \frac{d}{dz} - j\beta \right) a_+^*(z) &= 0 \\ \left( \frac{d}{dz} - j\beta \right) a_-(z) &= 0 & \left( \frac{d}{dz} + j\beta \right) a_-^*(z) &= 0 \end{aligned} \right| \quad (1.49)$$

where  $\beta$  is the line propagation constant defined by

$$\beta = +\omega\sqrt{LC} \quad (1.50)$$

In this form the transmission line equations are formally analogous to the simple oscillator (Eqs. 1.5), where distance plays the role of time, propagation constant plays the role of frequency, and average power flow plays the role of stored energy. The latter analog will become apparent below.

At a fixed  $z$ , the  $a_+$ - and  $a_+^*$ -modes can be visualized as two counter-rotating vectors, just as in the lumped circuit case of Section 1.1. Similarly,  $a_-$  and  $a_-^*$  are counterrotating vectors at a fixed  $z$ . It will be shown below that  $a_+$  and  $a_+^*$  are forward waves, whereas  $a_-$  and  $a_-^*$  are backward waves.

**Phase and group velocity.** The phase velocities of the two normal modes  $a_{\pm}$  are given by

$$v_{\pm ph} = \pm \frac{\omega}{\beta} = \pm \frac{1}{\sqrt{LC}} \quad (1.51)$$

where  $\beta > 0$ . Thus the  $a_+$ -mode travels along the positive  $z$ -direction and the  $a_-$ -mode travels along the negative  $z$ -direction.

It is again noted that  $a_+$  and  $a_-$  are called normal modes because the equations in the form of Eqs. 1.49 are decoupled and  $a_+$  and  $a_-$  represent two independent solutions of the transmission line "equations of motion."

If the phase velocity of a transmission line is different for various frequencies ( $v_{ph}$  is a function of frequency), the line is said to be dispersive. This dispersion must be known before the group velocity of the waves can be found. The dispersion law is found by solving for  $\beta$  versus  $\omega$  from Maxwell's equations for the particular structure under consideration. The direction of the group velocity gives the direction of power flow on the line, and the group velocity is defined by

$$v_{\pm gr} = \pm \frac{1}{\partial \beta / \partial \omega} = \frac{\pm v_{\pm ph}}{1 \mp \beta (\partial v_{\pm ph} / \partial \omega)} \quad (1.52)$$

where Eq. 1.51 has been used. For a dispersionless line,  $\partial v_{\pm ph} / \partial \omega = 0$ , and it is seen that the group and phase velocities are in the same direction. Thus the power flow is in the  $+z$ -direction for the  $a_+$ -mode, whereas it is in the  $-z$ -direction for the  $a_-$ -mode.

It might be noted that it is possible to devise a transmission line in which the phase and group velocities are in opposite direction by suitable choice of the dispersion. This line is used for a backward wave amplifier, which is treated in a later chapter. It is also discussed in Sections 1.7 and 1.8.

**Boundary conditions. Power flow in lossless line.** Consider first the boundary value problem. Assume that at  $z = 0$  the voltage and current are given by

$$\begin{aligned} V(0, t) &= V_m \cos(\omega t + \delta) \\ I(0, t) &= I_m \cos(\omega t + \epsilon) \end{aligned} \quad (1.53)$$

where  $\delta$  and  $\epsilon$  are arbitrary phases. It follows from Eq. 1.46 and the foregoing that

$$a_{\pm}(0) = \frac{1}{4\sqrt{Z_0}} (V_m e^{j\delta} \pm Z_0 I_m e^{j\epsilon}) \quad (1.54a)$$

Since the solutions of Eqs. 1.49 are given by

$$a_{\pm}(z) = a_{\pm}(0)e^{\mp j\beta z} \quad (1.54b)$$

it follows from Eq. 1.46a and the foregoing that

$$b_{\pm}(z, t) = a_{\pm}(0)e^{j(\omega t \mp \beta z)} + a_{\pm}^*(0)e^{-j(\omega t \mp \beta z)} \quad (1.54c)$$

Therefore,  $b_+$  is a forward wave made up of the  $a_+$ - and  $a_+^*$ -modes, and  $b_-$  is a backward wave made up of the  $a_-$ - and  $a_-^*$ -modes.

From Eq. 1.54a it follows that if

$$V_m = Z_0 I_m e^{j(\epsilon - \delta)}$$

since  $V_m$ ,  $Z_0$ , and  $I_m$  are real,  $\delta = \epsilon$  and  $a_-(0) = a_-^*(0) = 0$  and only the forward wave will be excited. In this case the voltage and current are in-phase at the input. This is the normal situation that occurs if a generator with internal impedance  $Z_0$  is applied at  $z = 0$  to an infinite line or to a line that is terminated in its characteristic impedance.

If, on the other hand,

$$V_m = -Z_0 I_m e^{j(\epsilon - \delta)}$$

again  $\epsilon = \delta$ , since  $V_m$ ,  $Z_0$ , and  $I_m$  are real and the voltage and current are out of phase at  $z = 0$ ; it follows that  $a_+(0) = a_+^*(0)$ , and only the backward wave is excited on the line. To excite this mode, a matched voltage generator must be applied to the line at  $z = L$ , and the end  $z = 0$  must be terminated with  $Z_0$  or the line must extend to  $z = -\infty$ . It is therefore seen that boundary conditions must be matched at  $z = L$  in order to excite a pure backward wave.

In general, if the voltage and current have an arbitrary phase at  $z = 0$ , both the forward and backward waves will be excited.

Consider next the average power transmitted down the line. It is shown in Appendix A that this average power is found by integrating Poynting's vector over a cross section normal to the direction of propagation. In the equivalent circuit representation this is given by

$$P = \overline{VI}$$

where the bar represents the time average. Now solve Eq. 1.46a for  $V(z, t)$  and  $I(z, t)$  in terms of  $b_{\pm}$ , and it follows that

$$P = \overline{VI} = \overline{b_+^2} - \overline{b_-^2}$$

By utilizing Eq. 1.54c, the foregoing expression reduces to

$$P = 2[|a_+(z)|^2 - |a_-(z)|^2] \equiv 2[|a_+(0)|^2 - |a_-(0)|^2] \quad (1.55)$$

The minus sign shows that the power flow in the backward mode is

opposite in direction from the forward mode. The group velocities of these modes are also in opposite directions.

It follows directly from Eq. 1.55 that  $dP/dz = 0$ , so that power is conserved.

The average power carried in the forward mode is  $2|a_+(z)|^2$ , whereas that carried in the backward mode is  $-2|a_-(z)|^2$ . From Eq. 1.54b it follows that

$$\frac{d}{dz} 2|a_{\pm}(z)|^2 = 0 \quad (1.56)$$

and the powers carried in these modes are separately conserved.

### 1.7 General Approach to Coupling of Two Lossless Modes of Propagation.

**Equations in coupled mode form.** Consider two waves with time dependence  $e^{j\omega t}$  which are weakly coupled. From the normal mode representation of the transmission-line equations (1.49) and an argument similar to that given in Section 1.5, it can be shown that the coupled equations can be written

$$\begin{aligned} \frac{da_1}{dz} &= -j\beta_1 a_1 + c_{12} a_2 & (a) \\ \frac{da_2}{dz} &= -j\beta_2 a_2 + c_{21} a_1 & (b) \end{aligned} \quad (1.57)$$

The  $c_{12}$  and  $c_{21}$  are the mutual coupling coefficients per unit length. The coupling is assumed uniform over the length of the coupler, so that  $c_{12}$  and  $c_{21}$  are independent of length. The modes are assumed lossless. In the absence of coupling, if  $\beta_1$  and  $\beta_2$  are positive, the phase velocities of both waves are in the positive  $z$ -direction; if  $\beta_1$  and  $\beta_2$  are negative, the phase velocities are in the negative  $z$ -direction; and if  $\beta_1$  and  $\beta_2$  are of opposite sign the phase velocities are in opposite directions. Any of these possible combinations can be described by Eqs. 1.57.

For weak coupling it is assumed that  $c_{12}$  and  $c_{21}$  are small compared with  $\beta_1$  and  $\beta_2$  and, furthermore, it is assumed that  $\beta_1 \cong \beta_2$ .

The mode or wave amplitudes are normalized so that  $2|a_{1,2}|^2$  represents approximately the average power carried by each mode.

**Power conservation.** Under the coupled mode approximation the total average power is given approximately by

$$2(|a_1(z)|^2 \pm |a_2(z)|^2) \cong \text{constant} \quad (1.58a)$$

(Compare Sections 1.3 and 1.4.) If the group velocities are in the same directions for the two modes, the + sign is to be taken, whereas if the power flow is in opposite directions for the two modes the - sign is to be taken. If Eq. 1.58a is to represent the average power, then it follows (see Section 1.5) that

$$c_{12} = \mp c_{21}^* \quad (1.58b)$$

where the upper sign is required for group velocities in the same direction and the lower sign is required for group velocities in opposite directions.

**Normal mode propagation constants.** Solutions of the coupled mode equations (1.57) are of the form  $e^{\gamma z}$ , where  $\gamma$  (see Section 1.2) is given by

$$\gamma_{1,2} = \pm \sqrt{\mp |c_{12}|^2 - \left(\frac{\beta_1 - \beta_2}{2}\right)^2 - j\left(\frac{\beta_1 + \beta_2}{2}\right)} \quad (1.59)$$

in which the upper sign of  $|c_{12}|^2$  is to be used if the group velocities of the uncoupled modes are in the same direction and the lower sign of  $|c_{12}|^2$  is taken if the group velocities are in opposite directions. The complete solution for  $a_1$  and  $a_2$  consists of a linear combination of the two modes,  $e^{\gamma_{1,2}z}$ , and the constants of integration are found from the boundary conditions. These are considered below.

### 1.8 The Directional Coupler.<sup>2, 3, 12-24</sup> Active and Passive Mode Coupling

It is sometimes useful in engineering practice to transfer power from one transmission line, partially or completely, to another. One means to accomplish this is by a directional coupler. By allowing appropriate coupling between the two lines in question, power can be transferred from one to the other. The coupled mode approach is ideal for visualizing the action of such a coupler.<sup>4</sup>

Two possible cases are considered in this section. The first is called a codirectional coupler in which the phase and group velocities of both coupled modes are in the positive  $z$ -direction. This case is shown schematically in Figure 1.6. Since power flow is to the right, boundary conditions must be matched at  $z = 0$  for both modes. Power in mode 1 couples into mode 2 and vice versa.

The second case treated is an example of a contradirectional coupler, shown schematically in Figure 1.7. The phase velocities of the two modes are taken in the positive  $z$ -direction, whereas the group velocity of the  $a_1$ -mode is in the positive  $z$ -direction and the power flow of the

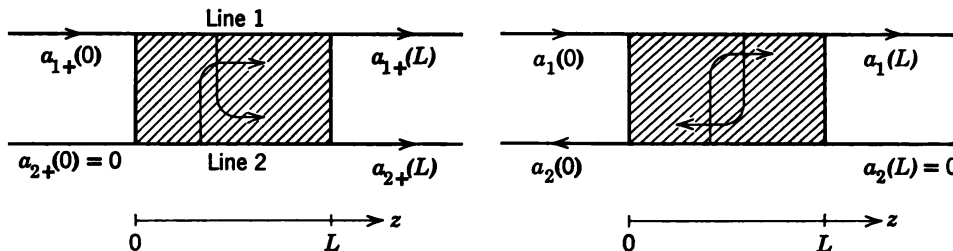


**Figure 1.6** Symbolic representation of a codirectional coupler in which the phase and group velocities of both modes are to the right.

**Figure 1.7** Symbolic representation of a contradirectional coupler in which the phase velocities of both modes are to the right but with group velocities in opposite directions.

$a_2$ -mode is in the negative  $z$ -direction. Accordingly, boundary conditions must be applied at  $z = 0$  for the  $a_1$ -mode and at  $z = L$  for the  $a_2$ -mode.

**A codirectional coupler. Passive mode coupling.** The propagation constants for the codirectional coupler (see Eq. 1.59) are

$$\gamma_{1,2} = -j(\beta_a \pm \beta_b) \quad (1.60)$$

where

$$\beta_a = \frac{\beta_1 + \beta_2}{2}$$

$$\beta_b = +\sqrt{\beta_d^2 + |c_{12}|^2} \quad (1.61)$$

$$\beta_d = \frac{\beta_1 - \beta_2}{2}$$

Before solving the boundary value problem, note that, since  $c_{12} = -c_{21}^*$ ,  $\gamma_1$  and  $\gamma_2$  are pure imaginary, and there can be no exponentially growing or decaying solutions. When  $\gamma$  is pure imaginary, the two modes are said to be *passively* coupled.

Now, given that  $a_{1,2}(0)$  are the mode input amplitudes at the beginning of the coupling region, it is straightforward to show by the method outlined in obtaining Eqs. 1.26 that the complete solutions of Eqs. 1.57 are given by

$$a_1(z) = e^{-j\beta_a z} \left[ \left( \cos \beta_b z - j \frac{\beta_d}{\beta_b} \sin \beta_b z \right) a_1(0) + \left( \frac{c_{12}}{\beta_b} \sin \beta_b z \right) a_2(0) \right] \quad (1.62)$$

$$a_2(z) = e^{-j\beta_a z} \left[ \left( \cos \beta_b z + j \frac{\beta_d}{\beta_b} \sin \beta_b z \right) a_2(0) + \left( \frac{c_{21}}{\beta_b} \sin \beta_b z \right) a_1(0) \right] \quad (1.63)$$

The average power transmitted on lines 1 and 2, respectively, is given approximately by

$$P_{1,2}(z) = 2 |a_{1,2}(z)|^2 \quad (1.64)$$

In order to obtain a picture of the power transfer, consider a few special cases.<sup>3</sup>

**Case 1. Synchronous Case.** Assume that, before coupling, the propagation constants of the two lines were identical, i.e.,  $\beta_1 = \beta_2$ , so that  $\beta_d = 0$ ,  $\beta_b = |c_{12}|$ , and  $\beta_a = \beta_1 = \beta_2$ . In this case, using Eqs. 1.62 and 1.64, it is seen that the average power on element 1 is given by

$$P_1(z) = 2 \{ \cos^2 (|c_{12}|z) |a_1(0)|^2 + \sin^2 (|c_{12}|z) |a_2(0)|^2 + \frac{1}{2} \sin (2|c_{12}|z) \left[ \frac{c_{12}}{|c_{12}|} a_2(0)a_1^*(0) + \text{c.c.} \right] \} \quad (1.65)$$

whereas the average power on element 2 is given by

$$P_2(z) = 2 \{ \sin^2 (|c_{12}|z) |a_1(0)|^2 + \cos^2 (|c_{12}|z) |a_2(0)|^2 - \frac{1}{2} \sin (2|c_{12}|z) \left[ \frac{c_{12}}{|c_{12}|} a_2(0)a_1^*(0) + \text{c.c.} \right] \} \quad (1.66)$$

It is clear that power transfer takes place between the two lines. Assume initially that all the power is on line 1, so that  $a_2(0) = 0$  and  $a_1(0) = \frac{1}{2}$ . Figure 1.8 then shows a sketch of the power in line 1 and line 2 as a function of distance along the coupler. It is seen that complete power transfer takes place in a length  $L$  given by

$$|c_{12}|L = \frac{\pi}{2} \quad (1.67)$$

Furthermore, the transfer takes place in exactly the same way if power is initially introduced on line 2, and complete power transfer will take place in the same length. By removing the coupling before  $z = L$ , any division of power between the two lines may be accomplished. For example, if the coupling is ended at  $|c_{12}|L = \pi/4$ , equal power will be in

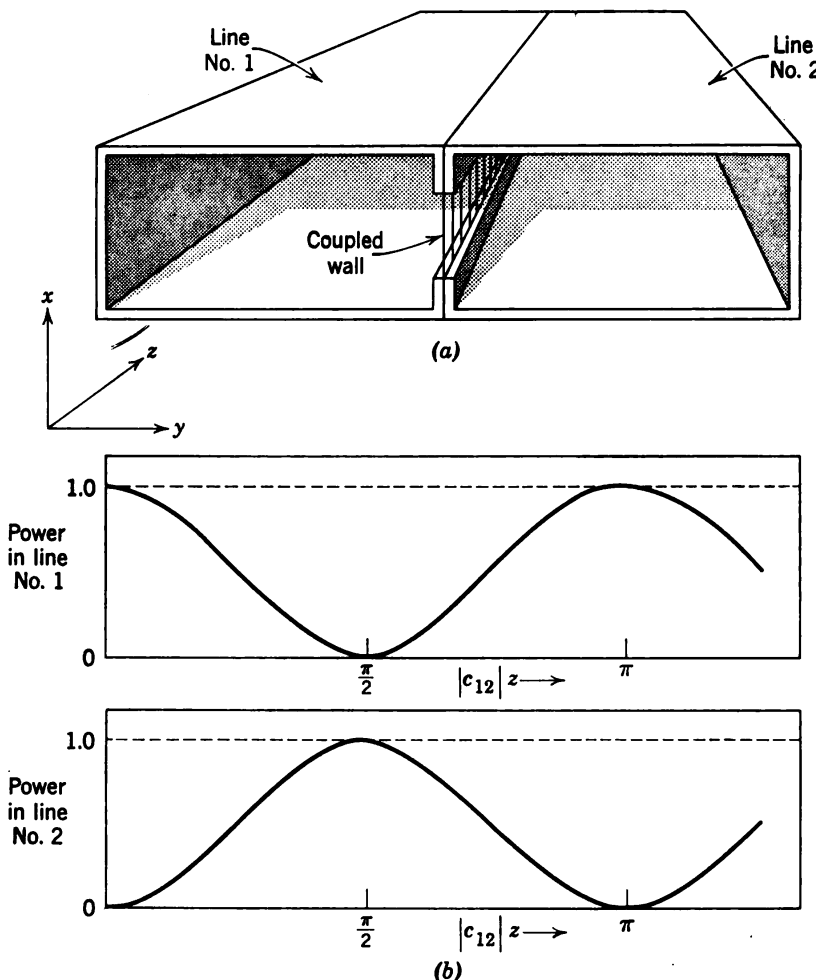


**Figure 1.8** (a) Two coupled waveguides used as a codirectional coupler; (b) power division between two lines when lines are identical before coupling. Only the dominant waveguide modes are considered. (From Cook, Reference 28.)

both lines. There are cases in which only partial power transfer is required, and the directional coupler offers a means of achieving this division.

Note that for uniform coupling, which has been treated here, complete power transfer is possible only for the synchronous case  $\beta_1 = \beta_2$ .

**Case 2. Nonsynchronous Case.** If  $\beta_1 \neq \beta_2$  and all the power is put on line 1 initially, then by Eqs. 1.62–1.64

$$\begin{aligned} P_1(z) &= 1 - F \sin^2 \beta_b z \\ P_2(z) &= 1 - P_1(z) \end{aligned} \quad (1.68)$$

Figure 1.9 shows a sketch of  $P_1(z)$  and  $P_2(z)$  in this case, in which

$$F = \left( \frac{|c_{12}|}{\beta_b} \right)^2 = \frac{1}{1 + \left( \frac{\beta_2 - \beta_1}{2|c_{12}|} \right)^2} \quad (1.69)$$

is the maximum fraction of power transferred. As  $|c_{12}| \rightarrow \beta_b$ , or  $\frac{\beta_2 - \beta_1}{|c_{12}|} \rightarrow 0$ , complete power transfer will take place.  $F$  will be recognized as the transfer factor introduced in Section 1.4.

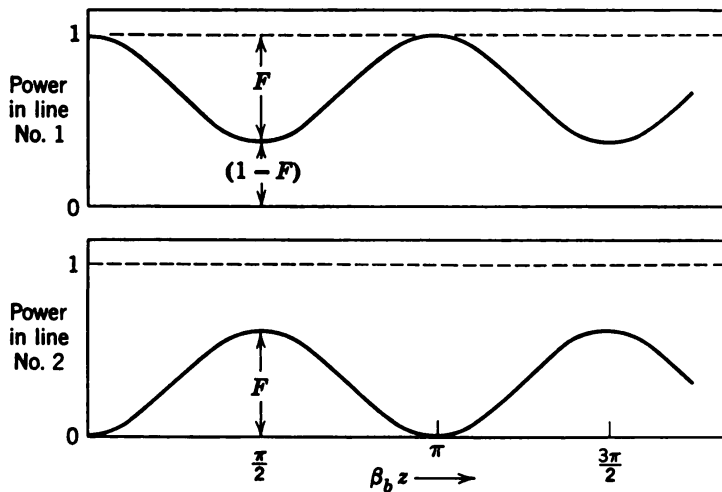


**Figure 1.9** Power division between two coupled transmission lines when propagation constants of the uncoupled lines are different. There is only partial power transfer, but it is periodic. (From Cook, Reference 28.)

**The contradirectional coupler. Active mode coupling.** Consider next a contradirectional coupler in which the phase velocities of the two modes are in the same direction and the group velocities are in opposite directions. From Eq. 1.59 the propagation constants are seen to be

$$\gamma_{1,2} = \pm\alpha - j\beta_a \quad (1.70)$$

where

$$\beta_a = \frac{1}{2}(\beta_1 + \beta_2)$$

$$\beta_d = \frac{1}{2}(\beta_1 - \beta_2) \quad (1.71)$$

$$\alpha = +\sqrt{|c_{12}|^2 - \beta_d^2}$$

Since  $\beta_1 \cong \beta_2$ , it follows that, if  $|c_{12}| > \beta_d$ ,  $\gamma$  will be complex, and there will be a growing and a decaying wave with the same phase velocity.

When  $\gamma$  can be complex, the two modes are said to be *actively* coupled.

The presence of growing waves may seem strange, since, clearly, there is no gain in the coupler. However, power removed must always be less than the power injected into the coupler. The explanation is that the direction of power flow in a given element will turn out to be the direction in which power is decreasing in that element. In order to have gain, power must increase in the direction of power flow. The situation here may be better visualized by applying boundary conditions. Assume that power is injected at  $z = 0$  in mode 1. Then  $a_2(L) = 0$  and  $a_1(0) = \frac{1}{2}$ . By a procedure analogous to that outlined for Eqs. 1.26, the power carried by the two modes is found to be

$$P_1(z) = 2|a_1(z)|^2 = \frac{1 + F \sinh^2 \alpha(z - L)}{1 + F \sinh^2 \alpha L} \quad (1.72)$$

$$P_2(z) = -2|a_2(z)|^2 = -\frac{F \sinh^2 \alpha(z - L)}{1 + F \sinh^2 \alpha L}$$

where

$$F = \left[ 1 - \left( \frac{\beta_1 - \beta_2}{2} \right)^2 \frac{1}{|c_{12}|^2} \right]^{-1} = \left( \frac{|c_{12}|}{\alpha} \right)^2 \quad (1.73)$$

A sketch of the power carried by each element is shown in Figure 1.10. The power in element 1 is seen to decrease in the positive  $z$ -direction, the direction of power flow, as power is fed into element 2 in agreement with the foregoing statement. So the presence of complex propagation constants (active mode coupling) does not necessarily imply gain.

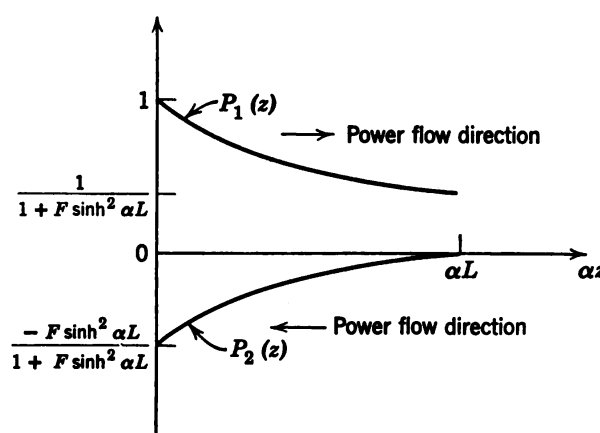


**Figure 1.10** Power flow in two actively coupled elements. The phase velocities of the two modes are in the same direction and the group velocities are in opposite directions.

Examples are given in Chapter 3 in which both active and passive coupling yield net power gain. Obviously, a source of energy must be available for gain to occur.

Only cases of distributed coupling have been treated in this chapter, since all examples in this book involve this type of coupling. However, there are important cases in which the coupling is discrete. Such cases have been treated by Pierce<sup>4</sup> in his initial paper on coupled mode theory. (See also Reference 24.)

Loss has been neglected in this chapter for simplicity, but it is included in the chapter on parametric amplifiers.

Fortunately, the examples treated in this book can be looked upon as coupling between only two elements. However, more than two modes are usually involved. The extension to these cases are made at the appropriate places as the need arises.

It is to be emphasized that the theory of coupling of modes is the unifying theme of the entire book; therefore, the reader should become thoroughly familiar with the concepts of this chapter.

### 1.9 Summary

Oscillating and wave propagating structures that are weakly coupled can be treated by using the method of coupled modes. To use this method, the coupling is first neglected. The decoupled equations are written in a normal mode form, and the mode or wave amplitudes are normalized so that they represent energy or power carried by the mode. The coupling is taken into account by writing the coupled equations in terms of the mode amplitudes of the decoupled elements. The coupling coefficients are then found either from the exact equations (Section 1.4) or by computing the energy or power transfer between the modes involved (Section 1.5). If some of the modes can be neglected, the solution of the equations can be simplified. A transfer factor (Section 1.4) has been defined as a means of deciding quantitatively whether some modes can be neglected. After this, the propagation constants must be found, and the boundary conditions applied, in order to have a complete solution to the problem.

It has been shown that the coupled mode approximation is equivalent to the weak coupling approximation. If the elements are not weakly coupled, more complex procedures are required.<sup>7</sup>

The bibliography<sup>25-32</sup> contains other references of possible interest in connection with Pierce's theory of coupled modes as well as broadband directional couplers.

## BIBLIOGRAPHY

1. H. Goldstein, *Classical Mechanics*, Addison-Wesley Press, Cambridge, Mass., 1950, Chapters 2, 7, and 10.
2. S. E. Miller, "Coupled Wave Theory and Waveguide Applications," *Bell System Tech. J.*, **33**, 661-720 (May 1954).
3. J. S. Cook, R. Kompfner, and C. F. Quate, "Coupled Helices," *Bell System Tech. J.*, **35**, 127-178 (January 1956).
4. J. R. Pierce, "Coupling of Modes of Propagation," *J. Appl. Phys.*, **25**, 179-183 (February 1954).
5. R. W. Gould, "A Coupled Mode Description of the Backward-Wave Oscillator and the Kompfner Dip Condition," *IRE Trans. PGED*, **ED-2**, 37-42 (October 1955).
6. H. A. Haus, "Electron Beam Waves in Microwave Tubes," *Mass. Inst. Technol. Research Lab. Electronics, Tech. Rep. No. 316* (April 8, 1958).
7. H. A. Haus, "Variational Principles Derived from Power Theorems," *Mass. Inst. Technol. Research Lab. Electronics, Internal Memorandum* (1959).
8. S. Ramo and J. R. Whinnery, *Fields and Waves in Modern Radio*, John Wiley and Sons, Second Edition, New York, 1953, p. 23.
9. R. I. Sarbacher and W. A. Edson, *Hyper and Ultrahigh Frequency Engineering*, John Wiley and Sons, New York, 1947, pp. 272-284, 320.
10. S. A. Schelkunoff, "Generalized Telegraphist's Equations for Waveguides," *Bell System Tech. J.*, **31**, pp. 784-801 (July 1952).
11. S. A. Schelkunoff, "Conversion of Maxwell's Equations into Generalized Telegraphist's Equations," *Bell System Tech. J.*, **34**, pp. 995-1044 (September 1955).
12. W. W. Mumford, "Directional Couplers," *Proc. IRE*, **35**, 160-165 (February 1947).
13. S. E. Miller and W. W. Mumford, "Multielement Directional Couplers," *Proc. IRE*, **40**, 1071-1078 (September 1952).
14. H. J. Riblet, "A Mathematical Theory of Directional Couplers," *Proc. IRE*, **35**, 1307-1313 (November 1947).
15. R. Kompfner, "Experiments on Coupled Helices," *AERE Rept. No. G/M98* (September 1951).
16. R. Kompfner, "Coupled Helices," presented at IRE Annual Conference on Electron Tube Research, Stanford, Calif. (1953).
17. G. Wade and N. Rynn, "Coupled Helices for Use in Traveling-Wave Tubes," *IRE Trans. PGED*, **ED-2**, p. 15 (July 1955).
18. M. Chodorow and E. L. Chu, "The Propagation Properties of Cross-Wound Twin Helices Suitable for Traveling-Wave Tubes," presented at IRE Annual Conference on Electron Tube Research, Stanford, Calif. (1953).
19. G. M. Branch, "A New Slow Wave Structure for Traveling-Wave Tubes," presented at IRE Annual Conference on Electron Tube Research, Stanford, Calif. (1953). G. M. Branch, "Experimental Observation of the Properties of Double Helix Traveling-Wave Tubes," presented at IRE Annual Conference on Electron Tube Research, Orono, Maine (1954).
20. B. L. Humphreys, L. V. Kite, and E. G. James, "The Phase Velocity of Waves in a Double Helix," *Rept. No. 9507, Res. Lab. G.E.E.*, England (September 1948).
21. L. Stark, "A Helical-Line Phase Shifter for Ultrahigh Frequencies," *Mass. Inst. Technol. Research Lab. Electronics Technical Rep. No. 59* (February 1954).

22. P. D. Lacy, "Helix Coupled Traveling-Wave Tube," *Electronics*, **27**, No. 11 (November 1954).
23. B. M. Oliver, "Directional Electromagnetic Couplers," *Proc. IRE*, **42**, 1686-1692 (November 1954).
24. D. A. Watkins, *Topics in Electromagnetic Theory*, John Wiley and Sons, New York, 1958, Chapter 3.

### Coupled Modes

25. J. R. Pierce, "The Wave Picture of Microwave Tubes," *Bell System Tech. J.*, **33**, 1343-1372 (November 1954).
26. C. C. Cutler, "A Mechanical Traveling Wave Amplifier," *Bell Labs Record*, 134-138 (April 1954).
27. A. Yariv, "On the Coupling Coefficients in the 'Coupled-Mode' Theory," *Proc. IRE*, **46**, 1956-1957 (December 1958).

### Broadband Directional Couplers

28. J. S. Cook, "Tapered Velocity Couplers," *Bell System Tech. J.*, **34**, 807-822 (July 1955).
29. W. H. Louisell, "Analysis of the Single Tapered Mode Coupler," *Bell System Tech. J.*, **34**, 853-870 (July 1955).
30. A. G. Fox, "Wave Coupling by Warped Normal Modes," *Bell System Tech. J.*, **34**, 823-852 (July 1955).
31. H. G. Unger, "Circular Waveguide Taper of Improved Design," *Bell System Tech. J.*, **37**, 899-912 (July 1958).

### General Perturbation Theory

32. D. Bohm, *Quantum Theory*, Prentice-Hall, New York, 1951, Chapter 18.

## Chapter 2

# Some normal modes on electron beams

Electron beams are capable of transmitting waves of various kinds under different conditions. There are many microwave devices that exploit the coupling of these beam modes to passive circuits such as a transmission line. In order to study these devices, therefore, it is most natural to use the coupled mode approach. It has been shown in Chapter 1 that in order to use the coupled mode approach it is first necessary to have a thorough knowledge of the uncoupled elements. This chapter is devoted to a study of some normal modes of propagation on an electron beam in preparation for later work in which the beam and circuit modes are coupled.

Specifically, a study will be made of the space-charge modes, the cyclotron modes, and the synchronous modes that propagate on an electron beam. Devices that utilize these modes are treated in later chapters.

### 2.1 Fundamental Equations Governing Wave Propagation on Electron Beams

An electron beam possesses a charge density distribution given by  $\rho(\mathbf{r}, t)$  (where  $\mathbf{r}$  is the position vector and  $t$  is the time) and a current density given by  $\mathbf{J}(\mathbf{r}, t)$ . These densities in turn set up an electric field  $\mathbf{E}(\mathbf{r}, t)$  and a magnetic field  $\mathbf{H}(\mathbf{r}, t)$ . Maxwell's equations in mks units for these fields are given by

$$\nabla \times \mathbf{H} = \mathbf{J} + \epsilon_0 \frac{\partial \mathbf{E}}{\partial t} \quad (2.1)$$

$$\nabla \times \mathbf{E} = -\mu_0 \frac{\partial \mathbf{H}}{\partial t} \quad (2.2)$$

$$\nabla \cdot \mathbf{E} = \frac{1}{\epsilon_0} \rho \quad (2.3)$$

$$\nabla \cdot \mathbf{H} = 0 \quad (2.4)$$

where all quantities are functions of  $(\mathbf{r}, t)$ ,  $\mu_0$  is the permeability, and  $\epsilon_0$  is the dielectric constant of free space.

The equation of continuity is derived from these equations by taking the divergence of both sides of Eq. 2.1 and using Eq. 2.3. Since  $\nabla \cdot \nabla \times \mathbf{A} = 0$  for any vector  $\mathbf{A}$ , it is seen that

$$\nabla \cdot \mathbf{J} + \frac{\partial \rho}{\partial t} = 0 \quad (2.5)$$

This equation is just an expression of the conservation of charge. Since Eq. 2.5 is a combination of Eqs. 2.1 and 2.3, Eq. 2.3 can be omitted and replaced by the equation of continuity.

The equation of motion is given by

$$\frac{d\mathbf{v}}{dt} = \frac{\partial \mathbf{v}}{\partial t} + \mathbf{v} \cdot \nabla \mathbf{v} = \frac{e}{m} (\mathbf{E} + \mathbf{v} \times \mathbf{B}) \quad (2.6)$$

where  $\mathbf{v}(\mathbf{r}, t)$  is the electron velocity,  $\mathbf{B} = \mu_0 \mathbf{H}$ , and  $e$  and  $m$  are the charge and mass of the particle (for electrons,  $e < 0$ ). The  $\mathbf{v} \times \mathbf{B}$  is the Lorentz force term. The term  $\partial \mathbf{v} / \partial t$  is the change in velocity at a fixed point, whereas the term  $\mathbf{v} \cdot \nabla \mathbf{v}$  is the change in velocity at a fixed time for different positions. This relation follows from the ordinary rules of differentiation, since  $\mathbf{v}$  is a function of  $\mathbf{r}$  and  $t$  and  $d\mathbf{r}/dt = \mathbf{v}$ .

If the spread in velocities of the electrons is small compared with the electron velocity, all electrons passing a given point can be assumed to have the same velocity. In this case, the current density and velocity are related by

$$\mathbf{J}(\mathbf{r}, t) = \rho(\mathbf{r}, t) \mathbf{v}(\mathbf{r}, t) \quad (2.7)$$

This completes the set of equations necessary to study wave propagation on electron beams. The equation of motion is seen to be nonlinear in the velocity, and  $\mathbf{J} = \rho \mathbf{v}$  is nonlinear in  $\rho$  and  $\mathbf{v}$ . In order to solve them analytically, they must be linearized. This is done by the small signal approximation which is taken up in the next section.

## 2.2 Small Signal Approximation

In order to linearize the fundamental equations of Section 2.1, it is assumed that all quantities can be broken up into the sum of a d-c or time-average part plus an a-c or time-varying part. Further, it is assumed that all a-c quantities are very small compared with the d-c quantities, so that all products of second order or higher in a-c quantities are omitted. Under these assumptions the equations will be linearized. Since it is well known that the superposition principle holds for linear systems, a sinusoidal excitation at only one frequency need be considered, and all quantities will vary with this same frequency. The solutions for excitations at different frequencies then need merely be added, as in Fourier analysis.

In accordance with the small signal approximation, all field quantities, current, and charge densities are expanded in the form

$$\mathbf{A}(\mathbf{r}, t) = \mathbf{A}_0(\mathbf{r}) + \mathbf{A}_1(\mathbf{r})e^{j\omega t} \quad (2.8)$$

where the first term is the time-average term and the second term is the a-c term, which is assumed to be small compared with the d-c term. Complex notation is used for mathematical convenience. It is understood tacitly that the real part of these expressions will be taken. It is also to be noted that the a-c amplitudes are complex.

Now substitute the expansions (Eq. 2.8) into Eqs. 2.1, 2.2, and 2.4–2.7. Omit all products of a-c quantities. The terms independent of  $t$  give the d-c equations, whereas the coefficients of  $e^{j\omega t}$  give the a-c equations:

	<i>Direct Current</i>	<i>Alternating Current</i>	
(a) <i>Maxwell</i>			
$\nabla \times \mathbf{H}_0 = \mathbf{J}_0$	(2.9)	$\nabla \times \mathbf{H}_1 = \mathbf{J}_1 + j\omega\epsilon_0\mathbf{E}_1$	(2.10)
$\nabla \times \mathbf{E}_0 = 0$	(2.11)	$\nabla \times \mathbf{E}_1 = -j\omega\mu_0\mathbf{H}_1$	(2.12)
(b) <i>Continuity</i>			
$\nabla \cdot \mathbf{J}_0 = 0$	(2.13)	$\nabla \cdot \mathbf{J}_1 = -j\omega\rho_1$	(2.14)
(c) <i>Motion</i>			
$\mathbf{v}_0 \cdot \nabla \mathbf{v}_0$		$j\omega\mathbf{u}_1 + \mathbf{v}_0 \cdot \nabla \mathbf{u}_1 + \mathbf{u}_1 \cdot \nabla \mathbf{v}_0$	
$= \frac{e}{m} (\mathbf{E}_0 + \mathbf{v}_0 \times \mathbf{B}_0)$	(2.15)	$= \frac{e}{m} (\mathbf{E}_1 + \mathbf{v}_0 \times \mathbf{B}_1$	
		$+ \mathbf{u}_1 \times \mathbf{B}_0)$	(2.16)
(d) <i>Current Density</i>			
$\mathbf{J}_0 = \rho_0 \mathbf{v}_0$	(2.17)	$\mathbf{J}_1 = \rho_0 \mathbf{u}_1 + \rho_1 \mathbf{v}_0$	(2.18)

where  $\mathbf{v}_0$  is the d-c and  $\mathbf{u}_1$  is the a-c velocity.

Now, the d-c equations are still nonlinear. In order to solve the linear a-c equations, it is seen that the d-c equations must first be solved. There are various artifices used to circumvent the nonlinear nature of the d-c equations. These are discussed later in specific cases. For the moment, merely assume that they have been solved so that  $v_0$  and  $\rho_0$  are known functions to be used in the a-c equations.

### 2.3 Small Signal Poynting Theorem

In order to derive the small signal Poynting theorem, which is the basis for kinetic power theorems to be developed later, scalar multiply both sides of the complex conjugate of Eq. 2.10 with  $E_1$  and both sides of Eq 2.12 with  $H_1^*$ . If these are subtracted from one another, the result is \*

$$\nabla \cdot (E_1 \times H_1^*) = -J_1^* \cdot E_1 - j\omega(\mu_0|H_1|^2 - \epsilon_0|E_1|^2) \quad (2.19)$$

This is the differential form of the *small signal* Poynting theorem, since the a-c quantities that appear are only approximate solutions of Maxwell's equations.

The integral form of this theorem is found by integrating both sides over a volume of space containing the electron beam. In the integral form it is found that  $E_1 \times H_1^*$  is related to the electromagnetic power flow per unit area crossing the surface enclosing the volume. The  $J_1^* \cdot E_1$  term is related to the kinetic power flow on the beam and is the rate of doing work by the electric force on the currents. The last two terms represent the average magnetic and electric energy stored per unit volume of the electromagnetic field.

The small signal Poynting theorem is used to derive the kinetic power theorems in later chapters when the beam is coupled to a circuit. The kinetic power theorems play an essential role in determining the coupling coefficients in the coupled mode formulations of various microwave devices to be treated.

It should be noted that only one frequency has been assumed. When more frequencies are involved, as in parametric devices, the entire analysis up to this point will have to be re-examined. However, the equations are still quite general—in fact, too general for ease of handling. Thus at this point the general analysis is broken off and various special cases are treated.

\* The vector identity  $\nabla \cdot (A \times B) = B \cdot \nabla \times A - A \cdot \nabla \times B$  has been used.

## 2.4 Space-Charge Waves in a One-dimensional Electron Beam in a Drift Region

**Simplifying assumptions.** Assume first that there is an infinite homogeneous d-c magnetic focusing field in the positive  $z$ -direction. Under this assumption, the beam is said to be in confined flow, since all electrons are confined to move in the  $z$ -direction: there will be only  $z$ -components of velocity and current density. Thus  $\mathbf{v}_0$  and  $\mathbf{u}_1$  are parallel to  $\mathbf{B}_0$ , so that  $\mathbf{v}_0 \times \mathbf{B}_0 = \mathbf{u}_1 \times \mathbf{B}_0 = 0$ . Further,  $\nabla \cdot \mathbf{J}_0 \rightarrow \partial J_0 / \partial z$  and  $\nabla \cdot \mathbf{J}_1 \rightarrow \partial J_1 / \partial z$ , since  $\mathbf{J}_0 \rightarrow J_0 \mathbf{e}_3$  and  $\mathbf{J}_1 \rightarrow J_1 \mathbf{e}_3$ , where  $\mathbf{e}_3$  is a unit vector in the  $+z$ -direction. Also, the term  $\mathbf{v}_0 \times \mathbf{B}_1$  in the a-c equation of motion (2.16) has only a component transverse to  $\mathbf{v}_0$ . Since  $\mathbf{B}_0$  is infinite and parallel to  $\mathbf{v}_0$ , there can be no transverse motion, and this term can be neglected.

Under this simplifying assumption (in addition to the small signal and single velocity assumptions made earlier), the fundamental equations (2.9–2.18) reduce to

<i>Direct Current</i>	<i>Alternating Current</i>
(a) <i>Maxwell</i>	
$\nabla \times \mathbf{H}_0 = J_0 \mathbf{e}_3$	(2.20)
$\nabla \times \mathbf{E}_0 = 0$	(2.22)
(b) <i>Continuity</i>	
$\frac{\partial J_0}{\partial z} = 0$	(2.24)
(c) <i>Motion</i>	
$v_0 \frac{\partial v_0}{\partial z} = \frac{e}{m} E_{0z}$	(2.26)
(d) <i>Current Density</i>	
$J_0 = \rho_0 v_0$	(2.28)
	(2.21)
	(2.23)
	(2.25)
	(2.27)
	(2.29)

The subscript  $z$  has been dropped wherever there is no tendency toward confusion.

These equations (2.20–2.29) apply to a finite as well as an infinite beam. Next, assume that the beam is of infinite extent in the  $x$ - and  $y$ -dimensions. This assumption is equivalent to requiring that all quantities, a-c and d-c, be independent of  $x$  and  $y$  so that  $\partial/\partial x = \partial/\partial y = 0$ . This implies further that any r-f excitation applied to the beam is independent of  $x$  and  $y$ .

As a consequence of the infinite beam assumption, it will be found that *only* two modes will propagate on the beam. These are the slow and fast space-charge modes to be derived immediately. A further consequence is that these two modes can be described completely by the a-c velocity and current density of the beam. This is in sharp contrast to the finite beam case to be taken up later, in which an infinite number of space-charge modes will be found to exist and in which, in general, the beam cannot be described by only the velocity and current but will require electric and magnetic field components.

The fact that the infinite-beam space-charge modes can be described by two independent variables will allow the equations to be put in the form of the transmission-line equations of Chapter 1.

The last simplifying assumption is that the beam is in a drift region. A drift region is defined as one in which there are no time-average forces acting on the beam. This simplifies the d-c equations. From the equation of motion (2.26),  $E_{0z} = 0$ , so that  $v_{0z}$  is a constant. By the equation of continuity,  $J_0$  is also a constant, and by Eq. 2.28  $\rho_0$  must be a constant.

One artifice used to cancel out the d-c space-charge forces (resulting in  $E_{0z}$ ) is to assume that there are heavy positive ions that neutralize the electron charge. Since the ions are at least 2000 times heavier than the electrons, they do not follow the r-f motion. However, the ions can follow the time-average fields and cancel the d-c electron charge.

Under these simplifying assumptions, Eqs. 2.21, 2.23, 2.25, 2.27, and 2.29 break up into two independent sets of equations. The first set corresponds to a *TEM*-mode of propagation on the beam. From the  $x$ - and  $y$ -components of Eqs. 2.21 and 2.23 it can be seen that  $E_{1x}$ ,  $E_{1y}$ ,  $H_{1x}$ , and  $H_{1y}$  are independent of  $E_{1z}$ . Waves that satisfy these equations propagate as though the beam were not present, since it is only  $E_{1z}$  that couples to the beam. These are clearly *TEM* electromagnetic waves that propagate at light velocity. Accordingly, they are omitted from further consideration.

**Space-charge wave equations.** Next consider the  $z$ -component of Eq. 2.21. It is

$$J_1 + j\omega\epsilon_0 E_{1z} = 0 \quad (2.30)$$

since the  $z$ -component of  $\nabla \times H_1 = 0$  under the second of the foregoing assumptions. This assumption is equivalent to considering a beam of infinite lateral dimensions. Since by the well-known right-hand rule a magnetic field encircles a current,  $\nabla \times H_1 = 0$  implies that the enclosing magnetic field is out at infinity and its curl is zero. Effectively, this

means that the net current is zero, which is what Eq. 2.30 says. That is, the conduction current is just canceled by the displacement current. This result is the distinguishing characteristic between a finite and an infinite beam.

There now remain to be considered Eqs. 2.25, 2.27, 2.29, and 2.30. Utilizing Eq. 2.30, Eq. 2.27 becomes

$$\left( \frac{d}{dz} + j \frac{\omega}{v_0} \right) u_1 = j \frac{e}{mv_0\omega\epsilon_0} J_1 \quad (2.31)$$

By utilizing Eq. 2.29, Eq. 2.25 is reduced to

$$\left( \frac{d}{dz} + j \frac{\omega}{v_0} \right) J_1 = j\omega \frac{\rho_0}{v_0} u_1 \quad (2.32)$$

Now, Eqs. 2.31 and 2.32 are the fundamental equations that govern wave propagation for a one-dimensional (infinite) beam in confined flow. They show first of all that wave propagation can be completely specified by two variables, which are taken here as the current density and the beam velocity. Equation 2.31 is essentially the equation of motion. It shows how the field set up by the current modulation (a-c space-charge forces) modulates the velocity. Equation 2.32 is essentially the continuity equation and shows how the velocity modulation couples to the current modulation.

The next task is to put these equations in normal mode form.

**Normal mode form.** First, define several new quantities. Let

$$V_1 = \frac{m}{|e|} v_0 u_1 \quad (2.33)$$

be the beam kinetic voltage<sup>1</sup>

$$\omega_p^2 = \frac{e\rho_0}{m\epsilon_0} \quad (2.34)$$

The quantity  $\omega_p$  is called the plasma frequency. It is the frequency at which a plasma of uniform density  $\rho_0$  will oscillate under the action of the space-charge repulsion forces. Further, let

$$\beta_p = \frac{\omega_p}{v_0} \quad (2.35)$$

be the plasma propagation constant and

$$\beta_e = \frac{\omega}{v_0} \quad (2.36)$$

the "electronic" propagation constant.

The d-c electron velocity is constant and is related to the d-c potential  $V_0$  by

$$\frac{m}{2} v_0^2 = |e| V_0$$

Further, recall that  $J_0 = \rho_0 v_0$ .

Now introduce these definitions (Eqs. 2.33–2.36) into Eqs. 2.30–2.32 and make the following simple change of variables:

$$\begin{aligned} V_1(z) &= V_1'(z)e^{-j\beta_e z} \\ J_1(z) &= J_1'(z)e^{-j\beta_e z} \end{aligned} \quad (2.37)$$

Equations 2.30–2.32 then reduce to

$$E_{1z} = j \frac{\beta_p^2}{\beta_e} \frac{2V_0}{|J_0|} J_1 \quad (2.38)$$

( $E_{1z}$  is the longitudinal space-charge field for the infinite beam.)

$$\begin{aligned} \frac{dV_1'}{dz} &= -j \frac{\beta_p^2}{\beta_e} \frac{2V_0}{|J_0|} J_1' \quad (a) \\ \frac{dJ_1'}{dz} &= -j\beta_e \frac{|J_0|}{2V_0} V_1' \quad (b) \end{aligned} \quad (2.39)$$

Put these equations in normal mode form. Let the mode amplitudes be

$$a_{\pm}'(z) = \frac{1}{4\sqrt{Z_0}} [V_1'(z) \pm Z_0(-J_1'(z))] \quad (2.40)$$

where

$$Z_0 = \frac{2V_0}{|J_0|} \frac{\omega_p}{\omega} \quad (2.41)$$

and the *normal mode form* of Eqs. 2.39 is

$$\begin{aligned} \frac{da_+'}{dz} &= j\beta_p a_+' \\ \frac{da_-'}{dz} &= -j\beta_p a_-' \end{aligned} \quad (2.42)$$

The conjugate equations are not written for simplicity. Recall that  $V_1'(z)$  and  $-J_1'(z)$  are complex quantities.

A word should be said about sign convention. Positive velocity and current are taken to be in the positive  $z$ -direction. Thus a convection

current of negative electrons moving with velocity in the positive  $z$ -direction is negative and  $-J_1'$  is explicitly positive. This accounts for taking  $(-J_1')$  in the foregoing mode amplitude definitions.

Equations 2.42 are formally the same as the transmission-line equations in normal mode form (Eqs. 1.49). By identifying line voltage,  $V(z)$ , with beam kinetic voltage,  $V_1'(z)$ , and line current,  $I(z)$ , with beam current density,  $-J_1'(z)$ , it is seen that the space-charge waves are equivalent to a lossless transmission line of series inductance per unit length  $L = \beta_p^2 2V_0 / \beta_e \omega |J_0|$  and shunt capacitance per unit length  $C = \beta_e |J_0| / 2V_0 \omega$ .

The beam-transmission-line analog is not perfect. The discrepancy lies in the phase shift introduced in Eqs. 2.37. To obtain the normal modes with the proper phase, define

$$a_{\pm} = a_{\pm}' e^{-j\beta_e z} = \frac{1}{4\sqrt{Z_0}} [V_1 \pm Z_0(-J_1)] \quad (2.43)$$

Put this back into Eqs. 2.42. This yields the *normal mode form* of the space-charge wave equations:

$$\begin{aligned} \left( \frac{d}{dz} + j(\beta_e - \beta_p) \right) a_+ &= 0 & (a) \\ \left( \frac{d}{dz} + j(\beta_e + \beta_p) \right) a_- &= 0 & (b) \end{aligned} \quad (2.44)$$

**Electromechanical nature of the waves.** The phase velocities of the normal modes in Eqs. 2.44 are given by

$$v_{p\pm} = \frac{\omega}{\beta_e \mp \beta_p} = \frac{v_0}{1 \mp (\omega_p/\omega)} \quad (2.45)$$

Since  $\omega_p/\omega \ll 1$  for microwave frequencies and charge densities usually used in microwave tubes, it is easy to see from Eq. 2.45 that the  $a_+$ -mode travels with a phase velocity slightly greater than the d-c velocity, whereas the  $a_-$ -mode travels with a phase velocity slightly less than the d-c velocity. Accordingly, the  $a_+$ -mode is called the fast space-charge mode, and  $a_-$  is called the slow space-charge mode. These phase velocities are sketched in Figure 2.1. The group velocity is given by

$$v_g \pm = \left( \frac{\partial \beta}{\partial \omega} \right)^{-1} = v_0 \quad (2.46)$$

since  $\beta = \beta_e \pm \beta_p$  and  $\beta_p$  is independent of frequency.

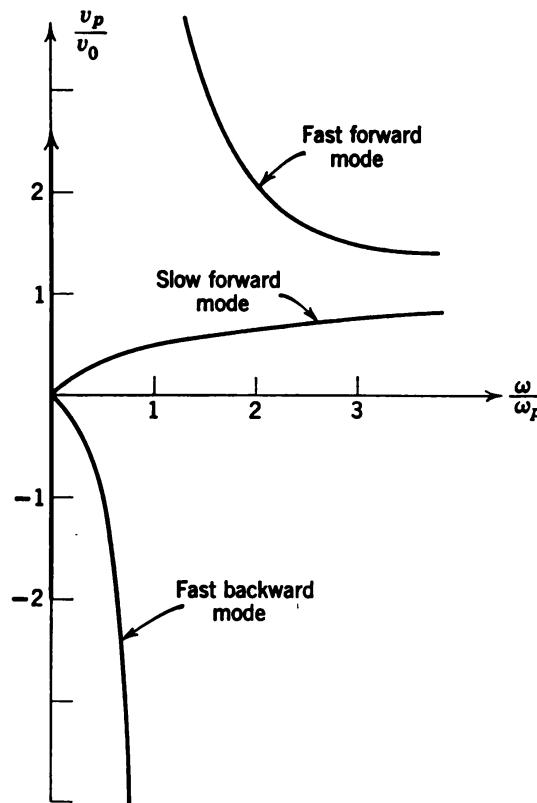


**Figure 2.1** Phase velocities of the fast and slow space-charge waves for a one dimensional beam in confined flow as a function of  $\omega/\omega_p$ .

It is a characteristic of waves that energy is propagated at the group velocity, which in this case is the d-c beam velocity. Energy is therefore mechanically transported by the electrons, which accounts for the waves being described as electromechanical.

For the space-charge waves in an infinite beam the magnetic field  $\mathbf{H}_1(\mathbf{r}, t) = 0$ , and there can be no electromagnetic power flow. This lends further credence to the power transport taking place by mechanical means.

**Kinetic power flow in space-charge waves.** By analogy with the transmission line, the kinetic power flow on the electron beam in the positive  $z$ -direction (see Eq. 1.55) is given by

$$P_k = \frac{1}{2} \operatorname{Re} [V_1(-J_1^*)] = 2(|a_+|^2 - |a_-|^2) = \text{constant} \quad (2.47)$$

whereas the d-c beam kinetic power is given by  $V_0|J_0|$ . This is the Chu kinetic power theorem<sup>1</sup> for an infinite beam in a drift region.

A considerable amount of effort must now be expended to bring out the significance of the negative sign in front of  $|a_-|^2$  in the kinetic power theorem (Eq. 2.47).

To begin, from the discussion of the power flow of the single transmission line of Chapter 1 it might be tempting to interpret the minus sign as signifying that the power flow in the fast and slow modes was in opposite directions; that the fast mode was a forward mode, whereas the slow mode was a backward mode. But this interpretation is not correct, since the group and phase velocities of both modes have been shown to be in the same direction.

Chu<sup>1</sup> has given the correct physical interpretation, viz., the power carried by the fast mode is positive kinetic power, and the power carried by the slow mode is negative kinetic power. This means that on the average the electron beam carries electrons with a larger kinetic energy when a fast mode is excited than it carries in the d-c state. Similarly, the beam carries, on the average, electrons with less kinetic energy when a slow mode is excited than it carries in the d-c state.

This may be stated another way. Consider a beam that is propagating a fast space-charge wave only. This means that  $a_-$  is zero, and from Eq. 2.43 it follows that the kinetic voltage and current are always in phase, since  $(-J_1) > 0$ . When the kinetic voltage (and therefore the velocity) is a maximum at some beam cross section, the current will also be a maximum. Thus when the velocity is a maximum there is an excess of electrons ( $J_1 < 0$ ) traveling at velocity  $v_0 + |u_1|$ . Therefore, it is concluded that the electron beam transports more kinetic energy in the presence of the fast wave than when there is only direct current.

A similar argument for the slow mode shows that the velocity and current are always  $180^\circ$  out of phase. Accordingly, when the velocity is a maximum,  $v_0 + |u_1|$ , there is a deficiency of electrons at this cross section. Therefore, the beam transports less kinetic energy when excited by a slow wave than under d-c conditions.

These arguments may be better visualized by reference to Figure 2.2.

Consider Figure 2.2a. If an observer travels with velocity  $v_0$ , then at time  $t$  the current wave  $(-J_1)$  on the beam will look like the solid curve. When  $(-J_1)$  is a peak (in the region marked +), there will be an excess of electrons, and when  $(-J_1)$  is in a trough (in the region marked -) there will be a deficiency of electrons. In the fast mode the velocity is in phase with the current. The arrows in line with  $u_1$  show that the a-c velocity is at its maximum value to the right in the excess current (+) region, whereas  $u_1$  is at its maximum value to the left in the charge deficient (-) region. Now, the space-charge forces will be zero at the centers of the (+) and (-) regions. The arrows on the line marked  $f$

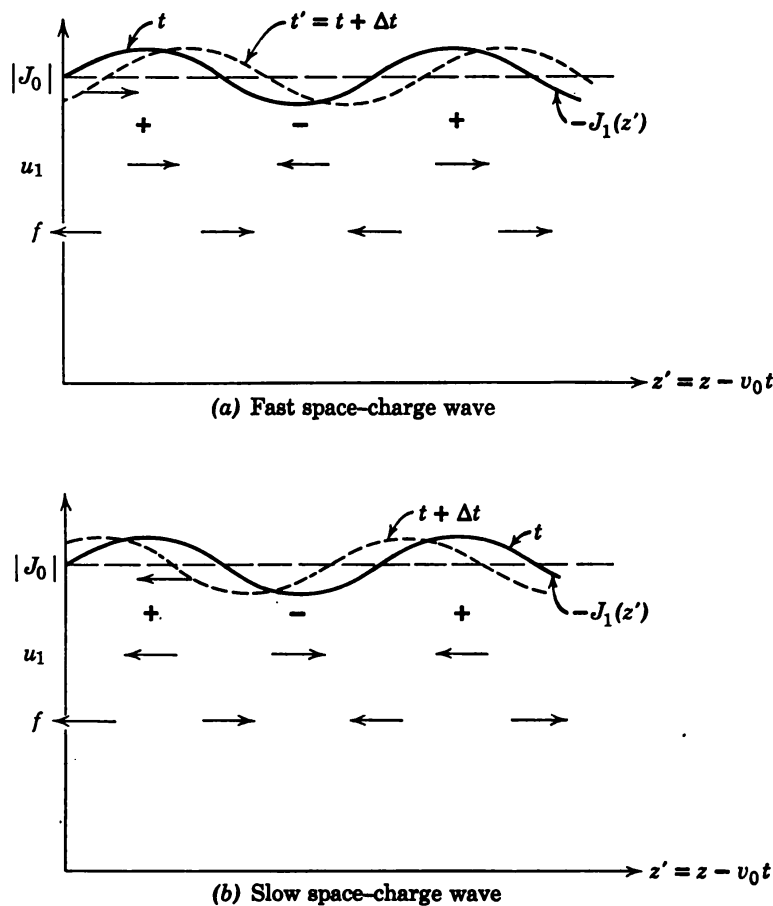


**Figure 2.2** Space-charge wave bunching in a moving frame of reference. The (+) regions are excess electron regions, whereas the (-) regions are electron deficient regions. The arrows in line with  $u_1$  show the direction of the a-c velocity maxima, and the arrows in line with  $f$  show the direction of the maximum space-charge forces.  $-J_1(z')$  gives the a-c current.

show the directions of the space-charge forces at the position of their maxima. The forces are away from the center of the (+) region where there is excess negative charge and toward the center of the (-) region where there is a deficiency. The particles in the (+) region are moving to the right at time  $t$  and the particles in the (-) region are moving to the left at time  $t$ . Thus they tend to form a bunch, or charge excess region, to the right of the bunch at  $t$ . In the region in which the new bunch tends to form the force is also to the right, so that the new bunch receives an excess velocity. The dotted curve, then, shows the  $(-J_1)$ -wave at a time  $t + \Delta t$ .

Relative to the moving observer, the phase velocity of this wave is

$v_+ - v_0 = v_0\omega_p/\omega$ . An individual electron, relative to a fixed observer, is moving to the right with the average velocity  $v_0$ . However, the individual electron in the moving frame executes simple harmonic motion along the  $z$ -axis at the plasma frequency  $\omega_p$ . Thus the fast space-charge wave “rides over” the electrons just as surface waves “ride over” water molecules. The positive power flow of the wave is to the right in relation to the moving observer, since the electron bunch moves to the right.

Figure 2.2b shows the analogous treatment for the slow mode. The (+) region shows excess charge so that the space-charge forces are again away from the center of the (+) regions as indicated by the force arrows on the  $f$ -axis. However, the velocity  $u_1$  is  $180^\circ$  out of phase with the current, and the arrows on the  $u_1$ -axis show the direction of the velocity maxima in the  $\pm z$ -directions. In this case, electrons in the (+) region are moving to the left at time  $t$ , and electrons in the (-) region are moving to the right in the (-) region, relative to the moving observer. The new bunch tends to form to the left of its position at time  $t$  in a region in which the force is to the left. Thus the wave moves to the left and the power flow is to the left, *relative to the moving observer*. Relative to a fixed observer, of course, the power flow is to the right. The dotted curve shows the slow space-charge wave at time  $t + \Delta t$ .

**Mode excitation.** In order to excite a fast space-charge wave, the kinetic voltage and current must be in phase at the input plane; in order to excite a slow mode they must be  $180^\circ$  out of phase. This follows from Eq. 2.43. In order to excite a fast wave, kinetic power must be given to the beam; to excite a slow mode, kinetic power must be extracted from the beam, since the slow mode carries negative power. Conversely, to remove a fast mode from the beam, power must be extracted from the beam, and to remove a slow mode power must be added to the beam.

Further, from Eq. 2.47 it is seen that no net power is required from the driving source if both modes are equally excited.

A more thorough discussion of these important concepts is given in Chapter 3 when the beam is coupled to a circuit that provides a means of interacting with the beam and thereby exciting these modes.

## 2.5 Space-Charge Waves in a Finite Cylindrical Beam in a Drift Region

It has been shown that the infinite beam in confined flow can propagate only two space-charge normal modes. Furthermore, these modes can be described completely by only two variables, viz., the current and velocity. The space-charge field has only a  $z$ -component and is related to

the current by Eq. 2.38. This relation states physically that the sum of the beam convection current and displacement current is zero. Alternatively, it shows that all the field lines are contained in the beam. Figure 2.3a shows these space-charge field lines schematically. They begin in an electron-deficient region and terminate in an electron-excess region. These regions are the result of the bunching feature previously discussed. Some electrons are speeded up and some are slowed down when a signal is impressed on the beam. The fast electrons overtake the slow ones, and this process continues until the space-charge forces are sufficient to repel the electrons. This causes a plasma oscillation at frequency  $\omega_p$  as the beam progresses.

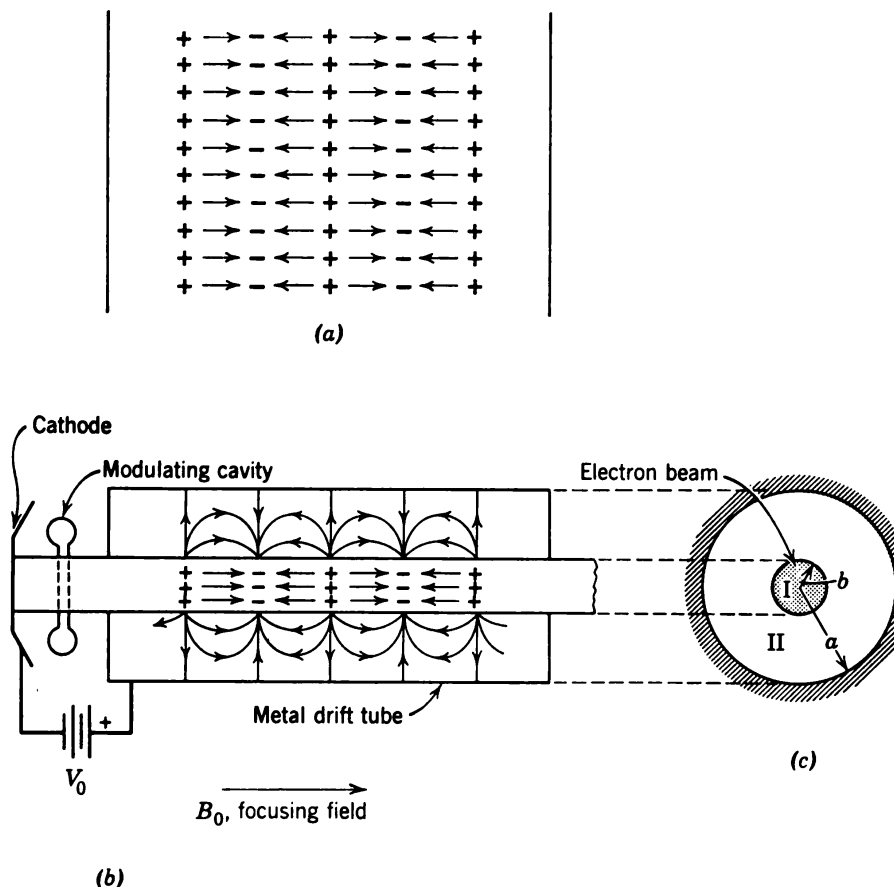


**Figure 2.3** (a) Space-charge lines of force in an infinite beam in confined flow. These forces are uniform across the beam and are entirely contained in the beam. (b) Space-charge lines of force in a thin finite beam in a drift tube. Some lines now go outside the beam so that for a given space-charge density the field in the beam is reduced. For a thin beam the lines are approximately uniform across the beam. (c) Cross-sectional view of beam and drift tube.

The situation is more complex<sup>2,3</sup> when the beam is of radius  $b$  in a metal drift tube of radius  $a$ . In this case some of the lines of force due to the space charge go outside the beam, as shown crudely in Figure 2.3b. For the same charge density the field inside the beam will therefore be reduced, since some lines terminate on the metal wall and some leave and re-enter the beam. As the wall is moved farther away, fewer lines go to the wall and more terminate on the beam. Inside the beam the space-charge field will no longer be perfectly uniform across the beam. Qualitatively, the same type of bunching will occur as in the infinite beam, but since the space-charge fields inside the beam are reduced the plasma oscillation frequency will be reduced. As the signal frequency is changed, the plasma frequency also changes.

This picture is somewhat oversimplified, since an infinite number of space-charge normal modes can propagate on a finite size beam, as shown in Appendix B. Only the lowest order modes are considered here. It is shown in the appendix that the relation between the  $z$ -component of the electric field and the current for the infinite beam (Eq. 2.38) can be taken over if the plasma frequency for the infinite beam  $\omega_p$  is replaced by a reduced plasma frequency  $\omega_q$ , where

$$\omega_q = \mathcal{R}\omega_p \quad (2.48)$$

and  $\mathcal{R}$  is called the plasma reduction factor. Branch and Mihran<sup>4</sup> have computed the reduction factors for beams of various shapes. Figure 2.4 shows the reduction factor for the lowest order space-charge mode, labeled "01," for a cylindrical beam of radius  $b$  in a metal tube of radius  $a$

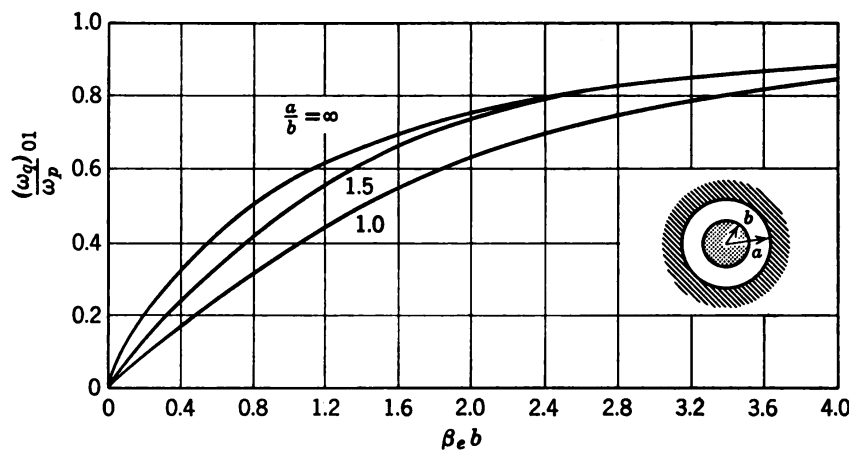


**Figure 2.4** Space-charge reduction factor  $\mathcal{R}$  for dominant space-charge mode of a cylindrical beam of radius  $b$  in a metal drift tube of radius  $a$  for  $a/b = 1.0, 1.5$ , and  $\infty$ . The beam is in confined flow and  $\mathcal{R} = (\omega_q/\omega_p)_{01}$  is plotted versus  $\beta_e b$ . (After Branch and Mihran, Reference 4.) The subscript "01" refers to the lowest order mode.

in confined flow as a function of  $\beta_e b$  for  $a/b = 1.0, 1.5$ , and  $\infty$ . This reduction factor takes into account the variation of the field and beam quantities with radius and allows the simplifications pointed out below. (Other references<sup>5-21</sup> are of interest for this problem. This listing, needless to say, is incomplete for the sake of brevity, since work in this field has been very active.)

By using the reduction factor, the equations for the infinite beam can be taken over completely for a finite beam by replacing  $\omega_p$  by  $\omega_q$  and  $\beta_p$  by  $\beta_q$ . Further, replace  $J_1$  and  $|J_0|$  by the a-c and d-c beam currents,  $i_1$  and  $|I_0|$ , wherever they occur. For example, the beam characteristic impedance (Eq. 2.41) becomes

$$Z_0 = \frac{2V_0}{|I_0|} \frac{\omega_q}{\omega} \quad (2.49)$$

and the mode amplitudes become

$$a_{\pm} = \frac{1}{4\sqrt{Z_0}} [V_1 \pm Z_0(-i_1)] \quad (2.50)$$

Similarly, the space-charge field is related to the current (compare Eq. 2.38) by

$$E_{1z} = j \frac{(\Omega\beta_p)^2}{\beta_e} \frac{2V_0}{|I_0|} i_1 \quad (a) \quad (2.51)$$

and the equations of motion and continuity, Eqs. 2.31 and 2.32 become

$$\left( \frac{d}{dz} + j\beta_e \right) V_1 = -j \frac{(\Omega\beta_p)^2}{\beta_e} \frac{2V_0}{|I_0|} i_1 \quad (b) \quad (2.51)$$

$$\left( \frac{d}{dz} + j\beta_e \right) i_1 = -j \frac{\beta_e |I_0|}{2V_0} V_1 \quad (c)$$

There is one point of minor difference between the finite and thick beam cases. The phase velocities of the two normal modes (cf. Eq. 2.45) are

$$v_{p\pm} = \frac{\omega}{\beta_e \mp \beta_q} = \frac{v_0}{1 \mp (\omega_q/\omega)} \quad (2.52)$$

whereas the group velocities are

$$v_{g\pm} = \left( \frac{\partial \beta}{\partial \omega} \right)^{-1} = v_0 \left( 1 \mp \frac{\partial \omega_q}{\partial \omega} \right)^{-1}$$

since  $\omega_q$  is now a function of frequency, as Figure 2.4 shows. This follows from the fact that there is a small amount of magnetic field left in the

beam, as shown in Appendix B, which accounts for the sum of the conduction and displacements no longer adding up to zero (Eqs. 2.51). Thus there is a small amount of electromagnetic power carried by the finite beam.<sup>22-24</sup>

All the remarks on the meaning of positive and negative kinetic power flow can be taken over directly to the thin beam.

It may be of interest to express the real current and kinetic voltage for an arbitrary excitation in terms of the mode amplitudes at the input plane  $z = 0$ . By Eqs. 2.50,

$$-i_1(z, t) = 2 \operatorname{Re} \left\{ \frac{1}{\sqrt{Z_0}} [a_+(z) - a_-(z)] e^{j\omega t} \right\} \quad (a)$$

(2.53)

$$V_1(z, t) = 2 \operatorname{Re} \{ \sqrt{Z_0} [a_+(z) + a_-(z)] e^{j\omega t} \} \quad (b)$$

in which  $a_{\pm}$  are the solutions of Eqs. 2.44 where  $\beta_p \rightarrow \beta_q$  and are

$$a_{\pm}(z) = a_{\pm}(0) \exp \left[ -j\beta_e \left( 1 \mp \frac{\omega_q}{\omega} \right) z \right] \quad (2.54)$$

where Eqs. 2.44 and 2.50 have been used. The method by which these modes can be excited is considered in Chapter 3, when coupling of the beam to a circuit is studied.

## 2.6 The Fast and Slow Cyclotron Normal Modes<sup>25-31</sup>

Space-charge normal modes were found to propagate on an electron beam in confined flow. There is another very useful class of normal modes that propagates on a beam moving in the  $z$ -direction with constant velocity  $v_0$  when there is a finite axial magnetic focusing field. In this case the a-c motion of the beam is no longer confined to the axial direction: there can be transverse a-c motion. In the case of transverse motion of the electrons in a finite field it is well known that the electrons will execute a circular motion at the cyclotron frequency. For this reason the normal modes are called cyclotron modes.

**Simplifying assumptions.** In order to find these modes in the simplest case, assume first that the axial d-c velocity  $v_0$  is a constant. This allows the terms  $\mathbf{u}_1 \cdot \nabla v_0$  to be omitted from the equations of motion (Eq. 2.16).

Next, assume that the beam is in a drift region so that there is no circuit to provide an r-f electric field ( $\mathbf{E}_1$ ) or a magnetic field ( $\mathbf{B}_1$ ). Also assume that the space-charge density is so small that the space-charge forces can be neglected compared with the magnetic restoring forces. This condition can be met if  $\omega_p^2 \ll \omega_c^2$ , where  $\omega_c$  is the cyclotron fre-

quency and allows the field  $\mathbf{E}_1$ , due to the space charge, to be neglected. Therefore, the terms  $\mathbf{E}_1$  and  $\mathbf{v}_0 \times \mathbf{B}_1$  in Eq. 2.16 may be taken to be zero. Also, if there is no coupling to the a-c electric or magnetic field, Maxwell's Eqs. 2.10 and 2.12, as well as Eqs. 2.14 and 2.18, may be entirely neglected.

When space charge is omitted, the electrons do not interact with one another, and the thickness of the beam is unimportant. Therefore, the velocity can be assumed uniform across the beam in analogy with the thin beam propagating the lowest order space-charge mode. All quantities are independent of  $x$  and  $y$ .

**Cyclotron wave equations (normal mode form).** It is worthwhile to clarify some notation before proceeding with the study of the cyclotron normal modes. The transverse a-c velocity components are given by

$$\mathbf{v}_1(z, t) = \operatorname{Re}(\mathbf{u}_1(z)e^{j\omega t}) \quad (2.55a)$$

and the transverse a-c displacements are given by

$$\mathbf{r}_1(z, t) = \operatorname{Re}(\xi_1(z)e^{j\omega t}) \quad (2.55b)$$

The introduction of  $\xi_{1x}$  and  $\xi_{1y}$  is necessary to keep in mind that  $\xi_1$  is a complex quantity, whereas  $\mathbf{r}_1 = (x_1, y_1)$  is real. Similarly,  $\mathbf{v}_1$  is real and  $\mathbf{u}_1$  is complex.

The  $x$ - and  $y$ -components of the equations of motion (Eq. 2.16), under the foregoing simplifying assumptions, are

$$\begin{aligned} \left( \frac{d}{dz} + j\beta_e \right) u_{1x} &= -\beta_c u_{1y} & (a) \\ \left( \frac{d}{dz} + j\beta_e \right) u_{1y} &= \beta_c u_{1x} & (b) \end{aligned} \quad (2.56)$$

where

$$\begin{aligned} \beta_e &= \frac{\omega}{v_0} \\ \beta_c &= \frac{\omega_c}{v_0} \equiv \frac{|e|B_0}{mv_0} \end{aligned} \quad (2.57)$$

These are the equations that describe the types of waves that can propagate on the beam in the form of a transverse velocity disturbance when the beam is subject to a finite magnetic focusing field. They are in a form analogous to the space-charge wave equations (2.31 and 2.32). They can be put in a form analogous to the transmission-line equations by a transformation of the type given in Eqs. 2.37. The normal mode form follows from a treatment analogous to that of Eq. 1.3 of Chapter 1.

Accordingly, define the normal mode amplitudes by

$$a_{1\pm} = k(u_{1x} \pm ju_{1y}) \quad (2.58)$$

where

$$k = \frac{1}{4} \sqrt{\frac{\omega}{\omega_c} \frac{|I_0|}{|e|} m}$$

and where  $|I_0|$  is the d-c beam current. (At this point the choice of the normalization constants can only be considered mysterious. Needless to say, they are chosen so that  $2|a_{1\pm}|^2$  gives the power carried by these modes, as shown in a later chapter.) The normal mode form of Eqs. 2.56 then becomes

$$\left( \frac{d}{dz} + j(\beta_e \mp \beta_c) \right) a_{1\pm} = 0 \quad (2.59)$$

and the solutions of these normal mode equations are

$$a_{1\pm}(z) = |c_{\pm}| \exp[-j(\beta_e \mp \beta_c)z + j\vartheta_{\pm}] \quad (2.60)$$

where  $|c_{\pm}| \exp(j\vartheta_{\pm})$  are arbitrary constants of integration.

Before discussing the nature of these modes, it should be noted that

$$\mathbf{v}_1(z, t) = \frac{d\mathbf{r}_1}{dt}(z, t) = \left( \frac{\partial}{\partial t} + v_0 \frac{\partial}{\partial z} \right) \mathbf{r}_1(z, t)$$

so that by using the notation of Eq. 2.55b it follows that

$$\left( \frac{d}{dz} + j\beta_e \right) \xi_{1x} = \frac{u_{1x}}{v_0}$$

$$\left( \frac{d}{dz} + j\beta_e \right) \xi_{1y} = \frac{u_{1y}}{v_0}$$

By multiplying the second equation by  $\pm j$  and adding to the first it follows that

$$\begin{aligned} \left( \frac{d}{dz} + j\beta_e \right) (\xi_{1x} \pm j\xi_{1y}) &= \frac{1}{v_0} (u_{1x} \pm ju_{1y}) \\ &= \frac{|A_{\pm}|}{v_0} \exp[-j(\beta_e \mp \beta_c)z + j\vartheta_{\pm}] \end{aligned} \quad (2.61)$$

where Eqs. 2.58 and 2.60 have been used and

$$|A_{\pm}| = \frac{1}{k} |c_{\pm}| \quad (2.62)$$

Now integrate Eqs. 2.61 and take the constants of integration zero. Therefore,

$$\xi_{1x} + j\xi_{1y} = -j \frac{|A_+|}{\omega_c} \exp [-j(\beta_e - \beta_c)z + j\vartheta_+] \quad (a)$$
(2.63)

$$\xi_{1x} - j\xi_{1y} = +j \frac{|A_-|}{\omega_c} \exp [-j(\beta_e + \beta_c)z + j\vartheta_-] \quad (b)$$

For convenience these modes are studied in terms of the displacements rather than velocities.

**Nature of the modes.** In order to study the characteristics of these modes, consider each separately. Accordingly, let  $A_- = 0$ . From Eq. 2.63b it then follows that  $\xi_{1x} = j\xi_{1y}$ , and Eq. 2.63a for the plus mode reduces to

$$\xi_{1x}^+ = j\xi_{1y}^+ = -j \frac{|A_+|}{2\omega_c} \exp \{ -j[(\beta_e - \beta_c)z - \vartheta_+] \} \quad (2.64a)$$

or, by using Eq. 2.55b, it follows that

$$x_1^+ = \frac{|A_+|}{2\omega_c} \sin [\omega t - (\beta_e - \beta_c)z + \vartheta_+] \quad (2.64b)$$

$$y_1^+ = -\frac{|A_+|}{2\omega_c} \cos [\omega t - (\beta_e - \beta_c)z + \vartheta_+]$$

The phase velocity of this mode is given by

$$v_{p+} = \frac{v_0}{1 - (\omega_c/\omega)} \quad (2.65)$$

If  $\omega > \omega_c$ , then  $v_{p+} > v_0$ , so that this is a fast forward cyclotron normal mode. If  $0 < \omega < \omega_c$ ,  $v_{p+}$  is negative and the mode travels backward. This phase velocity is plotted in Figure 2.5 for  $\omega/\omega_c > 0$ . It is seen that the phase velocity for this mode is zero when the signal frequency is zero and approaches minus infinity as  $\omega \rightarrow \omega_c$  from the left. As  $\omega \rightarrow \omega_c$  from the right, the phase velocity approaches plus infinity. When  $\omega \gg \omega_c$ , the phase velocity approaches the d-c beam velocity.

This mode can be considered from two viewpoints that prove helpful in visualizing the beam behavior. First, assume that an observer is fixed at a definite  $z$  and is watching different electrons as they pass this  $z$ -plane.

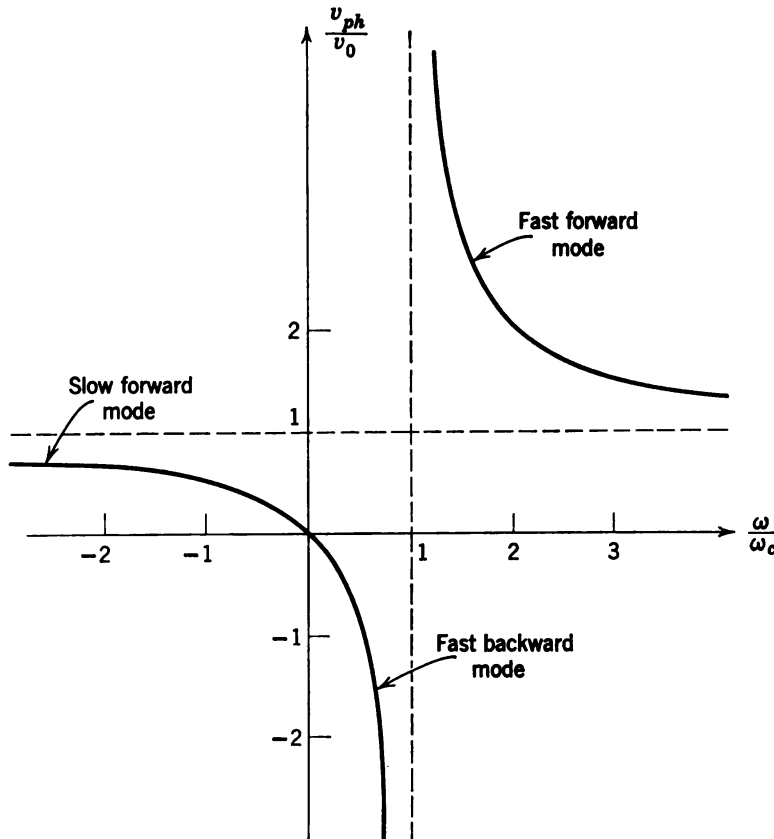


**Figure 2.5** The cyclotron mode dispersion curve.

For convenience, let  $\vartheta_+ = 0$  and  $z = 0$ . Equation 2.64b reduces to

$$x_1^+ = \frac{|A_+|}{2\omega_c} \sin \omega t$$

$$-y_1^+ = \frac{|A_+|}{2\omega_c} \cos \omega t$$

Figure 2.6a shows the position of an electron at  $t = 0$ , the position of a different electron at  $t = \pi/2\omega$ , etc. The fixed observer sees different electrons as time progresses, but it appears to be a single electron that is rotating counterclockwise, as viewed along the negative  $z$ -axis, at the signal frequency  $\omega$ . It is recalled <sup>32</sup> that this is the conventional sense of a left-handed circularly polarized wave. Accordingly, the fast cyclotron wave will be said to have left-handed polarization. Note that the observed frequency  $\omega$  is independent of the magnetic field ( $\omega_c$ ) or the d-c beam velocity. The sense of rotation of the wave at frequency  $\omega$  is always left-handed when  $\omega > 0$ .

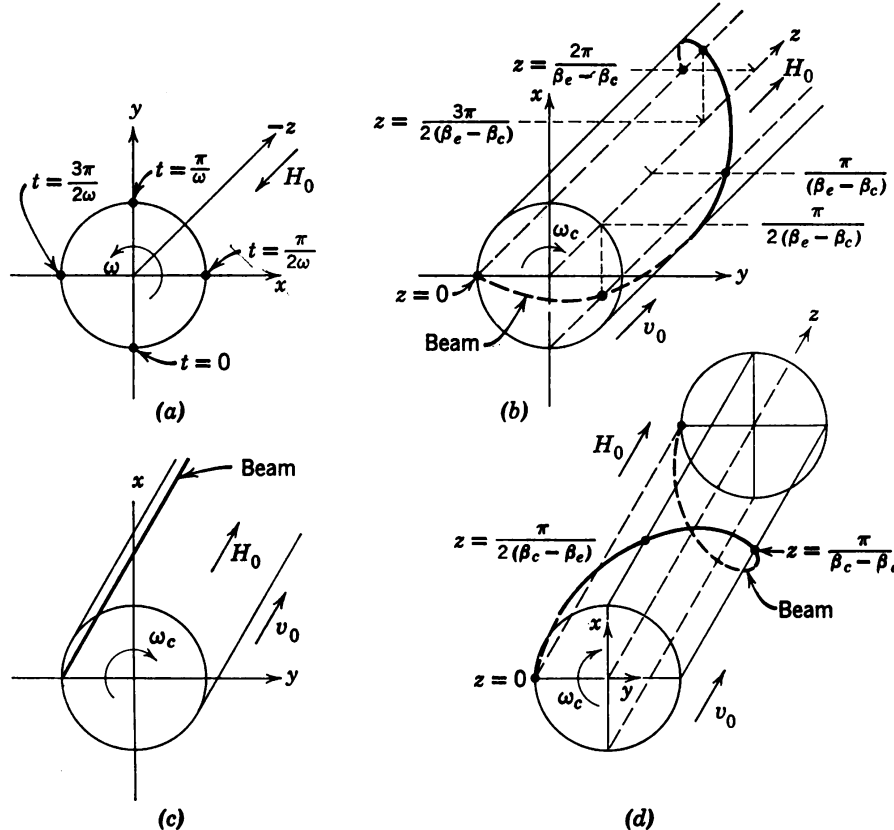


**Figure 2.6** The fast cyclotron mode  $a_{1+}$ . (a) View of different electrons at  $z = 0$  as time progresses. The wave is seen to be left-hand polarized. (b) Snapshot of the beam at  $t = 0$  when  $\beta_e > \beta_c$ . The beam lies on a helix that is wound counterclockwise, as viewed along positive  $z$ . (c) Snapshot of the beam at  $t = 0$  when  $\beta_e = \beta_c$ . All electrons lie on a straight line. (d) Snapshot of the beam at  $t = 0$  when  $0 < \beta_e < \beta_c$ . The beam lies on a clockwise-wound spiral, as viewed along positive  $z$ .

Next, consider a snapshot of the beam at a fixed time. Again for simplicity, assume  $t = 0$  and  $\vartheta_+ = 0$ . Then, by Eq. 2.64b,

$$\begin{aligned} x_1^+ &= -\frac{|A_+|}{2\omega_c} \sin (\beta_e - \beta_c) z \\ y_1^+ &= -\frac{|A_+|}{2\omega_c} \cos (\beta_e - \beta_c) z \end{aligned} \quad (2.66)$$

Consider now the position of the various electrons as given in Eqs. 2.66 for a sequence of values of  $\omega/\omega_c = \beta_e/\beta_c$ . Begin with the case in which  $\omega \gg \omega_c$ . Figure 2.6b shows that the electrons are located on a cylinder in the form of a very tightly wound spiral. As viewed along positive  $z$ , the spiral is wound counterclockwise. By convention, the

pitch of this  $+z$  counterclockwise wound spiral will be taken negative and is given by

$$p = -\frac{2\pi v_0}{\omega - \omega_c} \quad (2.67)$$

and, since  $\omega \gg \omega_c$ , the pitch is very small. From Figure 2.5 observe that under these conditions the wave phase velocity is approximately  $v_0$ .

Now let  $\omega$  decrease, keeping  $\omega_c$  fixed. The pitch of the  $+z$ -spiral is still negative but it increases, i.e., the spiral opens out. Finally, as  $\omega \rightarrow \omega_c$  from the foregoing, the pitch becomes (negatively) infinite. The spiral is now a straight line and all electrons are on it when the signal frequency equals the cyclotron frequency. This is shown in Figure 2.6c. From Figure 2.5 observe that under these conditions the wave phase velocity is infinite and positive.

As  $\omega$  continues to decrease below  $\omega_c$ , by Eq. 2.67 the pitch is very large but now positive, whereas from Figure 2.5 the phase velocity is now very large but negative. Thus, as the frequency continuously decreases from a value slightly greater than  $\omega_c$  to a value slightly below, the pitch changes from negative infinity to plus infinity and the phase velocity goes from plus infinity to minus infinity. As far as the beam itself is concerned, very little happens. Figure 2.6d shows an analogous snapshot when  $\omega < \omega_c$  when the spiral has positive pitch.

It is clear that each electron is rotating about the *positive z*-axis in a clockwise sense (left-hand polarization) and translating along the positive *z*-axis with velocity  $v_0$ . Imagine now that the electrons are glued to a cylinder in the form of a helix whose pitch is given by Eq. 2.67, which is rotating at frequency  $\omega_c$  from *x* to *y* and translating along  $+z$  with velocity  $v_0$ . A fixed observer will see an electron "wave" of frequency

$$\omega = \omega_c - \frac{2\pi v_0}{p} \quad (2.68)$$

pass by. Equations 2.67 and 2.68 are identical. Furthermore, the different snapshots given in Figures 2.6b, c, and d are obtained merely by changing the pitch of the electrons that are glued to the cylinder.

The difference between the fast forward and fast backward cyclotron modes, as labeled in Figure 2.5, is merely a difference in the sense in which the electrons are glued to the cylinder, and there is no mystery about what happens to the fast cyclotron mode as  $\omega$  "goes through"  $\omega_c$ .

Next consider the slow mode in the same way. In this case  $|A_+| = 0$ , and by an argument similar to that used to obtain Eq. 2.64b it follows that

$$x_1^- = -\frac{|A_-|}{2\omega_c} \sin [\omega t - (\beta_e + \beta_c)z + \vartheta_-]$$

$$y_1^- = - \frac{|A_-|}{2\omega_c} \cos [\omega t - (\beta_e + \beta_z)z + \vartheta_-]$$

The phase velocity of this mode is

$$v_{p-} = \frac{v_0}{1 + (\omega_c/\omega)} \quad (2.69)$$

so that it is a forward mode that travels with a velocity less than  $v_0$ . Accordingly, this is called the slow cyclotron mode. Compare now  $v_{p+}$  with  $v_{p-}$  (Eqs. 2.65 and 2.69). If  $\omega$  is allowed to be negative (mathematically), Eq. 2.65 reduces to Eq. 2.69. For this reason the phase velocity of the slow mode is plotted with  $\omega$  negative in Figure 2.5. This is a mathematical device that allows all the equations for the fast modes to describe the slow modes merely by letting  $\omega \rightarrow -\omega$ . However, the same treatment will be given for the slow waves as for the fast waves to bring out the physical distinction explicitly.

A fixed observer at  $z = 0$  and  $\vartheta_- = 0$  sees different electrons that appear to be a single electron rotating clockwise when viewed along the negative  $z$ -axis. This is the conventional sense of a right-handed circularly polarized wave.<sup>32</sup> Accordingly, the slow cyclotron mode will be said to have right-handed polarization. This is shown in Figure 2.7a.

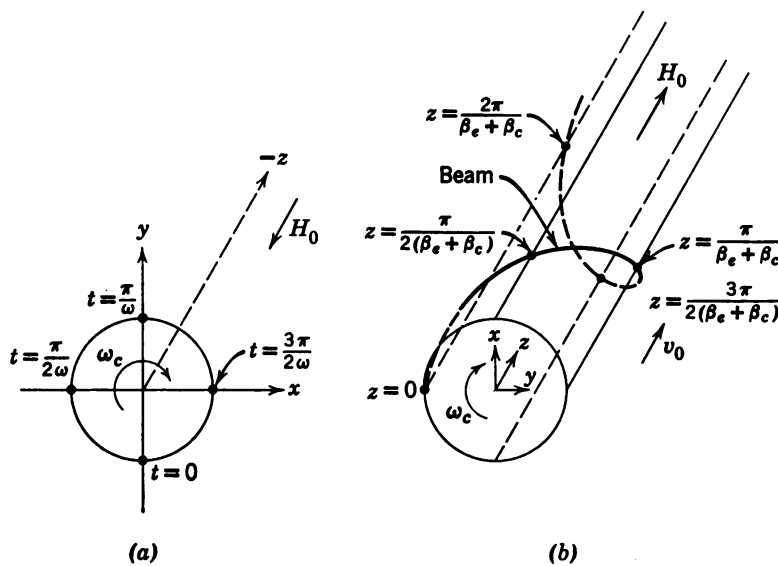


**Figure 2.7** The slow cyclotron mode  $a_{1-}$ . (a) View of different electrons at  $z = 0$  as time progresses. The wave is right-hand polarized, as viewed along negative  $z$ . (b) Snapshot of the beam at  $t = 0$ . Beam lies on right-hand wound spiral, as viewed along positive  $z$ .

Figure 2.7b shows a snapshot of the electrons at  $t = 0$  when  $\vartheta_- = 0$ . The spiral in this case is clockwise when viewed along positive  $z$  with pitch

$$p = \frac{2\pi v_0}{\omega + \omega_c} \quad (2.70)$$

which follows from Eq. 2.67 when  $\omega \rightarrow -\omega$ . As  $\omega \rightarrow \infty$ , the pitch, according to Eq. 2.70, approaches zero and the phase velocity approaches  $v_0$ . The spiral is always wound in the  $+z$  clockwise sense for the slow mode.

To summarize, the fast and slow cyclotron modes can be visualized by imagining a string of electrons glued to a cylinder in the form of a spiral with pitch

$$p = \frac{2\pi v_0}{\omega_c - \omega} \quad (2.67)$$

where  $\omega > 0$  for the fast mode and  $\omega < 0$  for the slow mode.  $p > 0$  implies the helix is wound from  $+x$  to  $+y$ , whereas for  $p < 0$  it is wound from  $+y$  to  $+x$ . This cylinder then rotates from  $+x$  to  $+y$  at frequency  $\omega_c$  and translates along the  $+z$ -direction with velocity  $v_0$ . For the fast wave a fixed observer facing in the  $+z$ -direction sees the beam rotate with the apparent frequency  $+\omega$ , whereas for the slow wave the apparent frequency is  $-\omega$ . Each electron, however, rotates with frequency  $+\omega_c$  and translates with velocity  $v_0$ .

An individual electron may be followed by letting  $z = v_0 t$  in Eqs. 2.63. Then, using Eq. 2.55b,

$$\begin{aligned} 2\omega_c x_1 &= |A_+| \sin(\omega_c t + \vartheta_+) + |A_-| \sin(\omega_c t - \vartheta_-) \\ 2\omega_c y_1 &= -|A_+| \cos(\omega_c t + \vartheta_+) - |A_-| \cos(\omega_c t - \vartheta_-) \end{aligned} \quad (2.71)$$

As expected, each electron rotates with frequency  $\omega_c$ . Finally, it can be shown for the cyclotron waves that

$$\overline{x_1^2} + \overline{y_1^2} = \frac{|u_{1x}|^2 + |u_{1y}|^2}{2\omega_c^2} \quad (2.72)$$

and

$$v_{1x}(z, t) = -\omega_c y_1(z, t)$$

$$v_{1y}(z, t) = +\omega_c x_1(z, t)$$

**Remarks.** *a.* It is of interest to note the analogy between the phase velocity of the fast and slow cyclotron modes and the fast and slow space-charge modes for the infinite beam. These are plotted in Figures 2.1 and 2.5. It turns out that devices that utilize space-charge modes operate

at frequencies such that  $\omega \gg \omega_p$ , where the phase velocity is almost independent of frequency, whereas devices that utilize cyclotron modes operate at frequencies near the cyclotron frequency ( $\omega \approx \omega_c$ ) where the phase velocity is extremely sensitive to any change in frequency.

b. The phase velocity (or dispersion curve) may be looked at as a Doppler frequency shift.<sup>25</sup> In the absence of space-charge forces, electrons emitted with transverse velocities in a magnetic field will travel in helical paths, rotating about the "unperturbed" path (parallel to the field lines) with the cyclotron frequency  $\omega_c$ . Assume now that an electromagnetic wave (a *TE* or a *TEM* wave) is also propagating in the axial direction. It is intuitively clear that the electrons will couple to the electromagnetic field when the electron experiences an r-f field pulsating at frequency  $\omega_c$ . In other words, when the r-f field is observed in the electron's moving frame of reference, its frequency must equal  $\omega_c$  for resonance to occur. But transforming the radio frequency to the moving electron frame just gives the familiar Doppler frequency shift, which is Eq. 2.65, the dispersion relation.

## 2.7 The Synchronous Normal Modes<sup>25-31</sup>

There are still two normal modes that propagate on a beam under the assumptions of Section 2.6 which have not yet been found. These are essentially transverse displacement modes in contrast to the cyclotron modes that are transverse velocity modes. In order to have cyclotron modes, the electrons must have transverse a-c velocity. The electrons then rotate at the cyclotron frequency and translate axially with velocity  $v_0$ . Consider now an electron that is injected with no transverse velocity. It will merely follow a magnetic field line with velocity  $v_0$ . Imagine that electrons are somehow injected off axis from a circular cathode sequentially around the circle with no transverse velocity. A disk with a small hole off axis placed in front of a cathode and rotated would serve the purpose. Each electron would follow a straight-line trajectory, but different electrons would lie on a spiral. This is the analog of the motion of water sent out from a garden-hose nozzle that is rotated, provided gravity is neglected. There will be two waves of this variety, depending on which way the garden hose is rotated. However, the phase velocity of each of these waves is the d-c electron velocity  $v_0$ . Furthermore, since the electrons have only a transverse displacement, these waves are called synchronous displacement modes.

The method of excitation here is, of course, fictitious. How they might actually be excited is postponed until the beam is coupled to a circuit in a later chapter.

Now consider the mathematical description of the synchronous modes. They arise essentially from the constant of integration of Eq. 2.61, which was taken zero in the solution given by Eq. 2.63.

Equations 2.56 have been put in normal mode form in Eq. 2.59. However, Eq. 2.61 is not in normal mode form, since the displacements and velocities are still coupled. Here is a situation in which four equations must be put in normal mode form. A general technique for putting any number of equations in normal mode form is given in Appendix C. In the present case a simpler method analogous to the method used in Eq. 1.3 of Chapter 1 can be used. The details are given in Appendix D and only the results are given here.

Define

$$r_{\pm} = k(\xi_{1x} \pm j\xi_{1y}) \quad (2.73)$$

and

$$a_{2\pm} = a_{1\pm} \mp j\omega_c r_{\pm} \quad (2.74)$$

where  $k$  is given by Eq. 2.58. The normal mode form of Eqs. 2.56 and 2.61 is

$$\left( \frac{d}{dz} + j(\beta_e \mp \beta_c) \right) a_{1\pm} = 0 \quad (2.75)$$

$$\left( \frac{d}{dz} + j\beta_e \right) a_{2\pm} = 0 \quad (2.76)$$

Of course, the  $a_{1\pm}$  normal modes are the cyclotron modes already discussed, and Eq. 2.75 is identical with Eq. 2.59. If this had not been the case, the  $a_{1\pm}$  would not have been normal modes. Recall that  $a_{1+}$  is the fast cyclotron mode and is left-handed circularly polarized, whereas  $a_{1-}$  is the slow cyclotron mode and is right-handed circularly polarized. Further, the phase velocities of these modes were frequency dependent.

Consider now the synchronous modes defined by Eq. 2.76. Note that the phase velocity of both modes is  $v_0$ , the d-c beam velocity, which accounts for their being called synchronous modes. It might be thought by looking at Eq. 2.76 that both modes are identical. However, it will now be shown that one is right-hand polarized and the other is left-hand polarized.

In order to obtain a physical picture of the nature of these modes, the same procedure is used as for the cyclotron modes.

The solutions of Eq. 2.76 are

$$a_{2\pm}(z) = |B_{\pm}| e^{-j\beta_e z \mp j\phi_{\pm}} \quad (2.77)$$

where  $|B_{\pm}| e^{j\phi_{\pm}}$  are constants of integration. Assume first that only the  $a_{2+}$ -mode is excited. Then  $a_{1+} = a_{1-} = a_{2-} = 0$ , and it follows from

Eqs. 2.58, 2.73, and 2.74 that

$$\begin{aligned}\xi_{1x} &= j\xi_{1y} & u_{1x} = u_{1y} &= 0 \\ a_{2+} &= -j\omega_c r_+ = -j\omega_c k 2\xi_{1x}\end{aligned}\quad (2.78)$$

Finally, by Eqs. 2.77, 2.78, and 2.55, the  $a_{2+}$ -mode is described by

$$\begin{aligned}x_1^+ &= -\frac{|B_+|}{2\omega_c k} \sin \left[ \omega \left( t - \frac{z}{v_0} \right) + \phi_+ \right] \\ y_1^+ &= \frac{|B_+|}{2\omega_c k} \cos \left[ \omega \left( t - \frac{z}{v_0} \right) + \phi_+ \right]\end{aligned}\quad (2.79)$$

Figure 2.8a shows what a fixed observer at  $z = 0$  (when  $\phi_+$  is taken as zero) sees as time progresses. The observer sees different electrons, but they look like a single electron that is rotating counterclockwise when viewed along the negative  $z$ -axis. Accordingly, the  $a_{2+}$  synchronous mode is said to have left-handed polarization.<sup>32</sup>

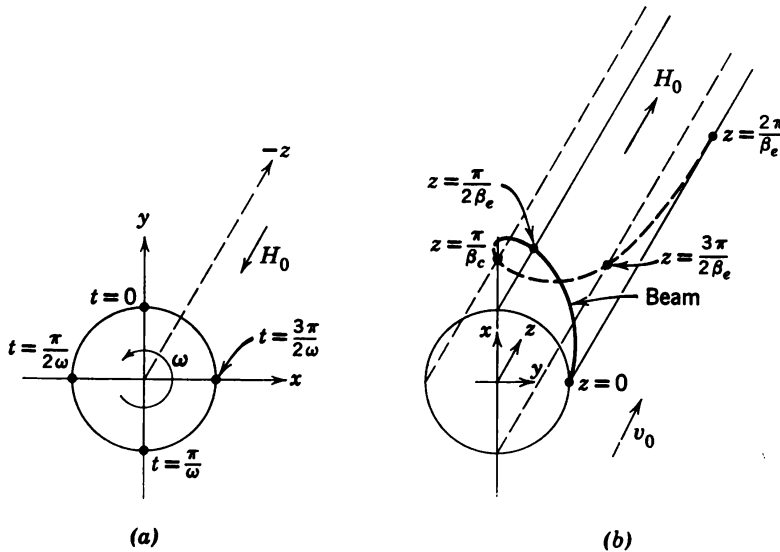


**Figure 2.8** The left-hand synchronous mode  $a_{2+}$ . (a) View of fixed observer,  $z = 0$ ; (b) snapshot at  $t = 0$ . Spiral is left-hand wound.

Figure 2.8b shows a snapshot of all the electrons at  $t = 0$  when  $\phi_+$  is zero. The electrons are seen to lie on a left-hand wound spiral looking in the positive  $z$ -direction with pitch

$$p = -\frac{2\pi v_0}{\omega} \quad (2.80)$$

in accordance with the convention adopted earlier.

For this mode it is clear from Eqs. 2.78 that the individual electrons have no transverse velocity. Therefore, all electrons propagating in the  $a_{2+}$  synchronous mode follow magnetic field lines with axial velocity  $v_0$ ; they are not executing cyclotron motion. The electrons in this mode can therefore be thought of as being glued to a cylinder in the form of a left-hand wound helix with pitch given by Eq. 2.80. The entire cylinder then merely translates axially with velocity  $v_0$ . This, then, is the garden-hose mode described earlier, in which the nozzle is rotated in a circle at frequency  $\omega$  in a clockwise direction when squirting in the positive  $z$ -direction.

Note that although the individual electrons have no transverse velocity the wave has a transverse velocity at a given transverse plane. A fixed observer would see the electrons going up and down.

The  $a_{2-}$ -mode can be treated in a similar manner. The results are shown in Figure 2.9. The  $a_{2-}$ -mode has right-handed circular polarization.

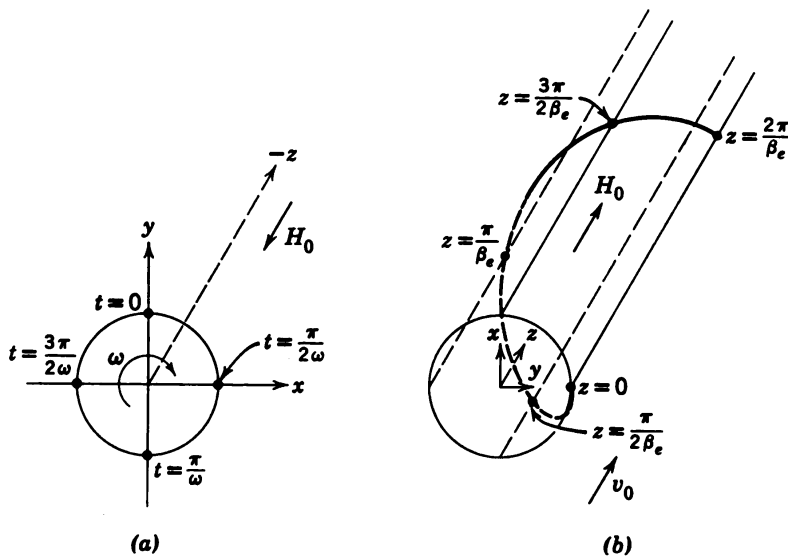


**Figure 2.9** The right-hand synchronous mode  $a_{2-}$ . (a) View of fixed observer,  $z = 0$ ; (b) snapshot at  $t = 0$ . Spiral is right-hand wound.

The synchronous modes therefore travel with the d-c beam velocity and are circularly polarized in opposite senses. Further, the electrons in these modes have only transverse displacement but no transverse velocity, so that they can be called displacement modes. However, the electrons in the cyclotron modes have both transverse velocity and displacement.

## 2.8 Remarks

a. The cyclotron and synchronous modes could have been treated together, since only boundary conditions differentiate among them. All can exist on the same beam under the same conditions. They were separated in order to make the presentation simpler. In a later chapter the excitation of these modes is considered when the beam is coupled to a circuit.

b. It has been shown that the fast space-charge wave carries positive kinetic power, whereas the slow space-charge wave carries negative kinetic power. This followed from the Chu power theorem, which was derived by noting the analogy between the space-charge wave equations and the transmission-line equations. (See Eq. 2.47.)

It has been shown that the fast and slow space-charge waves are independent, so that power carried in each mode is separately conserved, i.e.,  $|a_+(z)|^2 = \text{constant}$  and  $|a_-(z)|^2 = \text{constant}$ . If the power theorem [ $|a_+(z)|^2 - |a_-(z)|^2 = \text{constant}$ , Eq. 2.47] had not been known, it could not have been stated that one mode carried positive and the other carried negative power.

In the case of the cyclotron modes a corresponding power theorem has not yet been derived in the text. In a drift region power carried in the fast and slow cyclotron modes and the  $a_{2\pm}$  synchronous modes is separately conserved, and up to this point there is no way of deciding whether these waves carry positive or negative power. It is possible, therefore, to decide this question only when some measurement is made on the beam. This, for example, involves coupling a circuit to the beam. Any perturbation on the system that couples the modes will show whether the modes carry positive or negative power. In Chapter 8 a circuit is coupled to the cyclotron and synchronous modes, and then power can be compared with the circuit power to decide this important question. The result is that the fast cyclotron and  $a_{2-}$  synchronous modes carry positive kinetic power, whereas the slow cyclotron and  $a_{2+}$  synchronous modes carry negative kinetic power.

The presence of weak space-charge forces would also couple the modes, so that the sign of the mode powers could be compared with the space-charge mode power.

c. Table 2.1 gives a synopsis of the propagation constants, sign of kinetic power, and polarization of the modes discussed in this chapter.<sup>31</sup> The magnetic field points along positive  $z$ . Clockwise rotation viewed along negative  $z$  is right-hand polarization, counterclockwise rotation is left-hand polarization. (The opposite convention is also quite common.)

TABLE 2.1<sup>21</sup>

	Fast Cyclotron $a_{1+}$	Synchronous $a_{2+}$	Synchronous $a_{2-}$	Slow Cyclotron $a_{1-}$	Fast Space Charge $a_+$	Slow Space Charge $a_-$
$\beta$	$\beta_e - \beta_q$	$\beta_e$	$\beta_e$	$\beta_e + \beta_q$	$\beta_e - \beta_q$	$\beta_e + \beta_q$
Sign of kinetic power	+	-	+	-	+	-
Polarization	Left	Left	Right	Right		

d. The purpose of this chapter has now been fulfilled: the space charge, cyclotron, and synchronous modes have been introduced, and the equations have been put in normal mode form. Furthermore, a physical picture of the nature of these waves has been presented. It is now appropriate to return to the theory of coupled modes and consider the effect of weakly coupling a transmission line to a beam in confined flow that is propagating space-charge waves and to see the effect of the weak coupling on these waves. This leads to the theory of the traveling wave tube, backward wave amplifier, and Kompfner dip helices which are presented in Chapter 3.

e. Other references<sup>26-31</sup> to cyclotron and synchronous waves may be found in the bibliography.

## BIBLIOGRAPHY

1. L. J. Chu, "A Kinetic Power Theorem," presented at Annual IRE Conference on Electron Tube Research, Durham, N. H. (1951).
2. S. Ramo, "Space-Charge and Field Waves in an Electron Beam," *Phys. Rev.*, **56**, 276-283 (August 1939).
3. W. C. Hahn, "Small Signal Theory of Velocity Modulated Electron Beams," *Gen. Elec. Rev.*, **42**, 258-270 (June 1939).
4. G. M. Branch and T. G. Mihran, "Plasma Reduction Factors in Electron Beams," *IRE Trans. PGED*, **ED-2**, 3-11 (April 1955).
5. L. T. Zitelli, "Space-Charge Effects in Gridless Klystrons," *Stanford Univ. Microwave Lab., Rept. No. 149* (October 1951).
6. L. T. Zitelli, Errata to Reference 5, July 1952.
7. J. Labus, "Einfluss der Lorentzkraft auf die Raumladungswellen im Elektronenstrahl," *Arch. elektro. Übertr.*, **7**, 88 (February 1953).
8. W. W. Rigrod and J. A. Lewis, "Wave Propagation Along a Magnetically-Focussed Cylindrical Electron Beam," *Bell System Tech. J.*, **33**, 399 (March 1954).
9. J. Labus and K. Pöschl, "Raumladungswellen in ionenfreien Elektronenstrahlen," *Arch. elektro. Übertr.*, **9**, 39 (January 1955).
10. W. O. Schumann, "Über Wellenausbreitung in Plasma zwischen zwei unendlich gut leitenden Ebenen in Richtung eines aufgeprägten äusseren Magnetfeldes," *Z. Angew. Phys.*, **8**, 482 (October 1956).

11. G. R. Brewer, "Some Effects of Magnetic Field Strength on Space-Charge-Wave Propagation," *Proc. IRE*, **44**, 896 (July 1956).
12. R. Liebscher, "Raumladungswellen bei endlichem Magnetfeld an der Kathode einer zylindrischen Elektronenströmung," *Arch. elektr. Übertr.*, **11**, 214 (May 1957).
13. J. Labus, "Space-Charge Waves Along Magnetically Focussed Electron Beams," *Proc. IRE*, **45**, 854 (June 1957).
14. W. W. Rigrod and J. Labus, "Space-Charge Waves Along Magnetically Focussed Electron Beams," *Proc. IRE*, **46**, 358-359 (January 1958).
15. R. H. C. Newton, "On Space-Charge Waves," *J. Electronics Control*, **5**, 510 (December 1958).
16. R. W. Gould and A. W. Trivelpiece, "A New Mode of Wave Propagation on Electron Beams," *Symposium on Electronic Waveguides*, Polytech. Inst. Brooklyn (April 1958).
17. F. Paschke, "The Propagation of Perturbations along Magnetically Focussed Electron Beams," *R C A Rev.*, **20**, 254-283 (June 1959).
18. A. H. W. Beck, *Space-Charge Waves and Slow Electromagnetic Waves*, Pergamon Press, New York, 1958.
19. M. Chodorow, H. J. Shaw, and D. K. Winslow, "Current Distribution in Modulated Magnetically Focussed Electron Beams," *J. Appl. Phys.*, **29**, 1525 (November 1958).
20. *Noise in Electron Devices*, edited by L. D. Smullin and H. A. Haus, John Wiley and Sons, New York, 1959, Chapter 3.
21. L. Brillouin, "A Theorem of Larmor and Its Importance for Electrons in Magnetic Fields," *Phys. Rev.*, **67**, 260-266 (1945).
22. W. H. Louisell and J. R. Pierce, "Power Flow in Electron Beam Devices," *Proc. IRE*, **43**, 425 (April 1955).
23. L. R. Walker, "Stored Energy and Power Flow in Electron Beams," *J. Appl. Phys.*, **25**, 615 (May 1954).
24. L. R. Walker, "Power Flow in Electron Beams," *J. Appl. Phys.*, **26**, 1031 (August 1955).
25. R. Adler, O. M. Kromhout, and P. A. Clavier, "Transverse Field Traveling Wave Tubes with Periodic Electrostatic Focussing," *Proc. IRE*, **44**, 82-89 (January 1956).
26. R. Adler, "Parametric Amplification of the Fast Electron Wave," *Proc. IRE*, **46**, 1300-1301 (June 1958).
27. R. Adler, G. Hrbek, and G. Wade, "A Low-Noise Electron Beam Parametric Amplifier," *Proc. IRE*, **46**, 1756-1758 (October 1958).
28. J. R. Pierce, *Traveling Wave Tubes*, D. Van Nostrand, New York, 1950, Chapter 13.
29. A. E. Siegman, "The Waves on a Filamentary Electron Beam in a Transverse-Field Slow Wave Circuit," *J. Appl. Phys.*, **31**, 17-26 (January 1960).
30. C. C. Johnson, "Theory of Fast-Wave Parametric Amplification," *Technical Memorandum No. 540*, Research Labs., Hughes Aircraft Co., Culver City, Calif. (February 1959). Appendix by R. W. Gould.
31. J. W. Klüver, "Transverse-Field Interaction at Low Space-Charge Densities," *Bell Labs. Internal Memorandum 59-124-24* (July 9, 1959).
32. J. A. Stratton, *Electromagnetic Theory*, McGraw-Hill, New York, 1941, p. 280.

## Chapter 3

# Space-charge waves coupled to slow wave circuits

The theory of coupled modes was presented in Chapter 1 for two elements that were weakly coupled. The theory is now applied to a system, consisting of a thin electron beam in confined flow propagating space-charge waves, weakly coupled to a slow wave circuit.

A slow wave circuit can be thought of as a transmission line in which the phase velocity is adjusted to be approximately in synchronism with the d-c beam velocity. It is clear from the discussion on mode coupling in Chapter 1 that the circuit will couple most effectively to the beam when the uncoupled element phase velocities are in approximate synchronism. This accounts for the choice of a slow wave circuit to be used to couple to the space-charge waves.

In particular, the theory of weak coupling between a beam and circuit leads to the theory of the traveling wave tube, Kompfner dip helix, and the backward wave oscillator. They are all discussed in this chapter.

### 3.1 The Model

**The helix as a slow wave circuit.** The commonest slow wave circuit used in traveling wave tubes (abbreviated TWT) of low and medium power and in low power backward wave oscillators (abbreviated BWO) is the helix.<sup>1,2</sup> In order to visualize the slow phase velocity of the helix, consider Figure 3.1. This shows a wire wound with a uniform pitch on an imaginary cylinder of radius  $a$ . When an electromagnetic wave propagates in the axial direction  $z$ , Maxwell's equations must be solved, subject to boundary conditions on the helix. In order to match these boundary conditions, Pierce<sup>1</sup> introduced the artificial concept of a

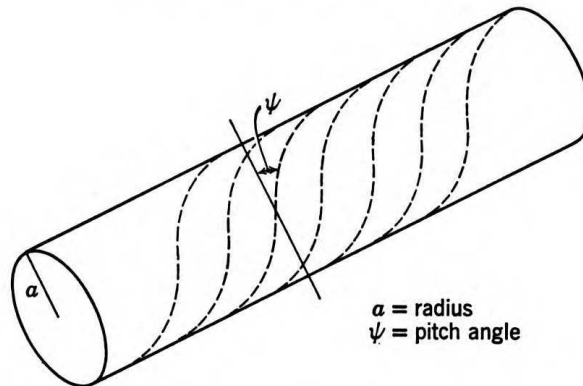


**Figure 3.1** Model of sheath helix. Cylinder is a perfect conductor in helical direction and a perfect insulator in direction normal to helix. (From Pierce, Reference 1.)

sheath helix. He assumed that the helix was a cylinder which was a perfect conductor in the helical direction and a perfect insulator in the direction normal to the helix. By this artifice, the boundary value problem can be solved, and an infinite number of normal modes are found to propagate. The fields found for the lowest order normal mode are sketched in Figure 3.2 at a given instant of time. As time progresses, this field pattern moves down the helix.

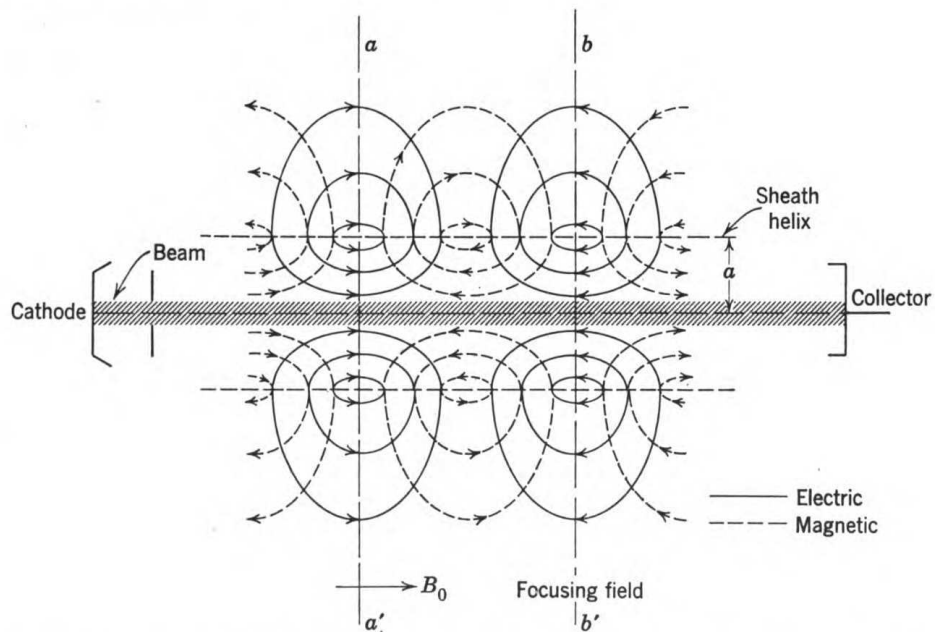


**Figure 3.2** Sketch of field distribution of lowest order mode on a sheath helix. The presence of a thin electron beam will modify this field distribution slightly. Electrons at the  $aa'$  are decelerated; those at  $bb'$ , accelerated. (From Watkins, Reference 2.)

Recall the discussion of the transmission line in Chapter 1. Associated with the electromagnetic fields, a current was induced in the lines and a voltage difference existed between the lines. If the fields of the helix are imagined to be generated by the current flowing in the helically wound wire, it seems reasonable that it would take the wave a longer time to go a given axial distance when the wire is wound in the form of a helix than when the wire is straight, since the current path is longer. This intuitive feeling is correct, and the phase velocity for small pitch angles  $\psi$  is given approximately<sup>1</sup> by

$$\frac{v_p}{c} \cong \sin \psi \cong \psi$$

where  $c$  is the velocity of light. The phase velocity of the wave can then be made synchronous with the d-c beam velocity by choosing the pitch angle sufficiently small.

It has been demonstrated in Chapter 1 that the lowest order modes of a transmission line can be represented by an equivalent distributed  $LC$  circuit. When this equivalent circuit can be used, the analysis is considerably simplified. The helix, propagating its lowest order mode, can also be shown to be equivalent to a distributed  $LC$  circuit. Figure 3.3 shows the transmission-line equivalent circuit for the sheath helix. The analysis of the TWT uses this equivalent circuit. Chu and Jackson<sup>2</sup> have given the corresponding field analysis for the TWT. However, because of its complexity, the field analysis has been omitted, since it leads to the same results as Pierce's equivalent circuit treatment in the simplest case.

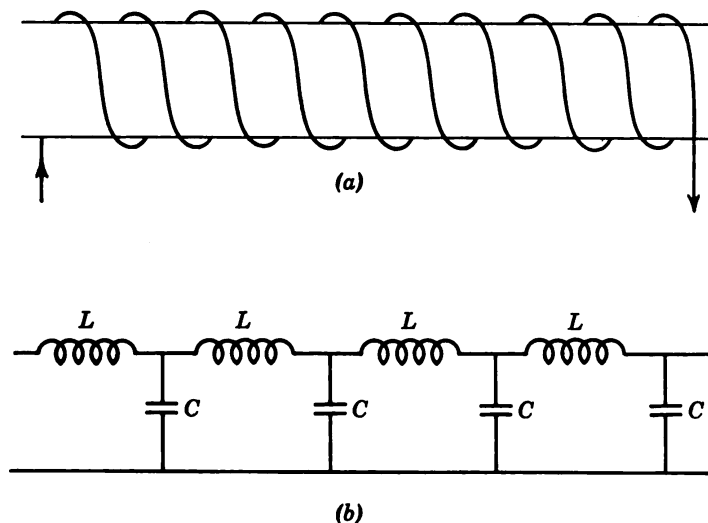


**Figure 3.3** (a) Sheath helix; (b) equivalent distributed circuit for lowest order helix mode.

Further discussion of the field analysis of the helix may be found in the bibliography.<sup>4, 5</sup>

**Beam coupled to circuit.** The next step consists of sending a thin beam down the center of the helix which is propagating its lowest order mode. A very large homogeneous magnetic focusing field in the axial direction is shown in Figure 3.2. The presence of the beam will alter the field of the circuit slightly. The problem now is to find the fields of the circuit and beam when both are weakly coupled. Qualitatively, it is seen that some electrons will be in accelerating electric field regions (plane  $bb'$ ) and some will be in decelerating field regions (plane  $aa'$ ). (The beam is assumed to be thin enough so that the fields are uniform over a cross section.) The accelerated electrons will overtake the decelerated electrons until the space-charge repulsion forces reverse the process. In this manner space-charge bunches made up of the space-charge normal modes discussed in Chapter 2 are formed.

This action obviously would not be cumulative unless the electromagnetic wave traveled in approximate synchronism with the beam. Therefore, it is seen that a slow wave circuit is needed to interact with the space-charge waves on the beam.

Consider now the mathematical description of the beam-circuit coupling. When the beam and circuit are decoupled, the circuit is equivalent to a lossless transmission line described by Eq. 1.45c and d in Chapter 1:

$$\begin{aligned} \frac{dV_c}{dz} &= -j\omega LI_c & (a) \\ \frac{dI_c}{dz} &= -j\omega CV_c & (b) \end{aligned} \quad (3.1)$$

where  $V_c$  and  $I_c$  are the complex voltage and current on the transmission line, and  $L$  and  $C$  are the distributed series inductance and shunt capacitance per unit length. The actual electric field in the region of the beam is seen to be approximately  $z$ -directed in Figure 3.2 and is given by  $E_{cz} = -dV_c/dz$ .

Consider the thin decoupled beam. It is described by Eq. 2.51 in Chapter 2:

$$\begin{aligned} \left( \frac{d}{dz} + j\beta_e \right) V_1 &= -j \frac{(\beta_q)^2}{\beta_e} \frac{2V_0}{|I_0|} i_1 = -E_{1z} & (a) \\ \left( \frac{d}{dz} + j\beta_e \right) i_1 &= -j\beta_e \frac{|I_0|}{2V_0} V_1 & (b) \end{aligned} \quad (3.2)$$

where  $\beta_q = \Re \beta_p$ .

Equation 3.2a is essentially the equation of motion and  $E_{1z}$  is the space-charge field, whereas Eq. 3.2b is essentially the equation of continuity.

Consider now how these "elements" are modified when they are weakly coupled in the sense of Chapter 1. The beam will induce a current in the circuit. The beam is coupled to the circuit capacitively, and a displacement current per unit length will be induced in the circuit given by  $di_1/dz$ . The modified circuit-beam equations (see Eqs. 3.1) are

$$\begin{aligned} \frac{dV_c}{dz} &= -j\omega L I_c & (a) \\ \frac{dI_c}{dz} &= -j\omega C V_c - \frac{di_1}{dz} & (b) \end{aligned} \quad (3.3)$$

Figure 3.4 shows schematically this induced current from an equivalent circuit standpoint.

The beam, in addition to the space-charge force, will experience a force due to the field of the circuit. The continuity equation remains

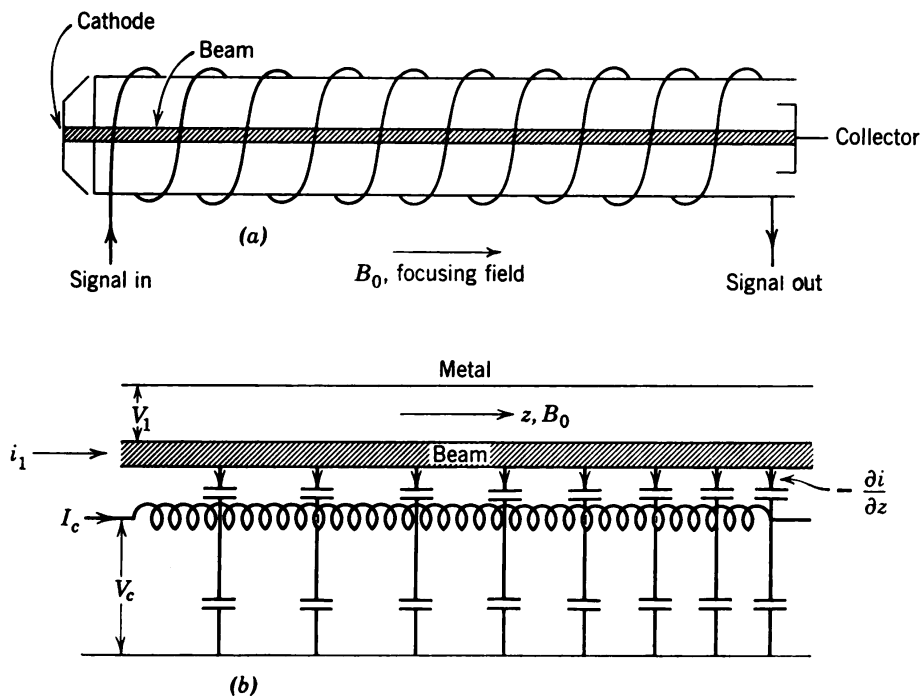


**Figure 3.4** (a) Beam coupled to a helix; (b) equivalent circuit. Beam is capacitively coupled to circuit and  $-\partial i_1/\partial z$  is the displacement current induced in the circuit. (From Pierce, Reference 1.)

unaltered, so that Eqs. 3.2 become

$$\left( \frac{d}{dz} + j\beta_e \right) V_1 = -j \frac{(\beta_q)^2}{\beta_e} \frac{2V_0}{|I_0|} i_1 + \frac{dV_c}{dz} \quad (c)$$
(3.3)

$$\left( \frac{d}{dz} + j\beta_e \right) i_1 = -j\beta_e \frac{|I_0|}{2V_0} V_1 \quad (d)$$

Equations 3.3 represent a beam that is weakly coupled to a circuit. The circuit equations are modified by the presence of an induced current due to the presence of the beam, and the force equation of the beam has been modified by the additional force of the field of the circuit.

The direct approach to coupled mode theory presented in Chapter 1 will now be used, and these equations will be put in coupled mode form.

**Coupled mode form of beam-circuit equations.** The coupled mode amplitudes (see Eqs. 1.46c, 1.47, 2.49, and 2.50) are

$$a_{1\pm} = \frac{1}{4\sqrt{Z_c}} (V_c \pm Z_c I_c) \quad (3.4)$$

$$a_{2\pm} = \frac{1}{4\sqrt{Z_b}} [V_1 \pm Z_b(-i_1)]$$

where

$$Z_c = \sqrt{\frac{L}{C}} \quad (3.5)$$

$$Z_b = \frac{2V_0}{|I_0|} \frac{\omega_q}{\omega}$$

It is shown in Appendix E that the coupled mode form of Eqs. 3.3 is

$$\left( \frac{d}{dz} \pm j\beta_c \right) a_{1\pm} = \pm \frac{1}{2} \sqrt{\frac{Z_c}{Z_b}} \frac{d}{dz} (a_{2+} - a_{2-}) \quad (a)$$
(3.6)

$$\left( \frac{d}{dz} + j(\beta_e \mp \beta_q) \right) a_{2\pm} = \frac{1}{2} \sqrt{\frac{Z_c}{Z_b}} \frac{d}{dz} (a_{1+} + a_{1-}) \quad (b)$$

where the uncoupled circuit propagation constant (Eq. 1.50) is

$$\beta_c = \omega \sqrt{LC} \quad (3.7)$$

and the reduced uncoupled plasma propagation constant is  $\beta_q = \omega_q/v_0$ .

That these equations are in coupled mode form may be seen by letting the coupling vanish. The left side of Eq. 3.6a is the normal mode form of the decoupled circuit equations (Eqs. 1.49), and the left side of Eq. 3.6b is the normal mode form of the decoupled space-charge normal modes (Eqs. 2.44), where  $\beta_p$  is replaced by  $\beta_q$  for the finite size beam. However, the coupling terms on the right side of Eqs. 3.6 involve derivatives of the mode amplitudes, which are different from the coupled mode form treated in Chapter 1. They can be put in the more conventional form if another approximation is made.

Solutions of these equations are of the form  $e^{\gamma z}$ . Since the coupling between the beam and circuit is weak, it will turn out that  $\gamma = -j\beta_e(1 + jC\delta)$ , where  $C\delta \ll 1$ . ( $C$  is a parameter that describes the strength of the coupling between the beam and circuit.) Accordingly, the derivatives in the coupling terms of Eqs. 3.6 can be approximately replaced by  $-j\beta_e$ . Equations 3.6 are then given by

$$\begin{aligned} \left( \frac{d}{dz} \pm j\beta_c \right) a_{1\pm} &= \mp c_{12}(a_{2+} - a_{2-}) \\ \left( \frac{d}{dz} + j(\beta_e \mp \beta_q) \right) a_{2\pm} &= -c_{12}(a_{1+} + a_{1-}) \end{aligned} \quad (3.8)$$

where the mutual coupling coefficient  $c_{12}$  is

$$c_{12} = \frac{j}{2} \sqrt{\frac{Z_c}{Z_b}} \beta_e \quad (3.9)$$

and  $\beta_c \cong \beta_e$ . These equations are now in the standard coupled mode form.

Pierce<sup>1</sup> has introduced two parameters that are so commonly used they must be defined. The first is the gain parameter  $C$ , defined by

$$4C^3 = \frac{Z_c |I_0|}{V_0} \quad (3.10a)$$

where in actual devices  $C \cong 0.01$ , and the second is the space-charge parameter  $\sqrt{4QC}$ , defined by

$$\frac{\omega_q}{\omega} \cong C \sqrt{4QC} \quad (3.10b)$$

where in actual devices  $4QC \cong 1$ . Physically,  $C$  measures the ratios of the uncoupled circuit impedance to the d-c uncoupled beam impedance. Recall that  $\omega_q$  is a measure of the reduced space-charge force in a finite beam, so it is reasonable to call  $\sqrt{4QC}$  the space-charge parameter.

In terms of these parameters, the mutual coupling coefficient  $c_{12}$  can be written<sup>6,7</sup>

$$c_{12} = +j \sqrt{\frac{\beta_e^3 C^3}{2\beta_q}} = \frac{j\beta_e C}{\sqrt{2}(4QC)^{1/4}} \quad (3.11)$$

If the circuit impedance is decreased,  $C$  will decrease (Eq. 3.10a). Further, if the d-c beam voltage is increased or the current decreased, the mutual coupling coefficient is decreased. Also, if the space-charge parameter is increased, the coupling is decreased.

Note that the forward and backward coupled circuit modes,  $a_{1+}$  and  $a_{1-}$ , are not directly coupled. Similarly, the fast and slow space-charge modes,  $a_{2+}$  and  $a_{2-}$ , are not directly coupled. Each of the forward and backward circuit modes is directly coupled to the fast and slow space-charge modes, and the beam modes are directly coupled only to the circuit modes.

Before specializing these equations, it is desirable to consider the small signal power theorem of Chu<sup>8</sup> so that power flow on the beam and circuit can be understood.

### 3.2 The Chu Kinetic Power Theorem<sup>8,9</sup>

The electromagnetic power carried by the circuit in the axial direction is obtained by integrating the small signal Poynting vector over a cross section of the beam and circuit in a manner analogous to the treatment of the transmission line of Chapter 1. This is equivalent (see Eq. 1.55) to

$$P_c = \frac{1}{2} \operatorname{Re} (V_c I_c^*) = 2(|a_{1+}|^2 - |a_{1-}|^2) \quad (3.12)$$

which is the power carried by the circuit in the absence of the beam. Further, the kinetic power carried by the beam in the absence of the circuit (see Eq. 2.47) is

$$P_k = \frac{1}{2} \operatorname{Re} [V_1(-i_1^*)] = 2(|a_{2+}|^2 - |a_{2-}|^2) \quad (3.13)$$

The weak coupling approximation neglects the mutual coupling power (see Chapter 1), so that the total power is approximately

$$P \cong P_c + P_k = 2(|a_{1+}|^2 - |a_{1-}|^2 + |a_{2+}|^2 - |a_{2-}|^2) \quad (3.14)$$

In order to show that  $dP/dz = 0$ , differentiate Eq. 3.14 with respect to  $z$  and use Eqs. 3.8 and their complex conjugates.  $P = \text{constant}$  is the Chu kinetic power theorem. It is derived on a more general basis in Appendix F, in which it is shown that Eq. 3.14 is an approximate expression of the Chu power theorem for a thin beam.

### 3.3 The Traveling Wave Tube<sup>1, 10, 11</sup>

**Coupling of forward circuit mode and slow space-charge mode.** A schematic representation of a TWT amplifier is shown in Figure 3.4a. An electron beam in confined flow moves axially down the center of a helix. A signal is applied at the input of the helix and an amplified signal is removed from the helix output. The spent beam is collected. The electric field of the helix slows the electron beam down, and the lost beam energy is supplied to the circuit wave. This energy transfer gives an exponentially growing wave on the helix.

Equations 3.8 describe the TWT interactions. However, special cases will be considered in which these equations can be simplified. In order to see under what conditions certain modes can be neglected, the transfer factors defined in Chapter 1, Eq. 1.28, are given next for all four modes in Eqs. 3.8.

#### TWT TRANSFER FACTORS. WEAK COUPLING APPROXIMATION

It has been stated that unless the uncoupled circuit phase velocity is in approximate synchronism with the d-c beam velocity there will not be much interaction between the beam and circuit. In order to express this approximate equality, introduce a parameter  $b$  defined by

$$\beta_c = \beta_e(1 + Cb) \quad (3.15)$$

where  $C$  is the gain parameter of Eq. 3.10a, and is typically 0.01, and  $b$  is a parameter<sup>1</sup> that measures the deviation of the uncoupled circuit phase velocity from the d-c beam velocity;  $b$  might typically range from -5 to +5. The transfer factors to be given immediately are more easily interpreted in terms of  $b$  than  $\beta_c$ .

Recall that the transfer factors for modes  $i$  and  $j$  (Eq. 1.28) were defined by

$$F_{ji} = F_{ij} = \left[ 1 + \left( \frac{c_{ii} - c_{jj}}{2} \right)^2 \frac{1}{c_{ij}c_{ji}} \right]^{-1} \quad (3.16)$$

The  $c_{ii}$  are the self-coupling coefficients [ $\pm j\beta_c$  or  $j(\beta_e \pm \beta_q)$ ], and the  $c_{ij}$  are the mutual coupling coefficients ( $\pm c_{12}$ ).

Only four transfer factors are distinct. They are given (see Eqs. 3.8–3.11, 3.15 and 3.16) by

$$F_{1+,2\pm} = \left[ 1 \pm \frac{(4QC)^{\frac{1}{2}}}{2} \left( b \pm \sqrt{4QC} \right)^2 \right]^{-1} \quad (a)$$

$$F_{1-,2\pm} = \left[ 1 \mp \frac{2(4QC)^{\frac{1}{2}}}{C^2} \right]^{-1} \quad (b)$$
(3.17)

Now  $F_{1+,2+}$  is the transfer factor between the forward circuit mode and the fast space-charge mode;  $F_{1+,2-}$  applies to the forward circuit and slow space-charge modes;  $F_{1-,2+}$  applies to the backward circuit and fast space charge; and  $F_{1-,2-}$  applies to the backward circuit and slow space-charge mode.

In order to neglect the backward circuit mode,  $|F_{1-,2+}|$  and  $|F_{1-,2-}|$  must be small compared with unity. These conditions will be simultaneously satisfied if  $C^2 \ll 2\sqrt{4QC}$ . As already noted,  $C \sim 0.01$ , whereas  $4QC$  is of order unity. Therefore, coupling to the backward circuit mode can be neglected. This is just the weak coupling approximation, since  $C$  measures the ratio of the uncoupled circuit impedance to the d-c uncoupled beam impedance and  $\sqrt{4QC}$  is a measure of the space-charge forces.  $C^2/(2\sqrt{4QC})$  is an effective coupling parameter of the beam and circuit.

There are three modes remaining, viz., the fast and slow space-charge modes and the forward circuit modes. In general, all three of these modes must be retained to discuss the quantitative TWT behavior. This is done below. However, there is a situation in which the general features of growth can be demonstrated and in which only the coupling between the slow space charge and circuit modes need be considered. The analysis is then simplified, and it is seen that the growth mechanism predominantly involves coupling between these two modes. The circumstances under which this occurs follows easily from the transfer factors (Eq. 3.17a). It is seen that if  $b = +\sqrt{4QC}$ , the forward circuit mode is in synchronism with the slow space-charge mode and  $F_{1+,2-} = 1$ , whereas  $F_{1+,2+} = [1 + 2(4QC)^{1/2}]^{-1}$ . Therefore, if  $4QC \gg 1$ , coupling to the fast space-charge mode can be neglected. This situation demonstrates the TWT gain mechanism in its simplest form and is now considered.

#### TWT SOLUTIONS, LARGE QC, CIRCUIT AND SLOW MODES SYNCHRONOUS. GAIN<sup>6</sup>

It has been shown that when the uncoupled forward circuit mode is in approximate synchronism with the uncoupled slow space-charge mode and when  $QC > 1$  the coupled mode equations (Eqs. 3.8) reduce to

$$\begin{aligned} \left( \frac{d}{dz} + j\beta_e(1 + Cb) \right) a_{1+} &= c_{12}a_{2-} \\ \left( \frac{d}{dz} + j\beta_e(1 + C\sqrt{4QC}) \right) a_{2-} &= -c_{12}a_{1+} \end{aligned} \quad (3.18)$$

These are in the form of Eqs. 1.57 of Chapter 1. Observe that the circuit mode and slow modes are actively coupled so that there will be ex-

ponentially growing waves when

$$(b - \sqrt{4QC})^2 < \frac{2}{\sqrt{4QC}} \quad (3.19)$$

(See Eqs. 1.59 and 3.11.) Assume solutions of the form  $\exp[-j\beta_e(1 + jC\delta)z]$ . The normal mode propagation constants then reduce to

$$\begin{aligned} \delta_{1,2} &= \pm \sqrt{\frac{1}{2\sqrt{4QC}} - \left(\frac{b - \sqrt{4QC}}{2}\right)^2} - j\left(\frac{b + \sqrt{4QC}}{2}\right) \\ &\equiv x_{1,2} + jy_{1,2} \end{aligned} \quad (3.20)$$

When the circuit phase velocity ( $b$ ) is in the range specified by Eq. 3.19, a growing wave and a decaying wave travel with the same phase velocity.

The active coupling in the present case is between two modes that carry power in the *same* direction. The circuit carries power in the positive  $z$ -direction, and the slow mode carries negative kinetic power (see Chapter 2) in the positive  $z$ -direction. To demonstrate that there is net power gain in this case, boundary conditions must be matched at the input. Assume that power is injected on the circuit and that the beam is initially unmodulated. Then  $|a_{1+}(0)| = \frac{1}{2}$  and  $|a_{2-}(0)| = 0$ . It is easy to show by the usual technique that the a-c power on the circuit is given by

$$P_c = 2|a_{1+}(z)|^2 = 1 + \left(\frac{1}{2\sqrt{4QC} x_1^2}\right) \sinh^2 \beta_e C x_1 z \quad (3.21a)$$

and the kinetic power carried by the beam is

$$P_b = -2|a_{2-}|^2 = -\left(\frac{1}{2\sqrt{4QC} x_1^2}\right) \sinh^2 \beta_e C x_1 z \quad (3.21b)$$

A sketch of the circuit and beam powers,  $P_c$  and  $P_b$ , is shown in Figure 3.5. It is seen that the total power,  $P_c + P_b = 2(|a_{1+}|^2 - |a_{2-}|^2)$ , is conserved, in agreement with the Chu power theorem. Furthermore, the circuit power is increasing in the direction of propagation. Compare this situation with the power flow in the contradirectional coupler shown in Figure 1.10.

The circuit gain in decibels in a length  $L$  is given by

$$\begin{aligned} \text{gain (db)} &= 10 \log_{10} \frac{P_c(L)}{P_c(0)} \\ &= 10 \log_{10} \left(1 + \frac{1}{2\sqrt{4QC} x_1^2} \sinh^2 2\pi x_1 C N\right) \quad (3.22) \end{aligned}$$

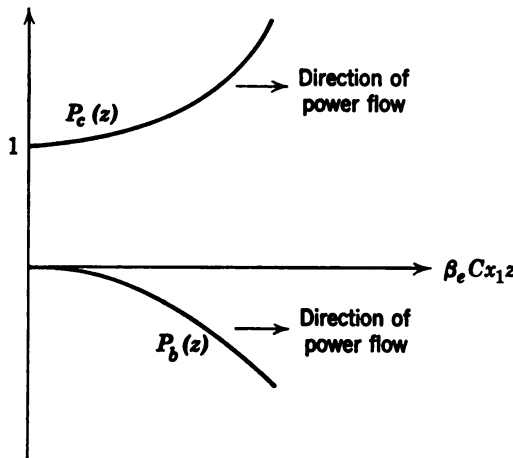


**Figure 3.5** Traveling wave tube gain. (Large  $QC$ .)  $P_c(z)$  is the circuit power and  $P_b$  is the beam power. Power flow is to the right on both beam and circuit.

where  $\beta_e L = 2\pi N$ . If the tube is long enough so that  $2\pi x_1 CN \gg 1$ , the gain can be written approximately as

$$\text{gain (db)} \cong 54.6 x_1 CN - 6 - 10 \log_{10} \left[ 1 - 2\sqrt{4QC} \left( \frac{b - \sqrt{4QC}}{2} \right)^2 \right] \quad (3.23)$$

so that maximum gain occurs when  $b = \sqrt{4QC}$ . Under this maximum gain condition, the gain is proportional to  $x_1$ , which by Eq. 3.20 is given by

$$(x_1)_{\max} = \frac{1}{\sqrt{2} (4QC)^{\frac{1}{4}}}$$

It is therefore seen that the maximum gain decreases as the space-charge parameter  $QC$  increases.

The physics of the gain mechanism, based on the Chu power theorem and the coupled mode approach, has been demonstrated in the most elementary case. In essence, all the important TWT features have been demonstrated.

This case may be treated from the general coupled mode approach<sup>7</sup> of Chapter 1. It is straightforward and is not repeated here, since no new information is to be gained.

**General TWT case.** Unfortunately, even if the circuit and slow modes are approximately synchronous,  $4QC$  may not be large compared with unity. Accordingly, both the fast and slow space-charge modes must be retained, although it is still legitimate to drop the backward circuit

mode. In this case, Eqs. 3.8 become

$$\begin{aligned} \left( \frac{d}{dz} + j\beta_e(1 + Cb) \right) a_{1+} &= -c_{12}(a_{2+} - a_{2-}) \\ \left( \frac{d}{dz} + j(\beta_e - \beta_q) \right) a_{2+} &= -c_{12}a_{1+} \\ \left( \frac{d}{dz} + j(\beta_e + \beta_q) \right) a_{2-} &= -c_{12}a_{1+} \end{aligned} \quad (3.24)$$

The coupled mode formulation has allowed only the backward circuit mode to be dropped. It still is helpful from a physical viewpoint in that it shows which modes are actively and which are passively coupled.

In order to solve these equations, assume solutions of the form  $\exp[-j\beta_e(1 + jC\delta)z]$ . Then  $\delta$  is found to satisfy the following cubic equation:

$$(\delta^2 + 4QC)(j\delta - b) = 1 \quad (3.25)$$

Now cubic equations can be solved algebraically,<sup>12</sup> but the work is quite tedious. Pierce<sup>1</sup> gives graphical solutions, and approximate analytic solutions that are fairly simple have been obtained by the author.<sup>13</sup> A sample graphical solution by Pierce is given in Figure 3.6 for  $QC = 0.25$ , where

$$\delta = x + jy \quad (3.26)$$

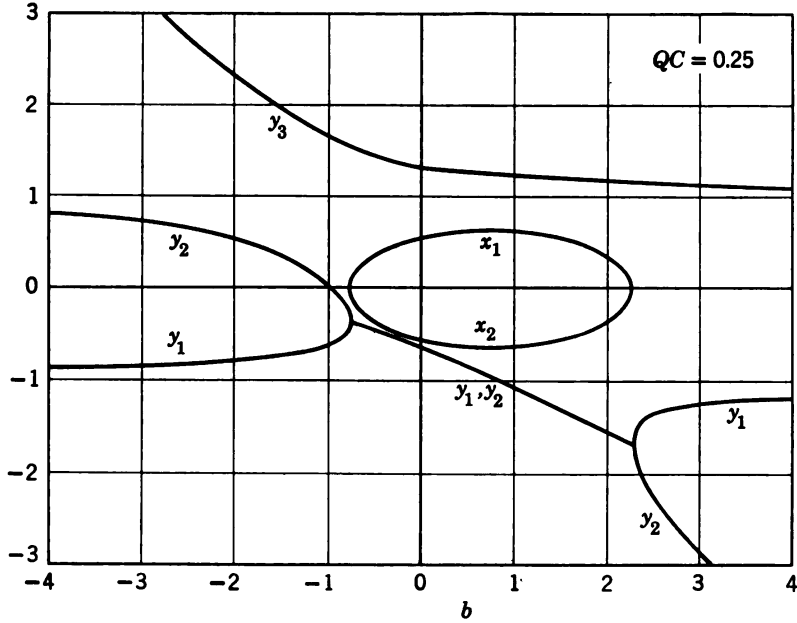


**Figure 3.6** TWT normal mode propagation constants for  $QC = 0.25$  versus the circuit phase velocity parameter  $b$ . Waves vary as  $\exp\{j[\omega t - \beta_e(1 + jC\delta)z]\}$  where  $\delta = x + jy$ . (From Pierce, Reference 1.)

Gaining waves are found for  $-0.75 < b < 2.25$  in approximate agreement with Eq. 3.19. Clearly, the discrepancy is accounted for, since  $4QC$  is not larger than one and the fast mode is interacting slightly. In the gain region the phase velocities for the growing and decaying normal modes are synchronous ( $y_1 = y_2$ ). For  $b < -3$ ,  $y_3$  represents the uncoupled circuit mode phase velocity approximately,  $y_2$  represents the uncoupled fast space-charge mode, and  $y_1$  represents the slow mode.

Power series solutions for the TWT equations (3.24) have been published.<sup>14,15</sup> They are most useful for tubes of short length and small  $QC$ . A convenient matrix method for their derivation is presented in Appendix G.

The boundary conditions are rather involved and have been treated in References 1 and 15. They can be expressed in terms of the power series in a straightforward way, as shown in Appendix G.

It should be clear that the simplicity with which the physical principles for the TWT were qualitatively explained by use of only two coupled modes is ample justification for the coupled mode approach.

It should be noted that the phase velocity of a helix can be designed so that it is independent of frequency over a very wide bandwidth. Accordingly, the TWT will amplify over large bandwidths, which is one of its most useful aspects.

### 3.4 The Kompfner Dip<sup>6, 15, 16, 17</sup> (Directional Coupler)

It is sometimes desirable to couple power from a circuit to a beam. One way of doing this is to use a helix in a region of operation in which there is no gain. The modes then consist of three sinusoidal waves which can interfere constructively or destructively with each other. Under certain operating conditions to be discussed below, all the power on the circuit can be transferred to the beam. The length of helix needed for this to occur is called the Kompfner dip length. Such a device can be thought of as a directional coupler or as a transducer, to use a more general term. Since, in general, three modes are involved, it is more complicated than the codirectional coupler treated in Chapter 1. If  $QC$  is large, however, the slow mode may be neglected and the analysis is simplified. Therefore, the large  $QC$  case is considered first.

**Coupling of forward circuit mode and fast space-charge mode.** Consider the mode transfer factors given in Eqs. 3.17. If  $b \cong -\sqrt{4QC}$ , then  $F_{1+,2+} \cong 1$  and  $F_{1+,2-} \cong [1 - 2(4QC)^{1/2}]^{-1}$ . Therefore, if  $4QC \gg 1$ , coupling to the slow space-charge mode may be neglected. In this case Eqs. 3.8 reduce to

$$\begin{aligned} \left( \frac{d}{dz} + j\beta_e(1 + Cb) \right) a_{1+} &= -c_{12}a_{2+} \\ \left( \frac{d}{dz} + j(\beta_e - \beta_q) \right) a_{2+} &= -c_{12}a_{1+} \end{aligned} \quad (3.27)$$

These equations are identical with those for a codirectional coupler treated in Chapter 1. It follows from the discussion in Section 1.8 that complete power transfer takes place (when  $\beta_1 = \beta_2$ )

$$b_{\text{dip}} = -\sqrt{4QC}) \quad (3.28a)$$

in a length (see Eq. 1.67) given by

$$\frac{\beta_e C}{\sqrt{2}(4QC)^{1/4}} L_{\text{dip}} = \frac{\pi}{2} (2n + 1) \quad (n = 0, \pm 1, \pm 2, \dots)$$

or

$$(CN)_{\text{dip}} = \frac{\sqrt{2}}{4} (4QC)^{1/4} \quad (3.28b)$$

where  $\beta_e L = 2\pi N$ . In this length,  $L_{\text{dip}}$ , all the power introduced on the circuit has been transformed to the fast space-charge mode on the beam, and it is this "dip" in the circuit voltage that gives the device its name.

Matching of the boundary conditions is done exactly as in Section 1.4 and will not be repeated. The results for the power on the circuit and beam when power is injected on the circuit, when  $\beta_1 \neq \beta_2$  (see Eqs. 1.68 and 1.69), are given for reference:

$$\begin{aligned} P_c(z) &= 2|a_{1+}(z)|^2 = 2|a_{1+}(0)|^2 \left( 1 - \frac{\sin^2 \beta_e C \beta_b z}{1 + 2\sqrt{4QC} \beta_d^2} \right) \\ P_b(z) &= 2|a_{2+}(z)|^2 = 2|a_{1+}(0)|^2 - P_c(z) \end{aligned} \quad (3.29)$$

where

$$\begin{aligned} \beta_b &= \sqrt{\frac{1}{2\sqrt{4QC}}} + \beta_d^2 \\ 2\beta_d &= b + \sqrt{4QC} \end{aligned} \quad (3.30)$$

These quantities are sketched in Figures 1.8 and 1.9 of Chapter 1. Complete power transfer takes place only under the dip conditions of Eqs. 3.28. The two modes interfere constructively and destructively for the periodic power transfer to take place.

As  $QC$  is increased, the length required for complete power transfer is increased but the weak coupling approximation becomes better.

The action is reciprocal in that fast mode power on the beam will be periodically transferred to the circuit under the same dip conditions.

Figure 3.7 shows a block diagram of an ideal fast mode coupler in which all the circuit power is converted to fast mode power on the beam, all the fast mode power on the beam is removed by the circuit, and the slow mode on the beam is unaffected.

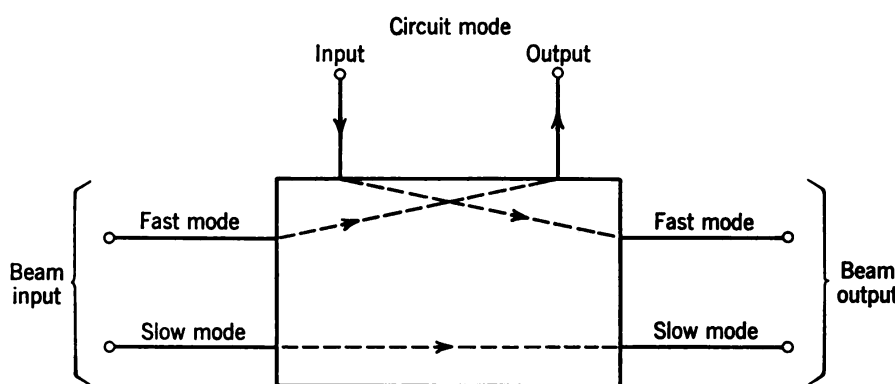
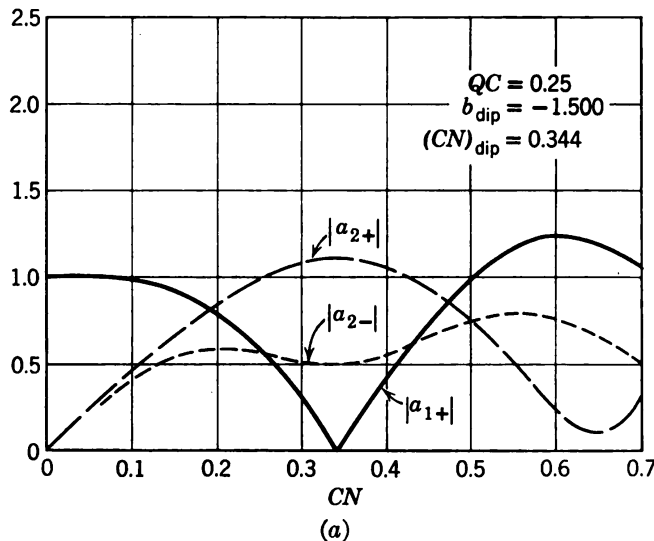


**Figure 3.7** Block diagram of an ideal fast mode coupler (Kompfner dip helix). (From Ashkin, Louisell, and Quate, Reference 15.)

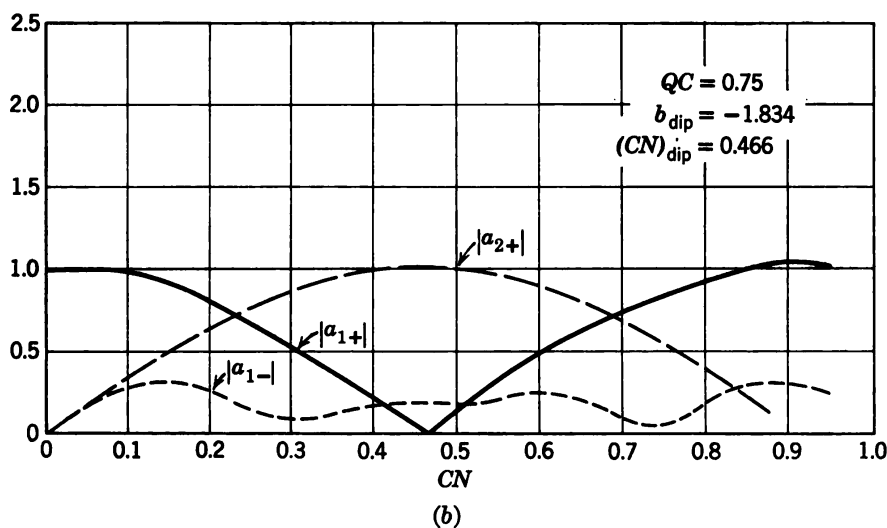
**General case, small QC.**<sup>15, 17, 18</sup> When  $QC$  is small, both the slow and fast modes become important. The general TWT equations (3.24) must then be used. Complete power transfer can still occur, as noted earlier. Figure 3.8a shows the mode amplitudes as a function of  $CN$  when Eqs. 3.24 are solved numerically under dip conditions. In this case  $b_{\text{dip}}$  is found to be  $-1.500$ , and the dip length occurs at  $CN_{\text{dip}} = 0.344$ . The circuit power is divided between the fast and slow modes. It is evident from this figure that the slow mode cannot be neglected. Figure 3.8b is a similar plot for  $QC = 0.75$ . In this case the amount of power in the slow mode is small enough to be neglected.

The solid curves in Figures 3.9 and 3.10 give graphical plots obtained numerically for  $b_{\text{dip}}$  and  $CN_{\text{dip}}$ , respectively, versus  $QC$  under conditions of complete power transfer. The approximate values of  $b_{\text{dip}}$  and  $CN_{\text{dip}}$  of Eqs. 3.28 are also plotted with a dashed curve on these figures. A comparison of these two curves shows the range of validity of the large  $QC$  approximation given in Eqs. 3.28.

For a given  $QC$  complete power transfer from the circuit to the beam occurs for a unique value of  $b$  and  $CN$ . This is useful in determining TWT circuit parameters experimentally.



(a)



(b)

**Figure 3.8** The forward circuit mode amplitude,  $|a_{1+}|$ , beam slow mode amplitude,  $|a_{2-}|$ , and beam fast mode amplitude,  $|a_{2+}|$ , plotted versus  $CN$  under dip conditions. (a)  $QC = 0.25$ . The slow mode must not be neglected. (b)  $QC = 0.75$ . The slow mode may be neglected. (From Ashkin, Louisell and Quate, Reference 15.)

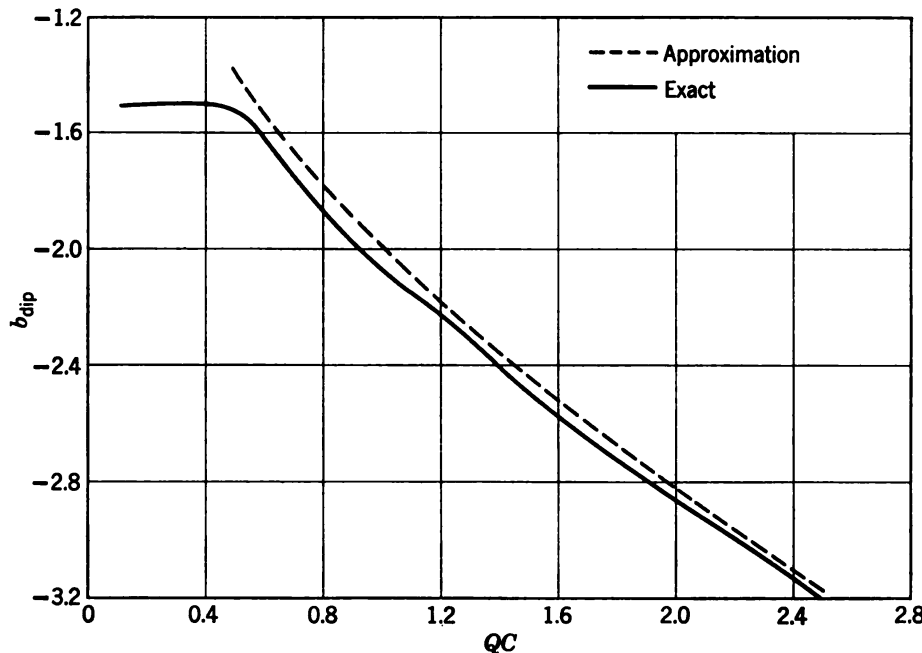


**Figure 3.9** Computed values of  $b_{\text{dip}}$  versus  $QC$  for the Kompfner dip helix. The dashed curve for  $QC > 0.5$  is a plot of Eq. 3.28a. (From Ashkin, Louisell, and Quate, Reference 15.)

### 3.5 The Backward Wave Amplifier and Oscillator<sup>6, 19-23</sup>

The TWT and Kompfner dip helix theories have used the lowest order mode of propagation on the helix. It has been pointed out that an infinite number of other helix modes is possible. Another mode, which is called the  $n = -1$ , has some interesting properties, viz., its group velocity is in the negative  $z$ -direction, whereas the phase velocity is in the positive  $z$ -direction. It is therefore possible for this mode to interact with the space-charge modes, which have both group and phase velocities in the positive  $z$ -direction. A study of this interaction leads to the explanation of the operation of the BWA and BWO, which is fundamentally different from the TWT.

For the  $n = -1$  mode of the sheath helix there is no axial electric field at the helix center, but there is an axial electric field near the helix. Accordingly, a hollow circular electron beam is used for a BWA that flows near the helix.

To study the BWA rigorously, as in the TWT case, a field solution is necessary. However, an equivalent circuit approach analogous to that of the TWT is possible and is, of course, much simpler than the field approach. The transmission line treated in Chapter 1 will not do for the

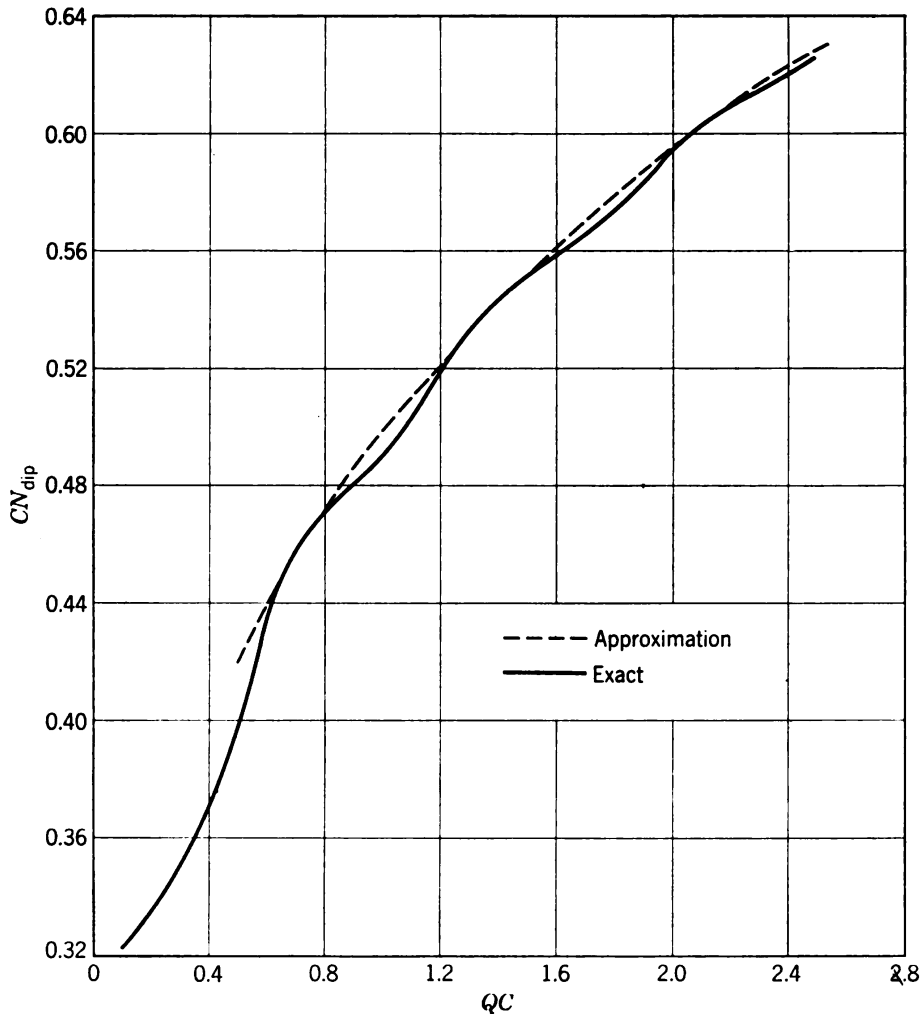
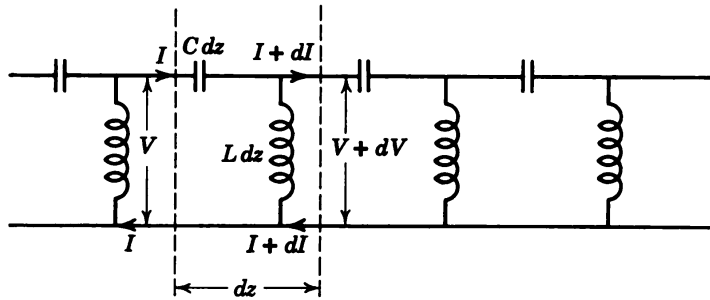


Figure 3.10 Computed values of  $(CN)_{\text{dip}}$  versus  $QC$  for the Kompfner dip helix. Dashed curve is plot of Eq. 3.28b. (From Ashkin, Louisell, and Quate, Reference 15.)

equivalent circuit of the  $n = -1$  helix mode, since the group and phase velocities are in the same direction. Figure 3.11 shows a distributed circuit that has the required characteristics, viz., the group and phase velocities of the modes are in opposite directions. The equations for this circuit are derived in a manner analogous to the transmission line of Section 1.6. They are

$$\begin{aligned} \frac{\partial^2 V_c}{\partial z \partial t} &= -\frac{1}{C} I_c \\ \frac{\partial^2 I_c}{\partial z \partial t} &= -\frac{1}{L} V_c \end{aligned} \quad (3.31)$$



**Figure 3.11** Equivalent distributed transmission-line circuit for the  $n = -1$  sheath helix mode (BWA mode). The group and phase velocities are in opposite directions. (From Pierce, Reference 1.)

Assume a sinusoidal time dependence of the form  $e^{j\omega t}$ , and they reduce to

$$\begin{aligned} \frac{dV_c}{dz} &= + \frac{j}{\omega C} I_c & (a) \\ \frac{dI_c}{dz} &= + \frac{j}{\omega L} V_c & (b) \end{aligned} \quad (3.32)$$

The propagation constant is

$$\beta = \frac{1}{\omega \sqrt{LC}} \quad (3.33)$$

where  $\beta > 0$ .

The phase velocities for the forward and backward modes are

$$v_p \pm = \pm \frac{\omega}{\beta} = \pm \omega^2 \sqrt{LC} \quad (3.34a)$$

and the group velocities are

$$v_g \pm = \pm \left( \frac{\partial \beta}{\partial \omega} \right)^{-1} = \mp \omega^2 \sqrt{LC} \quad (3.34b)$$

Therefore, the phase and group velocities of both the forward and backward modes are in opposite directions.

When the beam is coupled to the circuit, all the arguments of Section 3.1 can be repeated. The result is that  $-di_1/dz$  is added to the right side of Eq. 3.32b and Eqs. 3.3c and 3.3d are unmodified. By the usual procedure, these equations can be put in coupled mode form, and the resulting coupled mode equations analogous to Eqs. 3.8 for the TWT become

$$\begin{aligned} \left( \frac{d}{dz} \mp j\beta_c \right) a_{1\pm} &= \mp c_{12}(a_{2+} - a_{2-}) \\ \left( \frac{d}{dz} + j(\beta_e \mp \beta_q) \right) a_{2\pm} &= -c_{12}(a_{1+} + a_{1-}) \end{aligned} \quad (3.35)$$

where

$$\begin{aligned} a_{1\pm} &= \frac{1}{4\sqrt{Z_c}} (V_c \pm Z_c I_c) \\ a_{2\pm} &= \frac{1}{4\sqrt{Z_b}} [V_1 \pm Z_b(-i_1)] \end{aligned} \quad (3.36)$$

$$\begin{aligned} Z_c &= \sqrt{\frac{L}{C}}; \quad \beta_c = \frac{1}{\omega\sqrt{LC}} = \beta_e(1 + Cb) \\ c_{12} &= \frac{j}{2} \beta_e \sqrt{\frac{Z_c}{Z_b}} = \frac{j\beta_e C}{\sqrt{2}(4QC)^{1/4}} \end{aligned} \quad (3.37)$$

The only difference between these equations and Eqs. 3.8 is that  $a_{1+}$  is now the backward circuit mode,  $a_{1-}$  is the forward circuit mode, and the power is still  $2(|a_{1+}|^2 - |a_{1-}|^2)$  so that the group velocities of the two uncoupled circuit modes are in opposite directions. Note also that these equations come from Eqs. 3.8 directly if  $\beta_c \rightarrow -\beta_c$ .

Consideration of the transfer factors shows that the  $a_{1+}$ -mode can be neglected and only the backward group velocity mode,  $a_{1-}$ , need be retained. It has a phase velocity in the forward direction and can couple to the  $a_{2\pm}$ -modes.

In general, all three modes must be retained just as they are in the TWT. However, if  $QC$  is large and the circuit phase velocity is in approximate synchronism with the slow mode, ( $b \cong +\sqrt{4QC}$ ), the transfer factors between the circuit and fast mode will be small and the fast mode can be neglected. Only this special case will be treated. Write the resulting  $a_{1-}$  and  $a_{2-}$ -equations out, and it will be seen that these modes are passively coupled. Boundary conditions must be matched at  $z = 0$  for the beam,  $a_{2-}(0)$ , and at the far end,  $z = L$ , for the circuit. Assume power is injected on the circuit at  $z = L$ . (See Figure 3.12.) It is then easy to solve the boundary value problem. The power carried by the circuit is

$$P_c(z) = -2|a_{1-}|^2 = -\left(\frac{1 - F \sin^2 \beta_e C \beta_b z}{1 - F \sin^2 \beta_e C \beta_b L}\right) \quad (3.38a)$$

and the power carried by the beam is

$$P_b(z) = -2|a_{2-}|^2 = -\frac{F \sin^2 \beta_e C \beta_b z}{1 - F \sin^2 \beta_e C \beta_b L} \quad (3.38b)$$

where

$$F = \frac{1}{2\sqrt{4QC} \beta_b^2}$$

$$\beta_b = \sqrt{\frac{1}{2\sqrt{4QC}}} + \beta_d^2 \quad (3.39)$$

$$2\beta_d = \sqrt{4QC} - b$$

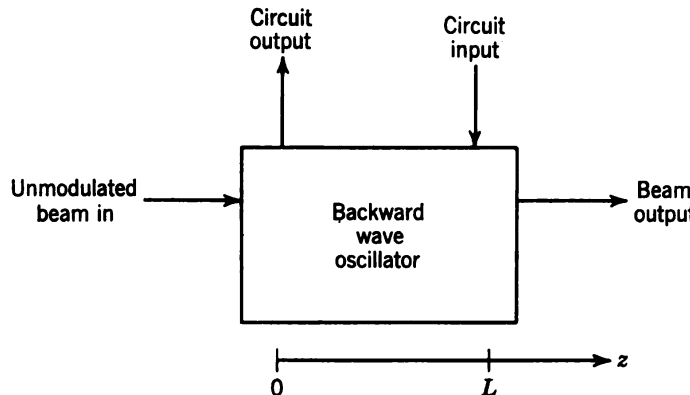


**Figure 3.12** Block diagram of BWA.

Now recall that power is injected on the line at  $z = L$ . There are no exponentially growing waves, but there can still be gain. The power out at  $z = 0$  is

$$P_c(0) = -(1 - F \sin^2 \beta_e C \beta_b L)^{-1} \quad (3.40)$$

and the input power at  $z = L$  is  $P_c(L) = -1$ . Accordingly, the gain in decibels is

$$\text{gain (db)} = 10 \log_{10} \frac{P_c(0)}{P_c(L)} = -10 \log_{10} (1 - F \sin^2 \beta_e C \beta_b L) \quad (3.41)$$

Since  $0 < F \leq 1$ , maximum gain will occur if  $L$  is chosen so that

$$\beta_e C \beta_b L_{\max} = \frac{\pi}{2} (2n + 1) \quad [n = 0, \pm 1, \pm 2, \dots] \quad (3.41a)$$

or

$$CN = \frac{(2n + 1)}{4} \sqrt{2} (4QC)^{\frac{1}{4}}$$

Note also that if in addition to Eqs. 3.41a the circuit is in exact synchronism with the slow space-charge mode,

$$b_{\text{osc}} = \sqrt{4QC} \quad (3.41b)$$

then  $F = 1$  and the gain is infinite. Therefore, any gain from zero to infinity can be achieved. Infinite gain means that the circuit will oscil-

late and the BWA becomes the BWO. Conditions given in Eqs. 3.41 are the start oscillation condition.

This amplifier is analogous to a familiar regenerative amplifier in that there is positive feedback. When the feedback is sufficiently large, the amplifier breaks into oscillation. The feedback effectively introduces a negative resistance in the circuit.

In order to achieve large gain, the amplifier must be operated near the threshold for oscillation, and there is always the danger that it will oscillate.

Figure 3.13 shows schematically the power on the beam and circuit for a nonsynchronous case ( $F < 1$ ) for a tube of length  $L_{\max}$  (Eqs. 3.41a). The circuit wave grows in the same direction as power flow, so that true gain is achieved.

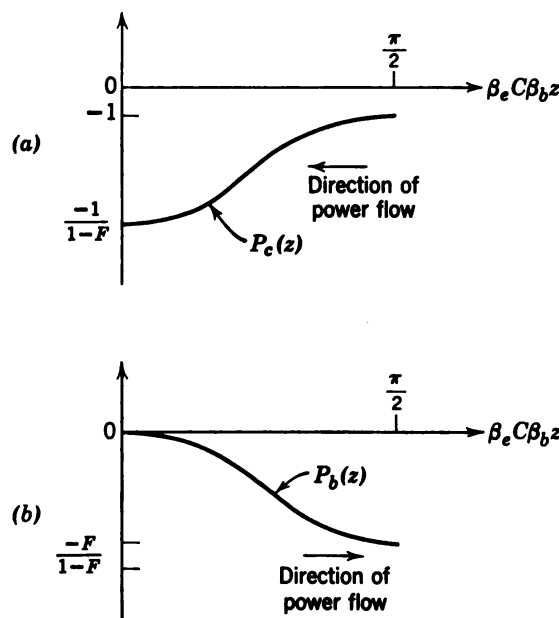


**Figure 3.13** BWA gain. (a) Power on circuit  $P_c(z)$ . Circuit power flows to the left. (b) Power on beam  $P_b(z)$ . Beam power flows to the right.

Note that the frequency of the oscillator and the gain can be controlled by the beam voltage. This is a voltage tuned oscillator, which is one of the BWO's remarkable features.

### 3.6 Remarks

- a. In this chapter the theory of coupled modes has been applied to TWT's, Kompfner dip helices, BWO's, and BWA's. From this treatment and the discussion on active and passive mode coupling of Chapter

it is evident that both types of coupling can lead to gain. The physical mechanism involved is different for active gain and passive gain.

b. The coupled mode approach, together with the power theorem, proves a very powerful analytical tool for the analysis of weakly coupled elements. The approach also leads to an understanding of the physical principles underlying the operation of such devices.

c. Many other devices can be analyzed by this method,<sup>1,2</sup> but space does not permit. A few that can be mentioned are the resistive wall amplifier,<sup>24,25</sup> the easitron,<sup>26</sup> the double stream amplifier,<sup>27</sup> the klystron, and noise waves in electron beams.<sup>28</sup>

d. C. C. Cutler<sup>29</sup> was among the first to explain the operation of the TWT in terms of coupling between an electromagnetic wave and a space-charge wave.

e. It might be thought that the coupled mode theory as presented to date is complete. However, there are cases in which the elements are not weakly coupled. It has been mentioned in Chapter 1 that Haus,<sup>7,30</sup> has treated the problem from a more general variational approach, which shows clearly the nature and validity of the weak coupling approximation, and has shown how to treat the stronger coupling cases. Unfortunately, the method is too involved to present here. Needless to say, it leads to the same results found in the present work under the weak coupling assumptions. P. A. Sturrock<sup>31</sup> has also given a variational principle formulation for the small signal electron beam problem.

f. Interest now shifts to a new class of low noise amplifiers which have been called parametric amplifiers. Chapter 4 is devoted to an explanation of the principles underlying their operation. The coupled mode theory is used as a technique to describe them.

## BIBLIOGRAPHY

1. J. R. Pierce, *Traveling Wave Tubes*, D. Van Nostrand, New York, 1950.
2. D. A. Watkins, "Topics in Electromagnetic Theory," John Wiley and Sons, New York, 1958, Chapter 2.
3. L. J. Chu and D. Jackson, "Field Theory of Traveling-Wave Tubes," *Proc. IRE*, **36**, 853-863 (July 1948).
4. S. Sensiper, "Electromagnetic Wave Propagation on Helical Conductors," Sc.D. Thesis, Mass. Inst. Technol., Cambridge, Mass., 1951; also *Proc. IRE*, **43**, 149-161 (February 1955).
5. S. Sensiper, "Electromagnetic Wave Propagation on Helical Structures" (A Review and Survey of Recent Progress), *Proc. IRE*, **43**, 149-161 (February 1955), and references contained therein.
6. R. W. Gould, "A Coupled Mode Description of the Backward-Wave Oscillator and the Kompfner Dip Condition," *IRE Trans. PGED*, **ED-2**, 37-42 (October 1955).

7. H. A. Haus, "Electron Beam Waves in Microwave Tubes," *Mass. Inst. Technol. Research Lab. Electronics, Tech. Rep. No. 316*, April 8, 1958.
8. L. J. Chu, "A Kinetic Power Theorem," presented at annual IRE Conference on Electron Tube Research, Durham, N. H. (1951).
9. *Noise in Electron Devices*, edited by L. D. Smullin and H. A. Haus, John Wiley and Sons, New York, 1959, Chapter 3.
10. R. Kompfner, "The Traveling Wave Tube as Amplifier at Microwaves," *Proc. IRE*, **35**, 124-127 (February 1947).
11. J. R. Pierce, "The Wave Picture of Microwave Tubes," *Bell System Tech. J.*, **33**, 1343-1372 (November 1954).
12. I. S. and E. S. Sokolnikoff, *Higher Mathematics for Engineers and Physicists*, McGraw-Hill, New York, 1941, p. 86.
13. W. H. Louisell, "Approximate Analytic Expressions for TWT Propagation Constants," *IRE Trans. PGED*, **ED-5**, 257-259 (October 1958).
14. J. A. Mullen, "A Power Series Solution of the Traveling Wave Tube Equations," *IRE Trans. PGED*, **ED-4**, 159-160 (April 1957).
15. A. Ashkin, W. H. Louisell, and C. F. Quate, "Fast Wave Couplers for Longitudinal Beam Parametric Amplifiers," *J. Electronics Control*, **7**, 1-32 (July 1959).
16. R. Kompfner, "On the Operation of the Traveling Wave Tube at Low Level," *British J. IEE*, **10**, 283-289 (August-September 1955).
17. H. R. Johnson, "Kompfner Dip Conditions," *Proc. IRE*, **43**, 874 (July 1955).
18. R. W. Gould, "Traveling-Wave Couplers for Longitudinal Beam Type Amplifiers," *Proc. IRE*, **47**, 419-426 (March 1959).
19. R. Kompfner and N. T. Williams, "Backward-Wave Tubes," *Proc. IRE*, **41**, 1603-1611 (November 1953).
20. H. Heffner, "Analysis of the Backward-Wave Traveling Wave Tube," *Proc. IRE*, **42**, 930-937 (June 1954).
21. L. R. Walker, "Starting Currents in the Backward-Wave Oscillator," *J. Appl. Phys.*, **24**, 854-859 (July 1953).
22. H. R. Johnson, "Backward-Wave Oscillators," *Proc. IRE*, **43**, 684-697 (June 1955) and references contained therein.
23. D. A. Watkins and E. A. Ash, "The Helix as a Backward-Wave Circuit Structure," *J. Appl. Phys.*, **25**, 782-790 (June 1954).
24. J. R. Pierce, "Waves in Electron Streams and Circuits," *Bell System Tech. J.*, **30**, 626-651 (July 1951).
25. C. K. Birdsall, G. R. Brewer, and A. V. Haef, "The Resistive Wall Amplifier," *Proc. IRE*, **41**, 865-875 (July 1953).
26. L. R. Walker, unpublished. See References 1, 11, and 23.
27. A. V. Haef, "The Electron Wave Tube—A Novel Method of Generation and Amplification of Microwave Energy," *Proc. IRE*, **37**, 4-10 (January 1949).
28. C. C. Cutler and C. F. Quate, "Experimental Verification of Space Charge and Transit Time Reduction of Noise in Electron Beams," *Phys. Rev.*, **80**, 875-878 (December 1950).
29. C. C. Cutler, "A Mechanical Traveling-Wave Oscillator," *Bell Labs. Record* (April 1954).
30. H. A. Haus, "Variational Principles Derived from Power Theorems," private communication.
31. P. A. Sturrock, "A Variational Principle for Small Amplitude Disturbances of Electron Beams," W. W. Hansen Laboratories of Physics, Stanford University, Stanford, California, *Internal Memorandum, M.L. No. 480* (February 1958).

## Chapter 4

# Parametric coupling principle for lumped circuits

The theory of coupled modes of vibration developed in Chapter 1 will now be extended to include cases in which two elements are weakly coupled by a time-varying circuit parameter. Just as a nonlinear circuit parameter can cause mixing of two different modes of vibrations (e.g., r-f signal and local oscillator modes in superheterodyne receivers), a time-varying circuit parameter can also provide frequency mixing. The mixing of frequencies allows energy supplied to the system at one frequency to be converted to another. The coupling of modes by a time-varying circuit parameter is called parametric coupling.

A simple mechanical example may help clarify the principle. Consider a child on a swing. The child "pumps up" the swing amplitude by lowering his center of gravity on the downswing and raising it on the up-swing. The "pumping frequency" is twice the swing resonant frequency, and energy is pumped into the swing amplitude. The raising and lowering of the center of gravity changes the effective length of the swing and is the time-varying circuit parameter that causes mixing between the two normal modes of the swing. (These are the two counter-rotating modes of the simple oscillator of Chapter 1.)

The swing illustration is a degenerate case of two independent resonant circuits which are coupled by a time-varying parameter. If the pump is applied at a frequency equal to the sum of the frequencies of the two uncoupled circuits, the modes are coupled by the pump and energy is fed into both circuits.

The purpose of this chapter is to extend the theory of coupled modes to include variable coupling elements and to show how the principle can be used for amplification. The main advantage of parametric amplifiers is their low noise characteristic. Therefore, a discussion is given of the theoretical noise figures of these devices.

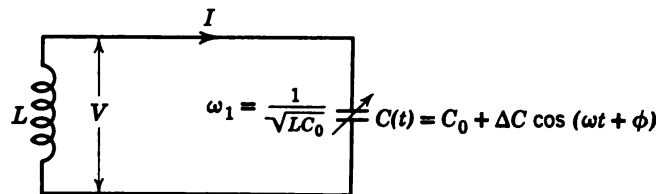


**Figure 4.1** Degenerate two-frequency parametric oscillator. The pump frequency  $\omega$  is twice the natural resonant frequency  $\omega_1$ .

#### 4.1 Mechanism of Energy Transfer

The principle of parametric coupling will now be illustrated for the simple  $LC$  circuit shown in Figure 4.1. Assume that it is possible to pull the condenser plates apart or to push them together, at will, mechanically. Since the capacitance depends on the plate separation, the condenser plays the role of a time-varying circuit parameter. Assume that the plates have been charged in the past and that the circuit is oscillating. Now, at an instant of time when the condenser is fully charged, pull the plates apart instantaneously a slight amount. Since the plates have opposite charges, work is required to separate them. The work done increases the energy in the electric field between the condenser plates, since the charge on the condenser cannot change instantaneously and the instantaneous decrease in capacitance causes a corresponding increase in the condenser voltage, ( $V = Q/C$ ). These changes are shown in Figure 4.2.

A quarter of a resonant period later there is no charge on the condenser. At that instant, no force is required to restore them to their original separation. Still another quarter period later, when the plates are charged with opposite sign, pull them apart again and more energy will be added to the circuit. In this way, energy at twice the resonant frequency can be pumped into the circuit, and the amplitude of oscillation at the resonant frequency will grow. This is analogous to the pumped swing discussed earlier.

The time-varying pump is now evident. By means of coupled mode theory, it will next be shown explicitly how the pump couples the two counterrotating modes of the oscillator and feeds energy into the circuit.

#### 4.2 Direct Coupled Mode Approach to the Degenerate Parametric Oscillator

The parametric oscillator of Figure 4.1 has been discussed qualitatively in Section 4.1. By pulling the condenser plates apart and pushing them together at twice the resonant frequency, it has been shown that energy

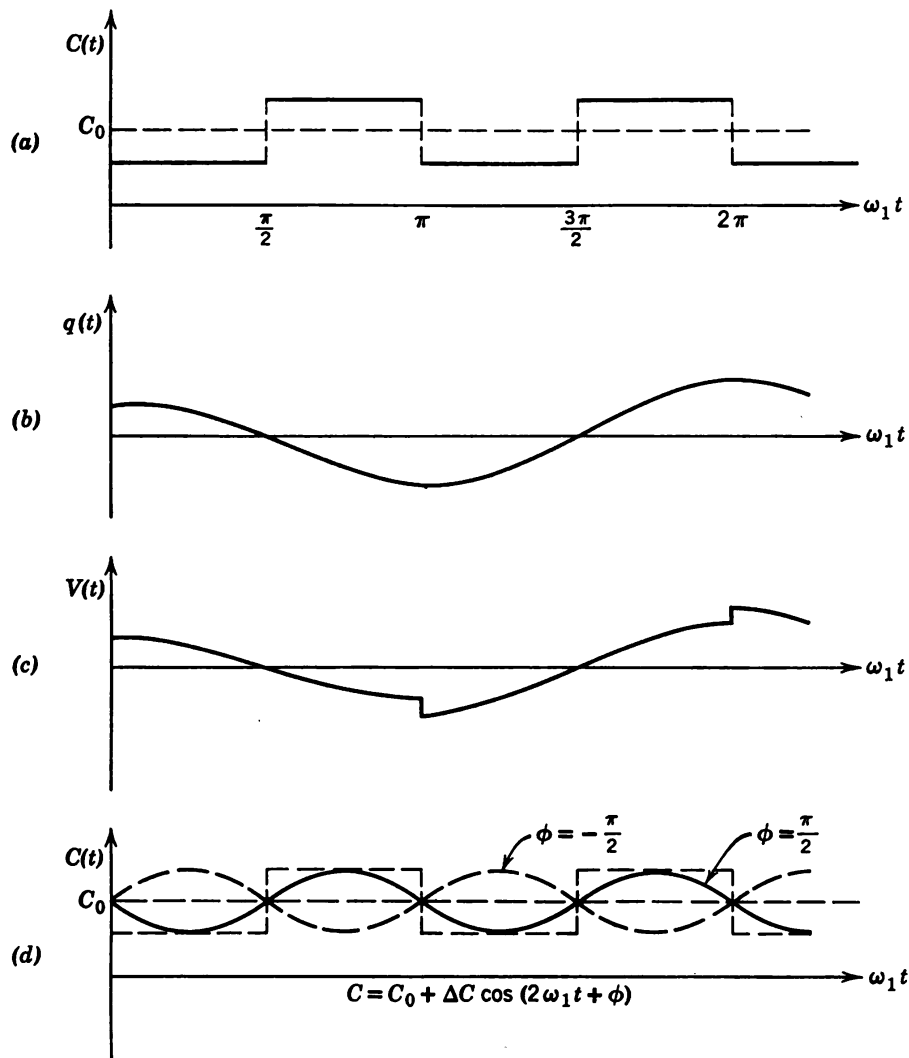


**Figure 4.2** Degenerate parametric oscillator behavior: (a) square wave capacitance (pump) variation; (b) growing charge oscillation; (c) voltage variation. The discontinuity occurs when the capacitance changes abruptly. (d) Square wave capacitance variation replaced by a sinusoidal variation,  $C = C_0 + \Delta C \cos(2\omega_1 t + \phi)$ . When  $\phi = \pi/2$ , a net amount of energy is fed into the circuit in each cycle by the pump, and the oscillations grow, whereas if  $\phi = -\pi/2$  a net amount of energy is extracted by the pump and the oscillations are damped out.

was fed into the resonant circuit. Note, however, that the phase of the pump relative to the charge on the condenser plates must be chosen properly; that is, in order to supply energy to the circuit, the plates must be pulled apart when fully charged and pushed together when the charge is zero. It is obvious that if the pump phase is changed so that the plates

are drawn together when they are fully charged the circuit will give up energy to the engine connected to the plates and the circuit oscillation will damp out rather than grow.

These qualitative arguments will now be formulated in terms of coupled mode theory. This theory was developed in Chapter 1 for the case of time-independent coupling. However, here the coupling is time dependent, and the theory must be extended to include this case.

Instead of the square wave capacitance variation shown in Figure 4.2a, assume a capacitance variation of the form (Figure 4.2d)

$$C(t) = C_0 + \Delta C \cos(2\omega_1 t + \phi) \equiv C_0 + C_p(t) \quad (4.1)$$

The arbitrary phase  $\phi$  is important here, for it will determine the phase of the pump relative to the charge on the condenser for growing oscillations to occur.

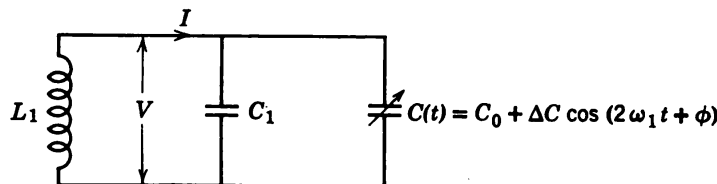


**Figure 4.3** Degenerate two-frequency parametric oscillator with a fixed capacitance in parallel with  $C(t)$ .

$$\omega_1^{-1} = \sqrt{L_1(C_1 + C_0)}$$

The circuit to be analyzed is shown in Figure 4.3. The voltage across the inductance is  $V$ , and the current through the inductance is  $I$ . The equations for the voltage and current are given by

$$\frac{dI}{dt} = -\frac{1}{L_1} V \quad (4.2a)$$

and

$$\frac{d}{dt} [(C_1 + C)V] = I \quad (4.2b)$$

The second equation follows, since  $C_1$  and  $C$  are in parallel, and the total charge on the two condensers is  $(C_1 + C)V = q$ . These coupled equations play the role of the Hamiltonian form of the equations of motion in Chapter 1, which is used because it lends itself more directly to the coupled mode form now sought. Since, by Eq. 4.1,  $C = C_0 + C_p(t)$ , Eq. 4.2b can be written as

$$\frac{dV}{dt} = \frac{1}{C_{11}} I - \frac{d}{dt} \left( \frac{C_p}{C_{11}} V \right) \quad (4.2c)$$

where  $C_{11} = C_1 + C_0$ .

The coupling coefficient  $C_p$  is a function of time. However, neglect this difficulty for the moment and proceed as in Chapter 1, Eq. 1.3, to try to put Eqs. 4.2 into normal mode form. Define, therefore, normal mode amplitudes

$$a = \frac{1}{2}\sqrt{L_1}(I + j\omega_1 C_{11} V) \quad (4.3)$$

$$a^* = \frac{1}{2}\sqrt{L_1}(I - j\omega_1 C_{11} V)$$

where

$$\omega_1 = \frac{1}{\sqrt{L_1(C_1 + C_0)}} = \frac{1}{\sqrt{L_1 C_{11}}} \quad (4.4)$$

and  $V(t)$  and  $I(t)$  are considered real variables.

Multiply Eq. 4.2c by  $\pm j\omega_1 C_{11}$  and add to Eq. 4.2a. Use the mode amplitude definitions of Eqs. 4.3 to show that these equations reduce to

$$\frac{da}{dt} = +j\omega_1 a - \frac{d}{dt}\left(\frac{C_p}{2C_{11}}(a - a^*)\right) \quad (a) \quad (4.5)$$

$$\frac{da^*}{dt} = -j\omega_1 a^* + \frac{d}{dt}\left(\frac{C_p}{2C_{11}}(a - a^*)\right) \quad (b)$$

When  $\Delta C \rightarrow 0$ ,  $C_p \rightarrow 0$ , and Eqs. 4.5 approach the normal mode form of the simple oscillator. However, when  $\Delta C \neq 0$ , it is evident that the pump couples the  $a$ - and  $a^*$ -modes, which are represented by two counterrotating vectors. As these equations stand, they are more complicated than the coupled mode formulation of Chapter 1, since  $C_p$  is time-dependent. However, they will now be simplified.

**Weak coupling approximation.** Strictly speaking, normal modes of the coupled system described by Eqs. 4.5 do not exist if  $\Delta C$  is comparable to  $C_{11}$ . However, it is now assumed that  $\Delta C \ll C_{11}$ , and this allows some simplifications to be made.

First of all, since  $\Delta C \ll C_{11}$ , the presence of the pump will alter the normal modes that existed before pumping only slightly; that is, any change that occurs in  $a$  or  $a^*$  will take place over many natural frequency ( $\omega_1$ ) cycles. Stated another way, if  $a(t) = A(t)e^{j\omega_1 t}$ ,  $A(t)$  will be a slowly varying function of time. Thus  $dA/dt \ll j\omega_1 A$ .

Next, since by Eq. 4.1  $C_p = \frac{1}{2}\Delta C\{\exp[j(2\omega_1 t + \phi)] + \exp[-j(2\omega_1 t + \phi)]\}$ , it is seen that the coupling terms on the right side of Eqs. 4.5 yield frequency components at  $\pm\omega_1$  and  $\pm 3\omega_1$ . When the circuit  $Q$  is high, the  $\pm 3\omega_1$  frequency components may be neglected. Furthermore,

in Eq. 4.5a the  $-\omega_1$  frequency term due to  $\{a \exp[-j(2\omega_1 t + \phi)]\}$  is very small compared with the  $+j\omega_1 a$  term (since  $\Delta C \ll C_{11}$ ) and may be neglected. Similarly, the  $\{a^* \exp[+j(2\omega_1 t + \phi)]\}$  term may be neglected in Eq. 4.5b. With these simplifications, Eqs. 4.5 reduce to

$$\frac{da}{dt} = j\omega_1 a + \frac{\Delta C}{4C_{11}} e^{j\phi} \frac{d}{dt} (e^{2j\omega_1 t} a^*) \quad (a) \quad (4.6)$$

$$\frac{da^*}{dt} = -j\omega_1 a^* + \frac{\Delta C}{4C_{11}} e^{-j\phi} \frac{d}{dt} (e^{-2j\omega_1 t} a) \quad (b)$$

Finally, since  $a = A e^{+j\omega_1 t}$  and  $dA/dt \ll j\omega_1 A$ , it follows that the coupling terms can be written approximately as

$$\begin{aligned} \frac{d}{dt} (e^{-2j\omega_1 t} a) &= e^{-j\omega_1 t} \left( \frac{d}{dt} - j\omega_1 \right) A \\ &\approx -j\omega_1 e^{-2j\omega_1 t} a \end{aligned}$$

[This is similar to the approximation used in the TWT equations (3.6) of Chapter 3 when  $C \ll 1$ .] Then, Eqs. 4.6 reduce to

$$\begin{aligned} \frac{da}{dt} &= j\omega_1 a + c_{12} e^{2j\omega_1 t} a^* \quad (a) \\ \frac{da^*}{dt} &= -j\omega_1 a^* + c_{21} e^{-2j\omega_1 t} a \quad (b) \end{aligned} \quad (4.7)$$

where

$$c_{12} = j\omega_1 \frac{\Delta C}{4C_{11}} e^{j\phi} = c_{21}^* \quad (4.8)$$

This will be taken as the standard form of the coupled mode equations when the coupling varies at twice the natural resonant frequency. The weak coupling approximation of Chapter 1 is equivalent to  $\Delta C \ll C_{11}$  in the present case. The time-varying capacitance is seen to couple the two counterrotating modes weakly.

Now, it might be thought that little real progress has been made toward a solution of Eqs. 4.5 after all these simplifications. As Eqs. 4.7 stand, they are a set of coupled equations with variable coefficients, just as Eqs. 4.5 are. However, there is a fundamental difference. By a simple transformation of variables, Eqs. 4.7 can be reduced to a set of coupled equations with *constant coefficients*, whereas no such transforma-

tion exists for Eqs. 4.5. Let

$$a(t) = A(t)e^{j\omega_1 t} \quad (4.9)$$

Put these into Eqs. 4.7, and it follows that

$$\begin{aligned} \frac{dA}{dt} &= c_{12}A^* \\ \frac{dA^*}{dt} &= c_{21}A \end{aligned} \quad (4.10)$$

It should be emphasized that such a transformation is possible only under the weak coupling assumption, viz.,  $\Delta C \ll C_{11}$  and the high circuit  $Q$  assumption so that other harmonics may be suppressed.

From Eqs. 4.10 it follows that normal modes of the weakly coupled system may be found. Assume solutions of the form  $\exp(st)$ . It follows that

$$s = \pm \omega_1 \frac{\Delta C}{4C_{11}} \quad (4.11)$$

and there is a growing and a decaying normal mode. The relation found in Eq. 4.8 between the coupling coefficients has assured that the pump couples the  $a$ -mode to the  $a^*$ -mode actively (see Chapter 1, Section 1.8) and that growing solutions are possible.

**Initial conditions.** The complete solution of the problem is found by the procedure that has been previously used:  $a(t)$  and  $a^*(t)$  are complex conjugates and can be expressed in terms of their initial values as

$$\begin{aligned} a(t) &= \frac{|a(0)|}{2} e^{j(\omega_1 t + \vartheta)} [(1 + je^{j(\phi - 2\vartheta)}) e^{|s|t} + (1 - je^{j(\phi - 2\vartheta)}) e^{-|s|t}] \\ a^*(t) &= \frac{|a(0)|}{2} e^{-j(\omega_1 t + \vartheta)} [(1 - je^{-j(\phi - 2\vartheta)}) e^{|s|t} + (1 + je^{-j(\phi - 2\vartheta)}) e^{-|s|t}] \end{aligned} \quad (4.12)$$

where by Eqs. 4.3

$$a(0) = |a(0)| e^{j\vartheta} = \frac{1}{2} \sqrt{L_1} [I(0) + j\omega_1 C_{11} V(0)] \quad (4.13)$$

and  $V(0)$  and  $I(0)$  are real quantities.

Consider now the case in which at  $t = 0$  the voltage is at its maximum,  $V(0) = V_m$ , and the current is zero,  $I(0) = 0$ . This is the situation shown in Figure 4.2b and c. It follows from Eq. 4.13 that  $\vartheta = \pi/2$  and  $|a(0)| = \frac{1}{2} \sqrt{C_{11}} V_m$ . Furthermore,  $C_p(0) = \Delta C \cos \phi$ , so that  $\phi$  is the phase of the pump relative to the initial voltage across the condenser. If this phase is chosen so that  $\phi = +\pi/2$ ,  $C_p(t) = -\Delta C \sin \omega t$  (Figure

4.2d), and it follows from Eqs. 4.12 that

$$\begin{aligned} a(t) &= \frac{j}{2} \sqrt{C_{11}} V_m e^{j\omega_1 t} e^{|s|t} \\ a^*(t) &= -\frac{j}{2} \sqrt{C_{11}} V_m e^{-j\omega_1 t} e^{|s|t} \end{aligned} \quad (4.14)$$

and pure exponential growing solutions occur. This agrees with the results shown in Figure 4.2d, where the square wave pumping is replaced by the sinusoidal pumping.

On the other hand, if the pump phase is chosen so that  $\phi = -\pi/2$ ,  $C_p(t) = \Delta C \sin \omega t$ , and it follows from Eqs. 4.12 that

$$\begin{aligned} a(t) &= \frac{j}{2} \sqrt{C_{11}} V_m e^{j\omega_1 t} e^{-|s|t} \\ a^*(t) &= -\frac{j}{2} \sqrt{C_{11}} V_m e^{-j\omega_1 t} e^{-|s|t} \end{aligned} \quad (4.15)$$

and only pure decaying solutions occur. This pump phase is again shown in Figure 4.2d and corresponds to pumping in such a phase that energy is extracted from the circuit in agreement with the qualitative results given earlier.

It has been shown that the phase of the pump relative to the voltage is important for growing oscillations. In general, if  $\phi - 2\vartheta = \pi(3 + 4n)/2$ , where  $n = 0, \pm 1, \pm 2, \dots$ , only growing solutions occur, whereas if  $\phi - 2\vartheta = \pi(1 + 4n)/2$ , where  $n = 0, \pm 1, \pm 2, \dots$ , only decaying solutions result. Note that  $\vartheta = \tan^{-1}[\sqrt{C_{11}} V(0)/\sqrt{L_1} I(0)]$ , which is the phase of the  $a$ -mode.

**Energy considerations. The Manley-Rowe relations.** The average energy stored in the  $a$ - and  $a^*$ -modes is equal and is given by

$$\begin{aligned} W_{\omega_1}(t) &= |a(t)|^2 = |a(0)|^2 [\cosh 2|s|t - \sin(\phi - 2\vartheta) \sinh 2|s|t] \\ &= W_{-\omega_1}(t) \equiv |a^*(t)|^2 \end{aligned} \quad (4.16)$$

so that the total average stored energy

$$W(t) = |a(t)|^2 + |a^*(t)|^2 \equiv 2|a(t)|^2 \quad (4.17)$$

is not constant. That is, energy in the oscillator is not conserved, regardless of the phase of the pump, if  $\Delta C \neq 0$ . Energy is continually being fed into or removed from the oscillator by the pump, depending on the phase of the pump relative to the voltage on the condenser. When  $\Delta C \rightarrow 0$ ,  $s = 0$  and  $W(t) \rightarrow 2|a(0)|^2$ , a constant.

Consider next two important power relations. The power fed into the

$a$ - and  $a^*$ -modes is defined by

$$P_{\omega_1}(t) = \frac{d}{dt} |a(t)|^2 \quad (4.18)$$

$$P_{-\omega_1}(t) = \frac{d}{dt} |a^*(t)|^2 \quad (4.19)$$

Since

$$P_{\omega_1}(t) = P_{-\omega_1}(t) \quad (4.20)$$

the total power supplied by the pump must be

$$P_T = 2P_{\omega_1}(t) = 2P_{-\omega_1}(t) \quad (4.21)$$

or

$$\frac{P_T}{2\omega_1} = \frac{P_{\omega_1}}{\omega_1} = \frac{P_{-\omega_1}}{\omega_1} \quad (4.22)$$

The two relations given in Eq. 4.22 are called the Manley-Rowe relations.<sup>1-7</sup> They were derived here for a very simple example, and a much more general derivation is given later. They show that power is supplied by the pump to the  $a$ - and  $a^*$ -modes in equal amounts. Further, the power associated with the modes is *not* separately conserved. The power given to or taken from the oscillator comes from the pump, so that the pump and oscillator powers taken together as a system are conserved.

#### 4.3 The General Coupled Mode Approach for Nondegenerate Parametrically Coupled Elements

One might ask what use the Manley-Rowe relations have for parametric amplifiers. Recall in Chapter 1, Section 1.5, that energy conservation led to a general relation that must be satisfied by the mutual coupling coefficients, viz.,  $c_{12} = -c_{21}^*$  (Eq. 1.33). In the parametric amplifier it has just been shown that energy is no longer conserved among the modes when the coupling coefficients are time-dependent. The Manley-Rowe relations, therefore, replace energy conservation in order to find the relationship among the time-dependent coupling coefficients when the general coupled mode approach analogous to Chapter 1, Section 1.5, is used.

**General equations.** To see how the general approach is used, write the coupled mode equations as

$$\begin{aligned} \frac{da_1}{dt} &= j\omega_1 a_1 + c_{12} e^{j\omega t} a_2^* & (a) \\ \frac{da_2^*}{dt} &= -j\omega_2 a_2^* + c_{21} e^{-j\omega t} a_1 & (b) \end{aligned} \quad (4.23)$$

A few words must be said about these equations. They are a generalization of Eqs. 4.7 in that  $\omega_1 \neq \omega_2$ . They represent coupling between counterrotating modes of different frequencies that can be realized if two resonant circuits of frequency  $\omega_1$  and  $\omega_2$  are coupled together by a time-varying inductance or capacitance, which varies, for example, as

$$C = C_0 + \Delta C \cos(\omega t + \phi) \quad (4.24)$$

Further, from the simplifying assumptions made to obtain Eqs. 4.7 it should be obvious that we must require that  $\Delta C \ll C_{11}$  and that the two circuits have ideal filters, as shown in Figure 4.4, so that circuit 1 supports only frequency  $\omega_1$  and circuit 2 supports only frequency  $\omega_2$ . Also, the pump frequency must be taken as

$$\omega = \omega_1 + \omega_2 \quad (4.25)$$

so that the  $a_1$ -mode will be actively coupled to the  $a_2^*$ -mode. (It will turn out that the  $a_1$ -mode is coupled passively to the  $a_2$ -mode if  $\omega = \omega_1 - \omega_2$  and no growing oscillations can occur.)

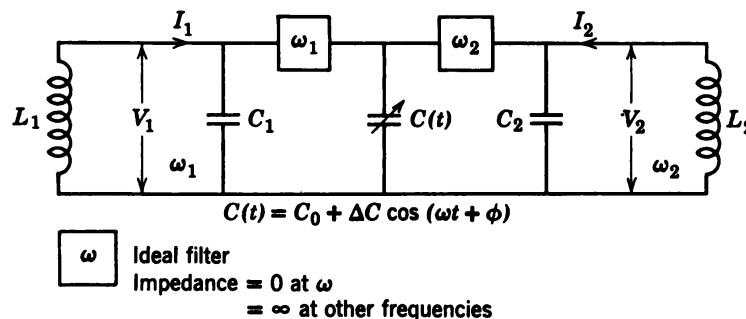


**Figure 4.4** Three-frequency parametric oscillator showing idler tank circuit.  $\omega_1 = [L_1(C_1 + C_0)]^{-\frac{1}{2}}$ ,  $\omega_2 = [L_2(C_2 + C_0)]^{-\frac{1}{2}}$ ,  $\omega = \omega_1 + \omega_2$ . (From Suhl, Reference 96.)

**Consequences of the Manley-Rowe relations.** It will be shown in Section 4.4 that the generalization of the Manley-Rowe relations given in Eq. 4.22 for the present case is

$$\boxed{\frac{P}{\omega} = \frac{P_{\omega_1}}{\omega_1} = \frac{P_{-\omega_2}}{\omega_2}} \quad (4.26)$$

where  $P = P_{\omega_1} + P_{-\omega_2}$ . From these relations it will be shown that

$$\boxed{\frac{c_{12}}{\omega_1} = \frac{c_{21}^*}{\omega_2}} \quad (4.27)$$

Conversely, if the mutual coupling coefficients satisfy Eq. 4.27, then Eq. 4.26 follows. This converse was proved in Section 4.3, in which  $c_{12} = c_{21}^*$  was proved by the direct coupled mode approach (Eq. 4.8 with  $\omega_1 = \omega_2$ ).

Assume now that the Manley-Rowe relations (Eq. 4.26) are satisfied. It follows that

$$\frac{d}{dt} \frac{|a_1|^2}{\omega_1} = \frac{d}{dt} \frac{|a_2^*|^2}{\omega_2} \quad (4.28)$$

By Eqs. 4.23 and their complex conjugates

$$\begin{aligned} \frac{d}{dt} \frac{|a_1|^2}{\omega_1} &= e^{j\omega t} \frac{c_{12}}{\omega_1} a_1^* a_2^* + e^{-j\omega t} \frac{c_{12}^*}{\omega_1} a_1 a_2 \\ \frac{d}{dt} \frac{|a_2^*|^2}{\omega_2} &= e^{-j\omega t} \frac{c_{21}}{\omega_2} a_2 a_1 + e^{j\omega t} \frac{c_{21}^*}{\omega_2} a_2^* a_1^* \end{aligned} \quad (4.29)$$

Since the Manley-Rowe relation of Eq. 4.28 must be identically true for all time, it follows from Eqs. 4.29 that  $c_{12}$  and  $c_{21}^*$  must be related by Eq. 4.27.

**Evaluation of the mutual coupling coefficients.** In the general coupled mode approach used in Chapter 1, a particular problem had to be considered in order to evaluate the  $c_{ij}$ 's. This situation is true here also.

Consider then the two resonant circuits shown in Figure 4.4 which are parametrically coupled by a time-varying capacitance whose variation is given by Eq. 4.24. Define the mode amplitudes by

$$\begin{aligned} a_1 &= \frac{1}{2} \sqrt{L_1} (I_1 + j\omega_1 C_{11} V_1) \\ a_2^* &= \frac{1}{2} \sqrt{L_2} (I_2 - j\omega_2 C_{22} V_2) \end{aligned} \quad (4.30)$$

where  $C_{11} = C_1 + C_0$ ,  $C_{22} = C_2 + C_0$ ,  $\omega_1^2 = (L_1 C_{11})^{-1}$ , and  $\omega_2^2 = (L_2 C_{22})^{-1}$ .  $V_{1,2}$  and  $I_{1,2}$  are real and are shown in the figure. Since only the  $a_1$ - and  $a_2^*$ -modes are coupled by the pump to any extent when  $\omega = \omega_1 + \omega_2$ , as may be seen if the direct coupled mode approach is used,  $a_1^*$  and  $a_2$  need not be considered. They will yield no new information and will be needed only to match boundary conditions.

In order to evaluate  $c_{12}$ , an argument analogous to that of Chapter 1, Section 1.5 may be used. The algebra is rather tedious and is carried out in Appendix H. The result is that

$$c_{12} = j \frac{\omega_1}{4} \frac{\Delta C e^{j\phi}}{\sqrt{C_{11} C_{22}}} = \frac{\omega_1}{\omega_2} c_{21}^* \quad (4.31)$$

**Initial conditions.** In order to solve the coupled equations (4.23), let

$$\begin{aligned} a_1 &= A_1(t)e^{j\omega_1 t} \\ a_2^* &= A_2^*(t)e^{-j\omega_2 t} \end{aligned} \quad (4.32)$$

This transformation reduces Eqs. 4.23 to

$$\begin{aligned} \frac{dA_1}{dt} &= c_{12}A_2^* \\ \frac{dA_2^*}{dt} &= c_{21}A_1 \end{aligned} \quad (4.33)$$

which have solutions of the form  $\exp(st)$  where

$$s = \pm \sqrt{c_{12}c_{21}} = \frac{\pm \sqrt{\omega_1\omega_2} \Delta C}{4\sqrt{C_{11}C_{22}}} \quad (4.34)$$

Therefore, the general solutions of Eqs. 4.23 are

$$\begin{aligned} a_1(t) &= e^{j\omega_1 t} \left( a_1(0) \cosh |s|t + j \sqrt{\frac{\omega_1}{\omega_2}} e^{j\phi} a_2^*(0) \sinh |s|t \right) \\ a_2^*(t) &= e^{-j\omega_2 t} \left( a_2^*(0) \cosh |s|t - j \sqrt{\frac{\omega_2}{\omega_1}} e^{-j\phi} a_1(0) \sinh |s|t \right) \end{aligned} \quad (4.35)$$

where  $a_1(0)$  and  $a_2^*(0)$  are found from Eqs. 4.30 in terms of the initial voltages and currents.

**Phase of the "pump" relative to the charge.** The average energy stored in the  $a_1$ - and  $a_2^*$ -modes is given by  $W_1 = 2|a_1(t)|^2$  and  $W_2 = 2|a_2^*(t)|^2$ , respectively. It is now easily seen that any phase of the pump relative to the charge on the condenser plates will lead to growth in contrast to the degenerate oscillator of Section 4.2. For, if there is to be no growth of oscillation, by Eqs. 4.35 it must be true that

$$a_1(0) = -j \sqrt{\frac{\omega_1}{\omega_2}} e^{j\phi} a_2^*(0) \quad (4.36)$$

Unless  $\omega_1 = \omega_2$ , this condition cannot be satisfied. The  $\omega_2$  circuit will therefore always start oscillating in the correct phase relative to the

pump and charge on the variable condenser at frequency  $\omega_1$  so that power will be fed into both tank circuits in agreement with Eq. 4.26.

Another way of stating this may prove useful. Suppose only tank circuit 1 is oscillating at  $t = 0$  when the pump is applied. Then  $a_2^*(0) = 0$ . To satisfy relation (Eq. 4.36)  $a_1(0)$  would have to be zero also, but this is trivial. In general, therefore, the oscillations will always grow regardless of the phase of the pump when an idler circuit is available. This was first pointed out by H. Suhl<sup>8</sup> and is very important when these devices are used for amplifiers. In an amplifier there can be no control over the phase of the incoming signal relative to the pump. If only the degenerate circuit were available, sometimes the signal would be amplified and sometimes attenuated. Therefore, the nondegenerate three-frequency circuit considered in this section must be used.

#### 4.4 The Manley-Rowe Relations<sup>1-7</sup>

The Manley-Rowe relations were derived in Section 4.2 for a time-varying capacitance under small signal conditions for the degenerate parametric oscillator. By using the same direct coupled mode approach, these relations could be derived for the nondegenerate case treated in Section 4.3. However, they were assumed to be true so that the general coupled mode approach could be used. A more rigorous proof<sup>7</sup> will now be given, since these relations are of much more general validity than would be indicated by the proof given in Section 4.2 and are of great importance in nonlinear phenomena.

Consider an arbitrary nonlinear capacitor whose characteristics are specified by giving the voltage as a function of the charge:

$$v = f(q) \quad (4.37)$$

where  $q$  is the charge on the nonlinear capacitor and  $v$  is the voltage across it. For a linear capacitor this reduces to

$$v = \frac{1}{C} q$$

where  $C$  is the capacitance. The analysis assumes that there is no hysteresis in the voltage, so that  $f(q)$  is a single-valued function but otherwise its shape is arbitrary.\*

Now assume that signals at two incommensurate frequencies,  $\omega_1$  and

\* The capacitor could equally well be described by giving the charge as a single-valued function of the voltage. The same analysis will apply to a nonlinear inductor by specifying the flux as a single-valued function of the current, or vice versa.

$\omega_2$ , are applied by signal generators to the capacitor. From considerations of a square law detector, for example, it will be seen that the nonlinear characteristic of the capacitor will give rise to sum and difference frequencies,  $\omega_1 \pm \omega_2$  as well as all frequencies of the form  $\Omega_{mn} = m\omega_1 + n\omega_2$ , where  $m$  and  $n$  take on all integral values, positive, negative, or zero.

It should be clear that power can be supplied to or taken from the capacitor at any of these frequencies. However, to do this a load must be connected to develop a voltage. Figure 4.5 shows the nonlinear capacitor connected to an equivalent external circuit consisting of a generator, which puts out a single frequency, a conductance, and an ideal filter, which has zero impedance at the generator frequency and infinite impedance at all other frequencies. If power is not being supplied to the nonlinear capacitor at a particular frequency, the generator voltage at this frequency is set equal to zero, leaving only the load and the filter. Thus, if power is being applied only at  $\omega_1$  and  $\omega_2$ , only these two branches will contain voltage generators and all other branches will contain only passive load impedances.

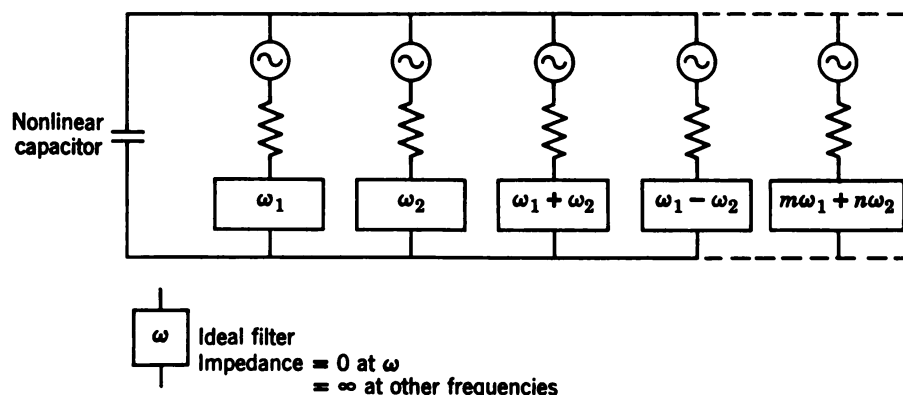


**Figure 4.5** Illustrative circuit connected to nonlinear capacitor. Each frequency flows in a separate circuit. If power is absorbed only at a particular frequency, the voltage of the corresponding generator is zero. (From Manley and Rowe, Reference 1.)

Now to the mathematical description. Since all frequencies  $\Omega_{mn}$  can exist, the charge flowing into the nonlinear capacitor can be written as a double Fourier series:

$$q = \sum_{m=-\infty}^{+\infty} \sum_{n=-\infty}^{+\infty} Q_{m,n} e^{j(mx+ny)} \quad (4.38)$$

where<sup>9</sup>

$$x = \omega_1 t, \quad y = \omega_2 t \quad (4.39)$$

Since  $q$  is real, the expansion coefficients,  $Q_{m,n}$ , must satisfy

$$Q_{m,n} = Q_{-m,-n}^* \quad \text{or} \quad Q_{-m,-n} = Q_{m,n}^* \quad (4.40)$$

The current flowing through the nonlinear capacitor is found by taking the total derivative of the charge (Eq. 4.38) with respect to time. Then

$$i = \frac{dq}{dt} = \sum_{m=-\infty}^{+\infty} \sum_{n=-\infty}^{+\infty} I_{m,n} e^{j(mx+ny)} \quad (4.41)$$

where

$$I_{m,n} = j\Omega_{mn} Q_{m,n} \equiv j(m\omega_1 + n\omega_2) Q_{m,n} = I_{-m,-n}^* \quad (4.42)$$

Similarly, expand the voltage across the capacitor:

$$v = \sum_{m=-\infty}^{+\infty} \sum_{n=-\infty}^{+\infty} V_{m,n} e^{j(mx+ny)} \quad (4.43)$$

where

$$V_{m,n} = V_{-m,-n}^* \quad (4.44)$$

The average power flowing into the nonlinear capacitor at the frequencies  $\pm |m\omega_1 + n\omega_2|$  is

$$\begin{aligned} P_{m,n} &= 2 \operatorname{Re} V_{m,n} I_{m,n}^* = -2(m\omega_1 + n\omega_2) \operatorname{Re} (jV_{m,n} Q_{m,n}^*) \\ &= P_{-m,-n} \end{aligned} \quad (4.45)$$

where Eqs. 4.40, 4.42, and 4.44 have been used.

Now assume that the nonlinear capacitor is lossless. The total average power flowing into the capacitor must be zero, since energy is conserved. Then

$$\sum_{m=-\infty}^{+\infty} \sum_{n=-\infty}^{+\infty} P_{m,n} = 0 \quad (4.46)$$

In order to obtain the desired Manley-Rowe relations, rewrite Eq. 4.46 by multiplying and dividing each term by its corresponding frequency:<sup>5</sup>

$$\sum_{m=-\infty}^{+\infty} \sum_{n=-\infty}^{+\infty} (m\omega_1 + n\omega_2) \frac{P_{m,n}}{(m\omega_1 + n\omega_2)} = 0 \quad (4.47)$$

Split this equation into two terms and rewrite it as

$$\omega_1 \sum_{m=-\infty}^{+\infty} \sum_{n=-\infty}^{+\infty} \frac{mP_{m,n}}{m\omega_1 + n\omega_2} + \omega_2 \sum_{m=-\infty}^{+\infty} \sum_{n=-\infty}^{+\infty} \frac{nP_{m,n}}{m\omega_1 + n\omega_2} = 0 \quad (4.48)$$

Consider the first double sum in Eq. 4.48. It can be rewritten as

$$\begin{aligned}
 \sum_{n=-\infty}^{+\infty} \sum_{m=-\infty}^{+\infty} \frac{mP_{mn}}{m\omega_1 + n\omega_2} &= \sum_{n=-\infty}^{+\infty} \left( \sum_{m=-\infty}^0 \frac{mP_{mn}}{m\omega_1 + n\omega_2} + \sum_{m=0}^{\infty} \frac{mP_{mn}}{m\omega_1 + n\omega_2} \right) \\
 &= \sum_{n=-\infty}^{+\infty} \left( \sum_{m=0}^{+\infty} \frac{-mP_{-m,-n}}{(-m\omega_1 - n\omega_2)} + \sum_{m=0}^{\infty} \frac{mP_{mn}}{m\omega_1 + n\omega_2} \right) \\
 &= 2 \sum_{n=-\infty}^{+\infty} \sum_{m=0}^{\infty} \frac{mP_{mn}}{m\omega_1 + n\omega_2} \tag{4.49}
 \end{aligned}$$

where in the first equality the sum over  $m$  has been split up from  $m = -\infty$  to 0 and from 0 to  $+\infty$ ; in the second equality  $m$  has been replaced by  $-m$  and  $n$  by  $-n$ ; in the final equality  $P_{-m,-n}$  has been replaced by  $P_{m,n}$  by Eq. 4.45.

A similar argument reduces the second term in Eq. 4.48, which can now be written as

$$\omega_1 \sum_{n=-\infty}^{+\infty} \sum_{m=0}^{\infty} \frac{mP_{mn}}{\Omega_{mn}} + \omega_2 \sum_{m=-\infty}^{+\infty} \sum_{n=0}^{\infty} \frac{nP_{mn}}{\Omega_{mn}} = 0 \tag{4.50}$$

by Eq. 4.49.

It will now be proved that both of the foregoing sums are separately equal to zero, i.e.,

$$\begin{aligned}
 \sum_{m=0}^{\infty} \sum_{n=-\infty}^{+\infty} \frac{mP_{mn}}{m\omega_1 + n\omega_2} &= 0 \\
 \sum_{m=-\infty}^{+\infty} \sum_{n=0}^{\infty} \frac{nP_{mn}}{m\omega_1 + n\omega_2} &= 0
 \end{aligned} \tag{4.51}$$

These are the desired Manley-Rowe relations.

To prove these relations, consider an extremely large number of identical nonlinear capacitors, which is called an ensemble, to use the language of statistical mechanics. Let the frequencies  $\omega_1$  and  $\omega_2$  be different for each element of the ensemble (capacitor). These are applied frequencies; the capacitors can be identical but yet have different frequencies. However, require that the voltage and charge expansion coefficients,  $V_{mn}$  and  $Q_{mn}$ , be identical for each element. In order to satisfy these requirements, the *external* impedances and generators in the equivalent circuit of Figure 4.5 will be different for each element of the ensemble, since  $\omega_1$  and  $\omega_2$  are all different. But these impedances and generators are external to the capacitors that are all identical. Since  $V_{mn}$  and  $Q_{mn}$  are identical for each element of the ensemble, it follows

from Eq. 4.45 that  $P_{mn}/(m\omega_1 + n\omega_2)$  will be identical for every element of the ensemble. Since each element has a different  $\omega_1$  and  $\omega_2$ , then  $P_{mn}/(m\omega_1 + n\omega_2)$  must be independent of  $\omega_1$  and  $\omega_2$ . Further, Eq. 4.50 must hold for every element of the ensemble, i.e., it must hold identically for all  $\omega_1$  and  $\omega_2$ . This can be true if and only if the coefficients of  $\omega_1$  and  $\omega_2$  are separately equal to zero, which yields Eqs. 4.51.

It is easy to see that if all frequencies except  $\omega_1$ ,  $\omega_2$ , and  $\omega_1 + \omega_2$  are shorted out, Eqs. 4.51 will reduce to

$$\begin{aligned} \frac{P_{10}}{\omega_1} + \frac{P_{11}}{\omega_1 + \omega_2} &= 0 \\ \frac{P_{01}}{\omega_2} + \frac{P_{11}}{\omega_1 + \omega_2} &= 0 \end{aligned} \quad (4.52)$$

This is just the special case used in the three frequency parametric oscillator in Eq. 4.26 of Section 4.3. If  $P_{10}$  and  $P_{01}$  are negative, power is being supplied *by* the capacitor at frequencies  $\omega_1$  and  $\omega_2$ , respectively. Then, by Eqs. 4.52 power,  $P_{11}$ , must be supplied *to* the condenser at frequency  $\omega_1 + \omega_2$ . Therefore, in Eq. 4.26  $P$  is the mechanical power supplied to the condenser, so that  $P = -P_{11}$  in order that Eqs. 4.26 and 4.52 may agree in sign.

Another special case occurs if only frequencies  $\omega_1$ ,  $\omega_2$ , and  $\omega_1 - \omega_2$  are present. Then Eqs. 4.51 reduce to

$$\begin{aligned} \frac{P_{10}}{\omega_1} + \frac{P_{1,-1}}{\omega_1 - \omega_2} &= 0 \\ \frac{P_{01}}{\omega_2} - \frac{P_{1,-1}}{\omega_1 - \omega_2} &= 0 \end{aligned} \quad (4.53)$$

These equations are used later for the frequency converter.

The derivation of Eqs. 4.51 applies to steady-state conditions, whereas the Manley-Rowe relations were used in Section 4.3 in connection with growing oscillatory conditions. However, it follows from Eqs. 4.23, 4.31, and 4.32 that the rate of growth is very slow, since

$$s^2 \ll \omega_1 \omega_2$$

so that the growth is a quasi-stationary process and the error involved should be small.

Several other points should be noted. The derivation of Eqs. 4.51 did not use a linearized theory, whereas the derivation in Section 4.2 linearized the system. Accordingly, the Manley-Rowe relations are valid for large or small signal theory.

There is no a priori reason why a specific nonlinear medium, such as an electron beam or ferrite, should obey the Manley-Rowe relations. However, it appears that many nonlinear media do obey these relations.<sup>10, 11, 12, 178</sup> They were derived for a nonlinear inductance or capacitance, but they do not apply to a nonlinear resistor.<sup>13</sup> Therefore, they must be shown to be valid for a medium before the general coupled mode approach can be used.

Finally, the general analysis was given for a nonlinear rather than a time-varying capacitor. It is very simple to give a plausibility argument that the two are equivalent. Expand the charge in a Taylor series in the voltage:

$$q = \sum_0^{\infty} a_n(v - v_0)^n \quad (4.54)$$

where  $v_0$  is some reference voltage. The capacitance may be defined as either  $dq/dv$  or  $q/v$ .<sup>14</sup> One must always be careful to note which definition is used. Let

$$C(v) = \frac{dq}{dv} = \sum_1^{\infty} a_n n(v - v_0)^{n-1} \quad (4.55)$$

If the voltage varies sinusoidally as  $v - v_0 = b \cos \omega t$ , then

$$\begin{aligned} C(v) \rightarrow C(t) &= \sum_1^{\infty} a_n n \left(\frac{b}{2}\right)^{n-1} (e^{j\omega t} + e^{-j\omega t})^{n-1} \\ &\equiv \sum_{-\infty}^{+\infty} C_n e^{jn\omega t} \end{aligned} \quad (4.56)$$

where the  $C_n$ 's are combinations of the  $a_n$ 's. Therefore, the nonlinear capacitor is equivalent to a time-varying capacitance. For small voltage variation

$$C \cong C_0 + C_1 \cos(\omega t + \phi) \quad (4.57)$$

where  $C_1 \ll C_0$ , which is the form that has been assumed in the equivalent circuits in the two preceding sections.

#### 4.5 The Three-Frequency Parametric Amplifier. Gain

It must now be shown how the three-frequency oscillator of Section 4.3 (Figure 4.4) can be used as an amplifier.\* Provision must be made

\* The degenerate case of Section 4.2 is not considered, since the gain is sensitive to the phase of the pump relative to the signal applied just as the condition for growing oscillations was found to be phase sensitive. It is therefore of no value as an amplifier. It has applications in computers, however.

for coupling a signal into the circuit at  $\omega_1$  (or  $\omega_2$ ) and for removing the enlarged signal at  $\omega_1$  (or  $\omega_2$ ). This may be accomplished with an isolator or a circulator.

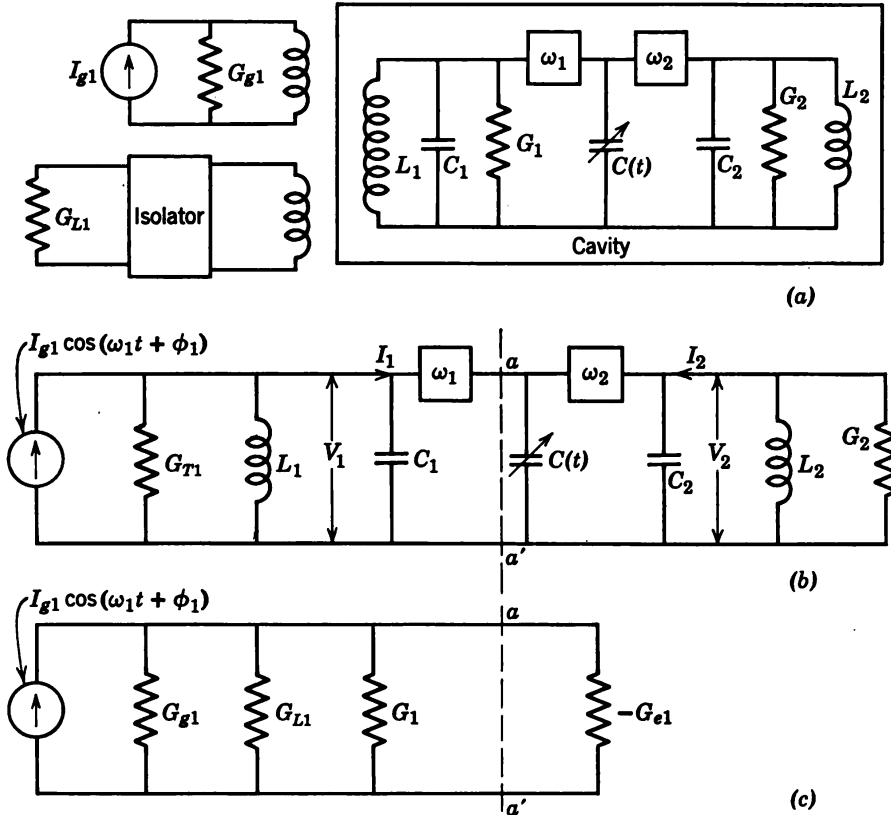


**Figure 4.6** (a) Schematic diagram of a transmission type, three-frequency parametric amplifier using an isolator; (b) equivalent circuit with variable capacitance; (c) equivalent circuit for gain calculation. (From Tien, Reference 16.)

Figure 4.6a shows a schematic diagram of a transmission-type cavity three-frequency parametric amplifier. The  $\omega_1$ - and  $\omega_2$ -circuits represent two resonant modes of the cavity. The cavity losses for each mode are given by conductances  $G_1$  and  $G_2$ , respectively. Ideal filters allow only current at frequency  $\omega_1$  to flow in the  $\omega_1$ -mode and current at  $\omega_2$  in the  $\omega_2$ -mode. The  $\omega_1$ -mode is coupled at the input terminal to a signal generator at frequency  $\omega_1$ , which has an internal conductance  $G_{g1}$ , and at the output terminal to a load,  $G_{L1}$ , through an isolator. Because of the isolator, the load is always matched to the cavity. Therefore, the equivalent circuit for this amplifier is shown in Figure 4.6b, where

$$G_{T1} = G_{g1} + G_{L1} + G_1 \quad (4.58)$$

Figure 4.7a shows a schematic diagram for a reflection-type cavity amplifier. Power from the signal generator at the  $\omega_1$ -circuit resonant frequency is fed to the cavity from port 1 through port 2 of a circulator. Power reflected from the cavity goes to the load at port 3, whereas power reflected from the load goes to port 4 where it is totally absorbed by a matched load. Therefore, by the nature of a circulator, the cavity is always matched to the generator and the load.

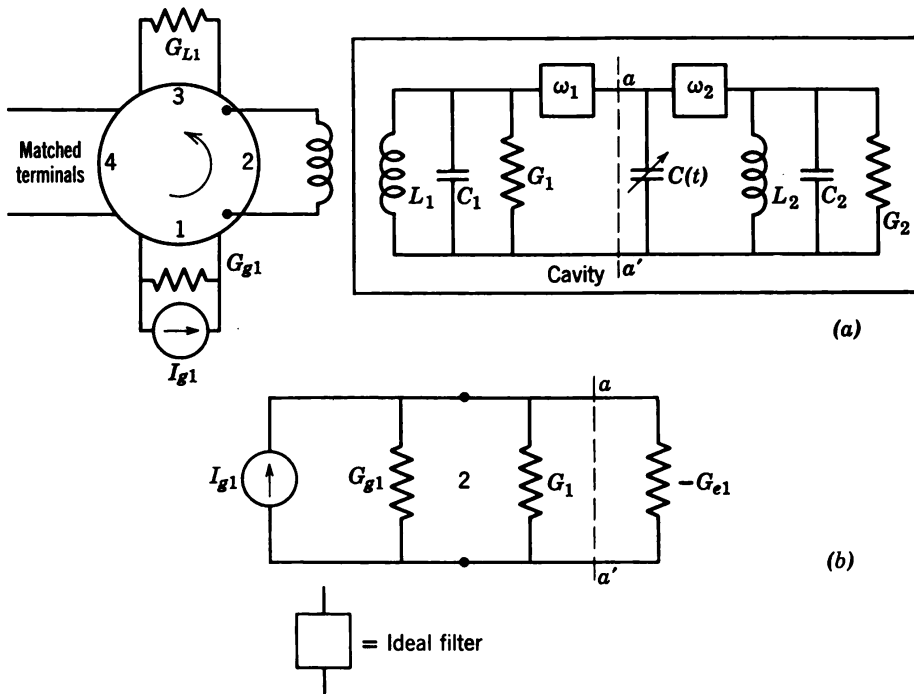


**Figure 4.7** (a) Schematic diagram of a reflection type, three-frequency parametric amplifier using a circulator; (b) equivalent circuit for gain calculation. (From Tien, Reference 16.)

Heffner and Wade<sup>15</sup> computed the gain and noise figure of the transmission-type amplifier, which is summarized in a review paper by Tien.<sup>16</sup> Their analysis uses a strict circuit theory point of view which gives a very useful method of treating the problem. However, the present treatment will use coupled modes in order to show how loss may be put in the theory. We consider first the transmission-type cavity.

In order to study the amplifier, it must be shown how a shunt conductance modifies the coupled mode theory. All loss has been neglected up to this point. The modification necessary when loss is considered is given in Appendix I. It is shown there that Eqs. 4.23 are modified by

letting

$$\begin{aligned}\omega_1 &\rightarrow \omega_1 \left( 1 + j \frac{1}{2Q_1} \right) \\ -\omega_2 &\rightarrow -\omega_2 \left( 1 - j \frac{1}{2Q_2} \right)\end{aligned}\quad (4.59)$$

where  $Q_1 = \omega_1 C_{11}/G_{T1}$ ,  $Q_2 = \omega_2 C_{22}/G_2$ . The mode amplitudes given in Eq. 4.30 are modified so that

$$\begin{aligned}a_1 &= \frac{1}{2} \sqrt{L_1} \left[ I_1 + j\omega_1 C_{11} \left( 1 - \frac{j}{2Q_1} \right) V_1 \right] \\ a_2^* &= \frac{1}{2} \sqrt{L_2} \left[ I_2 - j\omega_2 C_{22} \left( 1 + \frac{j}{2Q_2} \right) V_2 \right]\end{aligned}\quad (4.60)$$

The effect of loss on the coupling coefficients,  $c_{12}$  and  $c_{21}$ , in Eq. 4.31 is small and neglected.

One further modification of the coupled mode equations (4.23) is necessary, since a signal is applied at frequency  $\omega_1$  to tank 1. Since  $da_1/dt$  is proportional to  $\frac{1}{2} \sqrt{L_1} (dI_1/dt)$ , the time derivative of the signal driving current must be added to the right side of Eq. 4.23a and must also be multiplied by the normalizing constant  $\frac{1}{2} \sqrt{L_1}$ . Therefore, coupled mode form of the equations for two parametrically coupled oscillators with loss and a driving term become

$$\begin{aligned}\frac{da_1}{dt} &= c_{11}a_1 + c_{12}e^{j\omega t}a_2^* + D e^{j\omega_1 t} \\ \frac{da_2^*}{dt} &= c_{22}a_2^* + c_{21}e^{-j\omega t}a_1\end{aligned}\quad (4.61)$$

where

$$\begin{aligned}c_{11} &= j\omega_1 \left( 1 + j \frac{1}{2Q_1} \right) \\ c_{22} &= -j\omega_2 \left( 1 - j \frac{1}{2Q_2} \right) \\ c_{12} &= \frac{\omega_1}{\omega_2} c_{21}^* = \frac{j\omega_1 \Delta C e^{j\phi}}{4 \sqrt{C_{11} C_{22}}}\end{aligned}\quad (4.62)$$

$$D = j\omega_1 \sqrt{L_1} \frac{I_{g1}}{4} e^{j\phi_1}$$

where  $\frac{1}{2}I_g e^{j(\omega_1 t + \phi_1)}$  is the applied signal (see Figure 4.6) and the new mode amplitudes are given by Eqs. 4.60. It has been tacitly assumed that  $\omega = \omega_1 + \omega_2$ .

In order to remove the time-varying coefficients, let

$$\begin{aligned} a_1 &= A_1(t)e^{j\omega_1 t} \\ a_2^* &= A_2^*(t)e^{-j\omega_2 t} \end{aligned} \quad (4.63)$$

The resulting equations in  $A_1$  and  $A_2^*$  are

$$\begin{aligned} \left( \frac{d}{dt} + \frac{\omega_1}{2Q_1} \right) A_1 &= c_{12}A_2^* + D \\ \left( \frac{d}{dt} + \frac{\omega_2}{2Q_2} \right) A_2^* &= c_{21}A_1 \end{aligned} \quad (4.64)$$

There are two special cases to be considered, viz., the parametric oscillator and the parametric amplifier. The oscillator without loss was considered in Section 4.3.

**Case I. Oscillator.** For the oscillator,  $D = 0$  (no applied signal), and solutions of Eqs. 4.64 vary as  $\exp(st)$  where

$$s = -\frac{1}{4} \left( \frac{\omega_1}{Q_1} + \frac{\omega_2}{Q_2} \right) \pm \sqrt{\frac{1}{16} \left( \frac{\omega_1}{Q_1} - \frac{\omega_2}{Q_2} \right)^2 + \frac{\omega_1 \omega_2 (\Delta C)^2}{16 C_{11} C_{22}}} \quad (4.65)$$

This should be compared with Eq. 4.34, where  $Q_1$  and  $Q_2$  were infinite. From Eq. 4.65 it is seen that growing oscillations will now occur only if the square root term is larger than the decaying term  $-\frac{1}{4}(\omega_1/Q_1 + \omega_2/Q_2)$ . This condition is seen to be

$$\frac{\Delta C}{\sqrt{C_{11} C_{22}}} > \frac{2}{\sqrt{Q_1 Q_2}} \quad (4.66)$$

before growing oscillations can occur. This is typical of regenerative oscillators: an effective negative resistance must overcome the positive resistance (losses) before sustained oscillations will occur.

**Case 2. Amplifier.** To use this device as a regenerative amplifier, the pump is reduced to a value below the oscillation threshold (Eq. 4.66), so that an input sinusoidal signal will emerge as an enlarged sinusoidal signal that is proportional to the input amplitude. Therefore, if a signal is applied at frequency  $\omega_1$ , enlarged solutions of the form of Eqs. 4.63 are desired in which  $A_1(t)$  and  $A_2^*(t)$  are constants. These will represent the steady-state solutions (or particular integrals) due to

the driving term of Eqs. 4.61. To find these solutions, put  $d/dt = 0$  in Eqs. 4.64. These equations then merely become two algebraic equations for  $A_1$  and  $A_2^*$  in terms of  $D$ . It is easily found that

$$A_1 = j \frac{I_{g1}}{2} e^{j\phi_1} \frac{\sqrt{C_{11}}}{(G_{T1} - G_{e1})} \quad (4.67)$$

$$A_2^* = I_{g1} e^{j(\phi_1 - \phi)} \frac{G_{e1}}{(G_{T1} - G_{e1})} \frac{\sqrt{C_{11}C_{22}}}{\Delta C} \sqrt{L_1}$$

where

$$-G_{e1} = -\frac{\omega_1\omega_2(\Delta C)^2}{4G_2} \quad (4.68)$$

is the effective negative conductance across the circuit when the applied signal frequency is at the circuit resonance frequency  $\omega_1$ . Figure 4.6c shows the equivalent circuit when the variable capacitance and idler circuits are replaced by the negative conductance  $-G_{e1}$ .

Now compute the power gain of the amplifier. The voltage across the load,  $G_{L1}$ , is  $V_1 \cong -j(a_1 - a_1^*)/\sqrt{C_{11}}$  from Eqs. 4.60 when  $Q_1 \gg 1$ , and the current through  $G_{L1}$  is  $I_{G_{L1}} = V_1 G_{L1}$ , so that the average power supplied to  $G_{L1}$  is

$$\begin{aligned} P &= \overline{V_1^2} G_{L1} = -\overline{(a_1 - a_1^*)^2} \frac{G_{L1}}{C_{11}} \\ &= -\overline{(A_1 e^{j\omega_1 t} - A_1^* e^{-j\omega_1 t})^2} \frac{G_{L1}}{C_{11}} = 2|A_1|^2 \frac{G_{L1}}{C_{11}} \\ &= \frac{I_{g1}^2}{2} \frac{G_{L1}}{(G_{T1} - G_{e1})^2} \end{aligned} \quad (4.69)$$

where the last equality follows from Eqs. 4.67. The *available* signal input power is  $I_{g1}^2/4G_{g1} \cos^2(\omega_1 t + \phi_1) = I_{g1}^2/8G_{g1}$ . Therefore, the power gain of the transmission-type parametric amplifier is

$$\text{power gain} \equiv g^2 = \frac{4G_{g1}G_{L1}}{(G_{L1} + G_{g1} + G_1 - G_{e1})^2} \quad (4.70)$$

The gain is infinite when the pump power ( $\Delta C$ ) is adjusted so that  $G_{e1} = G_{T1}$ . It is easy to check that this is just the oscillation threshold given in Eq. 4.66. There is always danger that the amplifier will oscillate, since for large gain it is operated so that  $G_{e1} \cong G_{T1}$ .

Consider next the reflection type amplifier of Figure 4.7a. The effect of the variable reactor is to introduce the *same* negative conductance,

$-G_{e1}$ , across the line at  $a-a'$  as in the transmission type. Since the cavity is matched to the load and signal generator, Figure 4.7b is the equivalent circuit, and the power gain is just the square of the cavity reflection coefficient, viz.,

$$\text{power gain} \equiv g^2 = \left[ \frac{G_{g1} - (G_1 - G_{e1})}{G_{g1} + (G_1 - G_{e1})} \right] \quad (4.71)$$

This should be compared with the transmission gain of Eq. 4.70. The reflection gain is infinite when  $G_{e1} = G_{g1} + G_1$ .

#### 4.6 Noise Figure of Parametric Amplifiers

The principal virtue of parametric amplifiers is their low noise figure. In this section noise figure and excess noise temperature of an amplifier are defined and the noise figures for both transmission and reflection type amplifiers are discussed.

A microwave amplifier in its simplest form consists of a circuit and an active medium. In the TWT the circuit is usually a helix and the active medium is the electron beam. Any circuit loss will radiate Johnson thermal noise<sup>17</sup> which is proportional to the temperature. The active medium will also have noise associated with it. The beam, for example, is emitted from a hot cathode in a random manner which is a source of noise. In order to describe the amount of noise that an amplifier adds to a signal, Friis<sup>18</sup> defined a noise figure as the ratio of the noise-to-signal power ratio at the output to that at the input when the input is terminated with a matched resistance at 290° (room temperature). This resistance contributes an input thermal noise power of  $kTB$ , where  $k$  is Boltzmann's constant ( $1.38 \times 10^{-23}$  joule/degree),  $T = 290^\circ$ , and  $B$  is the amplifier bandwidth in cycles per second. Therefore, the noise figure is defined by

$$\begin{aligned} F &= \left( \frac{\text{output noise}}{\text{output signal}} \right) \times \left( \frac{\text{input signal}}{\text{input noise}} \right) \\ &= \frac{\text{output noise}}{kB \ 290^\circ} \times \frac{1}{\text{gain}} \end{aligned} \quad (4.72)$$

The noise figure is a pure number. If the amplifier introduces no noise, the output noise power is just the input noise  $kB$  290° times the gain and  $F = 1$ . If  $F = 2$ , the output noise-to-signal ratio is twice that at the input when the matched input termination is at 290°. The noise figure is frequently expressed in decibels. A zero-db noise figure corresponds to  $F = 1$ , whereas a 3-db noise figure corresponds to  $F = 2$ .

References 19 to 25 give thorough treatments of noise theory.

The foregoing noise figure is very useful for experiments that are performed at room temperature. However, in radio astronomy and satellite communication the input noise temperature is only a few degrees Kelvin when the antenna is pointed at the sky. In such applications it is more convenient to describe the noise performance of the amplifier by an "effective input noise temperature" or simply an "excess noise temperature." Gordon and White<sup>26</sup> define the effective input noise temperature of an amplifier as the temperature of a nonreflecting input termination that results in an output noise power double that which would occur if the same termination were at absolute zero. This excess noise temperature  $T_e$  can be related to the noise figure as follows: the total noise output power from the amplifier is given by

$$N_{\text{total}} = kBT_s g^2 + N_a \quad (4.73)$$

where  $T_s$  is the temperature of the nonreflecting input termination,  $g^2$  is the amplifier power gain, and  $N_a$  is the noise power contributed by the amplifier itself. By definition, when the input is at  $T_e$ , the output noise is twice the noise when  $T_s = 0$ , i.e.,  $N_{\text{total}} = 2N_a$ ; it follows that

$$N_a = kT_e B g^2 \quad (4.74)$$

This definition assumes that  $N_a$  is unaffected by the temperature of the input termination. Since the total noise out in Eq. 4.72 is

$$N_{\text{out}} = k 290^\circ B g^2 + N_a$$

the noise figure can be written as

$$\begin{aligned} F &= \frac{k 290^\circ B g^2 + kT_e B g^2}{k 290^\circ B g^2} \\ &= 1 + \frac{T_e}{290^\circ} \end{aligned} \quad (4.75)$$

It is then clear that a noise-free amplifier has a zero-degree excess noise temperature, and the noisier the amplifier, the higher the temperature.

Before giving the excess noise temperatures for parametric amplifiers, double and single sideband operation must be defined.

It is characteristic of parametric amplifiers that both a signal and idler mode exist. The energy in both of these modes or channels grows at the expense of the pump energy. This means that either or both channels can be used for amplification. If a signal is applied to one channel only, this is called single sideband operation; if it is applied to both channels, it is called double sideband operation. Normally, single sideband operation is used. However, in radio astronomy, double sideband operation

can be used. Regardless of the type of operation, noise is always present in both channels. Therefore, it is to be expected that the noise figure will be improved with double sideband operation.

The excess noise temperatures are now given. The derivations are omitted, since they are lengthy but may be found in References 15 and 16.

All the conductances in the circuit radiate thermal noise proportional to their temperatures. The excess noise due to these conductances is found to be

*a. Transmission type, single sideband*

$$T_e = \frac{G_1}{G_{g1}} T_c + \frac{\omega_1 G_{e1}}{\omega_2 G_{g1}} T_i + \frac{G_{L1}}{G_{g1}} T_L \left[ 1 - \left( \frac{G_{e1}}{g^2 G_{L1}} \right)^2 \right] \quad (4.76)$$

where  $T_c$  is the temperature of  $G_1$ ,  $T_i$  is the temperature of  $G_2$ ,  $G_{L1}$  is at 290°K,  $T_L$  is the isolator temperature,  $g^2$  is the gain given by Eq. 4.70, and  $G_{e1}$  is given by Eq. 4.68.

*b. Reflection type, single sideband*

$$T_e = \left( \frac{g+1}{g} \right)^2 \left( \frac{G_1}{G_{g1}} T_c + \frac{\omega_1 G_{e1}}{\omega_2 G_{g1}} T_i \right) \quad (4.77)$$

where  $g^2$  is given by Eq. 4.71.

*c. Reflection type, double sideband*

$$T_e = \frac{N_{11} + N_{21}}{kB(g_{11} + g_{21})} - 290^\circ \quad (4.78)$$

where

$$g_{11} = \left( \frac{G_{g1} - G_1 + G_{e1}}{G_{g1} + G_1 - G_{e1}} \right)^2 \quad (4.79)$$

$$g_{21} = \frac{\omega_1}{\omega_2} \frac{G_{g2}}{(G_{g2} + G_2)} \frac{4G_{g1}G_{e1}}{(G_{g1} + G_1 - G_{e1})^2} \quad (4.80)$$

$$N_{11} = k 290^\circ B g_{11} + \frac{4kT_c G_1 G_{g1}}{(G_{g1} + G_1 - G_{e1})^2} \quad (4.81)$$

$$N_{21} = \frac{\omega_1}{\omega_2} \frac{4kB(T_i G_2 + 290^\circ G_{g2}) G_{e1} G_{g1}}{(G_{g2} + G_2)(G_{g1} + G_1 - G_{e1})^2} \quad (4.82)$$

and  $G_{g2}$  is the generator conductance at the idler frequency which is taken at room temperature.

These expressions are too involved to discuss semiquantitatively as they stand. To simplify, assume that the amplifiers are operated just

below the oscillation threshold. Further, assume that the cavity conductances  $G_1$  and  $G_2$  are small compared to the generator conductances  $G_{g1}$  and  $G_{g2}$ . Under these conditions, it follows that the noise temperatures above reduce to

*a. Transmission, single sideband*

$$T_e \cong T_L + \frac{2\omega_1}{\omega_2} T_i \quad (4.83)$$

*b. Reflection, single sideband*

$$T_e \cong \frac{\omega_1}{\omega_2} T_i \quad (4.84)$$

*c. Reflection, double sideband*

$$T_e \cong \frac{1}{\omega_1 + \omega_2} \left( \frac{\omega_2 G_1}{G_{g1}} T_c + \frac{\omega_1 G_2}{G_{g2}} T_i \right) \quad (4.85)$$

It can now be seen from Eqs. 4.83 and 4.84 that a reflection-type cavity will give a lower excess noise temperature than a transmission type. This is not surprising, since a transmission-type cavity amplifier is loaded by both the generator and load conductances, whereas the reflection type is loaded only by the generator conductance. If the idler conductance is at  $290^\circ$  and  $\omega_1 = \omega_2$ , then the excess noise temperature of the reflection-type amplifier for single sideband operation is  $290^\circ$ . In order to obtain a lower noise temperature, the idler circuit must be cooled.

Compare next the reflection type for single and double sideband operation. If  $\omega_1 = \omega_2$ , from Eq. 4.85

$$T_e = \frac{1}{2} \left( \frac{G_1}{G_{g1}} T_c + \frac{G_2}{G_{g2}} T_i \right) \quad (4.86)$$

Then if the cavity losses are small ( $G_1 \ll G_{g1}$  and  $G_2 \ll G_{g2}$ ) and  $G_1$  and  $G_2$  are both at  $290^\circ$ ,  $T_e$  will be much smaller than  $290^\circ$  with no refrigeration. Therefore, double sideband operation is preferred.

The foregoing remarks should be sufficient to convince the reader of the low noise capabilities of parametric amplifiers over those of conventional microwave amplifiers. They compare very favorably with the noise temperatures obtained with masers.<sup>27-31</sup>

#### 4.7 The Frequency Converter

In the parametric amplifier and oscillator the pump is applied at a frequency  $\omega = \omega_1 + \omega_2$ . In this case it has been shown that the  $a_1$ - and

$a_2^*$ -modes are actively coupled. There is another case of interest, viz., when the pump frequency is given by  $\omega = \omega_1 - \omega_2$ , in which the direct coupled mode approach used in Section 4.2 will quickly show that the pump then couples the  $a_1$ - and  $a_2$ -modes passively. Equations 4.23 become

$$\begin{aligned}\frac{da_1}{dt} &= j\omega_1 a_1 + c_{12} e^{j\omega t} a_2 \\ \frac{da_2}{dt} &= j\omega_2 a_2 + c_{21} e^{-j\omega t} a_1\end{aligned}\quad (4.87)$$

Since all frequencies except  $\omega_1$ ,  $\omega_2$ , and  $\omega = \omega_1 - \omega_2$  are shorted, the Manley-Rowe relations given in Eqs. 4.53 must be used so that

$$\frac{P_{\omega_1}}{\omega_1} = - \frac{P_{\omega_2}}{\omega_2} \quad (4.88)$$

where  $P = (d/dt)2|a|^2$ . Use Eqs. 4.87 and 4.88 to show that

$$\frac{c_{12}}{\omega_1} = - \frac{c_{21}^*}{\omega_2} \quad (4.89)$$

This should be compared with the actively coupled case of Eq. 4.27.

In order to show that these modes are passively coupled, let

$$\begin{aligned}a_1 &= A_1 e^{j\omega_1 t} \\ a_2 &= A_2 e^{j\omega_2 t}\end{aligned}\quad (4.90)$$

Equations 4.87 then reduce to

$$\begin{aligned}\frac{dA_1}{dt} &= c_{12} A_2 \\ \frac{dA_2}{dt} &= c_{21} A_1\end{aligned}\quad (4.91)$$

and there are solutions of the form  $\exp(st)$  in which

$$s = \sqrt{c_{12} c_{21}} = \sqrt{-\left(\frac{\omega_1}{\omega_2}\right) |c_{12}|^2} \quad (4.92)$$

so that  $s$  is always pure imaginary and there can be no exponentially increasing solutions. This agrees with the definition of passively coupled modes given in Chapter 1. The frequency converter then looks like coupled transmission lines. Energy is continuously converted back

and forth between mode  $a_1$  and  $a_2$ . Therefore, if power is injected at frequency  $\omega_1$ , it is converted periodically to frequency  $\omega_2$ . If  $\omega_2 > \omega_1$ , by Eq. 4.88 there can be conversion gain if power is injected at  $\omega_1$  and removed at  $\omega_2$ . In this case the signal frequency is greater than the pump frequency ( $\omega_1 = \omega + \omega_2$ ), but there is no exponential growth, whereas for the amplifier the signal frequency is always smaller than the pump frequency ( $\omega_1 = \omega - \omega_2$ ).

#### 4.8 Remarks

*a.* This chapter has extended the theory of coupled modes presented in Chapter 1 to include cases in which the coupling coefficients are time-dependent. Only weakly coupled elements have been considered. It has been shown that the Manley-Rowe relations play the role of energy conservation when the elements are parametrically coupled. Further, the low noise feature of parametric amplifiers has been discussed.

*b.* There are several undesirable features of the lumped circuit parametric amplifier:

- i. The degenerate amplifier gain is sensitive to the phase of the pump relative to the signal. This feature can be circumvented by using an idler circuit that is nondegenerate.
- ii. The amplifier is a regenerative or negative resistance type. In order to obtain large gain, it must be operated near the oscillation threshold. Accordingly, the device is not unconditionally stable and may break into sustained oscillation.
- iii. The pump must be applied at a frequency higher than the signal frequency. This puts an upper limit on frequencies that can be amplified, since suitable pump sources are not yet available.

Objection ii can be remedied by using a distributed medium such as a transmission line. Distributed parametric amplifiers are discussed in detail in Chapter 5.

Objection iii can be overcome by suggestions of Hogan and co-workers<sup>32</sup> and Chang and Bloom,<sup>33-35</sup> which involve four frequencies. These are treated for the distributed parametric amplifier in Chapter 5, although they can also be adapted to the lumped circuit device.

*c.* In succeeding chapters materials that have been used to produce the time-varying circuit parameters in actual practice are discussed in detail. Specifically, semiconductor diodes, electron beams, and ferrites are covered, since most of the work to date has used them as active elements.

#### 4.9 Brief History of the Parametric Amplifier<sup>36</sup>

Recent interest in parametric amplifiers is due chiefly to their low noise characteristics and the technological development of materials, such as *PN* junction diodes and ferrites, which are suitable to use as variable reactance materials. In addition to the low noise feature, the diode and ferrite versions should have a very long life.

The parametric coupling principle is not new. Faraday<sup>37</sup> (1831), Melde<sup>38</sup> (1859), and Lord Rayleigh<sup>39, 40, 41</sup> have published calculations on the principle for mechanical systems. Work on the *LC* circuit case, using a variable inductance,<sup>42, 43</sup> led to a device that was successfully used in radio-telephone communication between Berlin and Vienna prior to World War I. Zenneck,<sup>44</sup> Alexanderson,<sup>45, 46</sup> and Hartley<sup>47</sup> pioneered with theoretical and experimental contributions in the next few years.

Much work followed along these lines,<sup>48-64</sup> but interest in the device subsided when high-power vacuum tubes became available. Then, in 1948, Van der Ziel<sup>65</sup> pointed out the low noise possibilities of the device when nonlinear condensers were used. Van der Ziel and Landon<sup>66</sup> derived the gain relationships. Further work, which followed, is given in References 67 to 95. Another important step was made by Suhl,<sup>8</sup> who proposed that a ferrite could be used as the variable reactance material and recognized the need for an idling circuit to remove the phase sensitivity of the gain. Since then, the literature has increased at such a rapid pace<sup>96-206</sup> that an adequate survey is impossible in a short space. Even this impressive list is not complete and contains only a few papers published after July 1959.

#### BIBLIOGRAPHY

1. J. M. Manley and H. E. Rowe, "Some General Properties of Nonlinear Elements. I. General Energy Relations," *Proc. IRE*, **44**, 904-913 (July 1956).
2. H. E. Rowe, "Some General Properties of Nonlinear Elements. II. Small Signal Theory," *Proc. IRE*, **46**, 850-860 (May 1958).
3. M. T. Weiss, "Quantum Derivation of Energy Relations Analogous to Those for Nonlinear Reactances," *Proc. IRE*, **45**, 1012-1013 (July 1957).
4. B. Salzberg, "Masers and Reactance Amplifiers—Basic Power Relations," *Proc. IRE*, **45**, 1544-1545 (November 1957).
5. C. H. Page, "Frequency Conversion with Nonlinear Reactance," *J. Research Natl. Bur. Standards*, **58**, 227-236 (May 1957).
6. P. Penfield, Jr., "Power Flow in Some Lossless Systems," *Mass. Inst. Technol. Servomechanisms Lab. Rep. DSR 7672* (February 1959).

7. J. M. Manley and H. E. Rowe, "General Energy Relations in Nonlinear Reactance," *Proc. IRE*, **47**, 2115-2116 (December 1959).
8. H. Suhl, "Theory of the Ferromagnetic Microwave Amplifier," *J. Appl. Phys.*, **28**, 1225-1236 (November 1957).
9. W. R. Bennett, "New Results in the Calculation of Modulation Products," *Bell System Tech. J.*, **12**, 228-243 (April 1933).
10. H. A. Haus, "Power-Flow Relations in Lossless Nonlinear Media," *IRE Trans. PGMTT*, **MTT-6**, 317-324 (July 1958).
11. H. A. Haus, "The Kinetic Power Theorem for Parametric, Longitudinal, Electron-Beam Amplifiers," *IRE Trans. PGED*, **ED-5**, 225-232 (October 1958).
12. H. A. Haus, "On a Nonlinear Phenomenon in Plasmas," *Mass. Inst. Technol. Lab. Electronics Internal Memorandum No. 2* (March 27, 1959).
13. R. H. Pantell, "General Power Relationships for Positive and Negative Nonlinear Resistive Elements," *Proc. IRE*, **46**, 1910-1913 (December 1958).
14. J. D. Pearson and D. H. Trevena, "Definition of Capacitance," *J. Electronics Control*, **6**, 74 (January 1959).
15. H. Heffner and G. Wade, "Gain, Bandwidth, and Noise Characteristics of the Variable-Parameter Amplifier," *J. Appl. Phys.*, **29**, 1321-1331 (September 1958).
16. P. K. Tien, "Noise in Parametric Amplifiers," *Acta Electronica*, **4**, No. 4 (October 1960).
17. K. R. Spangenberg, *Vacuum Tubes*, McGraw-Hill, New York, 1948, pp. 298-309, 321-326.
18. H. T. Friis, "Noise Figure of Radio Receivers," *Proc. IRE*, **32**, 419-422 (July 1944).
19. A. van der Ziel, *Noise*, Prentice-Hall, New York, 1954.
20. *Noise in Electron Devices*, Edited by L. D. Smullin and H. A. Haus, John Wiley and Sons, New York, 1959.
21. J. R. Pierce, "General Sources of Noise in Vacuum Tubes," *IRE Trans. PGED*, **ED-1**, 135-167 (December 1954), and references contained therein.
22. J. L. Lawson and G. E. Uhlenbeck, *Threshold Signals*, MIT Rad. Lab. Series, Vol. 24, McGraw-Hill, New York, 1950.
23. J. B. Johnson, "Thermal Agitation of Electricity in Conductors," *Phys. Rev.*, **32**, 97-109 (July 1928).
24. W. Schottky, "Spontaneous Fluctuations in Electron Streams," *Ann. Physik*, **57**, 541-567 (December 1918).
25. D. O. North, "Absolute Sensitivity of Radio Receivers," *R C A Rev.*, **6**, 332-343 (January 1942).
26. J. P. Gordon and L. D. White, "Noise in Maser Amplifiers—Theory and Experiment," *Proc. IRE*, **46**, 1588-1594 (September 1958).
27. J. P. Gordon, H. J. Zeiger and C. H. Townes, "The Maser—New Type of Microwave Amplifier, Frequency Standard, and Spectrometer," *Phys. Rev.*, **99**, 1264-1274 (August 15, 1955).
28. J. Combrisson, A. Honig, and C. H. Townes, "Utilisation de la résonance de spins électroniques pour réaliser un oscillateur ou un amplificateur en hyper fréquences," *Compt. rend.*, **242**, 2451-2453 (May 1956).
29. G. Feher, J. P. Gordon, E. Buehler, E. A. Gere, and C. D. Thurmond, "Spontaneous Emission of Radiation from an Electron Spin System," *Phys. Rev.*, **109**, 221-222 (January 1, 1958).
30. N. Bloembergen, "Proposal for a New Type Solid-State Maser," *Phys. Rev.*, **104**, 324-327 (October 15, 1956).

31. H. E. D. Scovil, G. Feher, and H. Seidel, "Operation of a Solid-State Maser," *Phys. Rev.*, **105**, 762-763 (January 15, 1957).
32. C. L. Hogan, R. L. Jepsen, and P. H. Vartanian, "New Type of Ferromagnetic Amplifier," *J. Appl. Phys.*, **29**, 422-423 (March 1958). This device was also independently suggested by Professor H. Heffner of Stanford University.
33. S. Bloom and K. K. N. Chang, "Parametric Amplification Using Low Frequency Pumping," *J. Appl. Phys.*, **29**, 594 (March 1958).
34. S. Bloom and K. K. N. Chang, "Theory of Parametric Amplifiers," *R C A Rev.*, **18**, 578-593 (December 1957).
35. K. K. N. Chang and S. Bloom, "Parametric Amplifier Using Lower Frequency Pumping," *Proc. IRE*, **46**, 1383-1386 (July 1958).
36. W. W. Mumford,\* "Some Notes on the History of Parametric Transducers," *Proc. IRE*, **48**, 848-853 (May 1960).
37. Michael Faraday, "On a Peculiar Class of Acoustical Figures; and on Certain Forms Assumed by Groups of Particles upon Vibrating Elastic Surfaces," *Phil. Trans. Roy. Soc. London*, **121**, 299-340 (1831).
38. F. Melde, "Über die Erregung stehender Wellen eines fadenförmigen Körpers," *Ann. Physik Chemie*, Series 2, **109**, 193-215, 1859.
39. John William Strutt, Lord Rayleigh, "On the Crispations of Fluid Resting upon a Vibrating Support," *Phil. Mag.*, Series 5, **16**, 50-58 (1883).
40. John William Strutt, Lord Rayleigh, "On the Maintenance of Vibrations by Forces of Double Frequency, and on the Propagation of Waves Through a Medium Endowed with a Periodic Structure," *Phil. Mag.*, Series 5, **24**, Issue 147, 145-159 (August 1887).
41. John William Strutt, Lord Rayleigh, *Theory of Sound*, Second Edition, Macmillan, London, Vol. I, 1894, Vol. II, 1896.
42. R. Goldschmidt, "High Frequency Alternator for Radio Telegraphy," *Elektrotech. Z.*, **32**, 54-56 (January 1911).
43. L. Kühn, "Über Neues Radio-Telephonisches System," *Jahrb. drahtl. Telegr.*, **9**, 502-534 (1915).
44. J. Zenneck, "A Contribution to the Theory of Magnetic Frequency Doublers," presented orally at IRE meeting, New York City, September 1915.
45. E. F. W. Alexanderson and S. P. Nixdorff, "A Magnetic Amplifier for Radiotelephony," *Proc. IRE*, **4**, 101-129 (April 1916).
46. E. F. W. Alexanderson, U. S. Patent #1,206,643.
47. R. V. L. Hartley, U. S. Patent #1,287,982.
48. B. van der Pol, "On Relaxation-oscillations," *Phil. Mag.*, Series 7, **2**, 978-992 (1926).
49. B. van der Pol, "Nonlinear Theory of Electric Oscillations," *Proc. IRE*, **22**, 1051-1086 (1934).
50. R. V. L. Hartley, "Oscillations in Systems with Nonlinear Reactance," *Bell System Tech. J.*, **15**, 424-440 (July 1936).
51. W. L. Barrow, D. B. Smith, and F. W. Baumann, "A Further Study of Oscillatory Circuits Having Periodically Varying Parameters," *J. Franklin Inst.*, **221**, Part I, 403-416 (March 1936); Part II, 509-529 (April 1936).
52. L. W. Hussey and L. R. Wrathall, "Oscillations in an Electromagnetical System," *Bell System Tech. J.*, **15**, 441-445 (July 1936).
53. R. N. Smith, "The Theory of Mixers in Terms of Measurable Mixer Constants," *NDRC Report 14-259*, Purdue University, March 24, 1944.

\* Items 37-204 are taken from Reference 36.

54. L. Apker, "Note on Reciprocity Failure in Crystal Mixers," *NDRC Report 15-931-16*, March 9, 1945, Contract OEMSR-931, General Electric Company.
55. L. Apker, E. Taft, and J. Dickey, "Theory of a Double Mixer for Spectrum Analyzer Applications," *NDRC Report 931-17, 15-931-16*, General Electric Company, April 2, 1945.
56. H. C. Torrey, "Theory of the Negative IF Conductance of North's Welded Contact Germanium Rectifiers," *Mass. Inst. Technol. Research Lab. Electronics, Tech. Rep. No. 55* (May 22, 1945).
57. L. C. Peterson and F. B. Llewellyn, "The Performance and Measurements of Mixers in Terms of Linear Network Theory," *Proc. IRE*, **33**, 458-476 (July 1945).
58. H. Q. North, "Properties of Welded Contact Germanium Rectifiers," *J. Appl. Phys.*, **17**, 912-923 (November 1946).
59. J. M. Manley and E. Peterson, "Negative Resistance Effects in Saturable Reactor Circuits," *Trans. AIEE*, **65**, 870-881 (December 1946).
60. N. W. McLachlan, *Theory and Applications of Mathieu Functions*, Oxford Clarendon Press, pp. 69-70, 274-275, 1947.
61. Frank Rockett, "The Electron Art," *Electronics*, **21**, 190-195 (January 1948).
62. H. C. Torrey and C. A. Whitmer, *Crystal Rectifiers*, MIT Rad. Lab. Series, Vol. 15, McGraw-Hill, New York, 1948.
63. M. C. Waltz, *Crystal Rectifiers*, MIT Rad. Lab. Series, Vol. 15, p. 401, Torrey and Whitmer, McGraw-Hill, 1948.
64. R. V. Pound, *Microwave Mixers*, MIT Rad. Lab. Series, Vol. 16, McGraw-Hill, New York, 1948.
65. A. van der Ziel, "On the Mixing Properties of Nonlinear Condensers," *J. Appl. Phys.*, **19**, 999-1006 (November 1948).
66. V. D. Landon, "The Use of Ferrite Cored Coils as Converters, Amplifiers and Oscillators," *R C A Rev.*, **10**, 387-396 (September 1949).
67. W. R. Bennett, "A General Review of Linear Varying Parameter and Non-linear Circuit Analysis," *Proc. IRE*, **38**, 259-263 (March 1950).
68. J. M. Manley, "Some General Properties of Magnetic Amplifiers," *Proc. IRE*, **39**, 242-251 (March 1951).
69. H. S. Tsien, *Engineering Cybernetics*, McGraw-Hill, 1954.
70. J. von Neumann, "Nonlinear Capacitance or Inductance Switching, Amplifying and Memory Organs," U. S. Patent #2,815,488, filed April 28, 1954, issued December 1957.
71. D. Leenov, "Crystal Rectifiers," Bell Telephone Labs. Interim Reports on Task 8, Signal Corps Contract No. DA-36-039-sc5589; 1954 to present.
72. S. Kita and T. Fujii, "Microwave Amplification by Use of Crystal Diode," *E.C.L. Internal Report*, February 1954. Annual Convention, Inst. Elec. Commun. Eng. Japan, October 1954.
73. W. P. Mason and R. F. Wick, "Ferroelectrics and the Dielectric Amplifier," *Proc. IRE*, **42**, 1606-1620 (November 1954).
74. E. Goto, "New Parametron Circuit Element Using Nonlinear Reactance," *Kokusai Den. Den. Kenkyu Shiryo* (November 1954).
75. A. E. Bakanowski, "The Nonlinear Capacitor as a Mixer," 2nd Interim Report on Task 8, Crystal Rectifiers, Sig. Corps Project 2-7-323A, December 31, 1954.
76. R. J. Duffin, "Impossible Behavior of Nonlinear Networks," *J. Appl. Phys.*, **26**, 603-605 (April 1955).
77. E. Goto, "On the Application of Parametrically Excited Nonlinear Resonators," *J. Elec. Commun. Engrs. Japan*, **38**, 770-775 (October 1955).

78. S. Oshima, H. Enomoto, and S. Watanabe, "Oscillation Theory of Parametron and Method of Measuring Nonlinear Elements," *Kokusai Den. Den. Kenkyu Shiryo* (November 1955).
79. A. van der Ziel, "Theory of Shot Noise in Junction Diodes and Junction Transistors," *Proc. IRE*, **43**, 1639-1646 (November 1955).
80. S. Oshima, "Introduction to Parametron," *Denshi Kogyo*, **4**, No. 11, 4 (December 1955).
81. S. Oshima, "General Remarks on a Parametron Circuit," *Denshi Kogyo*, special issue.
82. H. Yamada, "A Parametron Circuit Examined from the Point of Mathematical Logic," *Denshi Kogyo*, special issue.
83. A. C. Macpherson, "An Analysis of Diode Mixer Consisting of Nonlinear Capacitance and Conductance and Ohmic Spreading Resistance," *NRL Report 4667* (February 13, 1956).
84. L. J. Giacoletto and J. O'Connell, "A Variable Capacitance Germanium Diode for UHF," *R C A Rev.*, **17**, 68-85 (March 1956); also R C A Labs. Transistors I, pp. 221-238 (1956).
85. F. Dill and L. Depian, "Semiconductor Capacitance Amplifier," *IRE Convention Record*, Part 3, pp. 172-174 (1956).
86. A. Uhlir, Jr., "High Frequency Shot Noise in P-N Junctions," *Proc. IRE*, **44**, 557-558 (April 1956).
87. A. Uhlir, "Frequency Conversion and Computation with P-N Junction Devices," Chap. I, 6th Interim Technical Report, "Crystal Rectifiers—Task 8," June 15, 1956. Signal Corps Contract DA-36-039-sc-5589.
88. W. H. Higa, "Theory of Nonlinear Coupling in a Novel Ferroelectric Device," *J. Appl. Phys.*, **27**, 775-777 (July 1956).
89. A. Uhlir, Jr., "Possible Uses of Nonlinear Capacitor Diodes," Bell Telephone Laboratories, 8th Interim Report on Task 8, Signal Corps Contract DA-36-039-sc-5589; July 15, 1956.
90. J. E. Pippin, "Frequency Doubling and Mixing in Ferrites," *Proc. IRE*, **44**, 1054-1055 (August 1956).
91. A. Uhlir, Jr., "Two Terminal P-N Junction Devices for Frequency Conversion and Computation," *Proc. IRE*, **44**, 1183-1191 (September 1956).
92. A. E. Bakanowski, "Small Signal Admittance Measurements for a Retarding Field Diode," Chap. II, 9th Interim Technical Report, "Crystal Rectifiers—Task 8," October 15, 1956, Signal Corps Contract DA-36-039-sc-5589.
93. C. F. Edwards, "Frequency Conversion by Means of a Nonlinear Admittance," *Bell System Tech. J.*, **35**, 1403-1416 (November 1956).
94. A. C. Macpherson, "An Analysis of the Diode Mixer Consisting of Nonlinear Capacitance and Conductance and Ohmic Spreading Resistance," *IRE Trans., MTT-5*, 43-51 (January 1957).
95. Symposium on the Role of Solid-State Phenomena in Electric Circuits, Proceedings, Publ. Polytech. Inst. Brooklyn, Interscience, New York, edited by Jerome Fox, 1957.
96. H. Suhl, "A Proposal for a Ferromagnetic Amplifier in the Microwave Range," *Phys. Rev.*, **106**, 384-385 (April 15, 1957).
97. J. L. Melchor, W. P. Ayres, and P. H. Vartanian, "Microwave Frequency Doubling from 9 to 18 kmc in Ferrites," *Proc. IRE*, **45**, 643-646 (May 1957).
98. M. E. Hines, "Amplification with Nonlinear Reactance Modulators," presented at Annual IRE Conference on Electron Tube Research, Berkeley, Calif. (1957).

99. S. Duinker, "General Properties of Frequency Converting Networks," Dissertation, Tech. Univ. Delft., Netherlands, June 1957.
100. R. Adler, "A New Principle of Signal Amplification," presented at Annual IRE Conference on Electron Tube Research, Berkeley, Calif. (1957).
101. F. Paschke, "On the Nonlinear Behavior of Electron-Beam Devices," *R C A Rev.*, **18**, 221-242 (June 1957).
102. M. T. Weiss, "Solid-State Microwave Amplifier and Oscillator Using Ferrites," *Phys. Rev.*, **107**, 317 (July 1, 1957).
103. R. W. DeGrasse and G. Wade, "Microwave Mixing and Frequency Dividing," *Proc. IRE*, **45**, 1013-1015 (July 1957).
104. A. E. Bakanowski, N. G. Cranna, and A. Uhlir, Jr., "Diffused Silicon Non-linear Capacitors," *IRE Trans.*, **ED-6**, 384-390 (October 1959).
105. L. J. Giacoletto, "Junction Capacitance and Related Characteristics Using Graded Impurity Semiconductors," *IRE Trans.*, **ED-4**, 207-215 (July 1957).
106. "New Ferrite Microwave Amplifier," *Bell Labs. Record*, **35**, 316-317 (August 1957).
107. A. Uhlir, Jr., and N. Bronstein, "Semiconductor Diodes Yield Converter Gain," *Bell Labs. Record*, **35**, 412 (October 1957).
108. H. Suhl, "Theory of the Ferromagnetic Microwave Amplifier," *J. Appl. Phys.*, **28**, 1225-1236 (November 1957).
109. Y. Miyakawa, "Amplification and Frequency Conversion in Propagation Circuits," Inst. Elec. Comm. Engrs. Japan, *National Conv. Record*, p. 8, November 1957 (in Japanese).
110. J. P. Wittke, "New Approaches to the Amplification of Microwaves," *R C A Rev.*, **18**, 441-457 (December 1957).
111. E. O. Keizer, "A Carrier-Energized Bistable Circuit Using Variable Capacitance Diodes," *R C A Rev.*, **18**, 475-485 (December 1957).
112. B. Lax, "Status of Microwave Applications of Ferrites and Semiconductors," *IRE Trans.*, **MTT-6**, 5-18 (January 1958).
113. "Varicap," *Radio Electronics*, **29**, 45 (January 1958).
114. A. L. Cullen, "A Traveling-Wave Parametric Amplifier," *Nature*, **181**, 332 (February 1, 1958).
115. T. J. Bridges, "A Parametric Electron Beam Amplifier," *Proc. IRE*, **46**, 494-495 (February 1958).
116. K. W. H. Stevens, "Amplification Using a Precessing Magnetic Moment," *J. Electronics Control*, **4**, 280-284 (March 1958).
117. M. T. Weiss, "Solid-State Microwave Amplifier and Oscillator Using Ferrite," *J. Appl. Phys.*, **29**, 421 (March 1958).
118. P. K. Tien and H. Suhl, "A Traveling-Wave Ferromagnetic Amplifier," *Proc. IRE*, **46**, 700-706 (April 1958).
119. W. H. Louisell and C. F. Quate, "Parametric Amplification of Space-Charge Waves," *Proc. IRE*, **46**, 707-716 (April 1958).
120. H. Suhl, "Quantum Analog of the Ferromagnetic Microwave Amplifier," *J. Phys. Chem. Solids*, **4**, 278-282 (1958).
121. Rufus P. Turner, "Using the Varicap," *Radio Electronics*, **29**, 57-59 (May 1958).
122. G. F. Straube, "A Voltage Variable Capacitor" (2 parts), *Electronic Inds.*, **17**, 69-73 (May 1958), 77-80 (July 1958).
123. R. S. Engelbrecht, "A Low-Noise Nonlinear Reactance Traveling-Wave Amplifier," Solid-State Devices Research Conference, Columbus, Ohio, June 18, 1958. (Presented orally.)

124. G. F. Herrmann, M. Uenohara, and A. Uhlir, Jr., "Noise Figure Measurements on Two Types of Variable Reactance Amplifiers Using Semiconductor Diodes," *Proc. IRE*, **46**, 1301-1302 (June 1958).
125. A. Uhlir, Jr., "The Potential of Semiconductor Diodes in High Frequency Communication," *Proc. IRE*, **46**, 1099-1115 (June 1958).
126. B. Salzberg and E. W. Sard, "A Low-Noise Wide-Band Reactance Amplifier," *Proc. IRE*, **46**, 1303 (June 1958).
127. S. Kita, "A Harmonic Generator by Use of the Nonlinear Capacitance of Germanium Diode," *Proc. IRE*, **46**, 1307 (June 1958).
128. R. Adler, "Parametric Amplification of Fast Electron Waves," *Proc. IRE*, **46**, 1300-1301 (June 1958).
129. H. Heffner and K. Kotzebue, "Experimental Characteristics of a Microwave Parametric Amplifier Using a Semiconductor Diode," *Proc. IRE*, **46**, 1301 (June 1958).
130. P. K. Tien, "Parametric Amplification and Frequency Mixing in Propagating Circuits," presented at Annual IRE Conference on Electron Tube Research, Quebec, Canada (1958).
131. C. B. Crumly, P. M. Fitzgerald, and G. Wade, "Multitank Microwave Parametric Converters and Amplifiers," Sixteenth Annual Conference on Electron Tube Research, Université Laval, Quebec, Canada, June 26, 1958.
132. A. Ashkin, "Parametric Amplification of Space-Charge Waves," presented at Annual IRE Conference on Electron Tube Research, Quebec, Canada (1958).
133. N. Minorsky, "On Parametric Excitation," *Compt. rend.*, **247**, 406-408 (July 28, 1958).
134. "Low-Noise Amplifier for High Frequencies Uses New Semiconductor Diodes," *Bell Labs. Record*, **36**, 250-251 (July 1958).
135. L. D. Buchmiller and G. Wade, "Pumping to Extend Traveling-Wave Tube Frequency Range," *Proc. IRE*, **46**, 1420-1421 (July 1958).
136. D. Leenov, "Gain and Noise Figure of a Variable Capacitance Up Converter," *Bell System Tech. J.*, **37**, 989-1008 (July 1958).
137. R. E. Beam, "Report of Advances in Microwave Theory and Techniques—1957," *IRE Trans., MTT-6*, 251-263 (July 1958).
138. A. Uhlir, Jr., "Shot Noise in P-N Junction Frequency Converters," *Bell System Tech. J.*, **37**, 951-987 (July 1958).
139. K. M. Poole and P. K. Tien, "A Ferromagnetic Resonance Frequency Converter," *Proc. IRE*, **46**, 1387-1396 (July 1958).
140. L. B. Valdes, "Circuit Conditions for Parametric Amplification," *J. Electronics Control*, **5**, 129-141 (August 1958).
141. H. Heffner and G. Wade, "Minimum Noise Figure of a Parametric Amplifier," *J. Appl. Phys.*, **29**, 1262 (August 1958).
142. A. Ashkin, T. J. Bridges, W. H. Louisell, and C. F. Quate, "Parametric Electron Beam Amplifiers," *IRE Wescon Convention Record, Part 3—Electron Devices*, pp. 13-17 (1958).
143. H. Heffner, "Masers and Parametric Amplifiers," *IRE Wescon Convention Record, Part 3—Electron Devices*, pp. 3-8 (1958).
144. K. K. N. Chang and S. Bloom, "A Parametric Amplifier Using Lower Frequency Pumping," *IRE Wescon Convention Record, Part 3—Electron Devices*, pp. 23-27 (1958).
145. M. E. McMahon and G. F. Straube, "Voltage Sensitive Semiconductor Capacitors," *IRE Wescon Convention Record, Part 3—Electron Devices*, pp. 72-82 (1958).

146. R. S. Engelbrecht, "A Low Noise Nonlinear Reactance Traveling-Wave Amplifier," *Proc. IRE*, **46**, 1655 (September 1958).
147. P. K. Tien, "Parametric Amplification and Frequency Mixing in Propagating Circuits," *J. Appl. Phys.*, **29**, No. 9, 1347-1357 (September 1958).
148. H. Heffner and G. Wade, "Gain, Bandwidth and Noise Characteristics of the Variable Parameter Amplifier," *J. Appl. Phys.*, **29**, 1321-1331 (September 1958).
149. S. Weber, "The Mavar: A Low Noise Microwave Amplifier," *Electronics*, **31**, 65-71 (September 26, 1958).
150. W. L. Whirry and F. B. Wang, "Phase Dependence of a Ferromagnetic Amplifier," *Proc. IRE*, **46**, 1657-1658 (September 1958).
151. R. Gardner, J. C. Greene, P. P. Lombardo, and E. W. Sard, "Application of Semiconductor Diodes to Microwave Low-Noise Amplifiers and Harmonic Generators." (1) Report 4589-M-1 Cont. AF30(602)-1854, September 1958. (RADC, Rome.) (2) Report 5872-I-1 Cont. 36-039-sc-78161 DA Project 3-99-15-106, October 15, 1958. (U. S. Army Sig. Corps Eng. Lab.)
152. H. Suhl, "The Ferromagnetic Microwave Amplifier," *Phys. Today*, **11**, 28-30 (September 1958).
153. S. Muroga, "Elementary Principles of Parametron and its Application to Digital Computers," *Datamation*, **4**, No. 5, 31-34 (September-October 1958).
154. R. Adler, G. Hrbek, and G. Wade, "A Low-Noise Electron Beam Parametric Amplifier," *Proc. IRE*, **46**, 1756-1757 (October 1958).
155. H. A. Haus, "The Kinetic Power Theorem for Parametric, Longitudinal Electron Beam Amplifiers," *IRE Trans.*, **ED-5**, 225-232 (October 1958).
156. Shigebumi Saito, "Parametric Amplification of Space-Charge Waves on a Thin Electron Beam," *J. Inst. Elec. Comm. Engrs. Japan*, **41**, No. 11, 1113-1120 (November 1958).
157. Microwave Parametric Device Lecture Series, San Francisco, *IRE Chapters PGED and PGM TT*, October 15, 22, 29 and November 5, 12, 19, 1958.
158. Bernard Salzberg, "General Characteristics of Nonlinear Energy Storage Elements," Microwave Parametric Device Lecture Series, San Francisco, *IRE PGED and PGM TT*, October 15, 1958. Résumé by Berin Fank in *Grid*, **5**, 16-18 (November 1958).
159. Kenneth Kotzebue, "Large Signal Properties of Parametric Amplifiers," Microwave Parametric Device Lecture Series, San Francisco, *IRE PGED and PGM TT*, October 29, 1958. Résumé by Berin Fank, *Grid*, **5**, 18-20 (November, 1958).
160. Hubert Heffner, "Back-Biased Diode Parametric Amplifiers," Microwave Parametric Device Lecture Series, San Francisco, *IRE PGED and PGM TT*, October 22, 1958. Résumé by Keith Hunton, *Grid*, **5**, 18 (November 1958).
161. James Gibbons, "The Characteristics of Back-Biased Diodes," Microwave Parametric Device Lecture Series, San Francisco, *IRE PGED and PGM TT*, November 5, 1958. Résumé by Keith Hunton, *Grid*, **5**, 16-18 (December 1958).
162. P. H. Vartanian, "Ferromagnetic Parametric Amplifiers," Microwave Parametric Device Lecture Series, San Francisco, *IRE PGED and PGM TT*, November 12, 1958. Résumé by Berin Fank, *Grid*, **5**, 18-24 (December 1958).
163. Robert Adler, "Beam Type Parametric Amplifiers," Microwave Parametric Device Lecture Series, San Francisco, *IRE PGED and PGM TT*, November 19, 1958. Résumé by Berin Fank, *Grid*, **5**, 24-26 (December 1958).

164. Electrons at Work, "Parametric Amplifier Ups Scatter Range," *Electronics*, **31**, 96 (November 7, 1958).
165. F. S. Harris, "The Parametric Amplifier," *CQ*, **14**, 74 *et seq.* (November 1958).
166. Ross Bateman and Walter F. Bain, "New Thresholds in VHF and UHF Reception, the World Below KTB," *QST*, **42**, No. 12, 30 *et seq.* (December 1958).
167. R. H. Pantell, "General Power Relationships for Positive and Negative Non-linear Resistive Elements," *Proc. IRE*, **46**, 1910-1913 (December 1958).
168. A. Ashkin, "Parametric Amplification of Space-Charge Waves," *J. Appl. Phys.*, **29**, 1646-1651 (December 1958).
169. Wesley G. Matthei, "Recent Advances in Solid-State Receivers," *Microwave Journal*, **2**, 19-24 (January 1959).
170. B. Lax, "Microwaves and the Solid State," *Microwave Journal*, **2**, 5 (January 1959).
171. F. A. Brand, W. G. Matthei, and T. Sard, "The Reactron—a Low-Noise Semiconductor Diode, Microwave Amplifier," *Proc. IRE*, **47**, 42-44 (January 1959).
172. B. Oguchi, S. Kita, N. Inage, and T. Okajima, "Microwave Parametric Amplifier by Means of Germanium Diode," *Proc. IRE*, **47**, 77-78 (January 1959).
173. H. Heffner, "Solid-State Microwave Amplifiers," *IRE Trans., MTT-7*, 83-91 (January 1959).
174. R. S. Engelbrecht and W. W. Mumford, "Some Data on the Performance of MAVARS," presented at the San Francisco Chapter IRE PGMTT meeting, January 20, 1959.
175. G. Wade and R. Adler, "A New Method for Pumping a Fast Space-Charge Wave," *Proc. IRE*, **47**, 79-80 (January 1959).
176. K. K. N. Chang, "Four-Terminal Parametric Amplifier," *Proc. IRE*, **47**, 81-82 (January 1959).
177. Ross Bateman and Walter F. Bain, "New Thresholds in VHF and UHF Reception Devices and Diodes," *QST*, **43**, No. 1, 11-15 (January 1959).
178. W. H. Louisell, "A Three Frequency Electron Beam Parametric Amplifier and Frequency Converter," *J. Electronics Control*, **6**, 1-25 (January 1959).
179. K. Kurokawa and J. Hamasaki, "Theoretical Analysis of Periodic Structures for Parametric Amplifiers," *Trans. of Microwave Transmission Research Committee of Japan*, January 1959 (in Japanese).
180. A. Uhrlir, Jr., "Amplification by Nonlinear Reactance," Digest of Technical Papers, 1959 Solid-State Circuits Conference, Philadelphia, Pa., February 12, 1959.
181. P. P. Lombardo, "Low-Noise 400 mc Reactance Amplifier," Digest of Technical Papers, 1959 Solid-State Circuits Conference, Philadelphia, Pa., February 12, 1959.
182. R. S. Engelbrecht, "Nonlinear Reactance (Parametric) Traveling-Wave Amplifiers for UHF," Digest of Technical Papers, 1959 Solid-State Circuits Conference, Philadelphia, Pa., February 12, 1959, p. 8.
183. K. L. Kotzebue, "Large-Signal Characteristics of Three-Frequency Cavity Parametric Amplifiers," Digest of Technical Papers, Solid-State Circuits Conference, Philadelphia, Pa., February 12, 1959, pp. 10-11.
184. Hsiung Hsu, "Multiple Frequency Parametric Devices," Digest of Technical Papers, Solid-State Circuits Conference, Philadelphia, Pa., February 12, 1959, pp. 12-13.
185. Ross Bateman and Walter F. Bain, "New Thresholds in VHF and UHF Reception—Circuit Theory and Diode Details," *QST*, **43**, No. 2, 28-35 (February 1959).

186. Fred Shunaman, "The Variable Reactance Amplifier," *Radio Electronics*, **30**, 78-82 (February 1959).
187. J. Sie and S. Weisbaum, "Noise Figure of Receiving Systems Using Parametric Amplifiers," *IRE National Convention Paper*, **7**, Part 3, 141-157 (1959); **7**, Part 3, 158 (1959).
188. T. B. Warren, "Low-Noise Parametric Amplifiers and Converters," *IRE National Convention Paper*, **7**, Part 3, 158 (1959).
189. Ross Bateman and Walter F. Bain, "New Thresholds in VHF and UHF Reception-Practical Results," *QST*, **43**, No. 3, 35-39 (March 1959).
190. W. E. Danielson, "Low-Noise in Solid-State Parametric Amplifiers at Microwave Frequencies," *J. Appl. Phys.*, **30**, No. 1, 8-15 (January 1959).
191. Hubert Heffner, "Masers and Parametric Amplifiers," *Microwave Journal*, **2**, No. 3, 33-38 (March 1959).
192. F. A. Olson, C. P. Wang, and G. Wade, "Parametric Devices Tested for Phase-Distortionless Limiting," *Proc. IRE*, **47**, 587-588 (April 1959).
193. R. D. Haun, Jr. and T. A. Osial, "Gain Measurements on a Pulsed Ferromagnetic Microwave Amplifier," *Proc. IRE*, **47**, 586-587 (April 1959).
194. R. C. Knechtli and R. D. Weglein, "Low Noise Parametric Amplifier," *Proc. IRE*, **47**, 584-585 (April 1959).
195. L. U. Kibler, "Directional Bridge Parametric Amplifier," *Proc. IRE*, **47**, 583-584 (April 1959).
196. E. D. Reed, "The Variable-Capacitance Parametric Amplifier," *IRE Trans. PGED*, **ED-6**, 216-224 (April 1959).
197. L. S. Nergaard, "Nonlinear-Capacitance Amplifiers," *R C A Rev.*, **20**, 3-17 (March 1959).
198. R. W. Gould, "Traveling-Wave Couplers for Longitudinal Beam Type Amplifiers," *Proc. IRE*, **47**, 419-426 (March 1959).
199. A. E. Siegman, "Phase-Distortionless Limiting by a Parametric Method," *Proc. IRE*, **47**, 447-448 (March 1959).
200. E. Mount and B. Begg, Parametric Devices and Maser, as annotated bibliography, *IRE Trans. MTT-8*, 222-243 (March 1960).
201. P. P. Lombardo and E. W. Sard, "Low Frequency Prototype Traveling-Wave Reactance Amplifier," *Proc. IRE*, **47**, 995-996 (May 1959).
202. G. M. Roe and M. R. Boyd, "Parametric Energy Conversion in Distributed Systems," *Proc. IRE*, **47**, 1213-1219 (July 1959).
203. B. B. Bossard, "Superregenerative Reactance Amplifier," *Proc. IRE*, **47**, 1269-1271 (July 1959).
204. J. J. Younger, A. G. Little, H. Heffner, and G. Wade, "Parametric Amplifiers as Superregenerative Detectors," *Proc. IRE*, **47**, 1271-1272 (July 1959).
205. A. Ashkin, W. H. Louisell, and C. F. Quate, "Fast Wave Couplers for Longitudinal Beam Parametric Amplifiers," *J. Electronics Control*, **7**, 1-32 (July 1959).
206. J. S. Cook and W. H. Louisell, "Fast Longitudinal Space-Charge Wave Parametric Amplifiers," *IRE WESCON Convention Record*, Part 3, 77-85 (August 18-21, 1959).

## Chapter 5

# Parametric coupling principle for distributed circuits

In Chapter 4 the theory of coupled modes of vibrations was extended to encompass time-varying coupling coefficients. This led to the theory of lumped circuit regenerative parametric oscillators, amplifiers, and frequency converters. Tien and Suhl<sup>1</sup> suggested that more stable operation might be achieved by using a distributed circuit rather than a lumped circuit.

It was shown in Chapter 1 that the theory of coupled modes of vibration and propagation are formally identical. It is therefore reasonable to expect that the parametric coupled mode theory of Chapter 4 can readily be adapted to parametrically coupled distributed circuits. The analysis will use the general coupled mode approach and the Manley-Rowe relations will be shown to be valid.

In the distributed parametric amplifier a transmission line propagates two forward normal modes at frequencies  $\omega_1$  and  $\omega_2$ , respectively. The shunt capacitance of the line is time-varying and, by changing the capacitance along the line in the proper way, a pump wave at frequency  $\omega$  will appear to propagate down the line (See Figure 5.1.) The capacitance is then a function of  $z$  and  $t$ . The pump wave will actively couple the signal and idler waves at frequency  $\omega_1$  and  $\omega_2$  and result in exponentially growing signal and idler waves.<sup>1</sup> The degenerate case ( $\omega_1 = \omega_2$ ) has been treated by Cullen.<sup>2</sup>

The device can be made into a frequency converter, if  $\omega = \omega_1 - \omega_2$ , or a backward wave amplifier or oscillator (see Chapter 3) if a circuit is chosen so that the group and phase velocities of the signal wave are in opposite directions.<sup>3</sup>

The general coupled mode theory for some of these devices is given in this chapter. The theory will be extended to cases in which more than two modes are strongly coupled. The noise figure is also discussed.

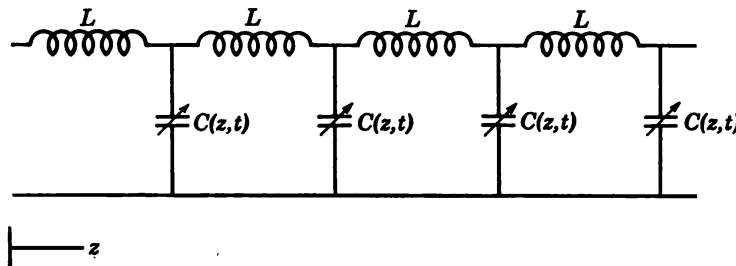


**Figure 5.1** Distributed (or traveling wave) parametric amplifier. This is a transmission line in which the shunt capacitances are made to vary with time and distance as  $C(z, t) = C_0 + \Delta C \cos(\omega t - \beta z)$ . This is a pump wave which propagates along the line in the positive  $z$ -direction. The line is dispersive, and if a forward signal wave of the form  $\cos(\omega_1 t - \beta_{12} z)$  is excited an idler wave will be generated by the pump and the signal of the form  $\cos(\omega_2 t - \beta_{22} z)$  where  $\omega = \omega_1 + \omega_2$  and  $\beta = \beta_1 + \beta_2$ . The pump couples the signal and idler waves. (From Tien and Suhl, Reference 1.)

### 5.1 Distributed Parametric Amplifier. General Coupled Mode Theory

The first case to be treated is the three-frequency distributed parametric amplifier shown in Figure 5.1 in which

$$\begin{aligned}\omega &= \omega_1 + \omega_2 \\ \beta &= \beta_1 + \beta_2\end{aligned}\tag{5.1}$$

$\omega_1$ ,  $\omega_2$ , and  $\omega$  are the frequencies of the signal, idler, and pump waves, respectively, and  $\beta_1$ ,  $\beta_2$  and  $\beta$  are the uncoupled propagation constants of these same waves which propagate on the same transmission line.

The shunt capacitance per unit length shown in Figure 5.1 is made to vary as

$$C(z, t) = C_0 + \Delta C \cos(\omega t - \beta z) \equiv C_0 + C_p(z, t)\tag{5.2}$$

where  $C_0$  may depend on frequency.  $C_p(z, t)$  looks like a pump wave propagating down the structure. (Discussion of an actual device that can yield such a capacitance variation is postponed until Chapter 6.)

In the absence of the pump ( $\Delta C = 0$ ), the transmission line can propagate a forward mode at frequency  $\omega_1$  and an independent forward mode at  $\omega_2$ . The equations for these two modes (see Eqs. 1.49) may be written as

$$\begin{aligned}\frac{da_{1+}}{dz} &= -j\beta_1 a_{1+} \\ \frac{da_{2+}^*}{dz} &= +j\beta_2 a_{2+}^*\end{aligned}\tag{5.3}$$

where

$$\begin{aligned}\beta_1 &= \omega_1 \sqrt{L_1 C_{01}} \\ \beta_2 &= \omega_2 \sqrt{L_2 C_{02}}\end{aligned}\quad (5.4a)$$

The series inductance may be frequency-dependent and is written  $L_{1,2}$  at  $\omega_{1,2}$ , respectively. Also  $C_{01}$  is  $C_0$  at  $\omega_1$  and  $C_{02}$  is  $C_0$  at  $\omega_2$ . Furthermore, the mode amplitudes (see Eqs. 1.46) are defined by

$$\begin{aligned}\frac{V_1(z, t)}{\sqrt{Z_{01}}} &= \sqrt{Z_{01}} I_1(z, t) = a_{1+}(z) e^{j\omega_1 t} + \text{c.c.} \\ \frac{V_2(z, t)}{\sqrt{Z_{02}}} &= \sqrt{Z_{02}} I_2(z, t) = a_{2+}(z) e^{j\omega_2 t} + \text{c.c.}\end{aligned}\quad (5.5)$$

since only forward modes are considered. Furthermore,

$$\begin{aligned}Z_{01} &= \sqrt{\frac{L_1}{C_{01}}} \\ Z_{02} &= \sqrt{\frac{L_2}{C_{02}}}\end{aligned}\quad (5.4b)$$

If  $\Delta C \ll \sqrt{C_{01}C_{02}}$ , the pump will couple the  $a_{1+}$ -mode to the  $a_{2+}^*$ -mode if  $\beta = \beta_1 + \beta_2$  by an argument similar to that given in Chapter 4. Accordingly, the coupled mode equations (see Eqs. 4.23) can be written

$$\begin{aligned}\frac{da_{1+}}{dz} &= - j\beta_1 a_{1+} + c_{12} e^{-j\beta z} a_{2+}^* \quad (a) \\ \frac{da_{2+}^*}{dz} &= j\beta_2 a_{2+}^* + c_{21} e^{j\beta z} a_{1+} \quad (b)\end{aligned}\quad (5.6)$$

The mode coupling coefficients,  $c_{12}$  and  $c_{21}$ , must be evaluated next. The general coupled mode approach of Section 1.5 will be used.

The power per unit length coupled into mode 1 due to the mixing with mode 2 is

---


$$- V_1(z, t) \frac{\partial}{\partial t} [C_p(z, t) V_2(z, t)] \quad (5.7a)$$

where the bar indicates the time average. This, in turn, must equal

$$\frac{d}{dz} 2|a_{1+}(z)|^2 \quad (5.7b)$$

since  $2|a_{1+}(z)|^2$  gives the power in mode 1. By using Eqs. 5.2 and 5.5, Eq. 5.7a is reduced to

$$\begin{aligned} -j\omega_1 \frac{\Delta C}{2} \sqrt{Z_{01}Z_{02}} (a_{1+}^* a_{2+} e^{-j\beta z} - a_{1+} a_{2+} e^{j\beta z}) \\ = 2(c_{12} e^{-j\beta z} a_{1+}^* a_{2+} + c_{12}^* e^{j\beta z} a_{1+} a_{2+}) \end{aligned}$$

where the latter equality follows from Eq. 5.7b when Eq. 5.6a and its complex conjugate are used. By identifying coefficients, it follows that

$$\begin{aligned} c_{12} &= -\frac{j}{4} \omega_1 \Delta C \sqrt{Z_{01}Z_{02}} \\ &= -\frac{j}{4} \sqrt{\frac{\omega_1}{\omega_2}} \frac{\Delta C}{\sqrt{C_{01}C_{02}}} \sqrt{\beta_1 \beta_2} \end{aligned} \quad (5.8a)$$

where Eqs. 5.4 have been used.

By a similar argument for the power increase in mode 2, it follows that

$$\frac{c_{12}}{\omega_1} = \frac{c_{21}^*}{\omega_2} \quad (5.8b)$$

When this relation is obeyed, the Manley-Rowe relations are satisfied and exponential growth occurs. The modes are said to be actively coupled when the mode coupling coefficients obey Eq. 5.8b.

It will now be shown that the Manley-Rowe relations are satisfied when  $c_{12}\omega_2 = c_{21}^*\omega_1$  and  $\omega = \omega_1 + \omega_2$ .

The Manley-Rowe relations for the lumped circuit, when only  $\omega_1 + \omega_2$ ,  $\omega_1$ , and  $\omega_2$  are present, are

$$\frac{P_{\omega_1}}{\omega_1} = \frac{P_{\omega_2}}{\omega_2} \quad (5.9)$$

For a distributed circuit they must be modified so that the power is measured in a length  $dz$ . In terms of the mode amplitudes, Eq. 5.9 becomes

$$\frac{d}{dz} \frac{2|a_{1+}|^2}{\omega_1} = \frac{d}{dz} \frac{2|a_{2+}^*|^2}{\omega_2} \quad (5.10)$$

since the power in mode 1 is defined as  $2|a_{1+}|^2$  and that in mode 2 is defined as  $2|a_{2+}^*|^2$ .

To show that Eq. 5.10 is satisfied, use Eqs. 5.6 and their conjugates and it follows that

$$\begin{aligned}\frac{d}{dz} \frac{2|a_{1+}|^2}{\omega_1} &= \frac{2}{\omega_1} (c_{12}e^{-j\beta z}a_{1+}*a_{2+}^* + \text{c.c.}) \\ \frac{d}{dz} \frac{2|a_{2+}^*|^2}{\omega_2} &= \frac{2}{\omega_2} (c_{21}^*e^{-j\beta z}a_{1+}^*a_{2+} + \text{c.c.})\end{aligned}\quad (5.11)$$

Then, if Eq. 5.8b is true, it follows that Eq. 5.10 is true. The converse is also true, and the Manley-Rowe relations are verified.

In order to show that relation 5.8b leads to growing waves (and, therefore, to active mode coupling) let

$$\begin{aligned}a_{1+}(z) &= e^{-j\beta_1 z} A_{1+}(z) \\ a_{2+}^*(z) &= e^{j\beta_2 z} A_{2+}^*(z)\end{aligned}\quad (5.12)$$

Substitute these equations in Eqs. 5.6, note that  $\beta = \beta_1 + \beta_2$ , and it will be seen that  $A_{1+}(z)$  and  $A_{2+}^*(z)$  vary as  $\exp(sz)$ , where

$$s = \pm \sqrt{c_{12}c_{21}} = \pm \frac{1}{4} \frac{\Delta C}{\sqrt{C_{01}C_{02}}} \sqrt{\beta_1\beta_2} \quad (5.13)$$

$s$  is real so that growing solutions occur, since Eq. 5.8b is satisfied.

It is next of interest to compute the gain. Assume a signal is applied at frequency  $\omega_1$ . It follows that the average power transmitted down the line at frequencies  $\omega_1$  and  $\omega_2$  is

$$\begin{aligned}P_1(z) &= 2|a_{1+}(z)|^2 = P_1(0) \cosh^2 |s|z \\ P_2(z) &= 2|a_{2+}^*(z)|^2 = \frac{\omega_2}{\omega_1} P_1(0) \sinh^2 |s|z\end{aligned}\quad (5.14)$$

These are sketched in Figure 5.2. The direction of power flow is in the direction of growth, so the power exponentially increases and gain can be achieved. It is easy to verify that

$$\frac{1}{\omega_1} \frac{dP_1}{dz} = \frac{1}{\omega_2} \frac{dP_2}{dz} = \frac{1}{\omega_1 + \omega_2} \frac{d}{dz} (P_1 + P_2) \quad (5.15a)$$

Also

$$\frac{P_1}{\omega_1} - \frac{P_2}{\omega_2} = \frac{P_1(0)}{\omega_1} \quad (\text{constant}) \quad (5.15b)$$

The power gain in decibels is given by

$$\text{gain(db)} = 10 \log_{10} \frac{P_1(L)}{P_1(0)} = 20 \log_{10} \cosh |s|L \quad (5.16a)$$

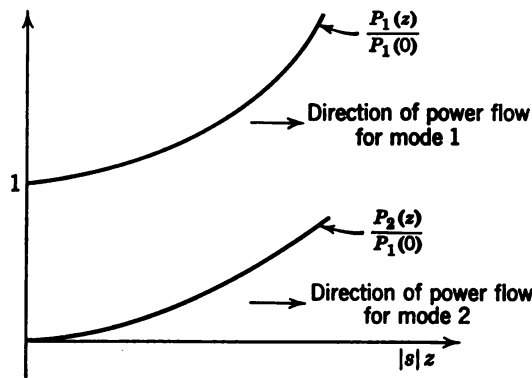


**Figure 5.2** Magnitude and direction of power flow for signal and idler waves of the distributed amplifier of Figure 5.1. Since the power grows in the direction of propagation, there is gain. (From Tien, Reference 3.)

For a tube long enough so that  $|s|L \gg 1$ ,

$$\text{gain} \cong (8.68|s|L - 6) \text{ db} \quad (5.16b)$$

It should be noted that since there is no loss and Eqs. 5.1 are satisfied there is no gain threshold. Consider now the case in which

$$\begin{aligned}\omega &= \omega_1 + \omega_2 \\ \beta &= \beta_1 + \beta_2 + \Delta\beta\end{aligned} \quad (5.17)$$

It will be shown that there is a gain threshold. Equations 5.6 are unmodified. Let

$$\begin{aligned}\beta_1' &= \beta_1 + \frac{1}{2}\Delta\beta \\ \beta_2' &= \beta_2 + \frac{1}{2}\Delta\beta\end{aligned} \quad (5.18)$$

for simplicity. Further, let

$$\begin{aligned}a_{1+}(z) &= A_{1+}(z)e^{-j\beta_1' z} \\ a_{2+}^*(z) &= A_{2+}^*(z)e^{j\beta_2' z}\end{aligned} \quad (5.19)$$

Equations 5.6 then become

$$\begin{aligned}\left(\frac{d}{dz} - j\frac{1}{2}\Delta\beta\right)A_{1+} &= c_{12}A_{2+}^* \\ \left(\frac{d}{dz} + j\frac{1}{2}\Delta\beta\right)A_{2+}^* &= c_{21}A_{1+}\end{aligned} \quad (5.20)$$

The solutions of these equations are also of the form  $\exp(st)$ , where

$$s = \pm \sqrt{\frac{(\Delta C)^2 \beta_1 \beta_2}{16 C_{01} C_{02}} - \left(\frac{\Delta \beta}{2}\right)^2} \quad (5.21)$$

This shows that the gain will be reduced if  $\Delta \beta \neq 0$ . Further, until the pump exceeds

$$\frac{\Delta C}{\sqrt{C_{01} C_{02}}} > \frac{2 \Delta \beta}{\sqrt{\beta_1 \beta_2}} \quad (5.22)$$

there will be no gain. Therefore, optimum gain is achieved when Eqs. 5.1 are satisfied.

It should be noted that the distributed parametric amplifier is a broadband device insofar as Eqs. 5.1 can be satisfied over a broad range of frequencies.

## 5.2 Distributed Frequency Converter <sup>3</sup>

From Section 4.7 of Chapter 4, a frequency converter results if

$$\begin{aligned} \beta &= \beta_1 - \beta_2 \\ \omega &= \omega_1 - \omega_2 \end{aligned} \quad (5.23)$$

In this case the Manley-Rowe relation (see Eq. 4.87) becomes

$$\frac{P_{\omega_1}}{\omega_1} = \frac{P_{\omega_2}}{-\omega_2} \quad (5.24)$$

where  $P_{\omega_1} = \frac{d}{dz} (2|a_{1+}|^2)$ ,  $P_{\omega_2} = \frac{d}{dz} (2|a_{2+}|^2)$ , and the coupling coefficients (see Eq. 4.88) satisfy

$$\frac{c_{12}}{\omega_1} = - \frac{c_{21}^*}{\omega_2} \quad (5.25)$$

In this case the  $a_{1+}$ - and  $a_{2+}$ -modes are passively coupled. There will be no exponentially growing solutions.

## 5.3 General Coupled Mode Theory When Many Modes Are Coupled

The experience that has now been obtained with coupled systems in which only a few modes have been coupled can be used to derive some relations among the mode coupling coefficients when  $n$ -modes are coupled. The first part of the section will apply to linearized time-invariant

systems of the type considered in Chapter 1, and the second part will apply to linearized systems with time-varying parameters of the type considered in Chapter 4 and Sections 5.1 and 5.2.

**Linearized time-invariant systems.** Consider a linearized system with constant coupling coefficients involving  $n$ -modes. The equations for such a system are

$$\frac{da_i}{dz} = \sum_{j=1}^n c_{ij}a_j \quad (i = 1, 2, \dots, n) \quad (5.26)$$

where the  $c_{ij}$  are constant mode coupling coefficients. The mode amplitudes are defined so that the average power carried by the  $i$ th mode is  $2|a_i|^2$ . The total average power is given by a power theorem which states that

$$\sum_{i=1}^n 2p_i|a_i|^2 = 0 \quad (5.27)$$

where  $p_i$  is called the parity of the mode and is

$$p_i = \begin{cases} +1 & \text{if the power flows in the positive } z\text{-direction and if the mode carries positive kinetic power} \\ -1 & \text{if the power flow is in the negative } z\text{-direction or if the mode carries negative kinetic power} \end{cases}$$

Note that the power theorem, or some equivalent information, must be known in order to determine the parity of the mode. For example, the Chu power theorem had to be known in Chapter 2 in order to determine that the slow mode carries negative power, since the fast and slow modes are not coupled if no circuit is present.

If the modes are coupled ( $c_{ij} \neq 0, i \neq j$ ), multiply Eq. 5.26 by  $p_i a_i^*$  and add it to its complex conjugate. This gives

$$\frac{d}{dz} p_i |a_i|^2 = \sum_{j=1}^n p_i c_{ij} a_i^* a_j + \sum_{j=1}^n p_i c_{ij}^* a_i a_j^* \quad (i = 1, 2, \dots, n) \quad (5.28)$$

Now sum all  $n$  of these equations:

$$\frac{d}{dz} \sum_{i=1}^n p_i |a_i|^2 = \sum_{i=1}^n \sum_{j=1}^n p_i c_{ij} a_i^* a_j + \sum_{i=1}^n \sum_{j=1}^n p_i c_{ji}^* a_j a_i^* \quad (5.29)$$

where the  $i$  and  $j$  have been interchanged in the second sum. This can be done, since the sum extends over all  $i$  and  $j$  and the order of taking the terms cannot alter a finite sum.

From the power theorem, Eq. 5.27, the left side of Eq. 5.29 is zero, and it follows that

$$\sum_{i=1}^n \sum_{j=-n}^n (p_i c_{ij} + p_j c_{ji}^*) a_j a_i^* \equiv 0$$

This sum will be identically satisfied for all  $z$  if and only if

$$c_{ij} = -\frac{p_j}{p_i} c_{ji}^* \quad (5.30)$$

If the parities of both modes are the same,  $c_{ij} = -c_{ji}^*$ , whereas if they are opposite  $c_{ij} = +c_{ji}^*$ . From the work of Chapter 1 it follows that if two modes with the same parity are coupled they must be passively coupled, but if they have opposite parities they must be actively coupled. (See Section 1.8 of Chapter 1.)

As an example, in the TWT the average power is given by  $|a_{1+}|^2 + |a_{2+}|^2 - |a_{2-}|^2 = \text{constant}$ . This may be verified by differentiating this expression with respect to  $z$  and using Eqs. 3.24 and their conjugates. Application of Eq. 5.30 shows that the  $a_{1+}$ -mode is actively coupled to the  $a_{2-}$ -mode but passively coupled to the  $a_{2+}$ -mode. ( $c_{12}$  is given by Eq. 3.11.)

**Linearized system with time-varying parameters.** Consider a linearized system with time-varying parameters which vary at frequency  $\omega$  and a signal at frequency  $\omega_1$ . Under the weak coupling assumption, it can be shown that the time-varying parameter will couple waves at frequencies

$$\Omega_i = \omega_1 + i\omega \quad (i = 0, \pm 1, \pm 2, \dots) \quad (5.31)$$

The coupled mode equations in this case become

$$\frac{da_i}{dz} = \sum_{j=-n}^{+n} c_{ij}(z) a_j \quad (i = 0, \pm 1, \dots, \pm n) \quad (5.32)$$

and the coupling coefficients are functions of  $z$ .

Assume that the system obeys the Manley-Rowe relations. They can be written as

$$\sum_{i=-n}^{+n} \frac{d}{dz} \frac{p_i |a_i|^2}{|\Omega_i|} = 0 \quad (5.33)$$

where  $p_i = \frac{|\Omega_i|}{\Omega_i} = \pm 1$ . Knowledge of the Manley-Rowe relations will therefore determine the parity. It cannot be correlated with direction of power flow in this case.

By an argument analogous to that used to obtain Eq. 5.30, it follows that if the Manley-Rowe relations are satisfied the coupling coefficients must satisfy

$$c_{ij}(z) = - \frac{p_j}{p_i} \left| \frac{\Omega_i}{\Omega_j} \right| c_{ji}^*(z) \quad (5.34)$$

From Eqs. 5.8b and 5.25 it can be stated that if the relative parities of two modes are opposite in sign the modes  $a_i$  and  $a_i^*$  are actively coupled, whereas if the relative parities of two modes are the same  $a_i$  is passively coupled to  $a_j$ .

As an example, assume  $\omega = \omega_1 - \omega_2$ . Then, by Eq. 5.31,  $\Omega_0 = +\omega_1$  and  $\Omega_{-1} = +\omega_2$ . Therefore,  $p_0 = +1$  and  $p_{-1} = +1$ ; and if  $\omega = \omega_1 - \omega_2$ , mode  $a_0$  will be coupled passively to  $a_{-1}$ . On the other hand, if  $\omega = \omega_1 + \omega_2$ ,  $\Omega_0 = \omega_1$  and  $\Omega_{-1} = -\omega_2$ . Therefore,  $p_0 = +1$  and  $p_{-1} = -1$ , and mode  $a_0$  will be actively coupled to mode  $a_{-1}^*$ .

If the relative parities of two modes are the same, the two modes can be visualized as two vectors rotating in the same sense for a fixed  $z$ , whereas if the parities are opposite the pump will couple two counter-rotating vectors for a fixed  $z$ . Coupling between two counterrotating vectors is necessary for parametric amplification.

#### 5.4 A Four-Frequency Traveling Wave Parametric Amplifier (Pump Frequency Lower Than Signal Frequency)

It was pointed out in Chapter 4 that one bad feature of the parametric amplifier is that the pump frequency is higher than the signal frequency when three frequencies are involved. If the pump frequency is less than the signal frequency, the modes are passively coupled, which leads to a frequency converter.

Hogan and co-workers<sup>4</sup> have suggested a device that utilizes two idler frequencies, and Chang and Bloom<sup>5,6,7</sup> have suggested using two pump frequencies in order to have the pump frequency less than the signal frequency.

Consider, then, the Hogan scheme in which waves of three frequencies,  $\omega_1$ ,  $\omega_2$ , and  $\omega_3$ , propagate on a transmission line and are coupled by a time-varying capacitance.<sup>8</sup>

$$C(z, t) = C_0 + \Delta C \cos(\omega t - \beta z) \quad (5.35)$$

Let the frequencies and phase constants satisfy the following relations:

$$\begin{aligned} \omega &= \omega_1 - \omega_2 & \beta &= \beta_1 - \beta_2 \\ \omega &= \omega_2 + \omega_3 & \beta &= \beta_2 + \beta_3 \end{aligned} \quad (5.36)$$

In this case three forward modes will be coupled. Since  $\omega = \omega_1 - \omega_2$ , the  $a_1$ - and  $a_2$ -modes will be passively coupled, as shown in Section 5.3. Also, since  $\omega = \omega_2 + \omega_3$ , modes 2 and 3 will be actively coupled. Since active coupling takes place between counterrotating vectors,  $a_2$  is coupled to  $a_3^*$ . The coupled mode equations are then given by

$$\begin{aligned}\frac{da_1}{dz} &= -j\beta_1 a_1 + c_{12} e^{-j\beta_2 z} a_2 \\ \frac{da_2}{dz} &= -j\beta_2 a_2 + c_{21} e^{j\beta_2 z} a_1 + c_{23} e^{-j\beta_3 z} a_3^* \\ \frac{da_3^*}{dz} &= +j\beta_3 a_3^* + c_{32} e^{j\beta_3 z} a_2\end{aligned}\quad (5.37)$$

(The plus subscripts are omitted, since only forward modes are involved.) The sign of  $e^{\pm j\beta z}$  is chosen so that Eqs. 5.36 will be satisfied, since for weak coupling  $a_1 \sim e^{-j\beta_1 z}$ ,  $a_2 \sim e^{-j\beta_2 z}$ , and  $a_3^* \sim e^{+j\beta_3 z}$ . There is no direct coupling of  $\omega_1$  and  $\omega_3$  by the pump by virtue of Eqs. 5.36, for it is seen that  $2\omega = \omega_1 + \omega_3$ , and *only frequencies that add up to the pump frequency will be coupled directly*.

From Eq. 5.34 it follows that

$$\frac{c_{12}}{\omega_1} = -\frac{c_{21}^*}{\omega_2} \quad \frac{c_{23}}{\omega_2} = \frac{c_{32}^*}{\omega_3} \quad (5.38)$$

since the 1 and 2 modes are passively coupled and the 2 and 3 modes are actively coupled.

The coefficients may be computed as usual from the power transferred between the modes. The result is

$$\begin{aligned}c_{12} &= -\frac{j}{4} \sqrt{\frac{\omega_1}{\omega_2}} \frac{\Delta C \sqrt{\beta_1 \beta_2}}{\sqrt{C_{01} C_{02}}} = -\frac{\omega_1}{\omega_2} c_{21}^* \\ c_{23} &= -\frac{j}{4} \sqrt{\frac{\omega_2}{\omega_3}} \frac{\Delta C \sqrt{\beta_2 \beta_3}}{\sqrt{C_{02} C_{03}}} = \frac{\omega_2}{\omega_3} c_{32}^*\end{aligned}\quad (5.39)$$

Needless to say, the direct coupled mode approach leads to the same result. These equations may be transformed by the usual substitution (see, for example, Eqs. 5.12), and solutions of the form  $\exp(sz)$  are easily found in which

$$s = 0; \quad s = \pm \frac{\Delta C \sqrt{\beta_2}}{4 \sqrt{C_{02}}} \sqrt{\frac{\beta_3}{C_{03}} - \frac{\beta_1}{C_{01}}} \quad (5.40)$$

Therefore, if  $\beta_3 C_{01} > \beta_1 C_{03}$ , there will be a growing, decaying, and unattenuated normal mode. For example,

$$a_1(z)e^{j\omega_1 t} = A_1(z)e^{j(\omega_1 t - \beta_1 z)} \quad (5.41)$$

in which

$$A_1(z) = c_1 + c_2 e^{|s|z} + c_3 e^{-|s|z}$$

where  $c_1$ ,  $c_2$ , and  $c_3$  are constants of integration. Similarly,  $A_2$  and  $A_3^*$  grow exponentially. A signal applied at any one of the three frequencies at the input will therefore be amplified, and the energy is supplied by the variable capacitance. If  $\omega_1$  is the signal frequency and  $\omega$  is the pump, then the signal frequency is higher than the pump frequency, which is the advantage of using two idler (or two pump) frequencies.

If  $\beta_3 C_{01} < \beta_1 C_{03}$ , all three waves are periodic in  $z$  ( $s$  becomes pure imaginary), the passively coupled modes dominate the actively coupled modes, and there is no further exponential gain. Power is converted among the various frequencies. This situation is equivalent to passively coupled transmission lines, and the device acts like a frequency converter. Part of the energy is then supplied by the pump and part is converted from the impressed signal (or signals).

### 5.5 Noise Figure of Distributed Parametric Amplifiers

The primary advantage of parametric amplifiers is their extremely low noise capabilities, as was pointed out in Chapter 4. A discussion of the noise figure of a distributed parametric amplifier will now be presented.

Every different medium used for parametric amplifiers has its own peculiar sources of noise. These sources are treated on an individual basis in later chapters. The lossless transmission line can, in principle, possess excellent low noise properties. Actual devices will, of course, have loss that will degrade the noise performance. The noise figure will be derived for a lossless distributed parametric amplifier in which the noise considered is the background noise in the absence of a signal. Only the result is given when there is loss.

Consider the distributed transmission line of Section 5.1. Assume that the pump, signal, and idler propagation constants before coupling satisfy Eqs. 5.1, viz.,  $\beta = \beta_1 + \beta_2$ , so that there will be no gain threshold. Further assume that the input is connected to a matched signal source at 290°K at frequency  $\omega_1$ . Assume that at  $\omega_2$  the input is matched to a passive impedance at temperature  $T$  and that the output end is matched to a load at temperature  $T_L$ . This is shown schematically in Figure 5.3.

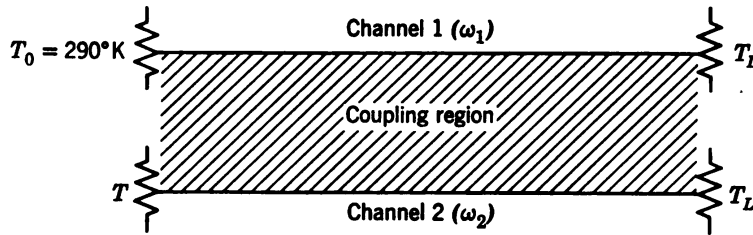


**Figure 5.3** Schematic representation of two channels for noise and signal in a distributed three-frequency parametric amplifier. The  $\omega_1$  input channel is terminated in a matched impedance at temperature  $T_0$ , the input of the  $\omega_2$  channel is terminated in a matched impedance at temperature  $T$ , and the outputs of the  $\omega_1$  and  $\omega_2$  channels are terminated in matched impedances at temperature  $T_L$ .

The noise figure given in Chapter 4, Eq. 4.72, is

$$F = \frac{\text{noise out}}{k 290^\circ B \text{ gain}} \quad (5.42)$$

The available input noise power at  $\omega_1$  is the Johnson thermal noise,  $kT_0B$ , from the matched signal source, where  $T_0 = 290^\circ\text{K}$ . If  $g^2$  is the power gain of the amplifier,

$$g^2 = \frac{S_{\text{out}}}{S_{\text{in}}} \quad (5.43)$$

the available output noise at  $\omega_1$  will be

$$N_0(\omega_1) = kT_0Bg^2 \quad (\text{watts}) \quad (5.44)$$

where  $k = 1.380 \times 10^{-23}$  joule/ $^\circ\text{K}$  (Boltzmann's constant) and  $B$  is the frequency bandwidth in cycles/second. This, of course, neglects thermal noise contributed by the loss in an actual device.

Further, the available noise output power at  $\omega_2$  due to  $kTB$  input at  $\omega_2$  is

$$N_0(\omega_2) = kTBg^2 \quad (5.45)$$

since the gain at  $\omega_1$  and  $\omega_2$  is the same and  $T$  is the temperature of the generator at  $\omega_2$ . Therefore, the excess noise at the output over the input at  $\omega_2$  is

$$\Delta N_0(\omega_2) = kTB(g^2 - 1) \quad (5.46)$$

Now, by the Manley-Rowe relation (Eq. 5.9), this power is converted to frequency  $\omega_1$ , so that

$$\Delta N_0(\omega_1) = \frac{\omega_1}{\omega_2} \Delta N_0(\omega_2) = \frac{\omega_1}{\omega_2} kTB(g^2 - 1) \quad (5.47)$$

Then the total available noise output power at  $\omega_1$  is the sum of Eqs. 5.44 and 5.47, viz.,

$$N_{0T}(\omega_1) = kT_0Bg^2 + \frac{\omega_1}{\omega_2} kTB(g^2 - 1) \quad (5.48)$$

whereas the total available input power at  $\omega_1$  is

$$N_{iT}(\omega_1) = kT_0B \quad (5.49)$$

If a signal is introduced at  $\omega_1$  only, then from the definition of gain (Eq. 5.43)

$$g^2 = \frac{S_{\text{out}}(\omega_1)}{S_{\text{in}}(\omega_1)} \quad (5.50)$$

and the noise figure (Eq. 5.42) is

$$F = 1 + \frac{\omega_1}{\omega_2} \frac{T}{T_0} \frac{(g^2 - 1)}{g^2} \quad (5.51)$$

where Eqs. 5.48–5.50 have been used.

The effective input noise temperature (by Eqs. 4.74 and 5.51) is

$$T_e = \frac{\omega_1}{\omega_2} T \frac{(g^2 - 1)}{g^2} \quad (5.52)$$

Consider the case of large gain,  $g^2 \gg 1$ . It is then seen that the single sideband noise figure (Eq. 5.51) can be improved by making  $\omega_2 \gg \omega_1$ . If, however,  $T \cong T_0$  and  $\omega_1 \cong \omega_2$ , the usual case, the effective noise temperature is  $290^\circ$ . Alternatively, it is seen that the noise figure can be improved by cooling the idler frequency termination  $T$ , just as in the cavity case of Chapter 4.

By arguments similar to the foregoing, when double sideband reception is used, it is easy to show that the total available input noise to both channels is

$$N_{\text{in}} = kB(T + T_0) \quad (5.53)$$

the total output noise is

$$N_{\text{out}} = \left( kT_0Bg^2 + \frac{\omega_1}{\omega_2} kTB(g^2 - 1) \right) + \left( kTBg^2 + \frac{\omega_2}{\omega_1} kT_0B(g^2 - 1) \right) \quad (5.54)$$

and the total signal input is

$$S_{\text{in}} = S_{\text{in}}(\omega_1) + S_{\text{in}}(\omega_2) \quad (5.55)$$

whereas the signal out is

$$\begin{aligned} S_{\text{out}} = & \left( g^2 S_{\text{in}}(\omega_1) + \frac{\omega_1}{\omega_2} S_{\text{in}}(\omega_2)(g^2 - 1) \right) \\ & + \left( g^2 S_{\text{in}}(\omega_2) + \frac{\omega_2}{\omega_1} S_{\text{in}}(\omega_1)(g^2 - 1) \right) \quad (5.56) \end{aligned}$$

The noise figure for double sideband reception is then

$$\begin{aligned} F = & \left( \frac{S_{\text{in}}}{N_{\text{in}}} \right) \left( \frac{N_{\text{out}}}{S_{\text{in}}} \right) = 1 + \frac{T_e}{290^\circ} \\ = & \frac{1 + \frac{\frac{\omega_1}{\omega_2} T + \frac{\omega_2}{\omega_1} T_0}{T + T_0} \left( \frac{g^2 - 1}{g^2} \right)}{1 + \frac{\frac{\omega_1}{\omega_2} S_{\text{in}}(\omega_2) + \frac{\omega_2}{\omega_1} S_{\text{in}}(\omega_1)}{S_{\text{in}}(\omega_1) + S_{\text{in}}(\omega_2)} \left( \frac{g^2 - 1}{g^2} \right)} \quad (5.57) \end{aligned}$$

Now, if  $\omega_1 = \omega_2$ , it is seen that  $F = 1$  or  $T_e = 0^\circ\text{K}$  and the device is perfect. That is, since the device is lossless and if both channels are used,  $F = 1$ , whereas if only one channel is used and  $\omega_1 = \omega_2$ ,  $T = T_0$  and  $g^2 \gg 1$ ,  $F = 2$ , or  $T_e = 290^\circ\text{K}$ .

When the  $\omega_1$ -mode has a loss per unit length,  $r_1$ , at temperature  $T_c$  and the  $\omega_2$ -mode has a loss per unit length,  $r_2$ , at temperature  $T_i$ , Tien<sup>8</sup> has shown that the excess noise temperature is given by

$$T_e = \frac{g^2 - 1}{g^2} \left( \frac{\alpha_1}{\mu - \alpha_1} T_c + \frac{\omega_1}{\omega_2} \frac{\mu}{\mu - \alpha_1} T_i \right) \quad (5.58)$$

where  $g^2$  is the power gain given by

$$g^2 = e^{(\mu - \alpha)l} \quad (5.59)$$

$l$  is the length of the amplifier,  $\mu$  is given by

$$\mu = \sqrt{\frac{\omega_1 \omega_2 \Delta L^2}{Z_{01} Z_{02}}} \quad (5.60)$$

$\alpha_1$  is a loss parameter given by

$$\alpha_1 = \frac{r_1}{Z_{01}} \quad (5.61)$$

$\Delta L$  is the amplitude of the variable inductance of the pump, and  $Z_{01}$

and  $Z_{02}$  are the characteristic impedances of the  $\omega_1$ - and  $\omega_2$ -modes, respectively. When the gain is large,

$$g^2 \gg 1 \quad \text{and} \quad \mu \gg \alpha_1 \quad (5.62)$$

It follows that

$$T_e \cong \frac{\alpha_1}{\mu - \alpha_1} T_c + \frac{\omega_1}{\omega_2} \frac{\mu}{\mu - \alpha_1} T_i \cong \frac{\omega_1}{\omega_2} T_i \quad (5.63)$$

which is exactly the same as the expressions given for the cavity in Chapter 4.

Tien <sup>3,8</sup> has also given a corresponding derivation for the noise figure of distributed parametric frequency converters. He finds that

$$F = \frac{\left( \frac{\omega_2}{\omega_1} T_0 + \frac{\omega_1}{\omega_2} T \right)}{T + T_0} \cdot \frac{[S_{in}(\omega_1) + S_{in}(\omega_2)]}{\left( \frac{\omega_2}{\omega_1} S_{in}(\omega_1) + \frac{\omega_1}{\omega_2} S_{in}(\omega_2) \right)} \quad (5.64)$$

## 5.6 Remarks

- a. It is tempting to include other cases treated by Tien <sup>3</sup> such as the backward wave parametric amplifier and oscillator. However, in the interest of brevity they are not included. It would be a worthwhile exercise to treat these devices from a coupled mode viewpoint, since Tien has treated them by using a more standard type of analysis.
- b. Another exercise of interest would be to treat the three-frequency distributed parametric amplifier from a direct coupled mode approach.
- c. The circuits considered in Chapters 4 and 5 are the analogs of actual devices that have been built. A large part of the remainder of the book is devoted to a study of active media that can be used to obtain parametric coupling.

## BIBLIOGRAPHY

1. P. K. Tien and H. Suhl, "A Traveling Wave Ferromagnetic Amplifier," *Proc. IRE*, **46**, 700-706 (April 1958).
2. A. L. Cullen, "A Traveling Wave Parametric Amplifier," *Nature*, **181**, 332 (February 1, 1958).
3. P. K. Tien, "Parametric Amplification and Frequency Mixing in Propagating Circuits," *J. Appl. Phys.*, **29**, 1347-1357 (September 1958).
4. C. L. Hogan, R. L. Jepsen, and P. H. Vartanian, "A New Type of Ferromagnetic Amplifier," *J. Appl. Phys.*, **29**, 422-423 (March 1958). This device was also independently suggested by Professor H. Heffner of Stanford University.

5. S. Bloom and K. K. N. Chang, "Theory of Parametric Amplifiers," *R C A Rev.*, **18**, 578-593 (December 1957).
6. S. Bloom and K. K. N. Chang, "Parametric Amplifiers Using Low Frequency Pumping," *J. Appl. Phys.*, **29**, 594 (March 1958).
7. K. K. N. Chang and S. Bloom, "Parametric Amplifiers Using Lower Frequency Pumping," *Proc. IRE*, **46**, 1383-1386 (July 1958).
8. P. K. Tien, "Noise in Parametric Amplifiers," *Acta Electronica*, **4**, No. 4 (October 1960).

## Chapter 6

# Semiconductor diode parametric amplifiers

It has been shown in Chapter 4 that if two resonant circuits are coupled by a time-varying capacitance the device can be used to amplify signals parametrically. The capacitance variation was achieved mechanically by pulling the condenser plates apart and pushing them together at a frequency  $\omega = \omega_1 + \omega_2$ , where  $\omega_1$  and  $\omega_2$  are the resonant frequencies of circuits 1 and 2, respectively. This method of achieving a time-varying capacitance is clearly useless for all but the very lowest frequencies.

In Chapter 4, Section 4.4, it was shown that a nonlinear condenser can act as a time-varying condenser by varying the voltage across it.<sup>1,2</sup> It will be shown qualitatively that a P-N junction diode<sup>3,4</sup> has a nonlinear voltage-capacitance characteristic, so that its capacitance may be made to vary sinusoidally by applying an r-f voltage across it. The development of low-loss semiconductor diodes is, in fact, one of the principal reasons for the revived interest in parametric amplifiers. The capacitance can be varied electrically, so that semiconductor diodes offer an ideal material to use for parametric amplifiers. Because of the nature of semiconductors, such devices should have an unlimited life, an important consideration.

The purpose of this chapter is to study the diode as a parametric circuit element. A brief discussion of the noise problem, as well as some of the remarkable experimental results with both lumped and distributed circuits achieved with these materials will be given. Some of the semiconductors that have been used are discussed briefly. Undoubtedly, materials research in the future will produce semiconductors that will give even better results than those reported here.

### 6.1 The P-N Junction Diode as a Variable Capacitance Element

A short plausibility argument is given to show that a P-N junction diode acts like a variable capacitance element.

Consider a semiconductor such as silicon or germanium. The atoms in the crystal are bonded covalently to each other. Now imagine that at one of the lattice sites an atom of germanium is replaced by an atom of arsenic. Arsenic has one more outer electron than germanium and is about the same physical size as germanium, so that it will go into a Ge lattice site, but there is an extra orbital electron of As that is not needed to bond covalently with the neighboring Ge atoms. This electron is therefore not bonded to the atoms and is free to roam around. In this case the Ge is said to be doped with As, and the resulting material is called *n*-type Ge. The As atoms are called donor atoms.

If, on the other hand, the Ge is doped with gallium, there is room for one more electron to complete the covalent bond with the Ge neighbors. This represents an electron deficient state and is called a hole. A free electron can move into the hole and complete the bond. Such material is called *p*-type Ge. The Ga atoms are called acceptor atoms.

Electrically, both the *p*-type and *n*-type materials are neutral. Consider a P-N junction when the *p* and *n* materials are in contact. Because of the different affinities of the materials for holes and electrons, electrons will migrate to the *p*-region and holes to the *n*-region. As the diffusion proceeds, an electric field is set up at the junction, which will ultimately become large enough to halt any further *net* transfer of charge between the two types of material. This will be a dynamic thermal equilibrium situation in which as many holes move one way as electrons move the other.

Figure 6.1a shows a P-N junction diode when thermal equilibrium has been established. The *p*-type material contains acceptor atoms that are bound to the crystal lattice and also holes, whereas the *n*-type material has donors and electrons. There is a transition region, sometimes called a depletion layer, between the *p*-type and *n*-type materials in which electrons have migrated to the *p*-type region and holes to the *n*-type region. Figure 6.1b shows the hole and electron concentration across the transition region as well as the donor and acceptor concentrations.

Figure 6.1c shows the net charge distribution in thermal equilibrium across the junction when there is no bias. This equilibrium net charge distribution is no longer zero once the *p*- and *n*-type materials are joined, but rather the charge forms a dipole layer: there is a net positive charge physically separated from a net negative charge. Figure 6.1d shows the equilibrium potential distribution across the junction.

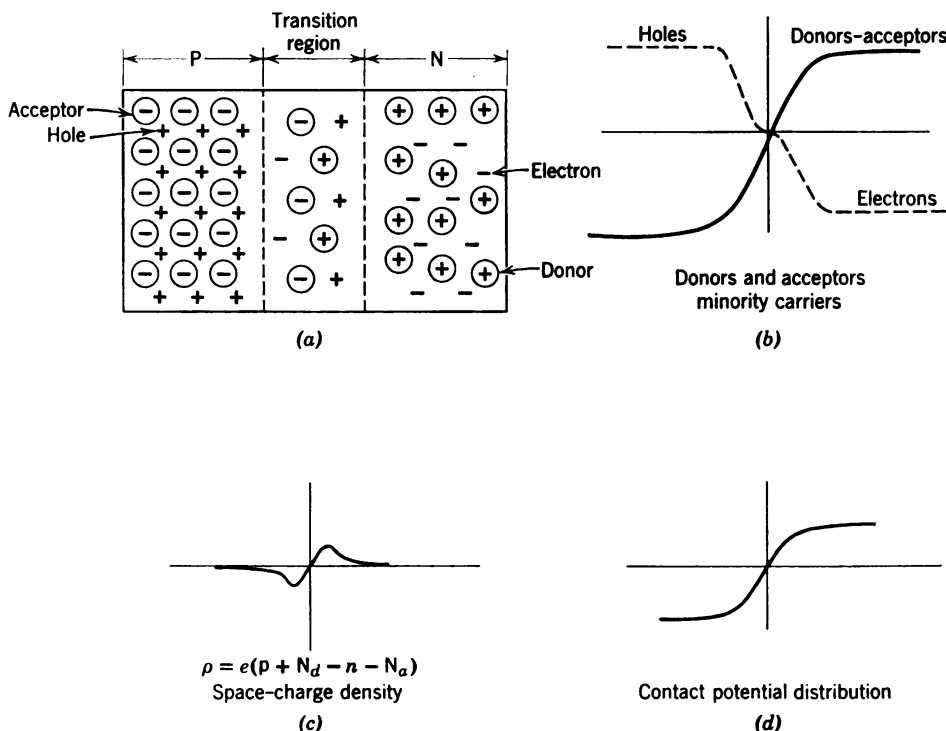


**Figure 6.1** (a) The P-N junction diode, showing donors, acceptors, holes, and electrons under zero bias conditions; (b) the concentration of impurities and carriers across a P-N junction diode; (c) net space-charge density distribution,  $\rho = e(p + N_d - n - N_a)$ ; (d) equilibrium contact potential distribution.

It is well known that charges of unlike sign on conductors that are physically separated possess a capacitance. Therefore, the diode looks like a parallel plate condenser. Consider what happens when a reverse bias is applied to the junction, as shown in Figure 6.2a. Under reverse bias, a negative potential is applied to the *p*-region so that holes are attracted to the negative electrode and electrons to the positive electrode. The densities of the holes and electrons are changed, but the donor-acceptor concentrations are relatively unaltered, since they are more tightly bound to the crystal lattice. The new equilibrium charge concentrations are shown in Figure 6.2b, and the charge distribution is shown in Figure 6.2c. The result is that the separation of the charges has increased from the zero bias state with a decrease in capacitance. The capacitance variation involves only very minute motions of the electrons and holes so that the variation can respond to fields at microwave frequencies.

Shockley<sup>3,4</sup> has computed the transition region capacitance for a planar P-N junction with a linearly tapered impurity density. He finds

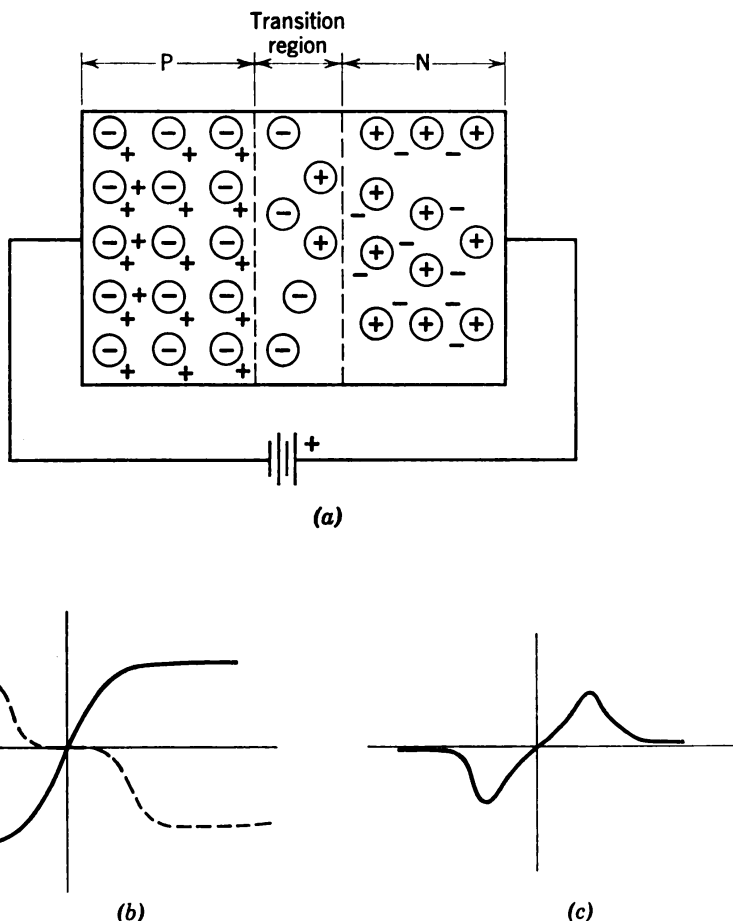


**Figure 6.2** The P-N junction diode when a negative bias is applied. (a) Schematic representation of diode; (b) impurity (solid) and carrier (dashed) concentration; (c) net charge distribution.

that it is a nonlinear function of the voltage across it and is given by

$$C_T \approx \frac{\epsilon A}{\left(\frac{12\epsilon}{ae}\Phi\right)^{\frac{1}{2}} \left(1 - \frac{V}{\Phi}\right)^{\frac{1}{2}}} = \frac{C(0)}{\left(1 - \frac{V}{\Phi}\right)^{\frac{1}{2}}} \quad (6.1)$$

where  $\epsilon$  is the dielectric constant of the material,  $A$  is the cross-sectional area of the junction,  $a$  is the constant gradient of the impurity density,  $\Phi$  is the contact potential of the junction,  $e$  is the electronic charge, and  $V$  is the voltage applied across the diode. Figure 6.3 shows a sketch of a capacitance-voltage plot of a graded Si junction diode.

If a small d-c reverse bias has an a-c generator added to it, whose amplitude is small, then, it is easy to see (Chapter 4, Section 4.4) that

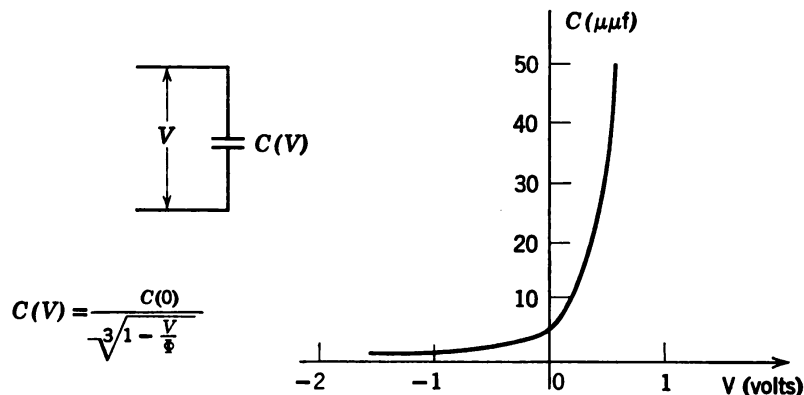


**Figure 6.3** Approximate capacitance voltage relation for a typical graded junction silicon diode used in experimental amplifiers.

$$C(V) \cong C(0) / \left[ 1 - \frac{V}{\Phi} \right]^{1/3}$$

(From Engelbrecht, Reference 21.)

the nonlinear capacitance is equivalent to a time-varying capacitance given approximately by

$$C(t) = C_0 + \Delta C \cos(\omega t + \phi) \quad (6.2)$$

where  $\omega$  is the frequency of the pump voltage applied across the capacitance.

Consider now how such a semiconductor diode might be used in an actual circuit. Figure 6.4a shows a rough sketch of a rectangular cavity operating in a  $TE_{011}$ -mode. The solid arrows show the electric field strength, which goes to zero at all the walls, and the dashed lines show the magnetic field. The electric field strength is largest at the center of the cavity, whereas the magnetic field is strongest near the walls of the cavity. It is well known that an  $LC$  circuit can be used as the equivalent circuit for such a cavity. The energy stored in the cavity magnetic field becomes the energy in the field of the inductance, and the cavity electric field energy becomes the energy associated with the capacitance. If the electric energy is changed, the equivalent circuit capacity is changed.

Figure 6.4b shows that a diode placed at the center of the cavity will cause the electric field lines, and, therefore, the electric field energy, to be even more concentrated in the center of the cavity, so that the capacitance in the equivalent circuit is changed.

Figure 6.4c shows how a d-c bias might be applied to the diode. An r-f choke must of course be provided, and pump power must be supplied. One method of applying pump power is by using a signal genera-

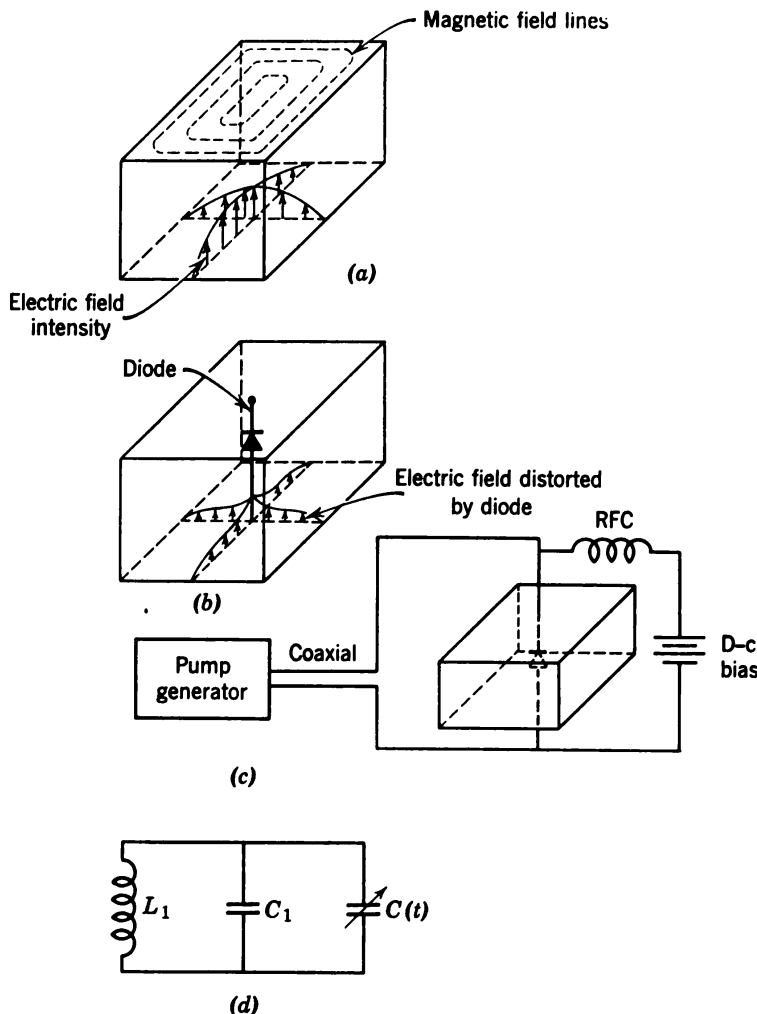


**Figure 6.4** (a) Sketch of r-f electric (arrows) and magnetic (dashed line) field lines for  $TE_{011}$ -mode in rectangular cavity; (b) distortion of field due to presence of diode; (c) possible method of applying d-c bias and pump power to diode; (d) equivalent circuit.

tor at frequency  $\omega$ , which is connected directly across the diode. A second method is to use a cavity that resonates in two modes: the signal,  $TE_{011}$ -mode, and a higher order mode at frequency  $\omega$ . The higher order pump mode is then excited by a probe in the usual way.

Finally, the equivalent circuit for degenerate operation is shown in Figure 6.4d. For nondegenerate operation the cavity must also be resonant to the idler frequency  $\omega_2$ . Once this equivalent circuit is established, the coupled mode theory developed in Chapter 4 is directly applicable.

## 6.2 Diode Amplifier Gain

It was pointed out in Chapter 4 that the lumped circuit parametric amplifier could be used as a transmission-type or reflection-type device. The equivalent circuits for gain calculations are shown in Figures 4.6 and 4.7, respectively. It is clear from the discussion in Section 6.1 that these are the equivalent circuits when a semiconductor diode is the active medium. For reference, the gain<sup>5,6</sup> for the transmission cavity (Eq. 4.70) was

$$\text{power gain} \equiv g^2 = \frac{4G_{g1}G_{L1}}{(G_{L1} + G_{g1} + G_1 - G_{e1})^2} \quad (6.3)$$

whereas for the transmission type (Eq. 4.71)

$$\text{power gain} \equiv g^2 = \left[ \frac{G_{g1} - (G_1 - G_{e1})}{G_{g1} + (G_1 - G_{e1})} \right]^2 \quad (6.4)$$

where

$$-G_{e1} = -\frac{\omega_1\omega_2(\Delta C)^2}{4G_2} \quad (\omega_1 \neq \omega_2) \quad (6.5a)$$

When  $\omega_1 = \omega_2$  (degenerate operation), it is easy to show that

$$-G_{e1} = -\frac{\Delta C\omega_1}{2} \quad (\omega_1 = \omega_2) \quad (6.5b)$$

Consider how the gain is changed if  $\omega$  is held constant while  $\omega_1$  and  $\omega_2$  are changed in such a way that  $\omega = \omega_1 + \omega_2$ . Assume that the pump power ( $\sim \Delta C$ ) is also constant and that  $G_2$ , the loss in circuit 2, is also unaltered. Then, by Eqs. 6.5,  $G_{e1} \sim \omega_1\omega_2 \sim \omega_1(\omega - \omega_2)$ . The greater the negative conductance, the larger the gain will be, and it follows that  $G_{e1}$  will be a maximum when  $\omega = 2\omega_1 = 2\omega_2$ . As  $\omega_1$  deviates far from  $\omega/2$ , the gain will be reduced.

Before considering the noise problem for the diode parametric amplifier, it should be noted in passing that the diode can be used to realize frequency converters and the lower pump frequency schemes of Hogan and co-workers<sup>7</sup> and Chang and Bloom.<sup>8</sup>

## 6.3 Diode Noise Considerations<sup>5,6,9</sup>

The noise figure for lumped circuit parametric amplifiers, in which the circuit, load, and generator losses were considered as noise sources, has

been given in Chapter 4. Any loss in the variable reactance itself was neglected. In a diode this is not a sufficiently accurate assumption. There is thermal noise in the diode due to the random scattering of the carriers (electrons and holes) across the transition region between the *p*- and *n*-type materials. This noise can be thought of as originating from a resistance,  $R_s$ , in series with the diode. The carriers can be scattered from the atoms of the parent semiconductor or by the impurity atoms. As the temperature of the diode is increased, the lattice atoms are in more rapid motion, and it turns out that scattering from the parent atoms is the most important source of resistance at high temperatures. When the temperature is reduced, scattering by the impurities is predominant. It might be thought that increasing the impurity concentration would increase  $R_s$ . This is partially true, but, as more impurities are added, more carriers are available, which reduces  $R_s$  more than the increased scattering increases it.

Another aspect of the thermal noise which depends on how the diode is made can change  $R_s$ . The diode can be made by growing a Ge crystal from a melt in which there is an excess of As atoms and then changing the melt to have an excess of Ga atoms gradually. This produces the graded junction diode, and the spreading resistance changes through the transition region. The spreading resistance can be reduced if pure *p*-type and pure *n*-type materials are put directly together. This is called an abrupt or step-junction diode. Unfortunately there are problems involved in bonding the two materials. Sometimes point contact diodes are used, and these approximate the step-junction diode. So it is seen that construction can alter the thermal noise of the diode by changing  $R_s$ .

The thermal noise attributed to the spreading resistance is believed to be the main source of noise of diode devices. However, there is another source of noise, called shot noise. This is generated in the junction of the diode and is "due to carriers that cross the junction in the forward direction, meander about as minority carriers for a while, and then, escaping any other fate, return in the reverse direction across the junction."<sup>10</sup> The random nature of this process gives a noise current fluctuation. Uhlir<sup>10</sup> has shown that this type of noise does not contribute significantly to the noise at the signal and idler frequencies in the microwave region and is neglected.

Another source of noise that has not been mentioned is pump noise that will give a fluctuation in the gain. However, this source of noise is probably negligible, since for proper adjustment of the amplifier the gain is essentially constant for small variations in the pump amplitude.

The actual derivation of the noise figure when loss is considered is

quite laborious. The detailed calculation is given by Uenohara,<sup>9</sup> and only a shortened plausibility derivation is presented here.

Figure 6.5 shows the equivalent circuit for a diode parametric amplifier of the reflection type using a circulator. It differs from the circuits of Chapter 4 in that a spreading resistance,  $R_s$ , is in series with the variable capacitance. Furthermore, noise arriving at the antenna at  $\omega_2$  excites the  $\omega_2$ -circuit if the circulator passes  $\omega_2$ , and this is represented by the conductance  $G_{L2}$  in the idler circuit.

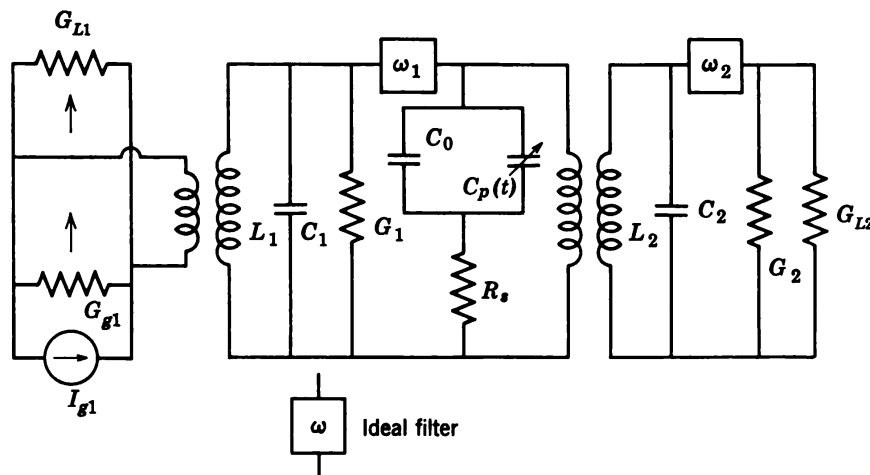


**Figure 6.5** Equivalent circuit for three-frequency parametric reflection-type amplifier with loss in circuits and diode. (From Uenohara, Reference 9.)

For noise calculations Figure 6.5 may be replaced by Figure 6.6. The diode spreading resistance contributes noise at both signal and idler frequencies, so that two noise voltage generators whose mean square voltages are given by  $e_{1p}^2 = e_{2p}^2 = 4kTBR_s$  are needed. For simplicity, all conductances and resistances are taken at the same temperature.

Since the spreading resistance of the diode is the main source of noise, the figure of merit for diodes is described<sup>9</sup> by a quality factor,  $Q = (\omega_1 C_0 R_s)^{-1}$ . The diode needs both a small  $R_s$  and  $C_0$  to have low noise potentialities. In good diodes  $C_0$  ranges from 0.4 to 3  $\mu\text{f}$ ,  $R_s$  ranges from 1 to 18 ohms, and  $Q$ , from 0.4 to 16 at 6 kmc. When  $Q \gg 1$  and the signal frequency is equal to the resonant frequency of tank 1, the circuit of Figure 6.6a can be replaced by the circuit shown in Figure 6.6b, as shown by Uenohara.<sup>9</sup> The effect of the diode loss at  $\omega_1$  and  $\omega_2$  has been combined with the loss in tanks 1 and 2, respectively, into a shunt conductance given by  $(Q^2 R_s)^{-1}$  when the  $Q$  is large. Ideal lossless filters at  $\omega_1$  and  $\omega_2$  are assumed to be in the circuit under high  $Q$  condi-

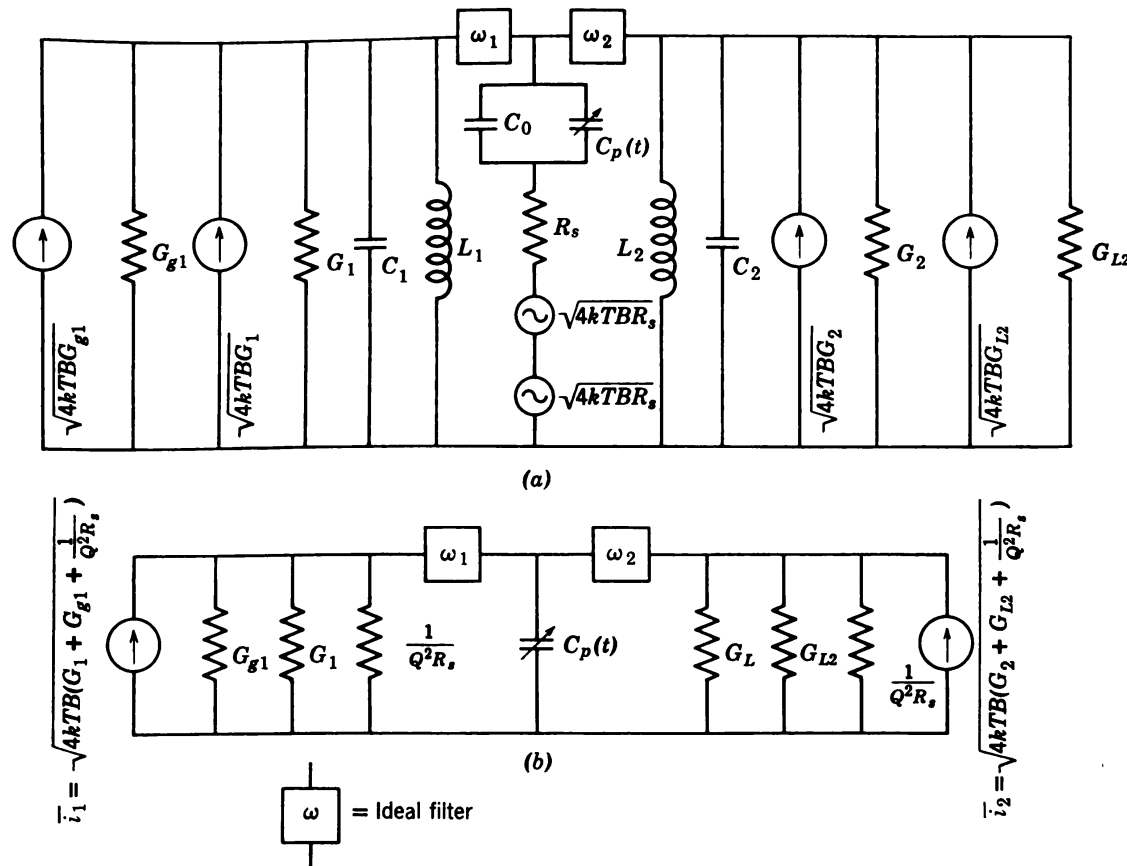


Figure 6.6 (a) Equivalent circuit for noise calculation; (b) equivalent circuit when  $\omega_1 C_0 R_s \ll 1$  and signal is applied at resonant frequency of tank 1. (From Uenohara, Reference 9.)

tions. The mean square noise current at  $\omega_1$  is

$$\bar{i_1^2} = 4kTB \left[ G_{g1} + G_1 + \left( \frac{1}{R_s Q^2} \right) \right]$$

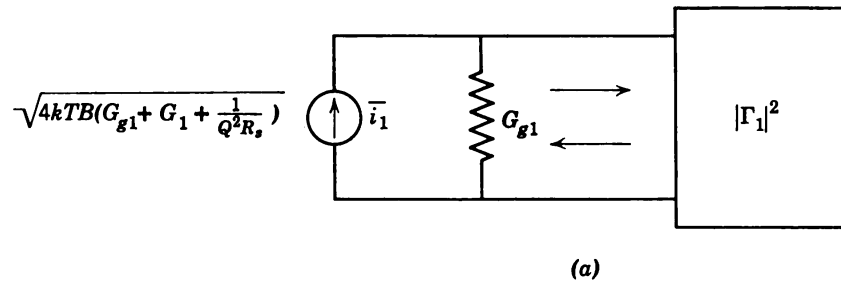
whereas the mean square noise current at  $\omega_2$  is

$$\bar{i_2^2} = 4kTB \left[ G_{L2} + G_2 + \left( \frac{1}{R_s Q^2} \right) \right]$$

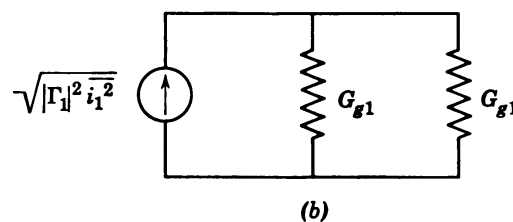
Consider first the noise power available from the amplifier output that originates at frequency  $\omega_1$  and is absorbed by the load at  $\omega_1$ . Let  $|\Gamma_1|^2$  be defined as the power gain of the amplifier. Figure 6.7a shows the noise current at  $\omega_1$ ,  $i_{1\text{rms}}$ , which is due to  $G_{g1}$ ,  $G_1$ , and  $1/Q^2 R_s$  in parallel. This noise signal is amplified and Figure 6.7b shows that the *available* output noise power to the matched load  $G_{g1}$  is

$$N_{01}(\omega_1) = \frac{\bar{i_1^2} |\Gamma_1|^2}{4G_{g1}} = \frac{kTB \left( G_{g1} + G_1 + \frac{1}{Q^2 R_s} \right)}{G_{g1}} |\Gamma_1|^2 \quad (6.6)$$

Next consider the noise power originating at  $\omega_2$ . It is amplified and converted to frequency  $\omega_1$  by the parametric mixing of the condenser and is absorbed in the load at frequency  $\omega_1$ . The gain will be the same if a



(a)



(b)

**Figure 6.7** (a) Circuit for noise originating at  $\omega_1$ ; (b) circuit to compute available noise power at  $\omega_1$ . (From Uenohara, Reference 9.)

signal is applied and removed at  $\omega_1$  as it is if it is applied and removed at  $\omega_2$ . However, if it is applied at  $\omega_2$  and removed at  $\omega_1$ , the gain is different. Therefore, let  $|\Gamma_2|^2$  be the power gain for a signal applied at  $\omega_2$  and removed at  $\omega_1$ .

Figure 6.8a shows the noise current developed at  $\omega_2$ , which is across  $G_{L2}$ . It is applied to the amplifier at  $\omega_2$  and removed at  $\omega_1$ . Figure 6.8b shows that the available output power at  $\omega_1$  across the matched load  $G_{g1}$  is

$$N_{02}(\omega_1) = \frac{\bar{i}_2^2 |\Gamma_2|^2}{4G_{g1}} = \frac{kTB \left( G_2 + G_{L2} + \frac{1}{Q^2 R_s} \right)}{G_{g1}} |\Gamma_2|^2 \quad (6.7)$$

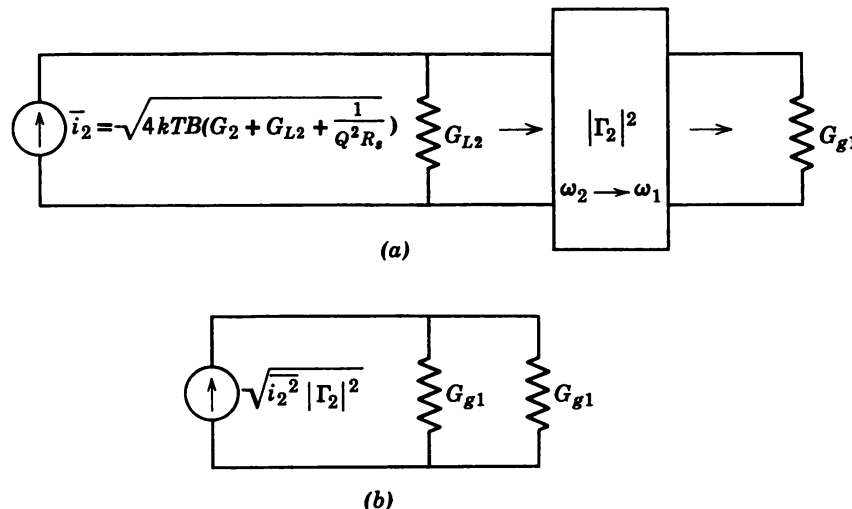


**Figure 6.8** (a) Circuit for noise originating at  $\omega_2$  which is converted to  $\omega_1$ ; (b) circuit to compute available noise power to load. (From Uenohara, Reference 9.)

For single sideband reception the available input noise is  $kTB$ , where  $T$  is  $290^\circ\text{K}$  and the ratio of available output signal power to input signal power at  $\omega_1$  is  $|\Gamma_1|^2$ . Since the noise figure is defined by Eq. 4.72,

$$F = \frac{\text{noise out}}{290^\circ \text{ } k \text{B gain}}$$

it follows from Eqs. 6.6 and 6.7 that

$$F = \frac{N_{\text{out}}}{kTB A} = \left( 1 + \frac{G_1}{G_{g1}} + \frac{1}{Q^2 R_s G_{g1}} \right) + \frac{|\Gamma_2|^2}{|\Gamma_1|^2} \left( \frac{G_2}{G_{g1}} + \frac{G_{L2}}{G_{g1}} + \frac{1}{Q^2 R_s G_{g1}} \right) \quad (6.8)$$

where  $A$  is the gain.

The foregoing derivation can be completely justified only when the problem is solved exactly.<sup>9</sup> Further, the ratio of  $|\Gamma_2|^2/|\Gamma_1|^2$  must be found from the exact analysis. In the noise figure calculation for the distributed amplifier treated in Chapter 5,  $|\Gamma_2|^2/|\Gamma_1|^2$  could be found from the Manley-Rowe relations because the circuit was lossless. However, in the present case the variable capacitance has loss and the Manley-Rowe relations must be modified. If  $Q = (\omega_1 C_0 R_s)^{-1} \gg 1$ , Uenohara shows that

$$\frac{|\Gamma_2|^2}{|\Gamma_1|^2} \cong \frac{\omega_1}{\omega_2} \frac{G_{e1}}{G_{L2}} \quad (6.9)$$

where  $G_{e1}$  is given by Eq. 6.5 and  $|\Gamma_1|^2$  is given by Eq. 6.4. For large gain  $G_{e1} \cong G_{g1}$  ( $G_1$  can be neglected since it is small), so that by Eqs. 6.8 and 6.9

$$F \cong 1 + \frac{G_1}{G_{g1}} + \frac{1}{Q^2 R_s G_{g1}} + \frac{\omega_1}{\omega_2} \left( 1 + \frac{G_2}{G_{L2}} + \frac{1}{Q^2 R_s G_{L2}} \right) \quad (6.10)$$

It might be noted that if the idler is at  $T_i$ ,  $G_1 \ll G_{g1}$ ,  $G_2 \ll G_{L2}$ , and  $Q^2 \gg 1$  the excess noise temperature is  $\omega_1 T_i / \omega_2$ , the results found in Chapters 4 and 5.

As pointed out in Chapters 4 and 5, the noise figure for single sideband reception can be improved by operating with  $\omega_2 \gg \omega_1$ . Further, as in the case of the distributed amplifier, double sideband reception will improve the noise figure. For double sideband reception, when  $G_1 = G_2$  and  $G_{L2} = G_{g1}$ ,  $F$  reduces to<sup>9</sup>

$$F \cong 1 + \frac{G_1}{G_{g1}} + \frac{1}{Q^2 R_s G_{g1}} \equiv 1 + \frac{T_e}{290^\circ} \quad (6.11)$$

if  $R_s \rightarrow 0$ , then  $F \cong 1$ , since  $G_1 \ll G_{g1}$  and  $T_e \cong 0^\circ K$ . It should be noted again that conventional operation is single sideband, whereas double sideband might be realized in radio astronomy. Experimental results for a diode cooled to liquid nitrogen temperature are given in Section 6.4.

#### 6.4 Experimental Results for Lumped Circuits

The experimental results quoted are for double sideband reception. For the equivalent single sideband noise figure 3 db must be added if  $\omega_1 = \omega_2$ .

Much work has been done with semiconductor diodes, as may be seen from the bibliography of Chapter 4. In the interest of brevity, only a small segment of this work is discussed here.

The block diagram of the experimental setup used by Uenohara is shown in Figure 6.9. The pump was supplied by a 12-kmc klystron to the amplifier. The signal at 6 kmc was applied at port 1 of a circulator. Port 2 supplies the signal to the amplifier and removes the amplified signal which emerges from port 3 of the circulator. This output signal goes through a mixer and the i-f to a detector. For noise measurements a noise generator is used, as shown in the figure.

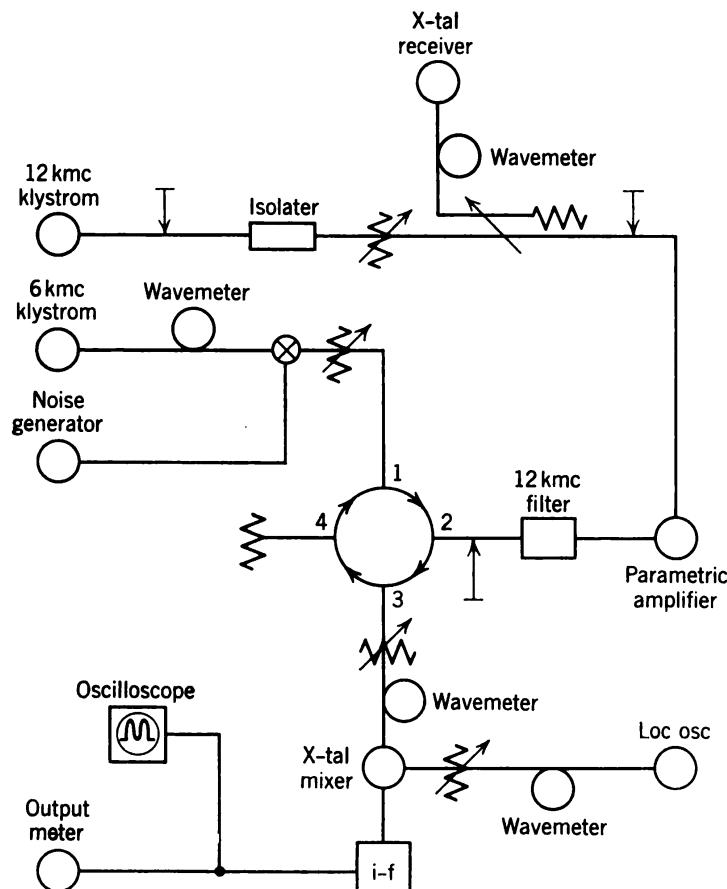


**Figure 6.9** Block diagram of experimental 6-kmc diode amplifier. (From Herrmann, Uenohara, and Uhlig, Reference 17.)

In one set of experiments seven Si P-N junction diodes, six Ge P-N diffused diodes, and one Ge gold-bonded diode were tested. Figure 6.10 shows a plot of the noise figures obtained versus the inverse quality factor,  $\omega_1 C_0 R_s$ , for the diodes together with the theoretical noise figure calculation (dotted curve). The input circuit loss was subtracted from the raw noise data to give the quoted results. The circles give the Si results, and the squares give the Ge results.

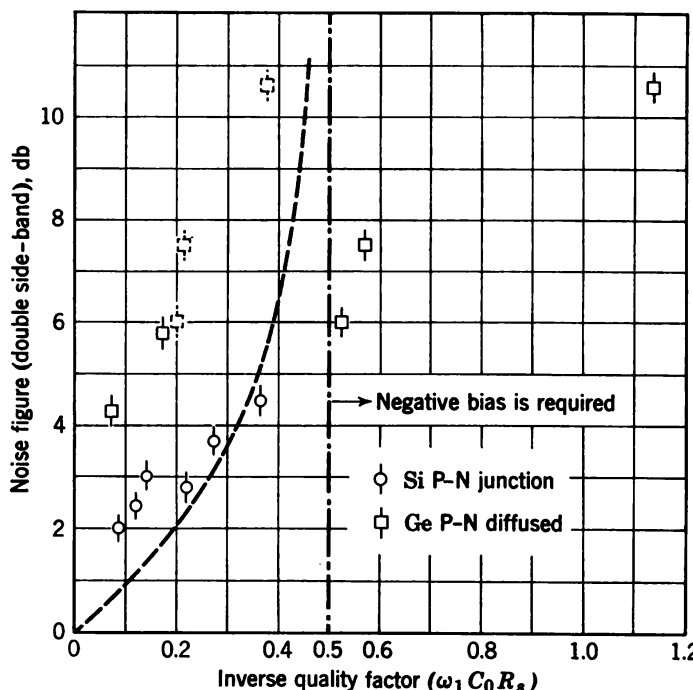


**Figure 6.10** Measured noise figure versus inverse diode quality factor. Dotted lines show theoretical noise figure versus  $\omega_1 C_0 R_s$ , circles give the measured results for Si diodes, and squares give results for Ge diodes. (From Uenohara, Reference 9.)

The possible discrepancy between theory and experiment may be due to higher order noise processes that have not been considered. This is discussed by Uenohara.<sup>9</sup>

Knechtli and Weglein<sup>11</sup> report a 1.3-db double sideband noise figure (100°K excess noise temperature) at 3.1 kmc when the amplifier is at room temperature. They used a gold-bonded Ge diode. When the diode was cooled to liquid nitrogen temperature, the effective noise temperature dropped to 50°K.

Uenohara and Bakanowski<sup>12</sup> have reported a  $0.60 \pm 0.05$  db noise figure (44°K excess noise temperature) at 6 kmc, using a Ge P-N junction diode cooled to 87°K.

The latest results<sup>13, 14, 15</sup> are for gallium arsenide (GaAs) point contact diodes at 6 kmc. A noise figure of 0.3 db ( $T_e \approx 20$ °K) for double sideband operation when the junction was cooled to liquid nitrogen temperature has been observed. This compound yields the lowest noise temperatures that had been measured at the time of writing.

Indium antimonide has been tried by Uenohara with very poor results. This compound is very active chemically and must be used in a vacuum to reduce surface contamination. However,  $C_0$  ( $\approx$  dielectric constant)

is very large for this compound, although  $R_s$  is small, and noise figure measurements indicate that it is inferior to GaAs. Other diode work is reported in References 16, 17, and 18.

### 6.5 Experimental Results for Distributed Circuits

It has been pointed out in Chapter 4 that since regenerative amplifiers are operated near oscillation threshold in order to achieve large gain they are inherently unstable. Further, since a nonlinear reactance is frequency-sensitive, it requires tuning elements for optimum operation. Also, since the nonlinear reactance element is a two-terminal device, the input and output exist across the same terminals. This requires the use of nonreciprocal circuit elements such as circulators or isolators to prevent oscillation.

A way of improving the bandwidth and stability is to make up a traveling wave structure, i.e., an artificial transmission line using P-N junction diodes as the variable capacity elements,<sup>19-21</sup> as shown in Chapter 5. Figure 5.1 shows an artificial single transmission line on which semiconductor diodes are used as the variable reactance elements. The signal and pump-phase velocities travel in approximate synchronism. An idler will be generated at frequency  $\omega_2 = \omega - \omega_1$ . The gain at frequencies  $\omega_1$  and  $\omega_2$ , given by Eqs. 5.14, is sketched in Figure 5.2.

In the experiments performed by Engelbrecht<sup>19-21</sup> a balanced structure, such as that shown in Figure 6.11, was used. The balanced structure permits independent control of signal and pump velocities and eliminates the need for band separating filters. One possible coaxial structure used by Engelbrecht is shown in the same figure.

Junction diodes developed by A. Uhlir, Jr., which required pump power in the milliwatt range, were used. Pump voltage amplitudes of about one volt can yield essentially full capacitance modulation. (See Figure 6.3.) The series resistance in these diodes was about  $1\ \Omega$  for  $5\ \mu\text{uf}$  diodes, so that low noise operation is to be expected. With only single sideband operation, the minimum noise figure is 3 db, as shown in Chapter 5.

Several experimental amplifiers have been built in coaxial and printed circuit forms. Balanced structures (with pairs of diodes at every stage) were used. This allowed independent adjustment of the phase velocities of  $\omega_1$  and  $\omega$ , so that  $\beta = \beta_1 + \beta_2$  (Chapter 5).

By using 2 to  $5\ \mu\text{uf}$  (zero bias) diodes to load uniform transmission lines, impedances from 10 to 100 ohms and phase shifts of about  $45^\circ/\text{stage}$  at 500 mc were obtained;  $90^\circ/\text{stage}$  at  $\omega$  was convenient for pump velocity adjustments without affecting the impedance.

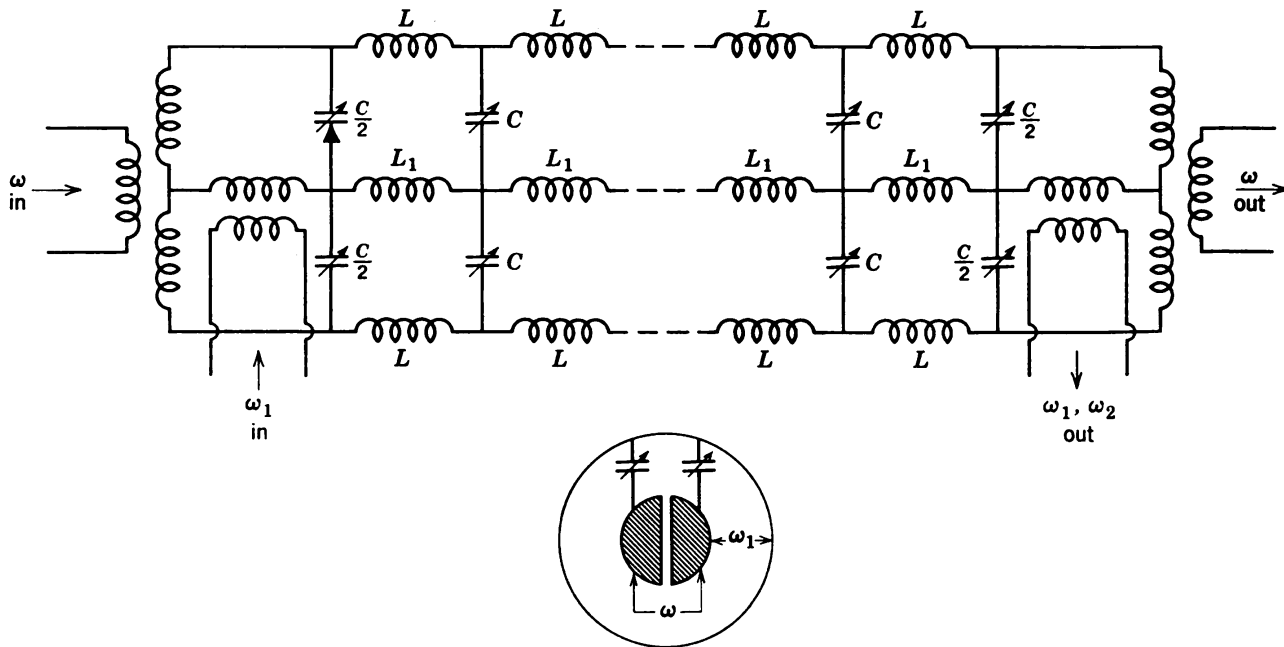


**Figure 6.11** Balanced distributed parametric amplifier structure using diodes. This arrangement permits independent control of the signal and pump velocities and eliminates the need for band separating filters. One possible actual coaxial structure is shown below. (From Engelbrecht, Reference 21.)

With only four stages in a coaxial structure, a gain of 10 db with a 100-mc bandwidth (Figure 6.12) was obtained with a pump power of 10 milliwatts. The equivalent input noise temperature measured at 380 mc was approximately 75°K for double sideband operation.

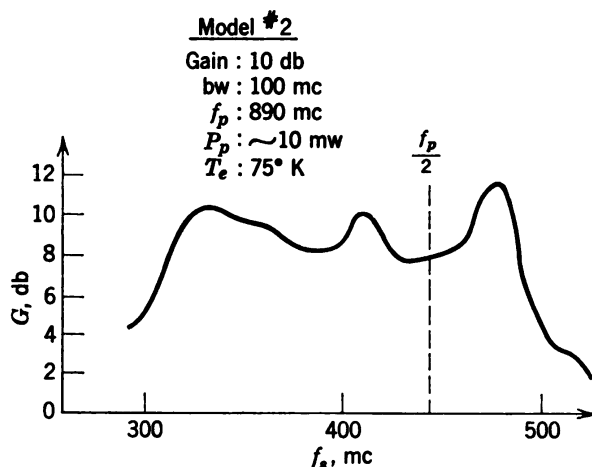


**Figure 6.12** Gain curve for a four-stage coaxial amplifier versus frequency. Individual tuning and external bias were used for all diodes. The structure used was similar to that shown in Figure 6.11. (From Engelbrecht, Reference 21.)

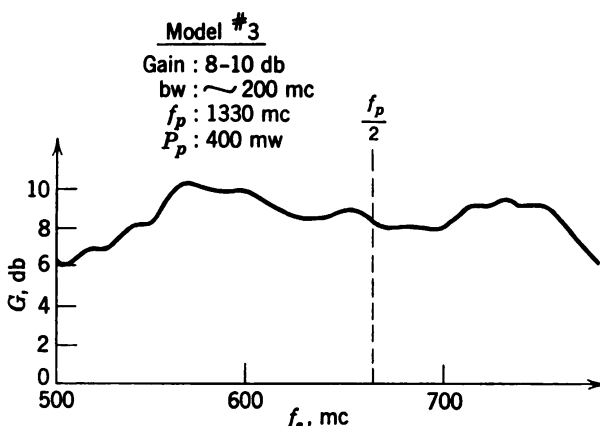


**Figure 6.13** Gain curve for a sixteen-stage printed circuit amplifier; strong self-bias (no d-c return on diodes), no individual tuning, and the diode capacitance spread was about  $\pm 10$  per cent. To avoid overlap with the idler band, the instantaneous bandwidth was limited to one side of  $\omega/2$ . (From Engelbrecht, Reference 21.)

A printed circuit structure with sixteen stages and  $\Delta C/C_0 \sim 0.6 - 0.7$  provided 8- to 10-db gain over a 200-mc band (Figure 6.13) requiring 400 milliwatts of pump power. Its reverse gain fluctuated with frequency between +1 db and -2 db.

### 6.6 Remarks

From the remarkable experimental results quoted for diode parametric amplifiers, the low noise predictions of van der Ziel<sup>1</sup> are amply justified. As materials research progresses, there is every reason to expect lower noise figures at higher frequencies than those used to date.

Chapter 7 considers a different nonlinear medium that can be used to obtain parametric mixing, viz., an electron beam that propagates space-charge waves.

### BIBLIOGRAPHY

1. A. van der Ziel, "On the Mixing Properties of Nonlinear Condensers," *J. Appl. Phys.*, **19**, 999-1006 (November 1948).
2. M. E. Hines, "The Theory of Amplification in Nonlinear Reactance Modulators," presented at IRE Annual Conference on Electron Tube Research, Berkeley, Calif. (1957).
3. W. Shockley, *Electrons and Holes in Semiconductors*, D. Van Nostrand, New York, 1950, p. 100.
4. E. Spenke, *Electronic Semiconductors*, McGraw-Hill, New York, 1958, pp. 107-112.
5. H. Heffner and G. Wade, "Gain, Bandwidth, and Noise Characteristics of the Variable Parameter Amplifier," *J. Appl. Phys.*, **29**, 1321-1331 (September 1958).
6. P. K. Tien, "Noise in Parametric Amplifiers," *Acta Electronica*, **4**, No. 4 (October 1960).
7. C. L. Hogan, R. L. Jepsen, and P. H. Vartanian, "A New Type of Ferromagnetic Amplifier," *J. Appl. Phys.*, **29**, 422-423 (March 1958).
8. K. K. N. Chang and S. Bloom, "Parametric Amplifier Using Lower Frequency Pumping," *Proc. IRE*, **46**, 1383-1386 (July 1958).
9. M. Uenohara, "Noise Considerations of the Variable Capacitance Parametric Amplifier," *Proc. IRE*, **48**, 169-179 (February 1960).
10. A. Uhlir, Jr., "High Frequency Shot Noise in P-N Junctions," *Proc. IRE*, **44**, 557-558 (April 1956).
11. R. C. Knechtli and R. D. Weglein, "Low Noise Parametric Amplifier," *Proc. IRE*, **47**, 554-555 (April 1959).
12. M. Uenohara and A. E. Bakanowski, "Low Noise Parametric Amplifier Using Germanium P-N Junction Diode at 6 kmc," *Proc. IRE*, **47**, 2113-2114 (December 1959).
13. M. Uenohara, "Extremely Low Noise Parametric Amplifier," talk presented at the Annual Conference on Electron Tube Research, Mexico City, Mexico, June 24-26, 1959.
14. W. M. Sharpless, "High Frequency Gallium Arsenide Point Contact Rectifiers," *Bell System Tech. J.*, **38**, 259-269 (January 1959).
15. M. Uenohara and W. M. Sharpless, "An Extremely Low Noise 6 kmc Parametric Amplifier Using Gallium Arsenide Point Contact Diode," *Proc. IRE*, **47**, 2114-2115 (December 1959).

16. M. Uenohara, "Parametric Amplifier at 6 kmc Using Semiconductor Diodes," presented at IRE Annual Conference on Electron Tube Research held at Quebec, Canada (1958).
17. G. F. Herrmann, M. Uenohara, and A. Uhlir, Jr., "Noise Figure Measurements on Two Types of Variable Reactance Amplifier Using Semiconductor Diodes," *Proc. IRE*, **46**, 1301-1303 (June 1958).
18. H. Heffner and K. Kotzebue, "Experimental Characteristics of a Microwave Amplifier Using a Semiconductor Diode," *Proc. IRE*, **46**, 1301 (June 1958).
19. R. S. Engelbrecht, "A Low Noise Nonlinear Reactance Traveling Wave Amplifier," *Proc. IRE*, **46**, 1655 (September 1958).
20. R. S. Engelbrecht, "A Low Noise Nonlinear Reactance Traveling Wave Amplifier," presented at the Solid State Device Research Conference, Columbus, Ohio, June 1958.
21. R. S. Engelbrecht, "Nonlinear Reactance (Parametric) Traveling Wave Amplifiers for UHF," presented at the 1959 Solid State Circuits Conference, Philadelphia, Pa. Session I, pp. 8-9, Lewis Winner, publisher.

## Chapter 7

# Parametric amplification of fast space-charge waves

In Chapter 6 it was shown that a semiconductor diode could be used as a variable reactance circuit element to provide parametric mixing between the signal and idler frequencies. Another nonlinear medium that can be used to provide parametric mixing between waves is an electron beam.

In Chapter 2 it was shown that an electron beam in confined flow will propagate a fast and slow space-charge wave. Further, it was shown that the equations governing space-charge wave (SCW) propagation were analogous to a transmission line. In Chapter 5 it was shown that if a pump wave in the form of a capacitance variation propagates down the line and if, in addition, a signal wave propagates down the line then an idler wave will be generated. The pump wave couples the signal and idler waves actively, and exponentially growing waves result. Now carry this analog back over to the beam case. The pump wave is taken as a fast space-charge wave at the pump frequency. This pump wave plays the role of the capacitance variation down the line. The signal is then applied to the beam in the form of a fast space-charge wave at the signal frequency. Because of the nonlinear nature of the beam, the pump and signal waves will mix and generate an idler wave, which will also be a fast space-charge wave at the idler frequency. The signal and idler waves will be actively coupled by the pump and both will grow exponentially at the expense of the power carried by the pump wave. In this manner the fast space-charge wave at the signal frequency will be parametrically amplified.

Amplification of the fast wave has some important consequences as far as noise is concerned. Recall from Chapter 2 that in order to remove a fast SCW power must be extracted from the beam; but in order to re-

move a slow SCW power must be added to the beam, since the slow SCW carries negative kinetic power. This means that only the part of the noise (associated with the generation of an electron beam) that is carried as a fast SCW can be removed. To remove noise from the slow SCW would require adding power to the beam. Since noise is random, this is clearly impossible. Therefore, if the fast SCW is amplified, the noise can first be removed from the beam, so that, in principle, the fast SCW parametric amplifier (FSCWPA) can be made noiseless.

For comparison, recall that the slow SCW is amplified in the TWT. This fact is the basis of the minimum noise figure theorems of Pierce<sup>1</sup> and Haus and Robinson.<sup>2,3</sup>

The theory of the FSCWPA, using the coupled mode formulation given in Chapter 5, will now be presented.

### 7.1 The Fast Space-Charge Wave Parametric Amplifier<sup>4</sup>

**Coupled mode form of equations.** Parametric amplification of a fast space-charge wave is considered by analogy with the distributed parametric amplifier treated in Chapter 5. However, the coupled mode equations and the coupling coefficients are derived in Appendix J by the direct coupled mode approach.

Consider an electron beam in a drift region in confined flow and assume that it is propagating a fast space-charge wave at frequency  $\omega$ . The current and voltage for this wave (Eqs. 2.53 and 2.54) are

$$-i(z, t) = 2 \operatorname{Re} \left( \frac{1}{\sqrt{Z_0}} |a_+(0)| \exp \{j[\omega t - (\beta_e - \beta_q)z]\} \right) \quad (7.1)$$

$$V(z, t) = 2 \operatorname{Re} (\sqrt{Z_0} |a_+(0)| \exp \{j[\omega t - (\beta_e - \beta_q)z]\})$$

since  $|a_-(0)| = 0$ ,  $\beta_e = \omega/v_0$ , and  $\beta_q = \omega_q/v_0$ . It follows from Eqs. 7.1 that  $V(z, t) = Z_0[-i(z, t)]$ . The arbitrary constant  $|a_+(0)|$  can be expressed as

$$-m|I_0| = \frac{2}{\sqrt{Z_0}} a_+(0) = |I_m| e^{j\phi} \quad (7.2)$$

where  $-|I_0|$  is the d-c current,  $I_m$  is the maximum a-c current amplitude,  $\phi$  is an arbitrary initial phase of the a-c current,  $m$  is the maximum depth of the a-c current modulation, and

$$Z_0 = \frac{2V_0}{|I_0|} \frac{\omega_q}{\omega} \quad (7.3)$$

where  $\omega_q$  is evaluated at frequency  $\omega$ .

This fast space-charge wave is called the pump wave, and it plays the role of the capacitance wave (in Eq. 5.2, viz.,  $C_p = \Delta C \cos(\omega t - \beta z)$ ) for the distributed parametric amplifier.

Next assume that the beam is propagating a fast space-charge wave at frequency  $\omega_1$  and another at  $\omega_2$ , where  $\omega = \omega_1 + \omega_2$ . Assume that the amplitudes of these modes are sufficiently small that they will not affect the pump mode. It is then expected by analogy with the distributed amplifier that the pump wave will actively couple the fast signal and idler waves. Therefore, define the mode amplitudes (Eqs. 2.53 and 2.54) by

$$-i_1(z, t) = 2 \operatorname{Re} \left\{ \frac{1}{\sqrt{Z_{01}}} [a_{1+}(z) - a_{1-}(z)] e^{j\omega_1 t} \right\} \quad (7.4)$$

$$V_1(z, t) = 2 \operatorname{Re} \{ \sqrt{Z_{01}} [a_{1+}(z) + a_{1-}(z)] e^{j\omega_1 t} \}$$

where

$$Z_{01} = \frac{2V_0 \omega_{q1}}{|I_0| \omega_1} \quad (7.5)$$

and  $\omega_{q1}$  is evaluated at  $\omega_1$ . The idler voltage and current are given above by replacing  $\omega_1$  by  $\omega_2$ . Then, by Eqs. 5.6, the coupled mode equations for the FSCWPA are

$$\begin{aligned} \frac{da_{1+}}{dz} &= -j\beta_1 a_{1+} + c_{12} e^{-j\beta z} a_{2+}^* \\ \frac{da_{2+}^*}{dz} &= +j\beta_2 a_{2+}^* + c_{21} e^{j\beta z} a_{1+} \end{aligned} \quad (7.6)$$

where

$$\begin{aligned} \beta_{1,2} &= \frac{\omega_{1,2}}{v_0} - \frac{\omega_{q1,2}}{v_0} \equiv \beta_{e1,2} - \beta_{q1,2} \\ \beta &= \frac{\omega}{v_0} - \frac{\omega_q}{v_0} \equiv \beta_e - \beta_q \end{aligned} \quad (7.7)$$

The foregoing argument cannot be considered as a derivation of the equations for a three-frequency SCWPA. They are therefore derived in Appendix J on a more rigorous basis. It is shown in the appendix that there will be passive coupling to the slow space-charge modes by the pump even though they are not initially excited. However, by considering the mode transfer factors, it is also shown in the appendix that if the beam is thin compared with the pump, signal, and idler wavelengths little power will be transferred to or from the slow modes and they may be neglected. This point is discussed again.

**The coupling coefficients. Manley-Rowe relations.** <sup>5,6</sup> In Appendix J the coupling coefficients are found to be

$$c_{12} = \frac{\omega_1}{\omega_2} c_{21}^* = -\frac{j}{4} \sqrt{\frac{\omega_1}{\omega_2}} m \sqrt{\beta_{q1}\beta_{q2}} \left( 1 + \frac{\alpha}{\alpha_1} + \frac{\alpha}{\alpha_2} \right) \quad (7.8)$$

where

$$\alpha = \frac{\omega_q}{\omega} \quad \alpha_{1,2} = \frac{\omega_{q1,2}}{\omega_{1,2}}$$

It is interesting to compare this expression with Eq. 5.8a of Chapter 5. Aside from the correction term  $[1 + (\alpha/\alpha_1) + (\alpha/\alpha_2)]$ , the depth of current modulation plays the role of depth of capacitance modulation and  $\beta_q$  plays the role of  $\beta$ .

From Chapter 5 it is seen that since  $c_{12}$  and  $c_{21}^*$  are related by Eq. 7.8 (compare Eq. 5.8b) it follows that the electron beam obeys the Manley-Rowe relations, i.e.,

$$\frac{1}{\omega_1} \frac{d}{dz} |a_{1+}|^2 = \frac{1}{\omega_2} \frac{d}{dz} |a_{2+}|^2 = \frac{1}{\omega} \frac{d}{dz} (|a_{1+}|^2 + |a_{2+}|^2) \quad (7.9)$$

(See Eq. 5.10.) The energy for the growing waves comes from the pump wave.

**Boundary conditions. Gain threshold.** In general, the pump propagation constant will not equal the sum of the signal and idler propagation constants. Therefore, let

$$\Delta\beta = \beta - \beta_1 - \beta_2 = -(\beta_q - \beta_{q1} - \beta_{q2}) \quad (7.10)$$

(See Eq. 5.17.) Then, by a procedure similar to that used in Eqs. 5.18–5.21, it follows that the solutions of Eqs. 7.6 are

$$\begin{aligned} a_{1+}(z) &= \exp \{ -j[(\beta + \beta_1 - \beta_2)/2]z \} [d_1 \exp(|s|z) + d_2 \exp(-|s|z)] \\ a_{2+}^*(z) &= \exp \{ j[(\beta - \beta_1 + \beta_2)/2]z \} \frac{1}{c_{12}} \left[ \left( |s| - j \frac{\Delta\beta}{2} \right) d_1 \exp(|s|z) \right. \\ &\quad \left. - \left( |s| + j \frac{\Delta\beta}{2} \right) d_2 \exp(-|s|z) \right] \end{aligned} \quad (7.11)$$

where  $d_1$  and  $d_2$  are arbitrary constants of integration and

$$s = \pm \sqrt{|c_{12}|^2 \frac{\omega_2}{\omega_1} - \left( \frac{\Delta\beta}{2} \right)^2} \quad (7.12)$$

It therefore follows that there is a threshold of pump modulation below which there will be no gain, since  $\Delta\beta \neq 0$  in general. Above threshold the growing and decaying fast modes travel at the same phase velocity. The phase velocity at the signal frequency above threshold is

$$v_{\omega_1} = \frac{2\omega_1}{\beta + \beta_1 - \beta_2} \quad (7.13a)$$

and at the idler frequency it is

$$v_{\omega_2} = \frac{2\omega_2}{\beta - \beta_1 + \beta_2} \quad (7.13b)$$

To find the gain, assume that power is injected at  $\omega_1$  so that  $a_2(0) = 0$ . It follows from Eqs. 7.10–7.12 that

$$\begin{aligned} \left| \frac{a_{1+}(z)}{a_{1+}(0)} \right|^2 &= 1 + F \sinh^2 |s| z \\ \left| \frac{a_{2+}(z)}{a_{1+}(0)} \right|^2 &= \frac{\omega_2}{\omega_1} F \sinh^2 |s| z \end{aligned} \quad (7.14)$$

where  $F$  is the transfer factor that is given by

$$F^{-1} = 1 - \frac{\omega_1}{\omega_2} \left( \frac{\Delta\beta}{2|c_{12}|} \right)^2$$

provided the pump modulation is above threshold. Figure 7.1 gives a sketch of the power at the two frequencies.

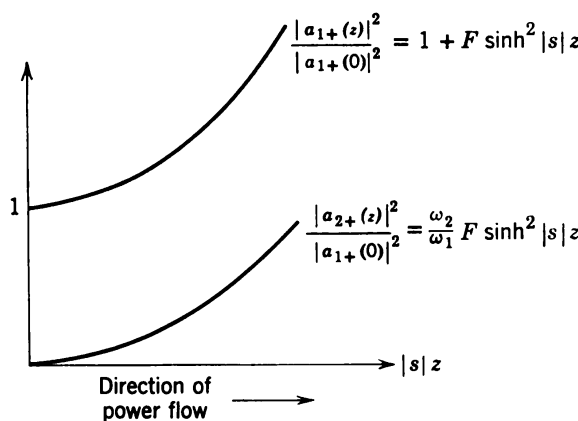


**Figure 7.1** Power carried by signal and idler channels versus distance in distributed parametric amplifier.

The gain in decibels at  $\omega_1$  in a length  $L$  is

$$\text{gain (db)} = 10 \log_{10} \left| \frac{a_1(L)}{a_1(0)} \right|^2 = 10 \log_{10} (1 + F \sinh^2 |s|L) \quad (7.15a)$$

When the tube is sufficiently long so that  $|s|L \gg 1$ , the gain is given approximately by

$$\text{gain (db)} \cong 8.68 |s|L - 6 + 10 \log_{10} F \quad (7.15b)$$

As pump modulation increases,  $\Delta\beta \rightarrow 0$  and  $F \rightarrow 1$ . The 6-db loss is due to the decaying wave, which is neglected in this approximation and which is excited by the signal.

The dependence of the gain on frequency can be seen by considering  $|s|$ . By Eqs. 7.8 and 7.12 it follows that

$$s^2 = \frac{|m|^2}{16} \beta_{q1}\beta_{q2} \left( 1 + \frac{\alpha}{\alpha_1} + \frac{\alpha}{\alpha_2} \right)^2 - \left( \frac{\beta_q - \beta_{q1} - \beta_{q2}}{2} \right)^2 \quad (7.16)$$

Since  $\omega_q$  is frequency-dependent, the frequency dependence of  $s$  is quite complicated. There are two extreme cases that can be handled analytically:

**Case 1. Infinitely Thick Beam.** For the thick beam,  $\omega_q = \omega_{q1} = \omega_{q2} = \omega_p$ , and  $\omega_p$  is independent of frequency. Then

$$s = \frac{\omega_p}{2v_0} \sqrt{|m|^2 - 1}$$

and  $s$  is frequency-independent. However, the gain threshold in this case requires  $|m| > 1$ . This means that the pump a-c current modulation would have to be greater than the d-c current. In such a case small signal theory breaks down so that the entire analysis fails. Qualitatively, it probably means that no gain can be achieved with an infinite beam.

**Case 2. Infinitely Thin Beam.** For an infinitely thin beam it can be shown that  $\alpha = \alpha_1 = \alpha_2$ ; that is, the fast space-charge waves travel with the same phase velocity, independent of frequency. The gain threshold is then reduced to zero;  $\Delta\beta = (\omega_q - \omega_{q1} - \omega_{q2})/v_0 \rightarrow \alpha(\omega - \omega_1 - \omega_2)/2 \rightarrow 0$ , since  $\omega = \omega_1 + \omega_2$ . In this case

$$s = \frac{3}{4}\alpha|m| \frac{\sqrt{\omega_1\omega_2}}{v_0}$$

where  $\alpha$  is frequency-independent. If the pump frequency is held constant, then it is seen that  $s$  will be a maximum when  $\omega_1 = \omega_2 = \omega/2$ .

But this is the degenerate case treated in preceding chapters, and the same condition was found true in the semiconductor diode amplifier of Chapter 6.

As might be expected, in the degenerate case the gain depends on the phase of the pump relative to the signal.<sup>4</sup>

**Validity of the weak coupling approximation.** In the foregoing coupled mode analysis, coupling to the slow modes has been neglected. This can be justified, since the transfer factors between the  $a_{1+}$ - and  $a_{2-}^*$ -modes, as well as between the  $a_{2+}^*$ - and  $a_{1-}$ -modes, are very small compared with unity when the beam is small compared with the wavelengths at the three frequencies considered. These are evaluated in Appendix J by using the definition of transfer factors of Chapter 1. However, these expressions are rather involved functions. Therefore, rather than argue from transfer factors, the equations were solved for the degenerate case  $\omega_1 = \omega_2$ , retaining the slow modes. Solutions of the form  $\exp(sz)$  were found where  $s = \beta_{q1}x_1$ . The exact values of  $x_1$  are plotted as the solid curves in Figure 7.2 for various values of  $|m|$  versus  $\omega_q/2\omega_{q1}$ . In addition, the approximate values of  $s$  from Eq. 7.16 are

$$\begin{aligned}s &= \beta_{q1} \sqrt{\frac{|m|^2}{16} \left(1 + \frac{\omega_q}{\omega_{q1}}\right)^2 - \left(1 - \frac{\omega_q}{2\omega_{q1}}\right)^2} \\ &= x_1 \beta_{q1}\end{aligned}$$

and these approximate values of  $x_1$ , where the slow modes were omitted, are plotted as the dashed curves in Figure 7.2. The agreement for small values of  $|m|$  is strikingly good, even for fairly thick beams. Since the theory is good for only small values of pump current modulation, neglecting the slow modes is completely justified in a three-frequency theory. The physical reason that the slow modes are unimportant is that the propagation constants of the slow modes are far enough out of synchronism with the pump mode that they do not couple very strongly.

It should be noted that  $\omega_q/2\omega_{q1} = 0.5$  for the infinitely thick beam, whereas  $\omega_q/2\omega_{q1} = 1.0$  for the infinitely thin beam.

Figure 7.3 gives a similar comparison when the slow modes are included (solid curve) and when they are neglected (dashed curve) for the modulation threshold needed for gain. Again, for the thin beam and small  $|m|$ 's, the slow modes can be neglected.

Similar comparisons have been made for the nondegenerate case, and the slow modes may indeed be neglected for thin beams when  $|m|$  is small.

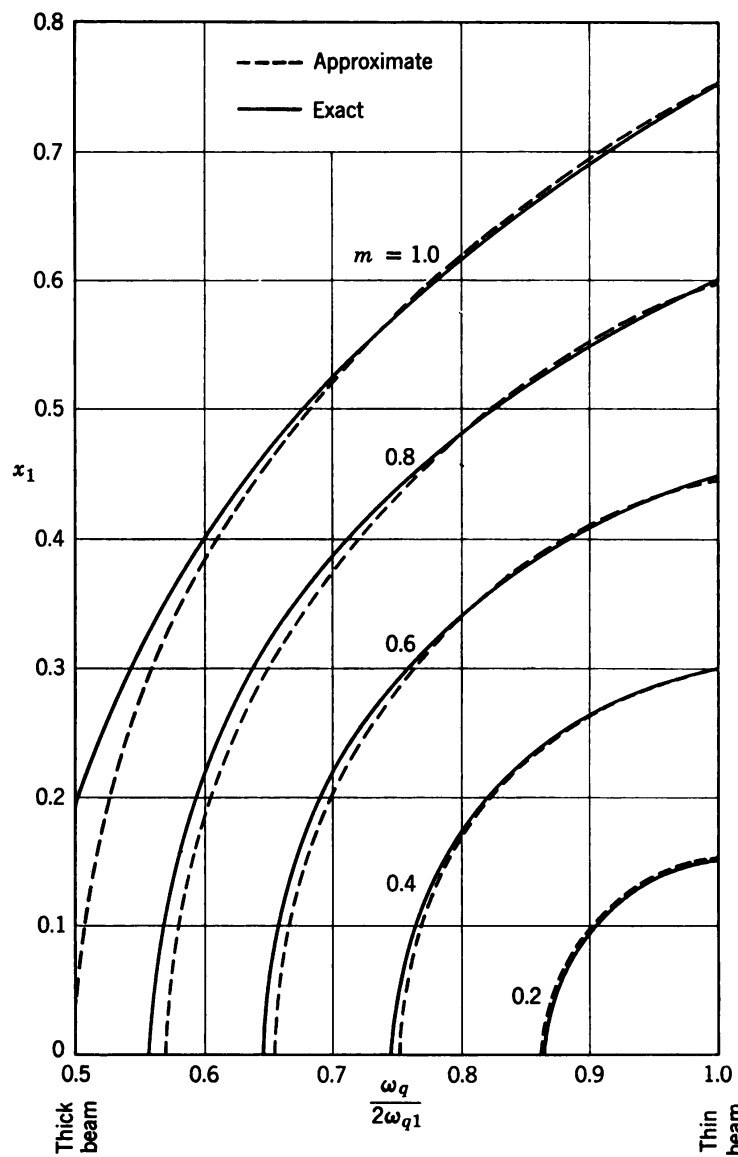


**Figure 7.2** Gain parameter ( $x_1$ ) for degenerate fast space-charge wave parametric amplifier versus beam thickness parameter ( $\omega_q/2\omega_{q1}$ ) for various values of pump modulation. The solid curves show  $x_1$  when both slow and fast signal (and idler) waves are present, and dashed curves show  $x_1$  when the slow modes are neglected. (From Louisell and Quate, Reference 4.)

**The frequency converter.<sup>5</sup>** It should also be mentioned that the beam can be used as a frequency converter. In this case  $\omega = \omega_1 - \omega_2$ . The  $a_{1+}$ - and  $a_{2+}$ -modes are strongly coupled, but the coupling is passive. The modes act like two passively coupled transmission lines, and power is continuously converted from  $\omega_1$  to  $\omega_2$  and vice versa. The equations

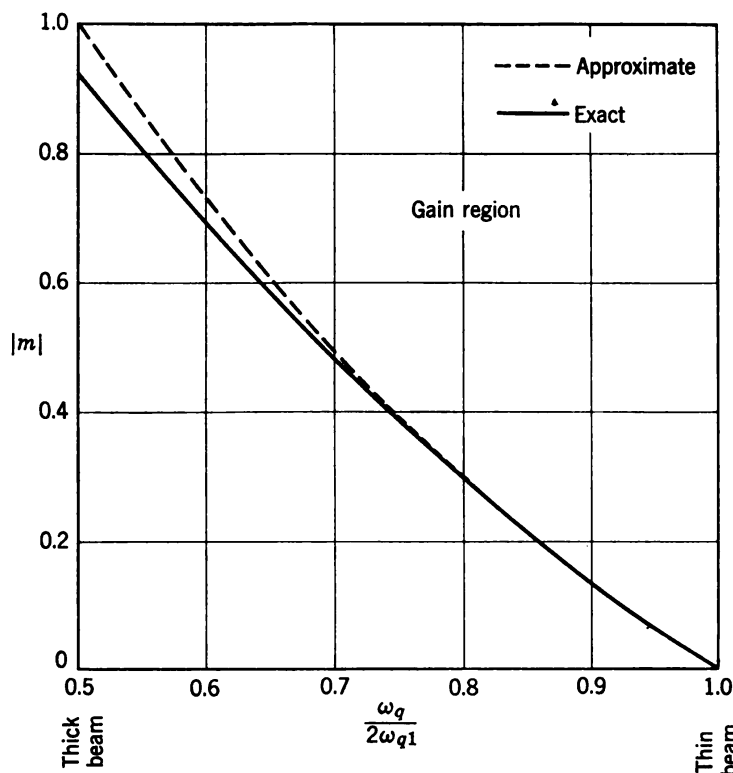


**Figure 7.3** A plot of the pump modulation ( $|m|$ ) threshold for gain versus beam thickness parameter. The solid curve includes the slow modes, and the dashed curve neglects the slow modes. There is a gain threshold even for this lossless system, since  $\beta \neq \beta_1 + \beta_2$  (see Chapter 5, Eq. 5.21). (From Louisell and Quate, Reference 4.)

for the frequency converter can be obtained from the amplifier equation simply by replacing  $\omega_2$  by  $-\omega_2$ .

## 7.2 Experimental Results

The first parametric beam experiments that were performed by A. Ashkin<sup>7</sup> were designed to demonstrate SCWPA gain only, and no attempt was made to excite only fast SCW's at the pump and signal frequencies and no attempt was made to remove the noise. Figure 7.4 shows a diagram of Ashkin's first experiment. A large magnetic focusing field was provided by a solenoid, and a beam of radius  $b = 0.040$  in. in a drift tube of radius  $a = 1.70$  in. was provided from a convergent Pierce gun. The signal wave was excited by allowing the beam to traverse a gap in an r-f cavity tuned to the signal frequency 4200 mc. In such a gap both the fast and slow SCW's are equally excited. Next, the pump fast and slow SCW's were applied by allowing the beam to traverse a

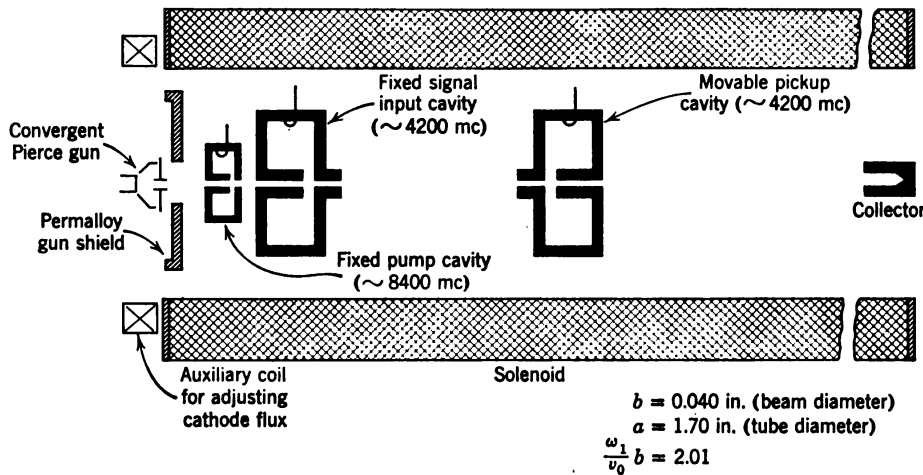


**Figure 7.4** Sketch of an experimental space-charge wave parametric amplifier used by Ashkin to demonstrate parametric gain. The signal and pump cavities excited both fast and slow modes. (From Ashkin, Reference 7.)

gap in a cavity tuned to the pump frequency 8400 mc. The beam was allowed to drift. It then went through another pickup cavity identical with the signal input cavity. Any current modulation on the beam at the signal frequency induced a current in the pickup cavity, which could be moved along the beam so that signal growth could be observed as a function of distance along the beam. Figure 7.5 shows the output from the pickup cavity as it was moved along the beam when only the signal wave was excited on the beam. The output shows the standing SCW setup by the beating of the slow and fast SCW's excited on the beam at the signal frequency.<sup>8,9</sup>

Figure 7.6 shows what happens when the pump wave is excited. It can be seen that the signal and idler waves grow exponentially as the three-frequency theory predicts. The observed gain was 13.2 db/plasma wavelength. The value of  $\omega_1 b / v_0$  was 2.01 for the experiment, and  $\omega_q / 2\omega_{q1}$  was 0.6. In order to compare this with the theoretical gain expressions, the pump power supplied must be related to the value of the current modulation at the pump frequency  $|m|$ . The value of  $|m|$  needed to give agreement with Eq. 7.15 would have been 0.84. An exact measurement of  $|m|$  was not made, but it was estimated that the actual value of  $|m|$  was considerably larger than 0.84.

Before discussing the probable cause of this discrepancy, it might be mentioned that the later experiments performed by Ashkin<sup>10-13</sup> have used fast wave couplers to excite pure fast SCW's on the beam. In this manner, fast wave noise can be removed at the signal frequency at the same time the fast signal mode is excited on the beam. The later experi-

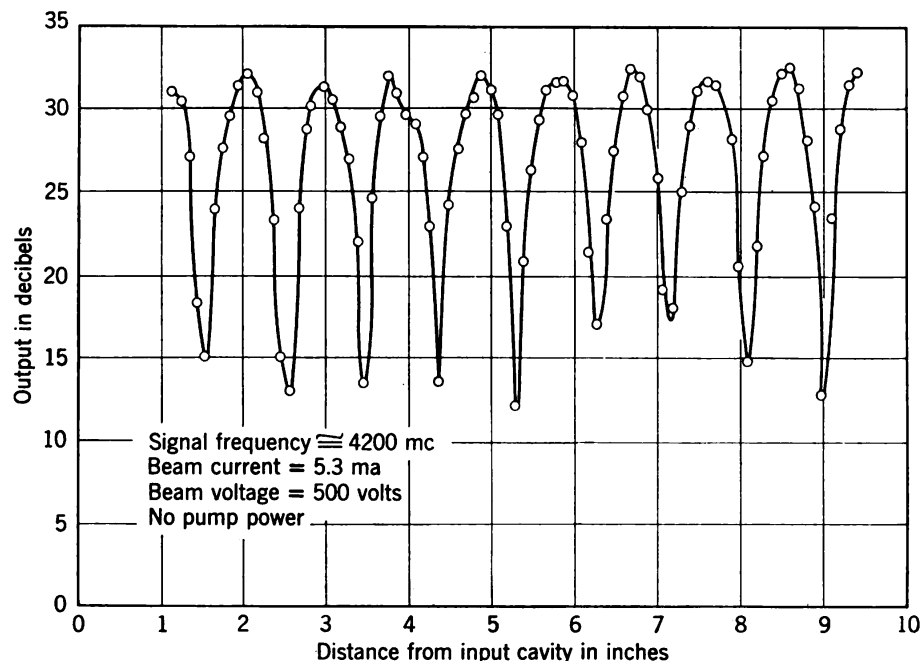


**Figure 7.5** Signal measured with movable cavity (Figure 7.4) as a function of distance when a signal but no pump was applied. This shows the standing waves set up by the interference of the fast and slow space-charge waves. For a discussion of the reason that the dips do not go to zero, see References 8 and 9. (From Ashkin, Reference 7.)

ments used a beam of radius  $b = 0.026$  in. in a tube of radius  $a = 0.060$  in. Further,  $\omega_1 b / v_0 = 0.6$ .

The discrepancy between theory and experiment is believed to be due to the presence of other idler frequencies, such as  $\omega + \omega_1 \equiv 2\omega_1 + \omega_2$  and  $\omega + \omega_2 \equiv \omega_1 + 2\omega_2$ , which are passively coupled to the signal by the pump. In this case the passive and active couplings counteract and reduce the gain drastically. The theory of these idlers is presented in Section 7.3.

To check this hypothesis, Ashkin<sup>14</sup> performed the following experiment. He first excited a fast SCW at the signal frequency  $\omega_1$  and observed the output measured at  $\omega_1$ . He compared this with an input signal at frequency  $2\omega_1 + \omega_2$ , when the output was again measured at frequency  $\omega_1$ . The pump was applied in the form of a fast wave. The conversion gain from  $2\omega_1 + \omega_2$  to  $\omega_1$  was indeed of the same order of magnitude as the straight  $\omega_1 \rightarrow \omega_1$  gain.

In addition to the foregoing idlers, another source of difficulty is the generation of pump harmonic waves at frequencies  $2\omega$ ,  $3\omega$ ,  $\dots$ . Paschke<sup>15,16</sup> and Mihran<sup>17</sup> have shown that by virtue of the nonlinear

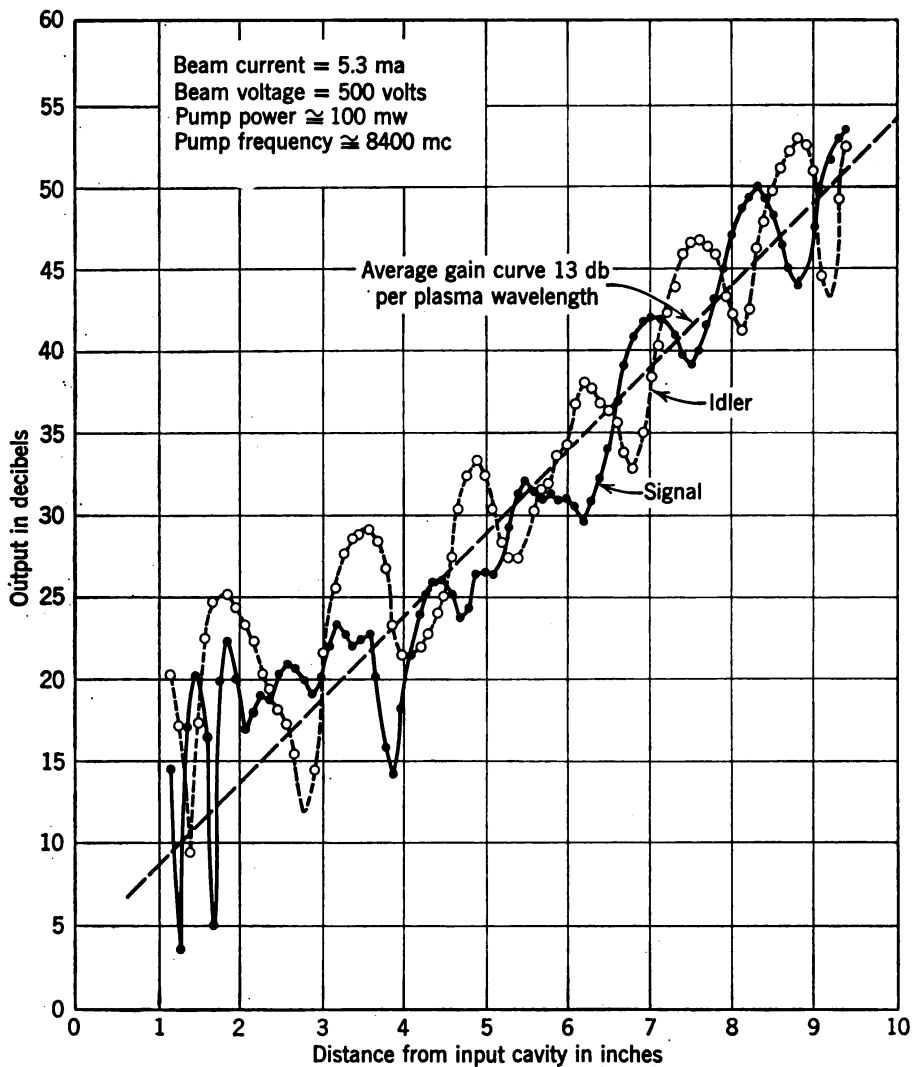


Figure 7.6 Measured signal output (see Figures 7.4 and 7.5) when pump power is applied when signal and idler frequencies differ by about 8 mc/sec. Interference between the fast and slow waves is still observed. Approximate exponential growth was observed of about 13 db/plasma wavelength. (From Ashkin, Reference 7.)

nature of the beam the strength of these pump harmonics will be very large. These harmonics give rise to unwanted interactions.

An analysis has also been carried out by Roe and Boyd<sup>18</sup> in which all harmonics are considered on a transmission line with no dispersion. They find that the gain will be decreased from the exponential gain when more harmonics are added. When a large number of harmonics is included, they find that the exponential gain disappears.

### 7.3 Effect of Higher Idler Frequencies on Gain

The analysis in which more idler frequencies are taken into account is quite laborious.<sup>19, 20</sup> The end result does not appear promising. Only a brief outline of the analysis, and a discussion of some of the results obtained, is given. The results point out the difficulties and show possible ways of overcoming them.

The analysis begins with Eqs. J.6 and J.7 of Appendix J in which the SCW's are described in terms of the beam velocity and current together with the reduced plasma frequency for a thin beam that is frequency dependent. These equations are essentially the equations of motion:

$$\frac{\partial^2 v}{\partial t^2} + \frac{\partial^2}{\partial z \partial t} \frac{v^2}{2} = -\omega_q^2 v_0 \frac{i}{|I_0|} \quad (7.17)$$

and the equation of continuity

$$v^2 \frac{\partial i}{\partial z} + v \frac{\partial i}{\partial t} - i \frac{\partial v}{\partial t} = 0 \quad (7.18)$$

The current and velocity are then expanded in a double Fourier series of the form

$$i(z, t) = \sum_{l=-\infty}^{\infty} \sum_{m=-\infty}^{\infty} i_{lm}(z) e^{i\Omega_{lm}t} \quad (7.19)$$

where  $\Omega_{lm} = l\omega_1 + m\omega_2$  with a similar expansion for the velocity. Since  $i(z, t)$  is real, it follows that the expansion coefficients must satisfy

$$i_{l,m}(z) = i_{-l,-m}^*(z) \quad (7.20)$$

with a similar requirement for  $v_{lm}(z)$ .

Consider now the physical meaning of these expansion coefficients. The term  $l = m = 0$  is clearly the d-c term in the expansion. The term  $l = m = 1$  is the pump, whereas  $l = m = 2$  is the second pump harmonic, etc. Therefore, the "diagonal" terms,  $l = m \neq 0$ , are the pump and pump harmonic terms. It is assumed that the pump and pump harmonics are fast SCW's whose amplitude of excitation decays as the order of the harmonic increases (see Paschke<sup>15, 16</sup>) and whose propagation constants are

$$\beta_{l\omega} = \frac{l\omega}{v_0} - \frac{\omega_q(l\omega)}{v_0} \quad (7.21)$$

where  $\omega_q$  is evaluated at frequency  $l\omega = l(\omega_1 + \omega_2)$ . The presence of pump harmonics ( $l > 1$ ) will present difficulties, as will be shown.

Further, since these are fast SCW's, the velocity and current are related by

$$\frac{v_{ll}}{v_0} = \frac{\omega_q(l\omega)}{l\omega} \frac{(-i_{ll})}{|I_0|} \quad (a)$$

where

$$\frac{i_{ll}}{|I_0|} = \frac{m_l}{2} e^{-j\beta_{l\omega} z} \quad (b)$$

and  $m_l$  measures the amplitude of current modulation of the harmonic  $l\omega$ .

The off-diagonal expansion coefficients ( $l \neq m$ ) are the a-c signal and idler terms. Therefore, amplitudes are assumed small compared with the pump and pump harmonic terms that are strongly excited.

The expansions of Eq. 7.19 and the similar one for the velocity are substituted in Eqs. 7.17 and 7.18. Products of a-c terms are neglected. Further,  $\omega_q$  evaluated at frequency  $\Omega_{lm}$  is always small compared with  $\Omega_{lm}$  for beams usually used in devices of this nature. This allows more terms to be neglected. Finally, the equations are put in coupled mode form and the slow modes are neglected. There still remains an infinite number of coupled equations in which fast SCW's at different frequencies are coupled by the pump. These are given by

$$\begin{aligned} & \left( \frac{d}{dz} + j(\gamma_{ln} - \beta_{q, ln}) \right) a_{ln} \\ &= -j \frac{\gamma_{ln}}{4} \sum_{s=-\infty}^{+\infty}' m_s e^{-j\beta_{s\omega} z} \sqrt{\alpha_{ln} \alpha_{l-s, n-s}} \left( 1 + \frac{\alpha_{ss}}{\alpha_{ln}} + \frac{\alpha_{ss}}{\alpha_{l-s, n-s}} \right) a_{l-s, n-s} \end{aligned} \quad (7.23)$$

where the prime on the sum indicates that the term  $s = 0$  is omitted. Also,

$$\begin{aligned} \gamma_{ln} &= \frac{\Omega_{ln}}{v_0} = \frac{l\omega_1 + n\omega_2}{v_0} \quad (a) \\ \beta_{q, lm} &= \frac{\omega_q(\Omega_{lm})}{v_0} \quad (b) \\ \alpha_{ij} &= \frac{\omega_q(\Omega_{ij})}{\Omega_{ij}} \quad (c) \end{aligned} \quad (7.24)$$

and  $a_{ln}$  is the fast SCW amplitude at frequency  $\Omega_{ln}$  in the absence of the pump. The double subscripts (e.g.,  $a_{ln}$ ) are integers and run from  $-\infty$  to  $+\infty$ .

It is an interesting exercise to correlate Eq. 7.23 with the general coupled mode equations of Chapter 5, Eqs. 5.31 and 5.32. It can be seen that the coupled frequencies are  $\omega_1$ ,  $-\omega_2$ ,  $2\omega_1 + \omega_2$ ,  $-\omega_1 - 2\omega_2$ ,  $3\omega_1 + 2\omega_2$ ,  $-2\omega_1 - 3\omega_2$ , etc. If  $\omega = \omega_1 + \omega_2$ , these frequencies can be written as  $\omega_1$ ,  $\omega_1 - \omega$ ,  $\omega_1 + \omega$ ,  $\omega_1 - 2\omega$ ,  $\omega_1 + 2\omega$ ,  $\omega_1 - 3\omega$ , etc., respectively. Therefore, the coupled frequencies are  $\Omega_i = \omega_1 + i\omega$ , where  $i = 0, \pm 1, \pm 2, \dots$  in agreement with Eq. 5.31. Only one subscript is needed to describe the modes that are coupled in agreement with Eq. 5.32.

When only  $\omega$ ,  $\omega_1$ , and  $\omega_2$  are assumed to be present, it is easy to verify that these equations reduce to Eqs. 7.6, where  $l = 1$ ,  $n = 0$ , and  $l = 0$ ,  $n = -1$ , in which case  $a_{0,-1} \equiv a_{2+}^*$ .

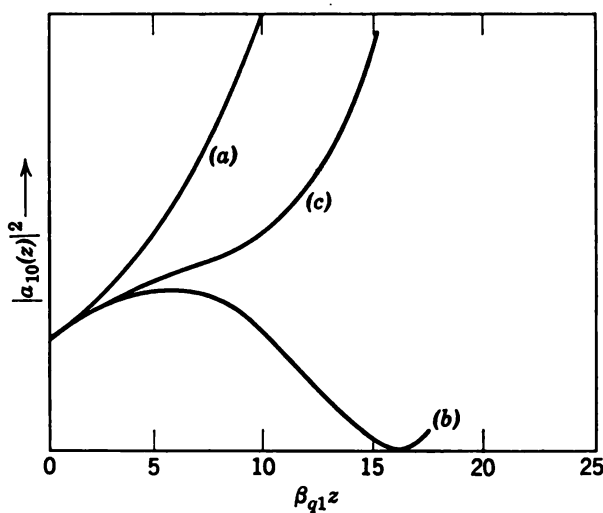
There is a fundamental difficulty if a pump harmonic, for example,  $2\omega$ , is allowed to propagate. In this case the standard change of variables, which has been used to remove the variable ( $z$ -dependent) coupling coefficients, will not work. However, even if only the pump primary is present, all frequencies  $\Omega_i = \omega_1 + i\omega$  are still coupled indirectly.

It can be seen by inspection of the coupling coefficients in Eq. 7.23, and using Eq. 5.34 when just the pump primary is present, that the  $\omega_1$  and  $-\omega_2$  modes are actively coupled and all others are passively coupled. Since the coupling coefficients obey Eq. 5.34 of Chapter 5, the Manley-Rowe relations follow immediately.

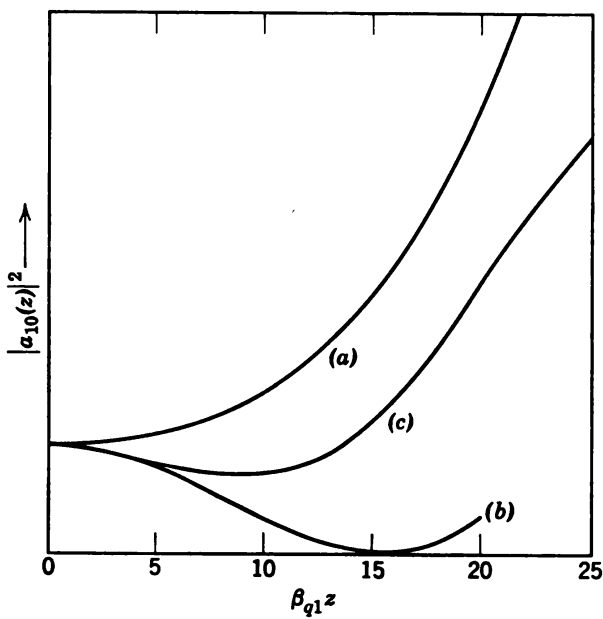
When more than a few idler frequencies are involved, Eq. 7.23 must be solved on the computer except in certain very special cases. Figure 7.7 (curve *a*) shows the computer solution of Eq. 7.23 when only three frequencies,  $\omega$ ,  $\omega_1$ , and  $\omega_2$  are allowed to propagate on a thin beam (no dispersion). The fast mode amplitude,  $|a_{10}(z)|^2$ , at  $\omega_1$  is plotted versus  $\beta_{q1}z$ , where  $\beta_{q1}$  is evaluated at  $\omega_1$ . This is the case treated analytically and yields the now familiar exponential growth. Curve *b* shows what happens to the output when two more frequencies ( $\omega + \omega_1 \equiv 2\omega_1 + \omega_2$  and  $\omega + \omega_2 \equiv \omega_1 + 2\omega_2$ ) are added, whereas curve *c* also contains frequencies  $2\omega + \omega_1$  and  $2\omega + \omega_2$ . All of these curves are for the degenerate case in which  $\omega_1 = \omega_2$  and the phase of the pump relative to the signal is adjusted for gain. From these results (compare with Reference 18) it is seen that the gain is reduced as more frequencies are added.

Figure 7.8 again shows  $|a_{10}(z)|^2$  versus  $\beta_{q1}z$  for the thin beam with an input at the signal frequency but for the case  $\omega_1 \approx \omega_2$ .  $|m| = 0.8$  for these curves is very large, but the same qualitative behavior was observed for smaller values of pump current modulation. Both the five- (curve *b*) and seven- (curve *c*) frequency cases are seen to give an initial loss.

For the infinitely thin beam, analytic solutions show that each time a



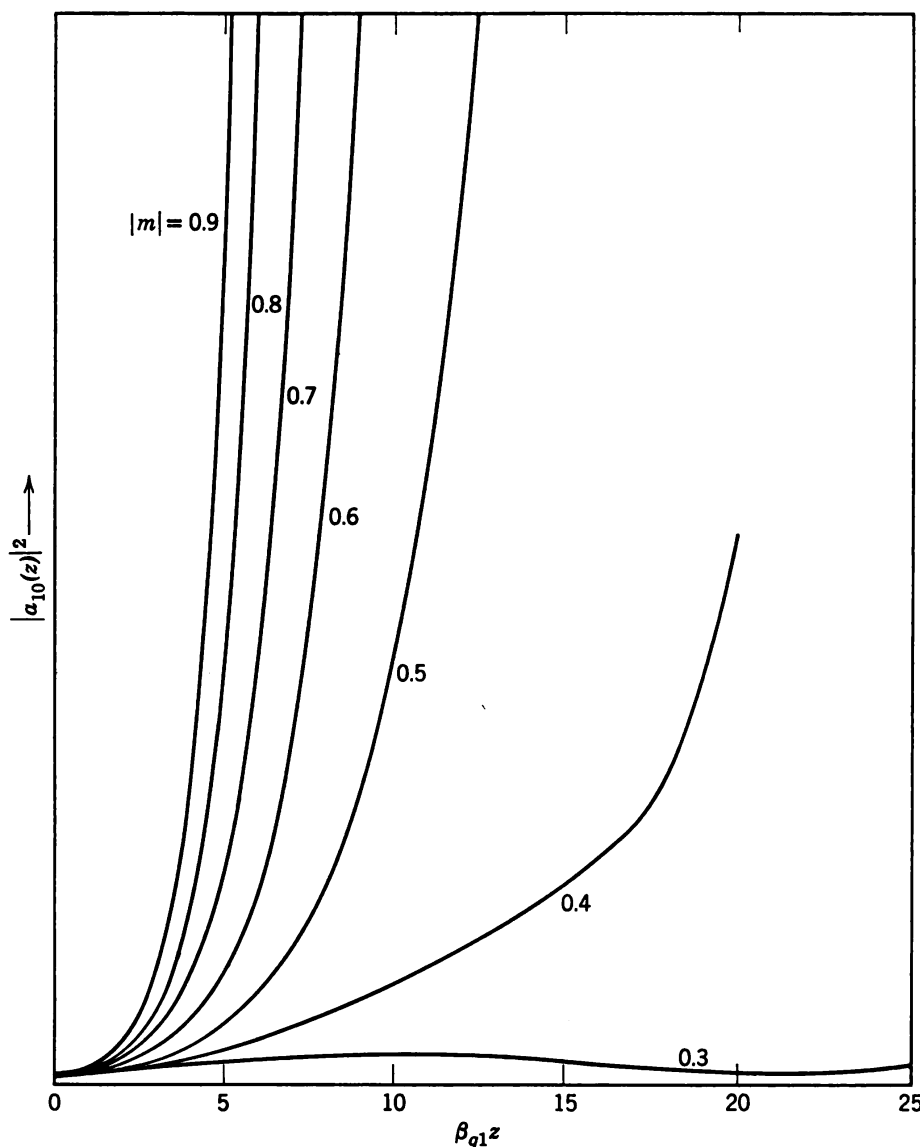
**Figure 7.7** Fast mode power output at signal frequency ( $|a_{10}(z)|^2$ ) versus distance for degenerate thin-beam amplifier. (a) Only frequencies  $\omega$  and  $\omega_1 = \omega_2$  are present. (Pump phase adjusted for maximum gain.) (b) Frequencies  $\omega + \omega_1$  and  $\omega + \omega_2$  ( $\omega_1 = \omega_2$ ) added. (c) Frequencies  $2\omega + \omega_1$  and  $2\omega + \omega_2$  added. As more frequencies are added, the tube must be made longer to obtain a given gain.



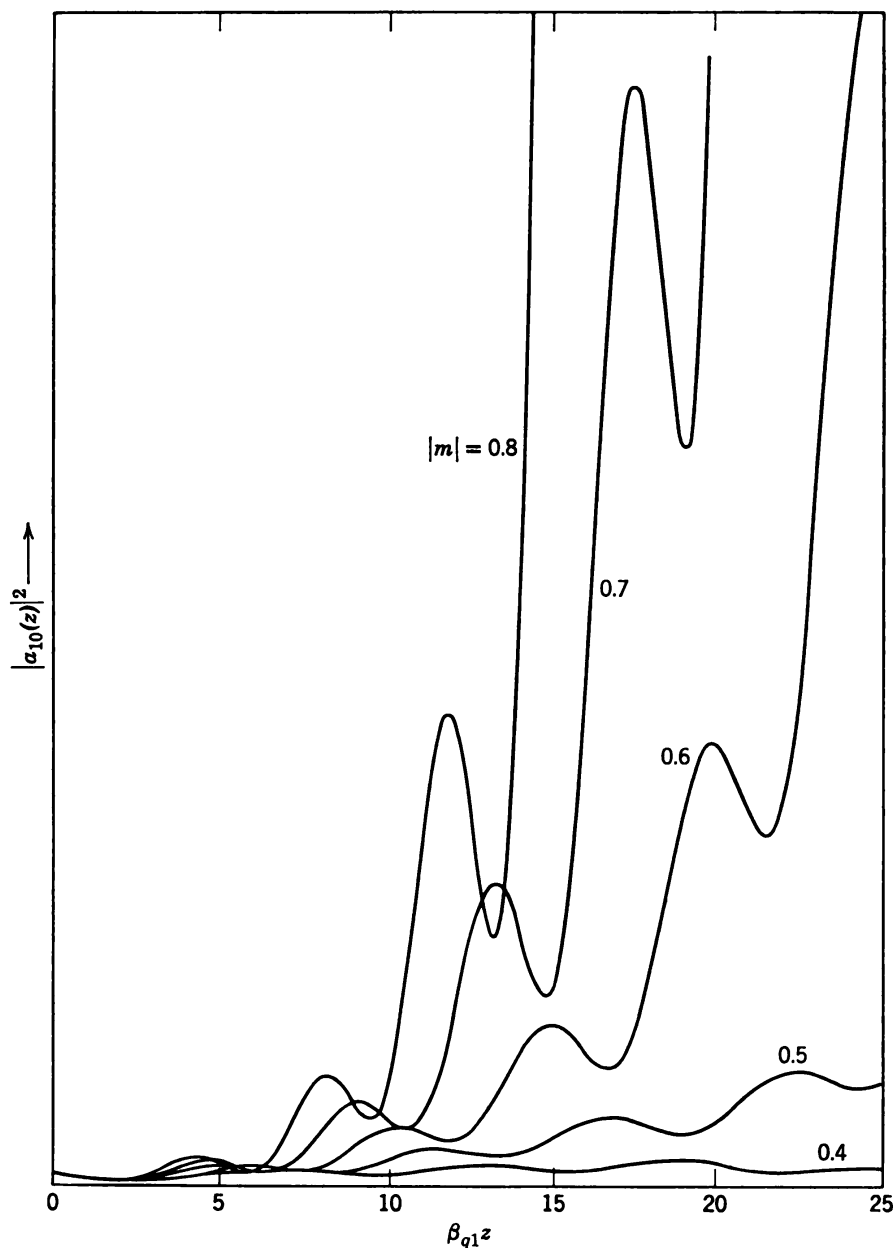
**Figure 7.8** Same as Figure 7.7, except  $\omega_1$  and  $\omega_2$  are slightly different.

new pair of idlers is added two growing and two decaying modes that travel with the same phase velocity are added. Initially these modes can interfere constructively or destructively, but eventually, as  $\beta_{q1}z$  increases, the growing waves predominate and win out. As long as only a finite number of idlers is considered, there will be exponential gain.

Figure 7.9 shows  $|a_{10}(z)|^2$  as a function of  $z$  with an input  $|a_{10}(0)|$

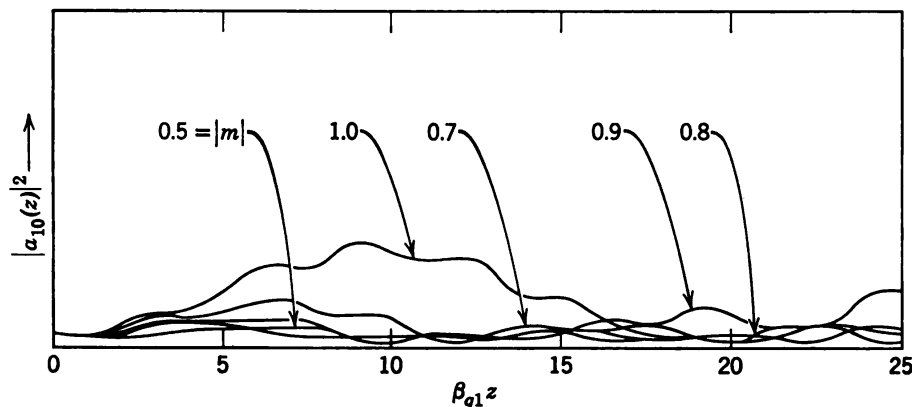


**Figure 7.9** Signal power versus distance for a finite size beam ( $\alpha/\alpha_1 = 0.75$ ) with only frequencies  $\omega$  and  $\omega_1 = \omega_2$  present. The gain is plotted for various values of pump modulation. The input level is at  $z = 0$ .



**Figure 7.10** Signal power versus distance when frequencies  $\omega$ ,  $\omega_1$ ,  $\omega_2$ ,  $\omega + \omega_1 = \omega_3$ , and  $\omega + \omega_2 = \omega_4$  are present on a finite beam.  $\alpha/\alpha_1 = \alpha/\alpha_2 = 0.75$  and  $\alpha/\alpha_3 = \alpha/\alpha_4 = 1.2$ . The gain is considerably reduced from the three-frequency case of Figure 7.9.

for various values of  $|m|$ . A finite beam was considered with  $\alpha/\alpha_1 = \alpha/\alpha_2 = 0.75$  for the three-frequency case. As found analytically in Chapter 6,  $|\alpha_{10}(z)|^2$  grows exponentially and the rate of growth increases with increasing  $|m|$ . Figure 7.10 shows the gain curves for various  $|m|$ 's for the five-frequency case. For these curves  $\alpha/\alpha_3 = \alpha/\alpha_4 = 1.2$ , where  $\omega_3 = \omega + \omega_1$  and  $\omega_4 = \omega + \omega_2$ . The gain is less when these frequencies are added and the gain curves are reminiscent of space-charge standing waves. Here, however, the slow modes are eliminated. The interference is between fast waves that grow at the same rate but travel with different phase velocities. When seven frequencies are added, Figure 7.11 shows that the gain is drastically reduced. The beam dispersion is not sufficient to prevent strong passive coupling to higher idler frequencies.



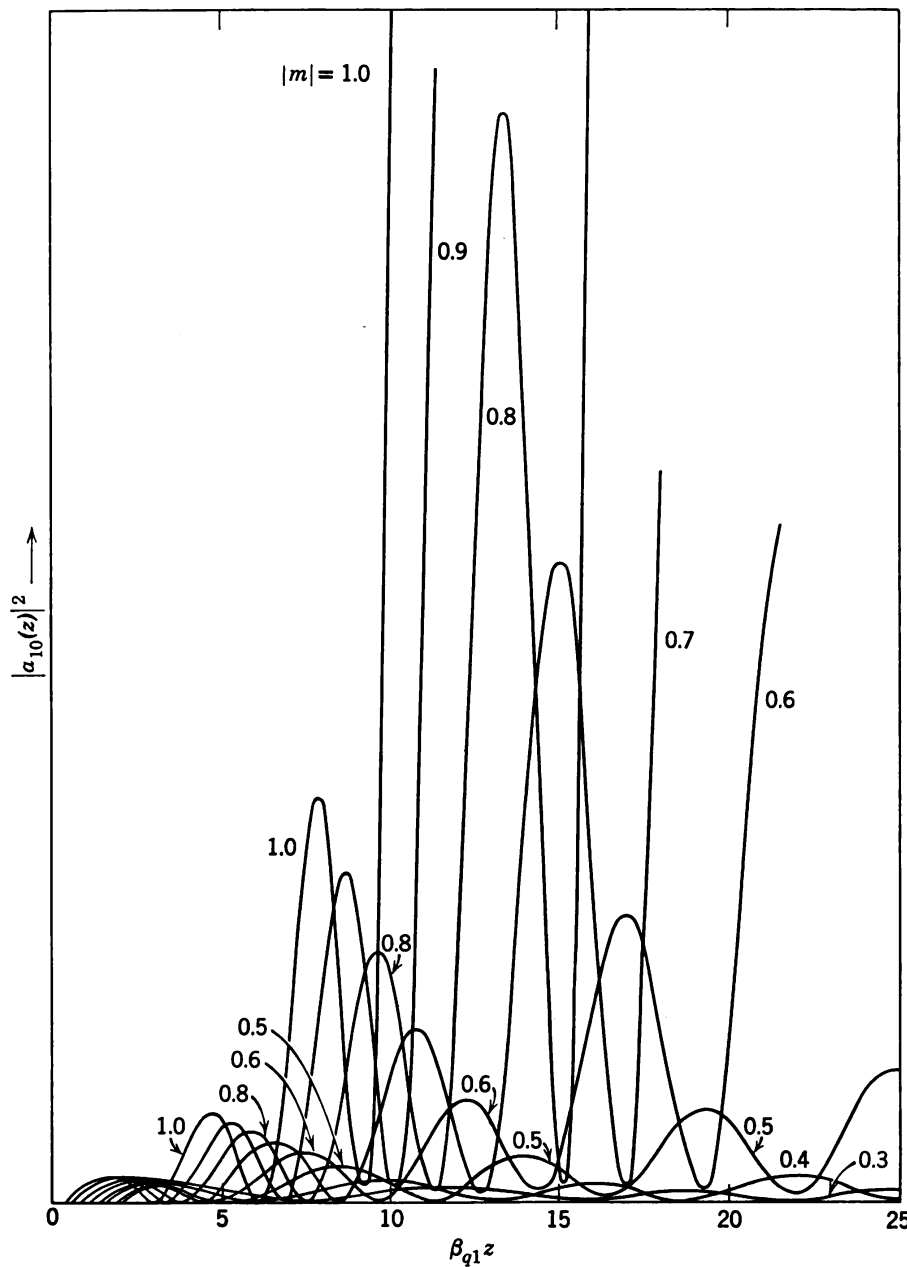
**Figure 7.11** When two more frequencies are added ( $2\omega + \omega_1$  and  $2\omega + \omega_2$ ) to Figure 7.10, the gain has disappeared.

Figure 7.12 shows the output at the signal frequency when there is an input at  $\omega_3$  for the five-frequency case. This bears out Ashkin's observations.<sup>14</sup>

The equations were also solved on the computer with the second pump harmonic, as well as five higher frequency idlers, and the results were disappointing. The gain never recovered to the five-frequency value.

#### 7.4 Remarks

- a. There are two serious drawbacks to the FSCWPA using the fast SCW at  $\omega$  to provide the pumping. Both are due to the small amount of dispersion of the SCW's. The first drawback is that passive coupling to higher idler frequencies reduces the gain. Fast mode noise in the higher



**Figure 7.12** Output power at signal frequency versus distance when signal is applied at frequency  $\omega_3 = \omega + \omega_1$ . There is a large amount of conversion gain.

idler frequencies couples down to frequency  $\omega_1$ . Therefore, noise has to be removed from a series of idler frequencies in addition to the signal frequency. Each frequency would require a separate coupler to remove the noise, so that the device in this form is not practical.

b. At least three proposals have been presented to circumvent these difficulties. Wade and Adler<sup>21</sup> have proposed using an external circuit to propagate a pump wave, instead of the fast SCW, which does not excite the fast SCW at the pump frequency. Since the mixing is done on the beam, presumably this wave will not couple to the higher idler frequency. Another proposal was made<sup>20</sup> in which the pump wave couples to a circuit. This coupling will alter the phase velocity with which the pump wave propagates on the beam. In this way coupling to the signal can be enhanced and coupling to the higher idler frequencies can be reduced. A third proposal<sup>18, 20</sup> couples a circuit to idler frequencies  $\omega + \omega_1$  and  $\omega + \omega_2$  only and shifts their phase velocities so that coupling to this idler will be reduced. Once these are out of the way, coupling to higher idlers will be reduced, since this coupling is via  $\omega + \omega_1$  and  $\omega + \omega_2$ , as may be seen if the equations are written out. So far no positive results are available on any of these proposals. Unfortunately, the detailed analysis of these schemes is too long to present here.

c. T. J. Bridges<sup>22</sup> proposed an electron beam parametric amplifier in which the beam goes through a single gap cavity which excites a fast and slow space-charge wave on the beam at the pump frequency  $2\omega_1$ . The modulated beam then traverses a double gap cavity tuned to the signal frequency  $\omega_1$ . The pump wave on the beam couples to the signal cavity and varies the r-f admittance of the cavity at  $2\omega_1$ . The equivalent circuit for this amplifier is the degenerate lumped circuit parametric amplifier of Chapter 4. Bridges observed a maximum gain of 20 db, using a beam voltage of 2450 volts, a beam current of 18 ma, signal frequency of 4150 mc, and a pump power of 140 mw.

d. Chapter 8 presents the theory of the fast cyclotron wave parametric amplifier.<sup>23, 24</sup> Since the dispersion for the cyclotron waves is so great, the coupling to higher idler frequencies can be neglected in this device.

## BIBLIOGRAPHY

1. J. R. Pierce, "A Theorem Concerning Noise in Electron Streams," *J. Appl. Phys.*, **25**, 931-933 (August 1954).
2. H. A. Haus and F. N. H. Robinson, "The Minimum Noise Figure of Microwave Beam Amplifiers," *Proc. IRE*, **43**, 981 (1955).
3. "Noise in Electron Devices," edited by L. D. Smullin and H. A. Haus, John Wiley and Sons, New York, Chapter 3, 1959.

4. W. H. Louisell and C. F. Quate, "Parametric Amplification of Space-Charge Waves," *Proc. IRE*, **46**, 707-716 (April 1958).
5. W. H. Louisell, "A Three Frequency Electron Beam Parametric Amplifier," *J. Electronics Control*, **6**, 1-25 (January 1959).
6. H. A. Haus, "The Kinetic Power Theorem for Parametric, Longitudinal, Electron Beam Amplifiers," *IRE Trans. PGED*, **ED-5**, 225-232 (October 1958).
7. A. Ashkin, "Parametric Amplification of Space-Charge Waves," *J. Appl. Phys.*, **29**, 1646-1651 (December 1958).
8. C. C. Cutler and C. F. Quate, "Experimental Verification of Space Charge and Transit Time Reduction of Noise in Electron Beams," *Phys. Rev.*, **80**, 875-878 (December 1, 1950).
9. A. van der Ziel, *Noise*, Prentice-Hall, New York, 1954, pp. 384-389.
10. A. Ashkin, "Parametric Amplification of Space-Charge Waves," presented at the IRE Annual Electron Tube Research Conference, Quebec, Canada (1958).
11. A. Ashkin, W. H. Louisell, and C. F. Quate, "Fast Wave Couplers for Longitudinal Beam Parametric Amplifiers," *J. Electronics Control*, **7**, 1-32 (July 1959).
12. R. W. Gould, "Traveling Wave Couplers for Longitudinal Beam Type Amplifiers," *Proc. IRE*, **47**, 419-426 (March 1959).
13. A. Ashkin, J. S. Cook, and W. H. Louisell, "Modification of the Space-Charge Wave Dispersion for Parametric Amplification," presented at IRE Annual Electron Tube Research Conference, Mexico City, Mexico (1959).
14. A. Ashkin, private communication.
15. F. Paschke, "On the Nonlinear Behavior of Electron Beam Devices," *R C A Rev.*, **18**, 221-242 (June 1957).
16. F. Paschke, "Generation of Second Harmonic in a Velocity Modulated Electron Beam of Finite Diameter," *R C A Rev.*, **19**, 617-627 (December 1958).
17. T. G. Mihran, "Measurement of Harmonic Currents in a Velocity Modulated Electron Beam," presented at the IRE Annual Conference on Electron Tube Research, Quebec, Canada (1958).
18. G. M. Roe and M. R. Boyd, "Parametric Energy Conversion in Distributed Systems," *Proc. IRE*, **47**, 1213-1218 (July 1959).
19. J. S. Cook and W. H. Louisell, "Traveling Wave Tube Equations Including the Effect of Parametric Pumping," *Proc. IRE*, **47**, 2016-2017 (November 1959).
20. J. S. Cook, W. H. Louisell, and C. F. Quate, "Space-Charge Wave Parametric Amplifiers," *J. Electronics Control*, **8**, 1-18 (January 1960).
21. G. Wade and R. Adler, "A New Method for Pumping a Fast Space-Charge Wave," *Proc. IRE*, **47**, 79-80 (January 1959).
22. T. J. Bridges, "A Parametric Electron Beam Amplifier," *Proc. IRE*, **46**, 494-495 (February 1958).
23. R. Adler, "Parametric Amplification of the Fast Electron Wave," *Proc. IRE*, **46**, 1300-1301 (June 1958).
24. R. Adler, G. Hrbek, and G. Wade, "A Low Noise Electron Beam Parametric Amplifier," *Proc. IRE*, **46**, 1756-1757 (October 1958).

## Chapter 8

# Fast cyclotron mode parametric amplifier

The present chapter has a two-fold purpose. First, it presents the theory of the effect of coupling a slow wave circuit weakly to an electron beam which propagates the cyclotron and synchronous modes treated in Chapter 2. The treatment is analogous to the coupling of a slow wave circuit to the space-charge waves in Chapter 3. However, the beam now propagates two cyclotron and two synchronous modes, so that two more coupled equations are involved. Depending on which of the modes is strongly coupled and the nature of the slow wave circuit, the theory can be used to describe a transverse field amplifier, backward wave amplifier, or directional coupler analogous to Chapter 3. The primary emphasis in the present discussion is on a directional coupler that can be used to excite the fast cyclotron mode on the beam.

The second aim is to show how the fast cyclotron mode can be parametrically amplified.<sup>1-3</sup> Experimental results that have been obtained are described.

### 8.1 Slow Wave Circuit Coupled to Cyclotron and Synchronous Modes<sup>4,5,6</sup>

The formal theory leading to the coupled mode equations when cyclotron and synchronous modes are coupled to a slow wave circuit is very similar to the treatment of space-charge waves coupled to a slow wave circuit treated in Chapter 3. Therefore, the detailed analysis of this problem is relegated to Appendix K, and the resultant coupled mode equations, together with a synopsis of the assumptions on which they

are based, will be immediately written down. The coupled mode equations are used to show that the fast cyclotron mode and one synchronous mode carry positive kinetic power, whereas the slow cyclotron mode and the other synchronous mode carry negative power. Finally, the directional coupler is treated in which the fast cyclotron mode is strongly coupled to the forward circuit mode.

**Coupled mode equations.** The coupled mode equations for the slow wave circuit coupled to the cyclotron and synchronous modes are derived in Appendix K. The beam moves in the positive  $z$ -direction with a uniform d-c velocity,  $v_0$ , small compared with the velocity of light. The uniform d-c magnetic focusing field,  $B_0$ , is in the positive  $z$ -direction. Space-charge forces are assumed small compared with the magnetic focusing forces ( $\omega_p^2 \ll \omega_c^2$ ), so that space-charge forces are neglected. Consequently, each electron is independent of the presence of other electrons. (See Chapter 2.) Therefore, only an infinitely thin beam need be considered. The usual time dependence  $e^{(j\omega_1 t)}$  and small signal approximations are made.

The effect of the circuit on the beam is accounted for by a transverse electric field term in the equations of motion in which the electric field is taken as the circuit field only. However, there will necessarily always be some longitudinal electric or transverse magnetic field present. Since they affect only the longitudinal velocities, their effects can be neglected in a first-order theory.

The actual slow wave circuit is replaced by an equivalent circuit<sup>7</sup> (a transmission line), as in Chapter 3. The beam induces a current in the circuit which represents the effect of the beam on the actual circuit. Only a-c transverse circuit fields are considered at the position of the beam. Since cyclotron and synchronous modes have only a-c transverse displacements and velocities, no coupling to the longitudinal beam motion need be considered.

The mode amplitudes are given by

$$a_{\pm}(z) = \frac{1}{4\sqrt{Z_0}} (V \pm Z_0 I)$$

= forward and backward circuit modes (Eq. 1.46c) (8.1a)

where  $V(z)$  and  $I(z)$  are complex,

$$a_{1\pm}(z) = k(u_{1x} \pm j u_{1y})$$

= fast and slow cyclotron modes (Eq. 2.58) (8.1b)

where  $u_{1x}(z)$  and  $u_{1y}(z)$  are complex,

$$\begin{aligned} a_{2\pm}(z) &= a_{1\pm} \mp j\omega_c r_\pm \\ &= \text{synchronous mode amplitudes (Eq. 2.74)} \end{aligned} \quad (8.1c)$$

where  $Z_0$  is the characteristic impedance of the line,

$$k = \frac{1}{4} \sqrt{\frac{\omega_1 |I_0|}{\omega_c |e|}} m \quad (8.2a)$$

and by Eq. 2.73

$$r_\pm = k(\xi_{1x} \pm j\xi_{1y}) \quad (8.2b)$$

$\xi_{1x}(z)$  and  $\xi_{1y}(z)$  are complex.

The six coupled mode equations (Eqs. K.18) are

$$\begin{aligned} \left( \frac{d}{dz} \pm j\beta_0 \right) a_\pm &= \pm c_{12} [f_+^*(a_{2+} - a_{1+}) - f_-^*(a_{2-} - a_{1-})] \\ \left( \frac{d}{dz} + j(\beta_e \mp \beta_c) \right) a_{1\pm} &= c_{12} f_\pm (a_+ + a_-) \\ \left( \frac{d}{dz} + j\beta_e \right) a_{2\pm} &= c_{12} f_\pm (a_+ + a_-) \end{aligned} \quad (8.3)$$

where  $\beta_0$  is the uncoupled line propagation constant,  $\beta_e = \omega_1/v_0$ ,  $\beta_c = \omega_c/v_0$ , and the mutual coupling coefficient is

$$c_{12} = \frac{1}{2D} \sqrt{\frac{Z_0 |I_0| \omega_1}{2V_0 \omega_c}} \quad (8.4)$$

A few words must be said about  $f_\pm$  and  $D$ . It was shown in Chapter 2 that the cyclotron ( $a_{1\pm}$ ) and synchronous ( $a_{2\pm}$ ) modes are circularly polarized. The factors  $f_+$  and  $f_-$  express the type of polarization of the circuit field.<sup>6</sup> If  $E_x$  and  $E_y$  are the actual transverse electric fields at the position of the beam, then

$$E_\pm = E_x \pm jE_y = -f_\pm \frac{V}{D} \quad (8.5)$$

where  $V$  is the voltage of the transmission line, which is taken as the equivalent circuit for the actual slow wave circuit, analogous to Chapter 3.  $D$  is a normalizing distance of the equivalent circuit. If  $f_+ = 0$ , the field of the circuit is circularly polarized in one sense, whereas if  $f_- = 0$  the circuit field is circularly polarized in the opposite sense. By using the parameters  $f_\pm$ ,<sup>6</sup> circular, linear, or elliptic polarized circuit fields

can be represented. The polarization parameters  $f_{\pm}$  are normalized, so that the magnitude of the actual circuit field is

$$|E_x|^2 + |E_y|^2 = \frac{V^2}{2D^2} \quad (8.6)$$

and

$$|f_+|^2 + |f_-|^2 = 1 \quad (8.7)$$

The coupled mode equations show that the circuit can be used to excite either cyclotron or synchronous modes. For example, the  $f_+$  circuit polarization couples directly to the fast cyclotron mode ( $a_{1+}$ ), which has left-handed polarization. That is, if the circuit field is polarized in the same sense as the beam mode, it will couple directly. In this case energy from the circuit is transformed into rotational beam kinetic energy.

**Power theorem.** It will now be shown that the fast cyclotron mode ( $a_{1+}$ ) and the synchronous mode ( $a_{2-}$ ) carry positive kinetic power, whereas the slow cyclotron mode ( $a_{1-}$ ) and the synchronous mode ( $a_{2+}$ ) carry negative kinetic power. These results were asserted in Chapter 2, but since the modes were uncoupled there was no reference power with which to compare the positive and the negative. In the present instance the mode power can be compared with the circuit power.

The total average power flow along the beam-circuit system is given by

$$P = 2(|a_+|^2 - |a_-|^2 + |a_{1+}|^2 - |a_{1-}|^2 - |a_{2+}|^2 + |a_{2-}|^2) \quad (8.8)$$

In order to show that  $P$  is independent of  $z$ , differentiate Eq. 8.8 with respect to  $z$  and substitute into this expression Eqs. 8.3 and their complex conjugates. It then follows immediately that  $dP/dz = 0$ . It is seen from the foregoing power theorem (Eq. 8.8) that  $a_{1+}$  and  $a_{2-}$  carry positive power with respect to the forward circuit mode, whereas  $a_{1-}$  and  $a_{2+}$  carry negative kinetic power.

The negative power carried by the  $a_{1-}$ - and  $a_{2+}$ -modes is due to the interaction of the beam with the longitudinal electric or transverse magnetic fields that necessarily exist when these modes are excited. These fields, which have been neglected, reduce the d-c beam velocity, so that on the average the beam kinetic power is less when these modes are excited than in their absence.

From the coupled equations it is seen, for example, that the forward circuit mode is passively coupled to the fast cyclotron mode and the slow cyclotron mode is actively coupled to the forward circuit mode, since  $c_{12}$  is real. The possibility of amplification of the slow cyclotron mode, therefore, exists, and this leads to the theory of the transverse field

amplifier, analogous to the traveling wave tube. The details are not worked out here, however. The principal interest is centered on the problem analogous to the Kompfner dip helix, in which the beam and circuit are used to excite a fast cyclotron wave on the beam and at the same time remove any noise in the fast cyclotron mode that exists on the beam.

**Fast cyclotron wave coupler.** Assume that the circuit provides a pure left-hand circularly polarized field. Then,  $f_- = 0$  and  $f_+ = 1$ . In this case the slow cyclotron and right-hand polarized synchronous mode amplitudes are not coupled. Further, coupling to the backward circuit mode  $a_-$  can be neglected. Equations 8.3 then reduce to

$$\begin{aligned} \left( \frac{d}{dz} + j\beta_0 \right) a_+ &= c_{12}(a_{2+} - a_{1+}) \\ \left( \frac{d}{dz} + j(\beta_e - \beta_c) \right) a_{1+} &= c_{12}a_+ \\ \left( \frac{d}{dz} + j\beta_e \right) a_{2+} &= c_{12}a_+ \end{aligned} \quad (8.9)$$

The transfer factor for  $a_{2+}$  and  $a_+$  is

$$F_{+,2+} = \left[ 1 - \left( \frac{\beta_0 - \beta_e}{2} \right)^2 \frac{1}{c_{12}^2} \right]^{-1} \quad (8.10)$$

Also note that the circuit will couple strongly to the fast cyclotron mode only if

$$\beta_0 \cong \beta_e - \beta_c \quad (8.11)$$

In this case, coupling to the  $a_{2+}$  mode can be neglected when  $\beta_c^2 \gg 4c_{12}^2$ . Equations 8.9 then reduce to

$$\begin{aligned} \left( \frac{d}{dz} + j(\beta_e - \beta_c) \right) a_{1+} &= c_{12}a_+ \\ \left( \frac{d}{dz} + j\beta_0 \right) a_+ &= -c_{12}a_{1+} \end{aligned} \quad (8.12)$$

But these are just the equations for two passively coupled modes (a directional coupler). Power injected on the line will periodically transfer back and forth to the beam. Further, noise on the beam will be periodically transferred to the circuit. (See Chapter 3, Section 3.4.) Therefore,

the coupler can be used to apply a signal to the beam and at the same time remove the noise in the fast cyclotron mode. The "dip" length  $L$  for maximum transfer is

$$\sqrt{\left(\frac{\beta_0 - \beta_e + \beta_c}{2}\right)^2 + c_{12}^2 L} = \frac{\pi}{2} \quad (8.13)$$

## 8.2 Parametric Coupling Principle Applied to Fast Cyclotron Wave

Section 8.1 has shown how a coupler can be used to excite a fast cyclotron signal wave on an electron beam and at the same time remove the fast cyclotron mode noise at the signal frequency from the beam. Adler, Hrbek, and Wade <sup>2</sup> proposed that if the beam, which is propagating a fast cyclotron wave, enters a transverse circularly polarized circuit pump field at frequency  $\omega = 2\omega_1$ , the signal wave will be parametrically amplified. It was shown <sup>2</sup> that such a field can be provided by a quadrupolar structure, described in Figure 8.1. A field with quadrupolar symmetry may be provided by four electrodes, as shown in the figure, or it might be provided by the  $TE_{11}$ -mode in a rectangular waveguide, a  $TE_{21}$ -mode in a circular waveguide, etc.

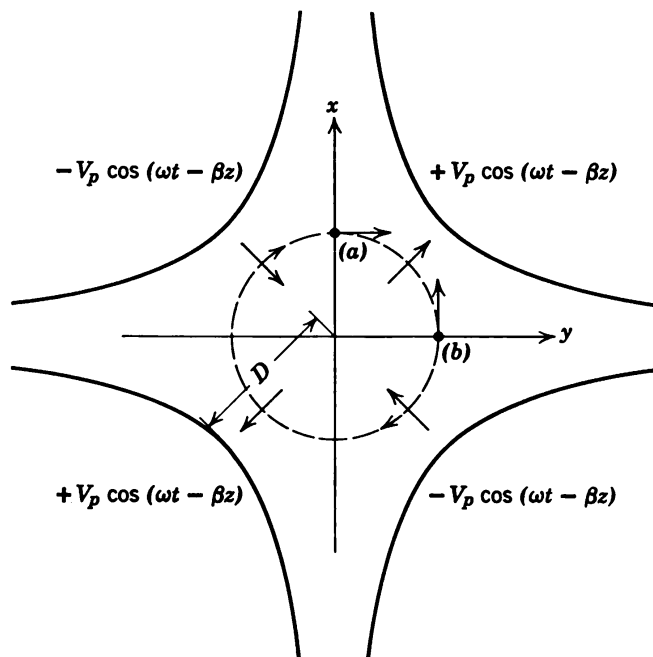


**Figure 8.1** Cross-sectional view of quadrupole pump structure for cyclotron wave amplifier. (From Adler, Hrbek and Wade, Reference 2.)

Figure 8.1 shows the field at an instant and given cross section in which the first and third quadrant electrodes are positive and the second and fourth are negative. A homogeneous d-c magnetic focusing field is directed into the plane of the paper. The electrons, on entering the pump region, are executing cyclotron motion on which there is a fast cyclotron wave. Points (a) and (b) represent two possible phases of the cyclotron wave electrons with respect to the pump field. The four arrows at 45, 135, 225, and 315° show the direction of the forces exerted on electrons in these regions. At these angles the forces are normal to the electron velocities and do no work. However, at (a) the force is tangential to the electron path and accelerates the electron, while at this same instant an electron at (b) is decelerated. Concentrate on electrons entering at (a). If the pump frequency  $\omega$  is twice the cyclotron frequency, by the time (a) gets to (b) it will again be accelerated, since the polarity of the pump field will have changed. The rotational energy that is given the electron motion by the pump goes into increasing its radius. As will be shown, the force also increases with the radius, and an exponential growth in radius is to be expected for this quadrupolar pump field. Thus the signal will be parametrically amplified at the expense of pump energy.

**The pump field.** The static potential of a quadrupole pump structure can be written as

$$V(x, y) = \frac{2V_p}{D^2} xy \quad (8.14)$$

which satisfies Laplace's equation, where  $V_p$  and  $D$  are constants. The hyperbolas  $xy = \text{constant}$  are equipotential surfaces. Therefore, the electrodes are taken as  $xy = \pm D^2/2$ , where  $D$  is shown in Figure 8.1, and  $V_p$  is the potential of the electrodes. Assume that a wave at frequency  $\omega$  and propagation constant  $\beta$  is propagating down the structure. Since  $\mathbf{E} = -\nabla V$ , the pump field may be written as

$$\begin{aligned} E_x &= -\frac{y}{2D^2} (V_p e^{j(\omega t - \beta z)} + \text{c.c.}) \\ E_y &= -\frac{x}{2D^2} (V_p e^{j(\omega t - \beta z)} + \text{c.c.}) \end{aligned} \quad (8.15)$$

Since

$$\overline{|E|} = \sqrt{\overline{E_x^2} + \overline{E_y^2}} = \frac{V_p}{2D^2} \sqrt{x^2 + y^2} = \frac{V_p}{2D^2} r \quad (8.16)$$

the electric field for this structure varies linearly with the radius.

It can be shown that Eqs. 8.15 represent approximately the  $TE_{11}$ -mode in a square waveguide near the center of the guide.

**Equations of motion in the pump region.** Assume that the beam enters the quadrupolar pump field modulated with a fast cyclotron wave at the signal frequency. The pump circuit propagates an electromagnetic wave at the pump frequency, but it is assumed that the circuit is cut off for the fast cyclotron wave at the signal and idler frequencies. Otherwise, the signal wave would couple passively to the pump circuit so that signal power would be transferred to the circuit.

The signal and idler frequencies are related to the pump by the usual relation

$$\omega = \omega_1 + \omega_2 \quad (8.17)$$

and, in order that there be no gain threshold, it is assumed that the uncoupled beam fast cyclotron mode propagation constants,  $\beta_{f_1} = \beta_1 - \beta_c$  and  $\beta_{f_2} = \beta_2 - \beta_c$ , where  $\beta_{1,2} = \omega_{1,2}/v_0$ , are related to the pump propagation constant by

$$\begin{aligned} \beta &= \beta_{f_1} + \beta_{f_2} \\ &= \beta_1 + \beta_2 - 2\beta_c \end{aligned} \quad (8.18)$$

(See Chapter 5.)

It is assumed that the pump amplitude is large compared with the signal and idler amplitudes and that it remains constant; that is, the amplitude of the pump is so large that the pump energy that is given to the beam is negligible. Stated differently, the pump field affects the electron motion, but the current induced in the pump circuit by the beam is neglected. The beam can be described by the equation of motion in the pump field. The pump field is then a driving term in the equations.

The coupled mode form of the equations is given in Appendix L. The left-hand polarized component of the pump field couples the fast cyclotron modes and the left-hand polarized synchronous modes at the signal and idler frequencies.

The mode amplitude notation previously used must be slightly modified. The fast cyclotron mode amplitudes at the signal and idler frequencies are defined by

$$\begin{aligned} A_{1+} &= k_1(u_{1x} + ju_{1y}) & (a) \\ A_{2+}^* &= k_2(u_{2x}^* - ju_{2y}^*) & (b) \end{aligned} \quad (8.19)$$

where

$$k_{1,2} = \frac{1}{4} \sqrt{m \frac{|I_0|}{|e|} \frac{\omega_{1,2}}{\omega_c}} \quad (8.20)$$

whereas the left-hand polarized synchronous mode amplitudes at  $\omega_1$  and

$\omega_2$  are

$$\begin{aligned} S_{1+} &= A_{1+} - j\omega_c r_{1+} & (c) \\ S_{2+}^* &= A_{2+}^* + j\omega_c r_{2+}^* & (d) \end{aligned} \quad (8.19)$$

where

$$\begin{aligned} r_{1+} &= k_1(\xi_{1x} + j\xi_{1y}) \\ r_{2+}^* &= k_2(\xi_{2x}^* - j\xi_{2y}^*) \end{aligned} \quad (8.21)$$

The coupled mode form of the equations (see Appendix L) is

$$\begin{aligned} \left( \frac{d}{dz} + j(\beta_1 - \beta_c) \right) A_{1+} &= -c_{12} e^{-j\beta z} (A_{2+}^* - S_{2+}^*) \\ \left( \frac{d}{dz} - j(\beta_2 - \beta_c) \right) A_{2+}^* &= -c_{21}^* e^{j\beta z} (A_{1+} - S_{1+}) \\ \left( \frac{d}{dz} + j\beta_1 \right) S_{1+} &= -c_{12} e^{-j\beta z} (A_{2+}^* - S_{2+}^*) \\ \left( \frac{d}{dz} - j\beta_2 \right) S_{2+}^* &= -c_{21}^* e^{j\beta z} (A_{1+} - S_{1+}) \end{aligned} \quad (8.22)$$

which is a typical set of parametrically coupled equations. The coupling coefficients are

$$c_{12} = \frac{V_p}{D^2 v_0 B_0} \sqrt{\frac{\omega_1}{\omega_2}} = \frac{\omega_1}{\omega_2} c_{21}^* \quad (8.23)$$

These equations can be reduced to equations with constant coefficients by the usual transformation of variables. Let

$$\begin{aligned} A_{1+}' &= A_{1+}(z) e^{-j(\beta_1 - \beta_c)z} \\ S_{1+}' &= S_{1+}(z) e^{-j(\beta_1 - \beta_c)z} \end{aligned} \quad (8.24)$$

and similar expressions for  $A_{2+}^*$  and  $S_{1+}^*$ . Equations 8.22 then reduce to

$$\begin{aligned} \frac{dA_{1+}'}{dz} &= -c_{12} (A_{2+}^{*\prime} - S_{2+}^{*\prime}) \\ \frac{dA_{2+}^{*\prime}}{dz} &= -c_{21}^* (A_{1+}' - S_{1+}') \\ \left( \frac{d}{dz} + j\beta_c \right) S_{1+}' &= -c_{12} (A_{2+}^{*\prime} - S_{2+}^{*\prime}) \\ \left( \frac{d}{dz} - j\beta_c \right) S_{2+}^{*\prime} &= -c_{21}^* (A_{1+}' - S_{1+}') \end{aligned} \quad (8.25)$$

Solutions of these equations of the form  $\exp(sz)$  exist where

$$s = \pm j\beta_c \sqrt{\frac{1}{2} \pm \frac{1}{2}\sqrt{1 + |\alpha|^2}} \quad (8.26)$$

and

$$\alpha = \frac{V_p}{V_0 D^2 \beta_c^2} \quad (8.27)$$

For  $|\alpha|^2 \ll 1$ , the approximate roots of Eq. 8.26 are

$$\begin{aligned} s_{1,2} &= \pm \frac{\beta_c}{2} |\alpha| \\ s_{3,4} &= \pm j\beta_c \left( 1 + \frac{|\alpha|^2}{8} \right) \end{aligned} \quad (8.28)$$

which shows that there is a growing and decaying normal mode resulting from the active coupling between the fast cyclotron modes and two non-growing solutions resulting from the passive coupling between the synchronous and cyclotron modes.

**Boundary conditions. Gain.** Boundary conditions must be matched at the input plane of the pump region. If noise is neglected, the synchronous mode amplitudes are initially zero and the fast cyclotron idler amplitude is zero. Under these circumstances, the gain in decibels for a pump region of length  $L$  is easily found to be

$$\text{gain (db)} = 20 \log_{10} \cosh \frac{1}{2} |\alpha| \beta_c L \quad (8.29a)$$

and when  $\frac{1}{2} |\alpha| \beta_c L \gg 1$

$$\text{gain} = (4.43 |\alpha| \beta_c L - 6) \text{ db} \quad (8.29b)$$

**Manley-Rowe relations.** The Manley-Rowe relations follow directly from the relations among the mutual coupling coefficients in the manner shown in previous work. They also follow directly from the equations by observing that

$$\frac{d}{dz} \left( \frac{|A_{1+}|^2 - |S_{1+}|^2}{\omega_1} - \frac{|A_{2+}|^2 - |S_{2+}|^2}{\omega_2} \right) = 0 \quad (8.30)$$

This can be verified by carrying out the indicated differentiation and utilizing Eqs. 8.25 and their complex conjugates.

The cyclotron idler wave in the linearized treatment carries negative kinetic power. As the power in the cyclotron signal wave increases at the expense of pump power, the power in the idler cyclotron wave also must increase.

It is evident from Eqs. 8.25 that the pump couples to the synchronous mode, but the coupling will be small. This is shown from the fact that the normal modes  $s_{3,4}$  (Eqs. 8.28) are just the synchronous modes slightly modified by the pump. However, noise in the synchronous modes will couple to the signal modes and thereby degrade the noise performance. Noise cannot be removed from the synchronous mode in the input coupler because it has negative power.

### 8.3. Description of Adler Tube.<sup>1-3</sup> Experimental Results

Figure 8.2 shows a schematic diagram of the cyclotron wave parametric amplifier. The beam goes through a coupler, which applies the signal to the beam and removes the noise. Rather than use a slow wave structure, Adler used a Cuccia coupler,<sup>8</sup> which is merely a parallel plate condenser. The beam enters the parametric quadrupolar pump region where the signal and idler are amplified. Finally, the amplified signal is removed from an output Cuccia coupler, which is identical with the input coupler.

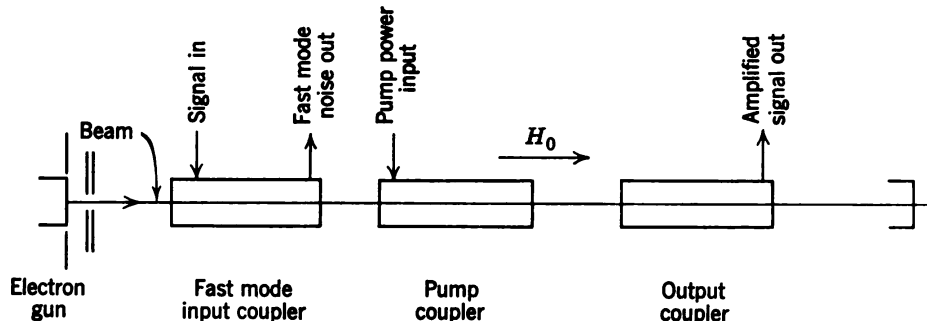


**Figure 8.2** Block diagram of fast mode parametric amplifier. (From Adler, Hrbek and Wade, Reference 2.)

The device is operated with the signal frequency near the cyclotron frequency. In this case the phase velocity of the fast cyclotron wave is very large. (See Chapter 2.)

Figure 8.3 shows schematically a tube used by Adler, Hrbek, and Wade.<sup>2,3,9</sup> With a few milliwatts of pump power, 20 db of gain was obtained at 560 mc (200 gauss) with 35  $\mu$ a beam current and 6 v beam voltage. The noise figure quoted for this tube was 1.3 db for double sideband reception of which 0.4 db was accounted for by input coupler losses. This was measured with a broadband noise source that excited both signal and idler. The input had to be accurately matched at both the signal and idler to achieve this noise figure.

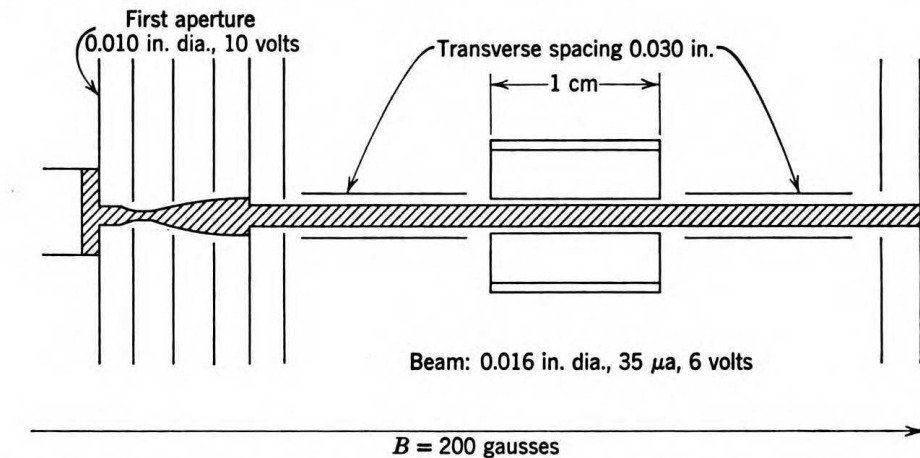


Figure 8.3 Diagram of experimental amplifier using Cuccia couplers. (From Adler, Hrbek and Wade, Reference 9.)

T. J. Bridges and A. Ashkin<sup>10</sup> have used r-f cavities for the signal and pump. Figure 8.4 shows the experimental tube. The signal cavity is similar, but two of the fins are omitted. In this tube the active lengths of the signal and pump cavities were 0.530 and 0.125 in., respectively. The magnetic field was approximately 1480 gauss, which corresponds to about 4140 mc. The beam current was about 70  $\mu$ A, the beam diameter was 0.026 in., and the beam voltage was 17.5 v. With a pump power of about 107 milliwatts, a gain of 20 db was achieved. The noise figure was 2.5 db for double sideband reception where the noise source excited both signal and idler.

The dynamic range of cyclotron wave parametric amplifiers is charac-

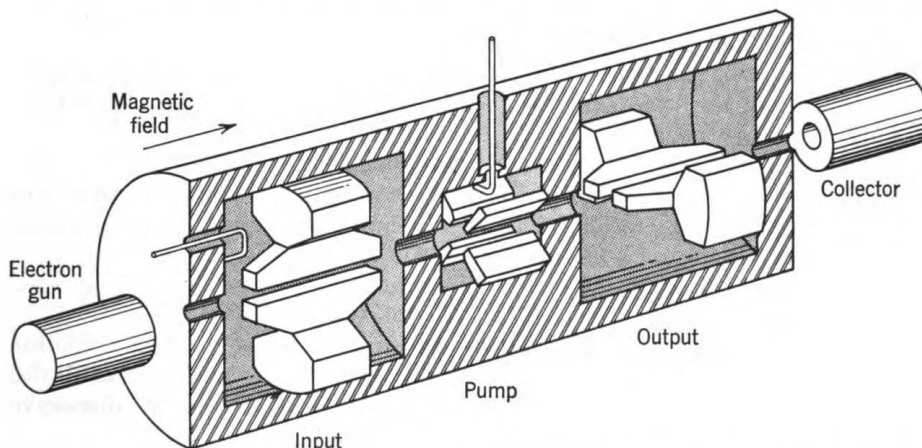


Figure 8.4 Diagram of cyclotron amplifier using cavities. (From Bridges and Ashkin, Reference 10.)

teristically very large. Bridges and Ashkin found, for example, that the gain of their amplifier was essentially independent of the input level over a range of 80 db. This is possible because saturation can occur only when the signal is so large that the orbiting electrons actually strike the pump circuit.

#### 8.4 Crossed Field Version

J. W. Klüver<sup>11</sup> has proposed a modification of the Adler tube in which a crossed electric and magnetic d-c field provide the focusing as the electrons move perpendicular to both of these fields. The advantage of this proposal is that the magnetic field gap is short compared with the Adler tube, in which, figuratively speaking, the field gap extends over the whole length of the beam.

The analysis of this device is very similar to that of the Adler case treated above and is not given here.

#### BIBLIOGRAPHY

1. R. Adler, "Parametric Amplification of the Fast Electron Wave," *Proc. IRE*, **46**, 1300-1301 (June 1958).
2. R. Adler, G. Hrbek, and G. Wade, "A Low-Noise Electron-Beam Parametric Amplifier," *Proc. IRE*, **46**, 1756-1757 (October 1958).
3. R. Adler, G. Hrbek, and G. Wade, "A Fast-Wave Transverse-Field Parametric Amplifier," presented at the IRE Annual Conference on Electron Tube Research, Quebec, Canada (1958).
4. J. W. Klüver, "Transverse-Field Interaction at Low Space-Charge Densities," *Bell Labs. Internal Memorandum* 59-124-24 (July 9, 1959).
5. A. E. Siegman, "The Waves on a Filamentary Electron Beam in a Transverse-Field Slow-Wave Circuit," *J. Appl. Phys.*, **31**, 17-26 (January 1960).
6. C. C. Johnson, "Theory of Fast-Wave Parametric Amplification," Technical Memorandum No. 540, Research Labs., Hughes Aircraft Company, Culver City, Calif. (February 1959). Appendix by R. W. Gould.
7. J. R. Pierce, *Traveling Wave Tubes*, D. Van Nostrand, New York, 1950.
8. C. L. Cuccia, "The Electron Coupler—A Developmental Tube for Amplitude Modulation and Power Control at Ultra-High Frequencies, Part I: Physical Theory," *R C A Rev.*, **10**, 270-303 (June 1949).
9. R. Adler, G. Hrbek, and G. Wade, "The Quadrupole Amplifier, a Low Noise Parametric Device," *Proc. IRE*, **47**, 1713-1723 (October 1959).
10. T. J. Bridges and A. Ashkin, "Parametric Amplification of the Fast Cyclotron Wave," presented at the Annual Conference on Electron Tube Research, Mexico City, Mexico, June 24-26, 1959. T. J. Bridges and A. Ashkin, "A Microwave Adler Tube," *Proc. IRE*, **48**, 361-363 (March 1960).
11. J. W. Klüver, "An M-Type Cyclotron Wave Parametric Amplifier," presented at the Annual Conference on Electron Tube Research, Mexico City, Mexico, June 24-26, 1959.

## Chapter 9

# Ferrite parametric amplifiers

The use of ferrites for parametric amplification was suggested by H. Suhl<sup>1</sup> in 1957. The term "ferrite" encompasses a rather large class of magnetic materials, which are insulators, in contrast to ordinary ferromagnetic materials, which are conductors. Since ferrites are insulators with relatively low ohmic and magnetic losses, electromagnetic waves can propagate through these materials. The relative dielectric constant is of order 10 for this class of compounds, and their saturation magnetization is of order 1000 oersteds.

A ferrite is a continuous magnetic medium that can be described by a magnetization vector,  $\mathbf{M}(\mathbf{r}, t)$ , which is the magnetic moment per unit volume of the specimen.  $\mathbf{r}$  is the position vector in the sample, and  $t$  is the time. Under the action of a magnetic field at  $\mathbf{r}$ , the magnetization will experience a torque. A time-varying field produces a time-varying torque, and the magnetization will vary. The equations governing the motion of  $\mathbf{M}$  are nonlinear, but under small signal conditions the solutions of the equations can be expressed in terms of normal modes, as should be expected. For wavelengths between the limits of approximately  $3 \times 10^{-8}$  cm (the shortest possible, since this is the lattice spacing in the crystal) and about  $3 \times 10^{-5}$  to  $3 \times 10^{-6}$  cm, it turns out that the normal modes are plane waves that propagate through the sample. These waves are called spin waves.<sup>2,3</sup> As the wavelength of the disturbance in the ferrite becomes comparable to or greater than the sample size, the modes are no longer suitably represented by plane waves. Under this condition, propagation can be neglected, and the problem of finding the normal modes becomes a magnetostatic one. Boundary conditions (shape of sample) become important, and the normal modes are then called magnetostatic modes.<sup>4</sup> Although the theory for these modes is too complicated to give in detail here, some further discussion of the modes is given later.

One feature of ferrites that makes their use possible for parametric amplification is the nonlinear nature of the magnetization equations of motion. Frequency mixing can occur, and the equations can be reduced to a set of coupled equations with time-varying coefficients of the type encountered in preceding chapters. The modes that are coupled for amplification may be the magnetostatic or cavity modes whose fields penetrate the sample. The spin waves could, in principle, be used, but in practice their wavelengths are so short that no method of coupling to any particular one of them exists. The longer wavelengths of the magnetostatic modes make coupling to individual modes possible.

The present chapter contains a discussion of the equations of motion for the magnetization, together with the derivation of one of the magnetostatic modes that will be used. A discussion of the parametric coupling, together with a brief account of three modes of operation of the amplifier suggested by Suhl,<sup>5-8</sup> is presented. The theory of one of these modes of operation is included in addition to a brief discussion of some of the experimental results. A traveling wave ferrite parametric amplifier<sup>9</sup> and a ferrite frequency converter<sup>10</sup> are described.

### 9.1 The Magnetization Equations of Motion<sup>11-15</sup>

To describe the behavior of a ferrite, Maxwell's equations are needed, in general, with the current and charge densities omitted. These equations involve the four field vectors,  $\mathbf{E}$ ,  $\mathbf{D}$ ,  $\mathbf{B}$ , and  $\mathbf{H}$ . For ferrites,  $\mathbf{D} = \epsilon\mathbf{E}$ , where  $\epsilon$  is a scalar quantity of order 10. However,  $\mathbf{B}$  and  $\mathbf{H}$  are related in a more complicated manner. In cgs units  $\mathbf{B} = \mathbf{H} + 4\pi\mathbf{M}$ , where  $\mathbf{M}$  is the magnetization. In nonmagnetic materials  $\mathbf{M}$  is proportional to  $\mathbf{H}$ , that is,  $\mathbf{M} = \chi\mathbf{H}$ , where  $\chi$  is a scalar, so that  $\mathbf{B} = (1 + 4\pi\chi)\mathbf{H} \equiv \mu\mathbf{H}$  and  $\mu$  is a scalar permeability. In ferrites the relation between  $\mathbf{M}$  and  $\mathbf{H}$  must be determined by the equations of motion of  $\mathbf{M}$ . It is found that  $\mathbf{M}$  and  $\mathbf{H}$  are related by a tensor so that the permeability is a tensor. (A derivation of this relation can be found in Reference 13.) This means, physically, that if a magnetic field is applied to the ferrite the magnetization will not be parallel to the magnetic field in general, as it will be in a nonmagnetic material. The tensor permeability gives rise to many unusual and interesting features, such as nonreciprocity in wave propagation through the ferrite, which is the property of interest for ferrite circulators. This feature is not necessary for parametric applications; therefore, the permeability relations<sup>12</sup> are omitted here. However, the nonlinear character of the equations of motion is important to the present discussion.

**Equations of motion.** In the range of frequencies, wavelengths, and temperatures of interest and in the absence of loss the equations of motion for the magnetization vector may be taken as

$$\frac{d\mathbf{M}}{dt} = \gamma(\mathbf{M} \times \nabla_{\mathbf{M}}\mathcal{E}) \quad (9.1)$$

where  $\gamma = -|e|/mc = -2.8$  mc/sec/oersted is the electron gyromagnetic ratio.  $\mathcal{E}$  is the magnetic energy of all kinds per unit volume of the specimen that depend on  $\mathbf{M}$ . This will be discussed in more detail presently. The gradient operator means differentiation with respect to  $M_x$ ,  $M_y$ , and  $M_z$ , the components of the magnetization. To make this equation plausible, the magnetization is proportional to the angular momentum, so that the left side is proportional to a torque.  $\nabla_{\mathbf{M}}\mathcal{E}$  is shown here to be an effective magnetic field, so that  $\mathbf{M} \times \mathbf{H}$  is the torque exerted on  $\mathbf{M}$  by the field  $\mathbf{H}$ . (A derivation is given in Reference 13.) Therefore, the magnetic field exerts a torque on  $\mathbf{M}$ , just as a bar magnet in a magnetic field experiences a torque. The torque causes  $\mathbf{M}$  to precess about the instantaneous direction of the magnetic field. The frequency of this precession is partly determined by  $\gamma$ , the value of which must be determined from the microscopic physics of the origin of the magnetization.

A consequence of these equations of motion is that the magnitude of the magnetization vector is constant. This follows easily by taking the scalar product of  $\mathbf{M}$  with both sides of the equation. Since  $\mathbf{M} \cdot (\mathbf{M} \times \mathbf{A}) \equiv 0$  for any vector  $\mathbf{A}$ , it follows that  $\mathbf{M} \cdot \frac{d\mathbf{M}}{dt} \equiv \frac{d}{dt} |\mathbf{M}|^2 = 0$ , and  $|\mathbf{M}| =$  constant.

Consider next the magnetic energy density  $\mathcal{E}$ , which depends on the magnetization  $\mathbf{M}$ . There are three sources of this energy. First, if the ferrite is placed in an external magnetic field,  $\mathbf{H}_a$ , it is well known<sup>16</sup> that the specimen will have a magnetic energy density given by  $\mathbf{M} \cdot \mathbf{H}_a$ . Since  $\nabla_{\mathbf{M}}(\mathbf{M} \cdot \mathbf{H}_a) \equiv \mathbf{H}_a$ , it is seen in this case that the foregoing statement that  $\nabla_{\mathbf{M}}\mathcal{E}$  is a magnetic field is justified.

The second type of magnetic energy density is the dipole-dipole energy. This arises because the magnetization, or magnetic moment per unit volume, has an associated magnetic field. Therefore, the magnetization at position  $\mathbf{r}$  in the specimen "sees" the magnetic field from the magnetization at  $\mathbf{r}'$ , another point in the sample, and there will be energy associated with this interaction of the form  $\mathbf{M}(\mathbf{r}) \cdot \mathbf{H}(\mathbf{r}')$ . This energy can be written as

$$\iint (\mathbf{M}(\mathbf{r}) \cdot \nabla_{\mathbf{r}})(\mathbf{M}(\mathbf{r}') \cdot \nabla_{\mathbf{r}'}) \frac{1}{|\mathbf{r} - \mathbf{r}'|} d\mathbf{r} d\mathbf{r}' \quad (9.2)$$

where the integration is over the entire specimen.<sup>16</sup> The d-c part of this integral yields the familiar demagnetizing fields<sup>17</sup> due to the magnetic poles on the surface of the sample. The a-c part of this integral can be called r-f demagnetizing energy, which on differentiating with respect to  $\mathbf{M}$  gives the r-f demagnetizing field.<sup>4</sup> For spherical samples the demagnetizing factors are antiparallel to  $\mathbf{M}$ .

The third source of magnetic energy is the exchange energy. It is due to the interplay of electrostatic forces and the exclusion principle of quantum mechanics, and no attempt will be made to justify its existence. It is equivalent to an extra energy between dipoles that are nearest neighbors in the crystal lattice over and above the dipole energy given in Eq. 9.2. This energy is proportional to the cosine of the angle between the dipoles of nearest neighbors in the lattice. If the constant of proportionality is negative, the exchange force arising from the exchange energy will tend to line up neighboring dipoles, and it is this force that causes a ferromagnetic material to remain in a state of permanent magnetization in the absence of an applied field. As the specimen is heated, the forces caused by thermal agitation increase, and when they exceed the exchange forces the specimen becomes demagnetized. The temperature at which this transition occurs is called the Curie temperature. In paramagnetic specimens the dipoles are so far apart that the exchange forces are too weak to cause this spontaneous self-alignment of dipoles. It can be shown in ferromagnetic materials with a continuous distribution of magnetization that the part of the exchange force that gives a torque is proportional to  $\nabla^2\mathbf{M}$ .

The total field given by  $\nabla_{\mathbf{M}}\mathcal{E}$  can now be written as

$$\mathbf{H}_{\text{total}}(\mathbf{r}, t) = \mathbf{H}_a(\mathbf{r}, t) + \mathbf{H}_d(\mathbf{r}, t) + \mathbf{H}_{\text{ex}}(\mathbf{r}, t) \quad (9.3)$$

where  $\mathbf{H}_a$  is the applied field,  $\mathbf{H}_d$  is the demagnetizing field, and  $\mathbf{H}_{\text{ex}}$  is the exchange field.

The relative orders of magnitudes of these fields are important. It is found that the relative magnitudes of  $\mathbf{H}_a$ ,  $\mathbf{H}_d$ , and  $\mathbf{H}_{\text{ex}}$  are as

$$H_a : 4\pi M_0 \cdot 10^6 (2\pi a/\lambda_0)^2$$

where  $a$  ( $\cong 3 \times 10^{-8}$  cm) is the lattice spacing in the crystal and  $\lambda_0$  is the wavelength of a disturbance in the sample. When  $\lambda_0$  is  $10^{-5}$  to  $10^{-6}$  cm, the exchange field is comparable to  $H_a$  and  $H_d$ . Since  $\lambda = a$  is the shortest possible wavelength, then for any wavelengths between  $3 \times 10^{-8}$  and  $3 \times 10^{-5}$  cm the exchange field is larger than  $H_a$  and  $H_d$  and they may be neglected. The solutions of the equations of motion for short wavelengths may then be taken as plane waves, which are called spin waves. The frequencies of the spin waves are determined mainly

by the exchange field but also to a lesser extent by the demagnetizing field. The demagnetizing field causes an anisotropy, so that the dispersion relation that characterizes the spin waves will be slightly different, depending on the direction of propagation through the sample relative to the applied magnetic field. Therefore, for a given wavelength disturbance, there is a finite band of frequencies that can propagate, depending on direction. As has already been mentioned, the wavelengths of these waves are so short that it is impossible to excite only one of the waves. It might be noted that the thermal energy of the sample is in the form of short wavelength spin waves.

For wavelengths comparable to the sample size, it is clear now that the exchange field can be neglected. Furthermore, propagation can be neglected so that Maxwell's equations reduce to  $\nabla \cdot \mathbf{B} = 0$  and  $\nabla \times \mathbf{H} = 0$ . Also  $\mathbf{B} = \mathbf{H} + 4\pi\mathbf{M}$  and

$$\frac{d\mathbf{M}}{dt} = \gamma\mathbf{M} \times (\mathbf{H}_a + \mathbf{H}_d) \quad (9.4)$$

Solutions of these equations together with the boundary conditions that the normal component of  $\mathbf{B}$  and the tangential component of  $\mathbf{H}$  are continuous at the sample boundary yield the magnetostatic modes.<sup>4</sup>

**The uniform precession mode.** The simplest magnetostatic mode is the uniform precession mode in a spherical sample of ferrite. This mode is used for convenience in the discussion of the parametric amplifier.

Assume that a d-c and a small a-c magnetic field are applied to a small ferrite sphere. The sphere is small enough so that field variations across the sample can be neglected. In the absence of the r-f field, it is assumed that the sample is magnetized to saturation. Let  $\mathbf{M}_0$  be the saturation magnetization and  $\mathbf{H}_0$  the applied d-c field. Both vectors are taken to lie along the positive  $z$ -axis. When the r-f field is applied at frequency  $\omega$ ,

$$\mathbf{H}_a = \mathbf{H}_0 + \mathbf{H}_1 e^{j\omega t} \quad (9.5a)$$

and this time-varying field will generate a time-varying magnetization which can be written as

$$\mathbf{M} = \mathbf{M}_0 + \mathbf{M}_1 e^{j\omega t} \quad (9.5b)$$

where the a-c amplitudes are small compared with the d-c amplitudes. Substitute these values of  $\mathbf{H}_a$  and  $\mathbf{M}$  into Eq. 9.4 ( $\mathbf{M} \times \mathbf{H}_d = 0$ , in this case), neglect products of a-c quantities, and it follows that

$$j\omega\mathbf{M}_1 \cong \gamma(\mathbf{M}_0 \times \mathbf{H}_1 + \mathbf{M}_1 \times \mathbf{H}_0) \quad (9.6)$$

Since  $\mathbf{M}_0$  and  $\mathbf{H}_0$  are parallel to the  $z$ -axis, there will be no  $z$ -component of  $\mathbf{M}_0 \times \mathbf{H}_1$  or  $\mathbf{M}_1 \times \mathbf{H}_0$ . Accordingly, it follows that

$$M_{1z} \cong 0 \quad (9.7)$$

That is, if the d-c saturation magnetization and the applied d-c fields are parallel, an applied r-f magnetic field will never induce a component of r-f magnetization parallel to this direction in a linearized theory.

Solve Eqs. 9.6 for  $M_{1x}$  and  $M_{1y}$ . It follows that the uniform precession mode is given by

$$M_+ = -\frac{\omega_M H_+}{4\pi(\omega - \omega_0)} \quad (a)$$

$$M_- = \frac{\omega_M H_-}{4\pi(\omega + \omega_0)} \quad (b) \quad (9.8)$$

where

$$M_{\pm} = \frac{1}{2}(M_{1x} \pm jM_{1y}) \quad (9.9)$$

and

$$\begin{aligned} H_{\pm} &= \frac{1}{2}(H_{1x} \pm jH_{1y}) \\ \omega_0 &= -\gamma H_0 = |\gamma| H_0 \\ \omega_M &= -4\pi\gamma M_0 = 4\pi|\gamma|M_0 \end{aligned} \quad (9.10)$$

where  $\omega_0$  is the gyromagnetic resonance frequency, which is described below, and  $\omega_M$  is a characteristic frequency of the material determined by  $M_0$ , the saturation magnetization.

The solutions found in Eqs. 9.8 demonstrate the gyromagnetic resonance phenomenon, for if the applied frequency is held fixed ( $\omega$ ) and the d-c magnetic field is varied ( $\omega_0$ ), when  $\omega_0 = \omega$ , it is seen from Eq. 9.8a that the magnetization becomes infinite. The magnetization would not be infinite in an actual sample, since loss terms which have not been taken into account so far will be present. This is analogous to the impedance of an  $LC$  circuit which is infinite at resonance if there is no loss but finite when loss is taken into account. It should also be mentioned that  $\omega_0$  can be held fixed while  $\omega$  is varied, and the resonance phenomenon will also be observed.

Physically, the resonance occurs for the following reason. The magnetization is precessing uniformly about the d-c field at a frequency given by  $\omega_0 = |\gamma| H_0$ . When the applied field is at the same frequency, energy is very easily coupled to the magnetization which will grow. The magnetization vector precesses with a larger angle between  $\mathbf{M}$  and  $\mathbf{H}_0$  when the precession is in resonance with the applied field. Again this is analogous to an  $LC$  circuit that is oscillating at a natural resonance frequency,

$\omega_0$ . When a driving field is applied at  $\omega_0$ , the amplitude of oscillation will grow exponentially until losses limit the growth.

Another aspect of Eqs. 9.8 should be noted. A right-hand polarized field induces a right-hand polarized magnetization, whereas a left-hand polarized field induces a left-hand polarized magnetization. However, the natural sense of precession is in the  $M_+$  direction about the d-c field, and the attempt to drive  $M$  in the opposite sense is less effective. Therefore, there is no resonance phenomenon if only an  $H_-$  polarized wave is applied to the sample when the d-c field is in the direction specified.

This mode is called the uniform mode, since the magnetization does not vary over the sample. Other modes are characterized by a magnetization that varies over the sample. Figure 9.1 shows the configuration of the transverse magnetization for another mode.<sup>18</sup>

One final remark. The precessing magnetization will generate a magnetic field in accordance with Eqs. 9.8.

## 9.2 Parametric Coupling Mechanism

In order to obtain parametric amplification, it is sufficient that two modes at frequencies  $\omega_1$  and  $\omega_2$  be actively coupled by a time-varying pump at frequency  $\omega = \omega_1 + \omega_2$ , as previously shown. In order to visualize the so-called electromagnetic mode of operation of a ferrite amplifier,<sup>10, 19</sup> consider a small spherical sample of ferrite in an r-f cavity. A d-c magnetic field,  $\mathbf{H}_0$ , is along the  $z$ -axis, and the ferrite is magnetized to saturation,  $\mathbf{M}_0$ , along the  $z$ -axis. The pump mode is taken as the uniform precession magnetostatic mode at the resonance frequency  $\omega = |\gamma|H_0$ . The signal and idler modes are taken as two electromagnetic modes of the cavity. The solution of the equation of motion

$$\frac{d\mathbf{M}}{dt} = -|\gamma|\mathbf{M} \times \mathbf{H} \quad (9.11)$$

can then be expanded in the form  $\mathbf{M} = \mathbf{M}_0 + \mathbf{M} + \mathbf{M}_1 + \mathbf{M}_2$ , where the subscripts refer to direct current, pump, and  $\omega_1$  and  $\omega_2$ , respectively, whereas the magnetic field can be expanded as  $\mathbf{H} = \mathbf{H}_0 + \mathbf{H} + \mathbf{H}_1 + \mathbf{H}_2$ . As usual, the pump mode amplitude is small compared with the direct current amplitude but large compared with the signal and idler terms, so that when these expansions are substituted into Eq. 9.11 products of signal and idler amplitudes are neglected.

Figure 9.2a shows the precession of the magnetization at the frequency  $\omega$ , the resonance frequency. As shown earlier, only the  $H_+(\omega)$  component of the pump field interacts strongly with the magnetization (Eqs. 9.8).

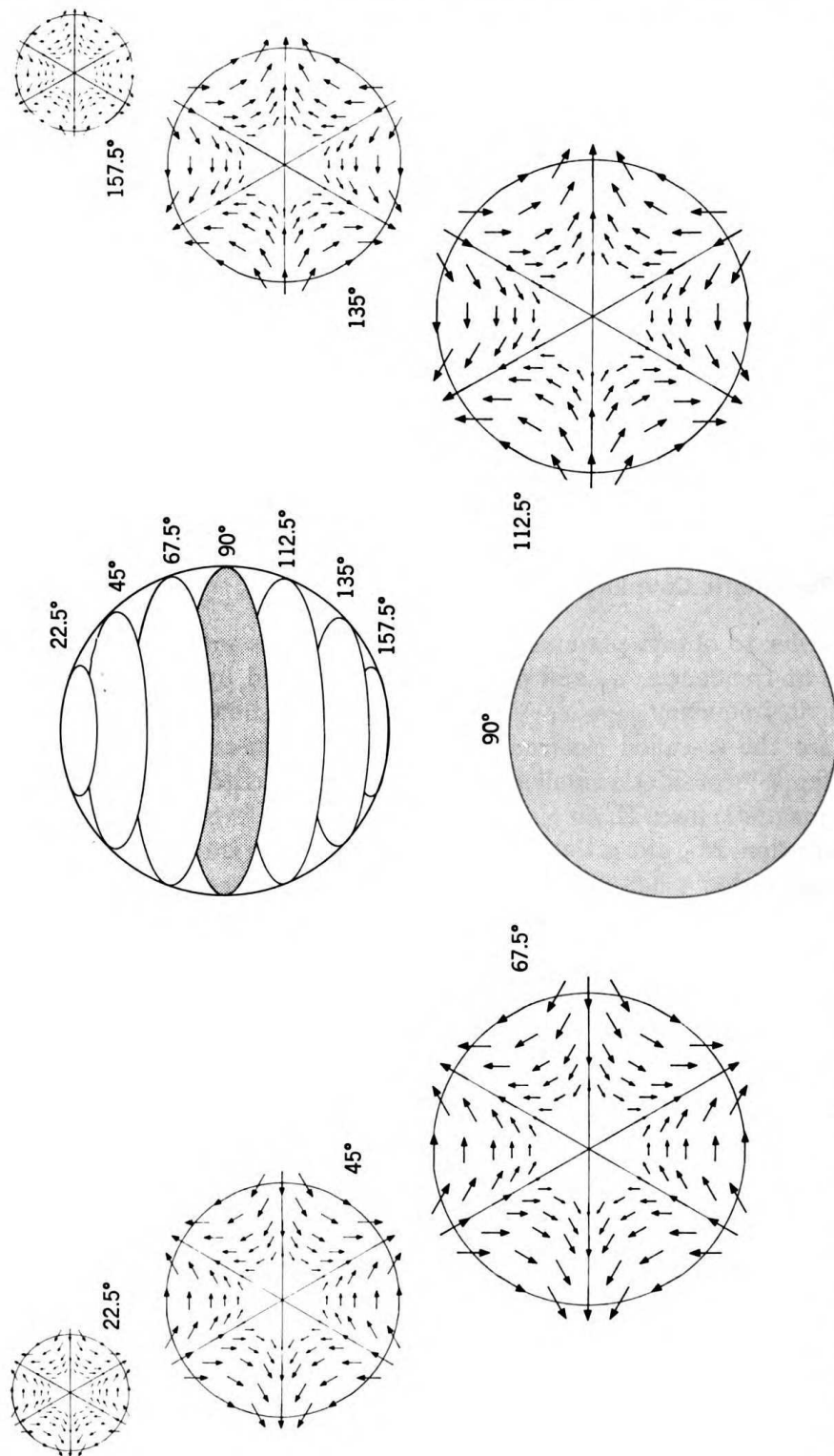


**Figure 9.1** The configuration of transverse magnetization seen in a rotating system for the  $(4, 3, 0)$  magnetostatic mode in a sphere. All the vectors precess together in this system. (From Walker, Reference 18.)

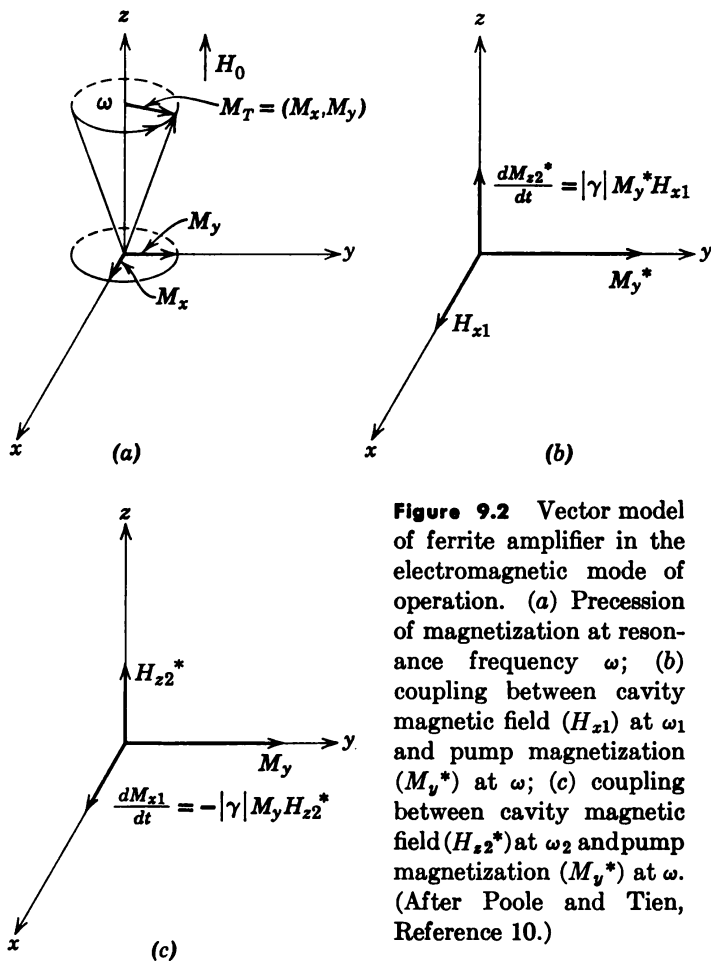


**Figure 9.2** Vector model of ferrite amplifier in the electromagnetic mode of operation. (a) Precession of magnetization at resonance frequency  $\omega$ ; (b) coupling between cavity magnetic field ( $H_{x1}$ ) at  $\omega_1$  and pump magnetization ( $M_y^*$ ) at  $\omega$ ; (c) coupling between cavity magnetic field ( $H_{z2}^*$ ) at  $\omega_2$  and pump magnetization ( $M_y^*$ ) at  $\omega$ . (After Poole and Tien, Reference 10.)

Consider Figure 9.2b. The cavity mode at the signal frequency has a component of magnetic field along the  $x$ -axis in the sample ( $H_{x1}$ ). This will mix with the  $y$ -component of the pump magnetization to generate a  $z$ -component of magnetization at the idler frequency ( $-\omega_2$ ); i.e., from Eq. 9.11 it follows that

$$\frac{dM_{z2}^*}{dt} = |\gamma| M_y^* H_{x1} \quad (9.12)$$

since  $\omega = \omega_1 + \omega_2$ . The component  $H_{y1}$  is parallel to  $M_y^*$  and gives no contribution. Therefore, the pump magnetization couples to the signal magnetic field to produce a change in the magnetization at the idler frequency along the  $z$ -axis. It has been noted that a changing magnetization will generate an electromagnetic field. The magnetic field at the sample in this case will be in the  $z$ -direction,  $H_{z2}^*$ . (See Figure 9.2c.)

$H_{z_1}$ \* again couples to  $M_y$  to give a change in  $M_{z_1}$  along the  $x$ -axis. The associated magnetic field  $H_{x_1}$  turns out to add in-phase with the original field, so that the amplitude of the original field will grow provided the pump amplitude is large enough to overcome the losses in the ferrite.

### 9.3 Three Modes of Operation

The analog to the three-frequency lumped circuit parametric amplifier treated in Chapter 4 should now be evident. The signal and idler circuits correspond to two cavity modes, and the pump mode is the analog of a time-varying inductance that couples the two circuits. This mode of operation has been called electromagnetic by Suhl. It is the simplest mode to treat theoretically and is considered in detail in Section 9.4.

It is also possible to use three different magnetostatic modes for the pump, signal, and idler. The pump mode can be the uniform precession mode, and the signal and idlers are two other modes whose frequencies add up to  $\omega$ . This is called the magnetostatic mode of operation by Suhl.

A third mode is the semistatic mode of operation. In this case two modes are magnetostatic, whereas the third is a cavity mode.

Walker<sup>4</sup> has shown that for samples that are ellipsoids of revolution the magnetostatic mode spectrum is limited to the frequency range  $|\gamma|(H_0 - N_z M_0) \leq \omega \leq |\gamma|(H_0 + 2\pi M_0)$ , where  $N_z$  is a factor that can vary between 0 and  $4\pi$ , depending on the shape of the sample. It is the demagnetizing factor arising from the magnetic dipole forces, as noted earlier. Figure 9.3 shows a typical arrangement of  $\omega$ ,  $\omega_1$ , and  $\omega_2$  for the three modes of operation discussed.

The device acts like the regenerative amplifier treated in Chapter 4. In all cases  $\omega = \omega_1 + \omega_2$ . If this condition is not met, there will be a gain threshold, even if loss is neglected, just like the threshold found in Chapter 5 when  $\beta = \beta_1 + \beta_2 + \Delta\beta$  for the lossless transmission line. The pump must alter the frequencies until the condition  $\omega = \omega_1 + \omega_2$  is satisfied before there will be gain. Furthermore, a signal must be coupled into the amplifier and an output load must be provided to one of the modes. The pump power is then raised to a value at which the *unloaded* circuit would be unstable but the loaded circuit is stable. Under these conditions, the gain will be large.

The magnetostatic mode of operation is not very efficient. There are many magnetostatic modes whose frequencies  $\omega_1'$  and  $\omega_2'$  lie close to  $\omega_1$  and  $\omega_2$  which add up very nearly to  $\omega$ . Their instability threshold will be slightly higher than the wanted pair of modes. However, the loading on the wanted pair may raise their instability threshold above that of

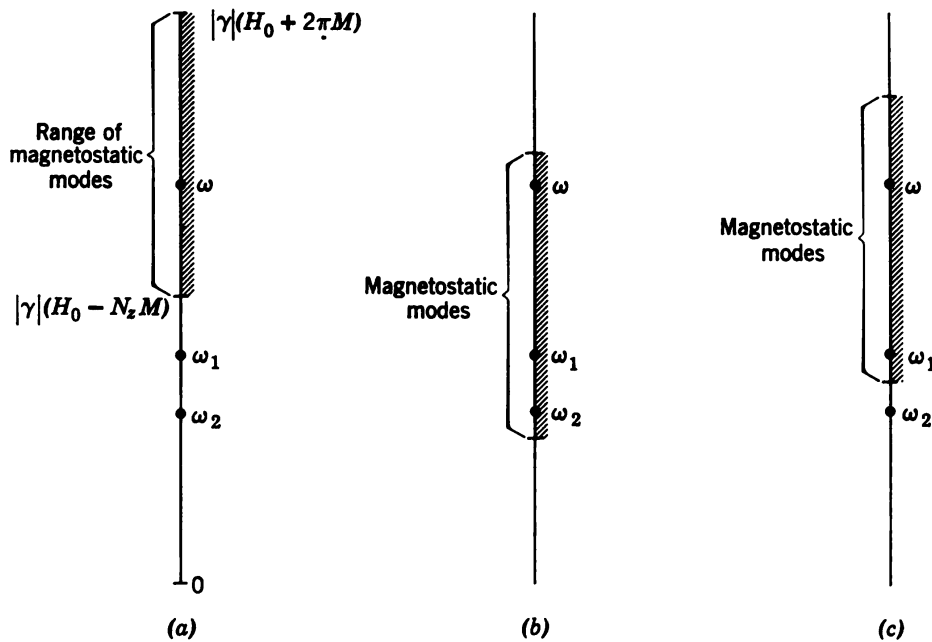


**Figure 9.3** Relation of pump, signal, and idler frequencies to magnetostatic mode spectrum for (a) electromagnetic, (b) magnetostatic and (c) semistatic modes of operation. The frequencies satisfy  $\omega = \omega_1 + \omega_2$ . In all cases the pump mode is the uniform precession mode.

neighboring unwanted pairs. As a result, the pump power will be fed into unwanted modes so that the efficiency is very low. This is similar to the problem of higher idler frequencies in the space-charge wave parametric amplifier.

In actual practice none of these modes of operation has proved very efficient. Other modes of operation have been proposed by Poole and Tien<sup>20</sup> and Berk, Kleinman, and Nelson,<sup>21</sup> who proposed a modified semistatic mode of operation in which the idler mode is the uniform precession mode and the pump and signal are cavity modes.

#### 9.4 Theory of Electromagnetic Operation<sup>1</sup>

Consider a small spherical sample of ferrite in a cavity that is resonant to the two amplifying modes ( $\omega_1$  and  $\omega_2$ ) and also resonant to the pump frequency. The latter requirement assures that the pump power will couple efficiently to the uniform precession mode of the ferrite. The sample is located in a region in which all three field configurations (pump, signal, and idler) are uniform. In this case the magnetization  $\mathbf{M}$  remains uniform throughout the sample and simplifies the calculation.

The first task is to determine the motion of the magnetization induced by the cavity fields. That is, the effect of the cavity coupling to the sample is considered. Next, the effect of the coupling of the sample on the cavity must be determined. This is the standard type of weak coupling that has been seen in the previous work.

The method of analysis used is somewhat simpler than that used by Suhl<sup>1</sup> and Poole and Tien<sup>10</sup> and is due to the latter two authors.<sup>20</sup> The theory could, of course, be developed by using the coupled mode approach.

**Landau-Lifshitz Equation.**<sup>11</sup> The equation of motion (9.11) for the magnetization has neglected loss in the ferrite. Landau and Lifshitz have added a phenomenological loss term

$$\frac{d\mathbf{M}}{dt} = -|\gamma|(\mathbf{M} \times \mathbf{H}) + \frac{\alpha}{M_0} \left( \mathbf{M} \times \frac{d\mathbf{M}}{dt} \right) \quad (9.13)$$

where  $\alpha$  is a loss parameter that is small compared with unity for the samples used. A qualitative picture of the effect of the loss term may be

obtained by reference to Figure 9.4. The effect of the loss term is to cause the angle between  $\mathbf{M}$  and  $\mathbf{H}_0$  to decrease so that the precession will damp out. Bloch<sup>14</sup> has also taken loss into account by introducing phenomenological relaxation times into the equations. However, the Landau-Lifshitz form is used here.

The loss term will be taken into account only in determining the motion of the magnetization under the action of the pump field for simplicity. The pump frequency is taken to be the ferromagnetic resonance frequency of uniform precession, whereas the signal and idler frequencies lie outside the magnetostatic mode spectrum that is necessary in order to make the foregoing simplifying assumption.

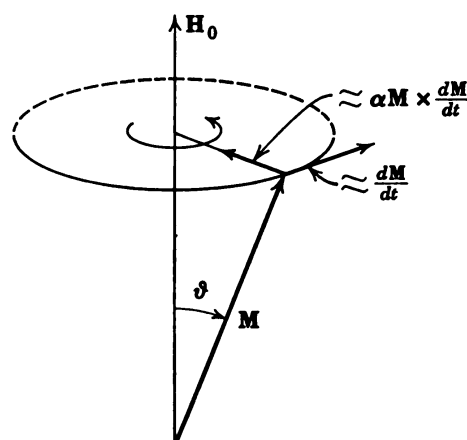


**Figure 9.4** Relation of  $\mathbf{M}$ ,  $d\mathbf{M}/dt$ , and  $\mathbf{M} \times (d\mathbf{M}/dt)$ . The loss term tends to decrease  $\vartheta$  and damp out the precession.

magnetic resonance frequency of uniform precession, whereas the signal and idler frequencies lie outside the magnetostatic mode spectrum that is necessary in order to make the foregoing simplifying assumption.

**The pump magnetization.** Consider now the steady-state motion of  $\mathbf{M}$  at the pump frequency  $\omega = \omega_0$ , the uniform mode resonance frequency, under the influence of an elliptically polarized magnetic field in the  $x$ - $y$ -plane. The d-c magnetic field  $\mathbf{H}_0$  is in the positive  $z$ -direction.

The applied pump field is given by

$$\begin{aligned} H_x(\omega_0) &= -\frac{h}{2j}(e^{j\omega_0 t} - e^{-j\omega_0 t}) \\ H_y(\omega_0) &= \frac{h\sigma}{2}(e^{j\omega_0 t} + e^{-j\omega_0 t}) \\ H_z &= H_0 \end{aligned} \quad (9.14)$$

where  $\sigma$  measures the ellipticity of the applied field. Further, the resonance frequency is given by

$$\omega_0 = |\gamma| H_0 \quad (9.15)$$

It is assumed that

$$h \ll H_0 \quad (9.16)$$

where  $h$  is the amplitude of the applied field.

Substitute the applied field (Eqs. 9.14) into Eq. 9.13 and neglect products of a-c terms. This results in

$$\begin{aligned} \frac{dM_x}{dt} &\cong -\omega_0 M_y - \alpha \frac{dM_y}{dt} + \frac{\omega_M}{4\pi} H_y \\ \frac{dM_y}{dt} &\cong \omega_0 M_x + \alpha \frac{dM_x}{dt} - \frac{\omega_M}{4\pi} H_x \\ \frac{dM_z}{dt} &\cong 0 \end{aligned} \quad (9.17)$$

where  $\omega_M = 4\pi|\gamma|M_0$ ,  $M_0$  is the saturation magnetization, and  $M_0 \cong M_z$  as far as the direct current is concerned. Now if  $\alpha \ll 1$ , an approximate steady-state solution of Eqs. 9.17 becomes

$$\begin{aligned} M_x(\omega_0) &\cong \frac{M_0 h}{2\Delta H} (1 + \sigma)(e^{j\omega_0 t} + e^{-j\omega_0 t}) \\ M_y(\omega_0) &\cong \frac{M_0 h}{2j \Delta H} (1 + \sigma)(e^{j\omega_0 t} - e^{-j\omega_0 t}) \\ M_z(\omega_0) &\cong 0 \end{aligned} \quad (9.18)$$

where

$$|\gamma| \Delta H = 2\omega_0 \alpha \quad (9.19)$$

$\Delta H$  is effectively the width of the resonance line due to the losses in the

ferrite and is defined in terms of  $\alpha$  above. It can be related to the angle  $\vartheta$  of uniform precession seen in Figure 9.5. From Eq. 9.13 it follows that  $\mathbf{M} \cdot (d\mathbf{M}/dt) = 0$  or  $|\mathbf{M}|^2 = \text{constant}$ . If  $\mathbf{M}_t = (M_x, M_y)$ ,

$$\cos \vartheta = \frac{|M_z|}{|\mathbf{M}|} = \sqrt{1 - \frac{|M_t|^2}{|\mathbf{M}|^2}} \cong \sqrt{1 - \frac{|M_t|^2}{M_0^2}} \quad (9.20)$$

so that for small precession angles it follows that

$$\vartheta \cong \frac{|M_t|}{M_0} = \frac{h}{2\Delta H} (1 + \sigma) \equiv \frac{h}{4H_0\alpha} (1 + \sigma) \quad (9.21)$$

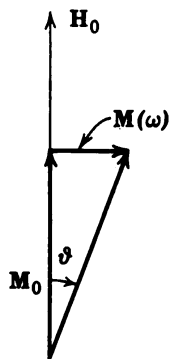


**Figure 9.5** Angle of uniform precession  $\vartheta$ .  $\mathbf{M}_0$  is the saturation magnetization.

The field  $h$  is, of course, a measure of the strength of the applied pump field. However, equally important is  $\Delta H$ , the line width. It should be obvious even at this stage that the gain will depend on  $\vartheta$  so that a sample with a narrow resonance line width will require less pump power to achieve a given gain. Damon and Eshbach <sup>22</sup> have given a discussion of pump power requirements for various modes of operation in terms of the sample line width.

The effect of the ferrite resonance on the cavity pump field has been neglected in the present approximation. Further, in line with other parametric approximations that have been used before, the effect of the signal and idler on the pump will be neglected, since the signal and idler quantities are assumed small compared with the pump terms.

**Parametric coupling.** The pump field is given by Eqs. 9.14 and the pump magnetization with loss by Eqs. 9.18. Now expand the magnetic field and magnetization as

$$\mathbf{H} = \mathbf{H}_0 + \mathbf{H}(\omega) + \mathbf{H}^*(\omega) + \mathbf{H}(\omega_1) + H^*(\omega_1) + \mathbf{H}(\omega_2) + H^*(\omega_2) \quad (9.22)$$

$$\mathbf{M} = \mathbf{M}_0 + \mathbf{M}(\omega) + \mathbf{M}^*(\omega) + \mathbf{M}(\omega_1) + \mathbf{M}^*(\omega_1) + \mathbf{M}(\omega_2) + M^*(\omega_2)$$

where, for example,  $\mathbf{H}(\omega_1) \sim e^{j\omega_1 t}$ ,  $\mathbf{M}^*(\omega_2) \sim e^{-j\omega_2 t}$ , etc. Assume, as usual, that  $\omega = \omega_0 = \omega_1 + \omega_2$  and that the signal and idler terms are small compared with the pump terms, which are in turn small compared with the d-c terms. The equations of motion then at the signal and idler

frequencies are ( $\alpha = 0$ )

$$\begin{aligned}\frac{dM_{x_1}}{dt} &= -\omega_0 M_{y_1} + \frac{\omega_M}{4\pi} H_{y_1} - |\gamma| M_y^* H_{z_2} \\ \frac{dM_{y_1}}{dt} &= \omega_0 M_{x_1} - \frac{\omega_M}{4\pi} H_{x_1} + |\gamma| M_x H_{z_2}^* \\ \frac{dM_{z_2}^*}{dt} &= -|\gamma| (M_x^* H_{y_1} - M_y^* H_{x_1})\end{aligned}\quad (9.23)$$

where in the equations of motion  $\mathbf{M}(\omega_0) \gg \mathbf{H}(\omega_0)$  at resonance,  $\mathbf{H}_2^*$  is of the same order as  $\mathbf{M}_2^*$ , and  $\mathbf{H}_1$  is of the same order as  $\mathbf{M}_1$ . The subscript 1 refers to  $\omega_1$  and 2 to  $\omega_2$ . Further, the pump quantities are found by comparing the expansion coefficients in Eqs. 9.22 with Eqs. 9.14 and 9.18.

From Eqs. 9.23 it is seen that  $M_{x_1}$  and  $M_{y_1}$  are coupled by the pump to  $M_{z_2}^*$  via  $H_{x_1}$  and  $H_{y_1}$  and  $H_{z_2}^*$ . Therefore, only these components of magnetic field and magnetization need be considered, since they are the only ones coupled. The magnetic fields are the fields of the cavity which are "seen" by the ferrite sample. Therefore, assume that the cavity fields at the ferrite and the magnetization are given by

$$\begin{aligned}H_{x_1} &= \frac{1}{2} h_{x_1}(\mathbf{r}) e^{j\omega_1 t} & M_{x_1} &= \frac{1}{2} m_{x_1}(t) e^{j\omega_1 t} \\ H_{y_1} &= \frac{1}{2} h_{y_1}(\mathbf{r}) e^{j\omega_1 t} & M_{y_1} &= \frac{1}{2} m_{y_1}(t) e^{j\omega_1 t} \\ H_{z_2}^* &= \frac{1}{2} h_{z_2}^*(\mathbf{r}) e^{-j\omega_2 t} & M_{z_2}^* &= \frac{1}{2} m_{z_2}^*(t) e^{-j\omega_2 t}\end{aligned}\quad (9.24)$$

To find the steady-state solutions of Eqs. 9.23, substitute Eqs. 9.24 into Eqs. 9.23 and then let  $d/dt = 0$ . This means that  $m_{x_1}$ ,  $m_{y_1}$ , and  $m_{z_2}^*$  are constant with time. It then follows that

$$m_{x_1} \cong \frac{1}{\Delta_1} \left( -\frac{j\omega_1 \omega_M}{4\pi} h_{y_1} - \frac{\omega_0 \omega_M}{4\pi} h_{x_1} + \frac{\omega_M}{4\pi} \vartheta h_{z_2}^*(\omega_1 + \omega_0) \right) \quad (a)$$

$$m_{y_1} \cong \frac{1}{\Delta_1} \left( \frac{j\omega_1 \omega_M}{4\pi} h_{x_1} - \frac{\omega_0 \omega_M}{4\pi} h_{y_1} - j \frac{\omega_M}{4\pi} \vartheta h_{z_2}^*(\omega_1 + \omega_0) \right) \quad (b)$$

$$m_{z_2}^* \cong \frac{1}{\Delta_1} \frac{\omega_M}{4\pi} \vartheta (h_{x_1} + j h_{y_1})(\omega_0 + \omega_1) \quad (c)$$

where  $\vartheta$  is given by Eq. 9.21 and

$$\Delta_1 = \omega_1^2 - \omega_0^2 \quad (9.26)$$

If the pump amplitude  $h$  goes to zero, Eqs. 9.25a and b are simply the

usual Polder tensor relations<sup>12,13</sup> between the magnetization and the applied r-f fields. The last term in Eq. 9.25a when  $h \neq 0$  is just the  $x$ -component of the magnetization arising from the frequency mixing. It is proportional to the  $y$ -component of the magnetization at the pump frequency and the  $z$ -component of the idler magnetic field. Similarly, the last term in Eq. 9.25b is the frequency mixing term for the  $y$ -directed signal magnetization.

Equations 9.25 represent the effect of the cavity fields on the magnetization. The effect of the ferrite on the cavity fields must next be considered.

The a-c magnetization at the signal and idler frequencies have been related to the r-f magnetic fields at these frequencies. The power generated in the cavity due to the motion of the magnetization is given by<sup>23,24</sup>

$$P = -\frac{1}{2} \operatorname{Re} \iiint_{\text{sample}} \frac{d\mathbf{M}}{dt} \cdot \mathbf{H}^* dv \quad (9.27)$$

where  $\operatorname{Re}$  means the real part of.  $P$  is positive if energy flows from the sample to the cavity. Therefore, the power generated at  $\omega_1$  is

$$\begin{aligned} P(\omega_1) &= -\frac{1}{2} \operatorname{Re} \iiint_{\text{sample}} \left( \frac{dM_{x_1}}{dt} H_{x_1}^* + \frac{dM_{y_1}}{dt} H_{y_1}^* \right) dv \\ &= -\operatorname{Re} \frac{j\omega_1}{8} \iiint_{\text{sample}} (m_{x_1} h_{x_1}^* + m_{y_1} h_{y_1}^*) dv \end{aligned} \quad (9.28)$$

whereas at  $\omega_2$

$$\begin{aligned} P(\omega_2) &= -\frac{1}{2} \operatorname{Re} \iiint_{\text{sample}} \frac{dM_{z_2}^*}{dt} \cdot H_{z_2} dv \\ &= \operatorname{Re} \left( \frac{j\omega_2}{8} \iiint_{\text{sample}} m_{z_2}^* h_{z_2} dv \right) \end{aligned} \quad (9.29)$$

For the oscillation threshold condition these must be balanced by the losses in the cavity at the respective frequencies. From the definition of the cavity  $Q$  the power lost is given by

$$\begin{aligned} P_{\text{lost}}(\omega_1) &= \frac{\omega_1}{8\pi Q_1} \iiint_{\text{cavity}} |\mathbf{H}_1|^2 dv \\ &= \frac{\omega_1}{32\pi Q_1} \iiint_{\text{cavity}} (|h_{x_1}|^2 + |h_{y_1}|^2) dv \end{aligned} \quad (9.30)$$

and

$$P_{\text{lost}}(\omega_2) = \frac{\omega_2}{32\pi} \frac{1}{Q_2} \iiint_{\text{cavity}} |h_{z_2}|^2 dv \quad (9.31)$$

where  $Q_1$  and  $Q_2$  are the total  $Q$ 's at  $\omega_1$  and  $\omega_2$ , respectively, including any external loading. Thus, for oscillations to build up,

$$\begin{aligned} P(\omega_1) &= P_{\text{lost}}(\omega_1) \\ P(\omega_2) &= P_{\text{lost}}(\omega_2) \end{aligned} \quad (9.32)$$

By utilizing Eqs. 9.25 and 9.28–9.31, Eqs. 9.32 can be reduced to

$$\frac{1}{Q_1} \int_{\text{cavity}} |h_1|^2 dv = - \frac{\omega_M h(1 + \sigma)}{2\Delta H(\omega_1 - \omega_0)} \text{Re} \int_{\text{sample}} jh_{z_2}^*(h_{x_1}^* - jh_{y_1}^*) dv \quad (9.33)$$

$$\frac{1}{Q_2} \int_{\text{cavity}} |h_{z_2}|^2 dv = \frac{\omega_M h(1 + \sigma)}{2\Delta H(\omega_1 - \omega_0)} \text{Re} \int_{\text{sample}} jh_{z_2}(h_{x_1} + jh_{y_1}) dv \quad (9.34)$$

where

$$\int_{\text{cavity}} |h_1|^2 dv \equiv \iiint_{\text{cavity}} (|h_{x_1}|^2 + |h_{y_1}|^2) dv \quad (9.35)$$

Define the following filling factors:

$$F_1 = \frac{\text{Re} \int_{\text{sample}} jh_{z_2}(h_{x_1} + jh_{y_1}) dv}{\int_{\text{cavity}} |h_1|^2 dv} \quad (a) \quad (9.36)$$

$$F_2 = \frac{\text{Re} \int_{\text{sample}} jh_{z_2}(h_{x_1} + jh_{y_1}) dv}{\int_{\text{cavity}} |h_{z_2}|^2 dv} \quad (b)$$

If Eqs. 9.33 and 9.34 are combined and Eqs. 9.36 are used the pump threshold can be given by

$$\vartheta = \frac{h}{2\Delta H} (1 + \sigma) \geq \frac{\omega_2}{\omega_M} \frac{1}{\sqrt{Q_1 Q_2 F_1 F_2}} \quad (9.37)$$

This represents the magnitude of the pump field necessary for the pump power to exceed the cavity losses. Typical numbers might be useful. Assume  $\sigma = 1$  (circular polarization),  $\Delta H = 1$  oersted,  $F_1 = F_2 = 10^{-1}$ ,  $Q_1 = Q_2 = 10^3$ , and  $\omega_2 = \omega_M$  ( $\sim 5.6$  kmc). Then  $h \cong 10^{-2}$  oersted. This figure represents a good design and the best materials. On the other hand, if  $\Delta H = 100$  oersteds,  $F_1 = F_2 = 10^{-2}$ , then  $h \cong 10$  oersteds. In this case pulsed operation would be necessary because of the high pump power density required to achieve an r-f field of 10 oersteds at the sample.

### 9.5 Experimental Results

M. T. Weiss <sup>25</sup> has reported experimental results on a ferrite amplifier. The pump frequency was  $\omega/2\pi = 9$  kmc/sec, and the signal frequency,  $\omega_1/2\pi = 4.5$  kmc/sec. With a pumping pulse of 20 kw peak power and 3  $\mu$ sec duration, a pulse of oscillation at 4.5 kmc/sec with an output power of 100 watts was observed. The amount of pump power actually absorbed by the ferrite was not measured.

By reducing the pump power below oscillation threshold, a range of amplification was observed. By reducing the 9 kmc/sec drive about 1 db below oscillation threshold, a gain of 8 db was observed at 4.5 kmc/sec. As the signal was detuned from 4.5 kmc/sec, its image  $\omega_2$  was displaced from  $\omega_1$  and beats were observed.

Another experiment was made in which  $f_1$  and  $f_2$  ( $\omega_{1,2}/2\pi$ ) were 4.0 and 4.8 kmc/sec, respectively. Frequency conversion and oscillation were observed at the foregoing frequencies. The oscillations had a peak power of 50  $\mu$ watts and were jittery in amplitude.

Whirry and Wang <sup>26</sup> have reported results on polycrystalline yttrium garnet with  $\Delta H = 75$  oersteds, using Suhl's electromagnetic mode of operation with  $\omega_1 = \omega_2$ . In this case the phase sensitivity of the pump and signal was observed. With pulsed operation, the threshold of pump power needed for oscillation was 8 kw peak. For a 0.1 mw signal input a peak gain of 47 db with a 1-mc bandwidth was observed.

### 9.6 Traveling Wave Version

Tien and Suhl <sup>9</sup> have proposed that more bandwidth and greater stability might be achieved by using a propagating structure rather than a resonant circuit. In this case two transmission lines (or two propagating modes of a transmission line) are embedded in a ferromagnetic medium. Figure 9.6 shows a cross-sectional view of such a system. It consists essentially of two pairs of parallel wires which act as two transmission

lines. The  $y$ -axis is the direction of propagation. A d-c field  $H_0$ , uniform over the entire cross section of the structure, is applied in the  $z$ -direction. Line No. 1 has its two wires in the  $y$ - $z$ -plane and line No. 2 has its wires in the  $x$ - $y$ -plane. All the wires are parallel to the direction of propagation and are totally embedded in the ferrite medium. The entire structure is surrounded by a circular waveguide which carries the energizing wave supplied by the pump. To use the pump power efficiently, the pump generator must be operated at the frequency of the ferromagnetic resonance, viz.,  $\omega_0 = |\gamma| \sqrt{H_0(H_0 - 2\pi M)}$ , where  $\gamma$  is the gyromagnetic ratio,  $H_0$  is the applied d-c magnetic field, and  $M$  is the total magnetization of the medium. This formula applies to a rod of ferrite which is transversely magnetized and is different from the resonance frequency of the sphere treated earlier.

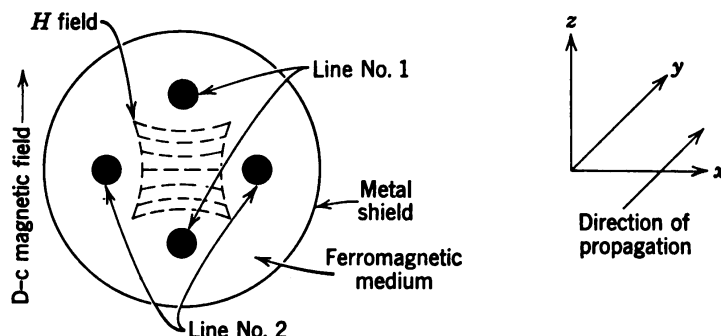


**Figure 9.6** A ferromagnetic traveling wave amplifier with parallel wire structure. (From Tien and Suhl, Reference 9.)

The equivalent circuit for this structure is shown in Figure 5.1 of Chapter 5. The time-varying coupling is provided by the ferromagnetic medium.

Tien and Suhl<sup>9</sup> find that the net gain of the amplifier is given approximately by

$$\left( \frac{\vartheta}{4} \frac{\omega_M}{\omega_2} \sqrt{\beta_1 \beta_2} - \alpha \right) \text{nepers/cm}$$

where  $\vartheta$  = precession angle

$$\vartheta = \sqrt{\frac{\Delta H}{2\pi M}}$$

$$\omega_M = 4\pi|\gamma|M$$

$$\omega_1 = \text{signal frequency}$$

$\omega_2$  = idler frequency

$$\beta_1 \cong \frac{\omega_1}{c} \sqrt{\frac{\epsilon(\mu^2 - \kappa^2)}{\mu}}$$

$$\beta_2 \cong \frac{\omega_2}{c} \sqrt{\epsilon}$$

$\mu$  and  $\pm j\kappa$  are the components of the permeability tensor (see Reference 13),  $c$  is the velocity of light,  $\epsilon$  is the ferrite dielectric constant,  $\alpha$  is a ferrite loss term, and  $\Delta H$  is the line width of the ferrite sample.

As a numerical example for yttrium-iron garnet,

$$4\pi M = 2000$$

$$\epsilon = 10$$

$$\Delta H = 3 \text{ oersteds}$$

$$H_0 = 3750 \text{ oersteds}$$

$$\frac{\omega_0}{2\pi} = \frac{|\gamma|}{2\pi} \sqrt{H_0(H_0 - 2\pi M)} = 9 \text{ kmc}$$

$$\frac{\omega_M}{2\pi} = 2|\gamma|M = 5.6 \text{ kmc}$$

The lower limit of the magnetostatic mode is

$$\frac{1}{2\pi} |\gamma|(H_0 - 2\pi M) = 7.7 \text{ kmc}$$

Instability will not occur therefore by choosing

$$f_1 = 6.5 \text{ kmc}$$

$$f_2 = 2.5 \text{ kmc}$$

$$\vartheta = \frac{1}{20}$$

By ignoring circuit copper losses, the gain in decibels per centimeter is

$$\text{gain (db/cm)} = 0.551 \text{ db/cm}$$

Since  $\Delta H = 3$  oersteds, the energizing field required is

$$h_{\text{energizing}} = \Delta H \times \vartheta = 0.15 \text{ oersted}$$

To maintain this field, power must be supplied by a local oscillator mainly because of ferromagnetic loss of the sample. If the sample

volume is  $V_S$  cm<sup>3</sup>, the ferromagnetic loss at the pump frequency is

$$\begin{aligned} P_m &= \frac{\omega}{8\pi} \frac{4\pi M}{\Delta H} (h_{\text{energizing}})^2 V_S \times 10^{-7} \text{ watt} \\ &= 3.375 \times 10^3 V_S \text{ watts} \end{aligned}$$

Therefore, although this figure may be slightly pessimistic, orders of magnitude improvement must be achieved before such a device appears practical.

### 9.7 Ferromagnetic Frequency Converter

Poole and Tien<sup>10</sup> have suggested that a ferrite be used for a frequency converter. The equivalent circuit for this case has been worked out in Chapter 5 and is not repeated. The theory of the ferrite device itself is worked out by Poole and Tien in detail. The work is mainly of importance as a means of verifying the theory. Since the analysis is involved and the future of ferrite devices is open to question at the moment by virtue of the high pump power requirements, only the experimental results are discussed. Perhaps future technology will change this situation.

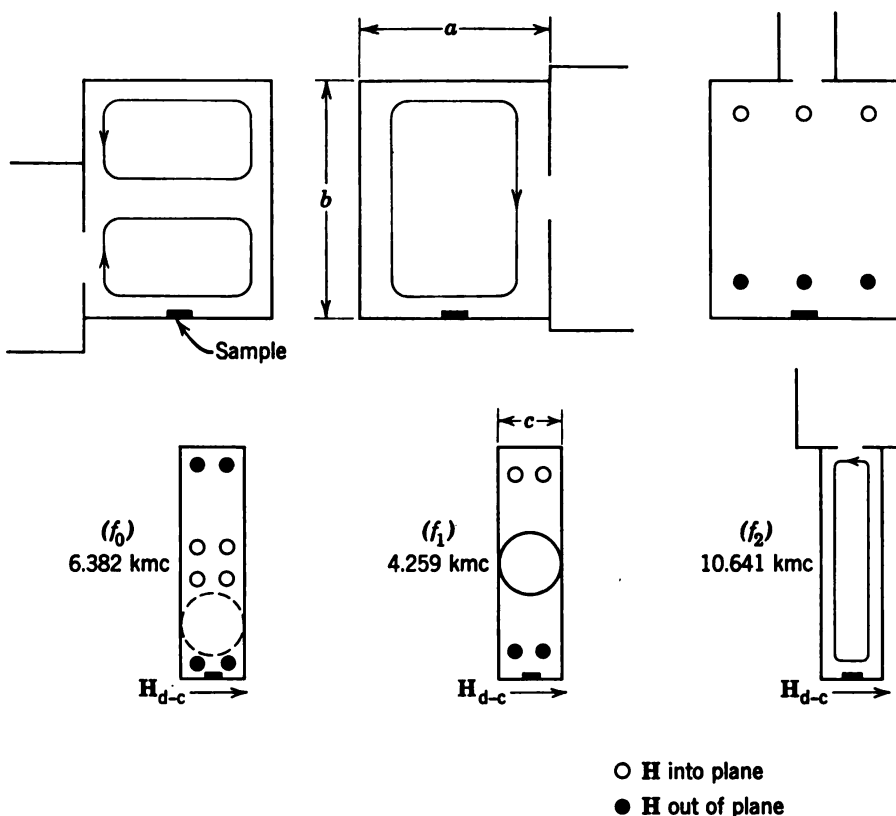
The cavity used was a triply resonant rectangular cavity. The design was governed by several conditions; the cavity modes had to be chosen so that in some region of the cavity strong microwave magnetic fields of all three modes coexisted in the appropriate directional arrangement; simultaneously, it must be possible to choose the cavity dimensions to satisfy  $\omega_2 = \omega + \omega_1$ .

Figure 9.7 shows the cavity modes in question and the arrangement of the coupling irises and waveguides. The ferrite sample is a disk 0.0023 in. thick and 0.046 in. in diameter cut in the 110 plane from a single crystal of yttrium-iron garnet. The frequencies of the modes are shown in the figure.

Figure 9.8 shows a plot of the output conversion gain measurements as a function of signal and energizing powers. The theoretical curves are drawn from the relationship

$$P_{\text{output}} = CP_{\text{signal}}P_{\text{energize}}$$

which is based on the assumption that the line width (hence the related parameters of the microwave resonance) are independent of signal level. The figure shows a deviation of the order of 2 db from the idealized model.



**Figure 9.7** Magnetic field patterns of resonant modes of cavity. (Coupling waveguides and irises shown only on sketch of corresponding mode.) (From Poole and Tien, Reference 10.)

The relevant measured parameters when the pump power was substantially higher than the signal power are given by

Signal frequency	4.259 kmc/sec
Loaded $Q$	1690
Incident power	$5 \times 10^{-2}$ watt
Power transmission factor of coupling iris	0.395
Energizing frequency	6.382 kmc/sec
Loaded $Q$ (at ferromagnetic resonance)	1170
Incident power	3 watts
Resonance line width	11 oersteds
Power transmission factor	0.8
Output frequency	10.641 kmc/sec
Loaded $Q$	6000
Output power	$3.7 \times 10^{-10}$ watt
Power transmission factor	0.35

(Measured by use of external generator.)

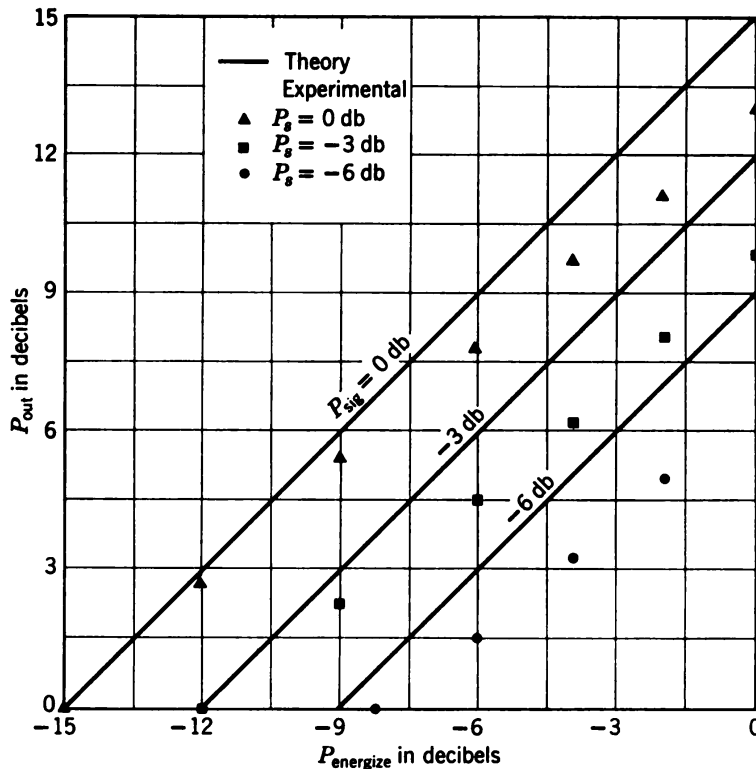


**Figure 9.8** Output power at 10.641 kmc as function of signal power (at 4.259 kmc) and energizing power (at 6.382 kmc). (From Poole and Tien, Reference 10.)

Poole and Tien have compared these values with the theory and find a remaining 2-db discrepancy. This discrepancy was less than the accumulated errors, which were estimated at 3 to 4 db.

### 9.8 Conclusions

As of the date of this writing, pump power requirements look prohibitive for the ferrite amplifiers. Other modes of operation and lower loss ferrites that will change this picture may become available.

### BIBLIOGRAPHY

1. H. Suhl, "Theory of the Ferromagnetic Microwave Amplifier," *J. Appl. Phys.*, **28**, 1225-1236 (November 1957).
2. F. Bloch, "Zur Theorie des Ferromagnetismus," *Z. Physik*, **61**, 206-219 (1930).
3. C. Kittel, *Introduction to Solid-State Physics*, John Wiley and Sons, New York, 1954, pp. 360-362.

4. L. R. Walker, "Magnetostatic Modes in Ferromagnetic Resonance," *Phys. Rev.*, **105**, 390-399 (January 1957).
5. H. Suhl, "Proposal for a Ferromagnetic Amplifier in the Microwave Range," *Phys. Rev.*, **106**, 384-385 (April 15, 1957).
6. H. Suhl, "The Ferromagnetic Microwave Amplifier," *Phys. Today*, **11**, 28-30 (September 1958).
7. H. Suhl, "Quantum Analog of the Ferromagnetic Microwave Amplifier," *J. Phys. Chem. Solids*, **4**, 278-282 (1958).
8. H. Suhl, "Origin and Use of Instabilities in Ferromagnetic Resonance," *J. Appl. Phys.*, **29**, 416-421 (March 1958).
9. P. K. Tien and H. Suhl, "A Traveling Wave Ferromagnetic Amplifier," *Proc. IRE*, **46**, 700-706 (April 1958).
10. K. M. Poole and P. K. Tien, "A Ferromagnetic Resonance Frequency Converter," *Proc. IRE*, **46**, 1387-1396 (July 1958).
11. L. Landau and E. Lifshitz, "On the Theory of the Dispersion of Magnetic Permeability in Ferromagnetic Bodies," *Physik. Z. Sowjetunion*, **8**, 153-169 (June 1935).
12. D. Polder, "On the Theory of Ferromagnetic Resonance," *Phil. Mag.*, **40**, 99-115 (1949).
13. D. A. Watkins, *Topics in Electromagnetic Theory*, John Wiley and Sons, New York, 1958, Chapter 4.
14. F. Bloch, "Nuclear Induction," *Phys. Rev.*, **70**, 460-474 (October 1946).
15. See Reference 3, pp. 155-156, 170-171.
16. J. A. Stratton, *Electromagnetic Theory*, McGraw-Hill, New York, 1941, Chapters 2, 4.
17. See Reference 3, Chapter 6.
18. L. R. Walker, "Resonant Modes of Ferromagnetic Spheroids," *J. Appl. Phys.*, **29**, 318-323 (March 1958).
19. A. G. Fox and M. T. Weiss (see Reference 1).
20. K. M. Poole and P. K. Tien, "A Study of Possible CW Ferrimagnetic Amplifiers," *Bell Labs. Internal Memorandum 59-124-9* (March 30, 1959).
21. A. D. Berk, L. Kleinman, and C. E. Nelson, "Modified Semistatic Ferrite Amplifier," *IRE WESCON Convention Record*, **2**, Part III, 9 (1958). This mode of operation was independently proposed by M. T. Weiss.
22. R. W. Damon and J. R. Eshbach, "Theoretical Limitations of Ferrite Parametric Amplifier Performance," talk presented at PGMTT Symposium, Harvard University, Cambridge, Massachusetts, June 1959.
23. H. B. G. Casimir, *Philips Research Reports*, **6**, 162 (1951).
24. H. A. Bethe and J. Schwinger, *NDRC Report D1-117*, Cornell University (1943).
25. M. T. Weiss, "Solid-State Microwave Amplifier and Oscillator Using Ferrites," *Phys. Rev.*, **107**, 317-318 (July 1957).
26. W. L. Whirry and F. B. Wang, "Phase Dependence of a Ferromagnetic Microwave Amplifier," *Proc. IRE*, **46**, 1657-1658 (September 1958).

## Appendix A

# Coaxial cable as a transmission line

This appendix is presented to demonstrate the type of analysis that must be carried out in order to evaluate the parameters, for example,  $L$ ,  $C$ , which are used in the equivalent circuit of a transmission line in terms of the dimensions, type of dielectric, etc. This must be done in order to design a transmission line. A very simple case is treated, viz., a *TEM*-mode of propagation of an electromagnetic wave in the dielectric between two concentric metallic cylinders. (See Figure A.1.)

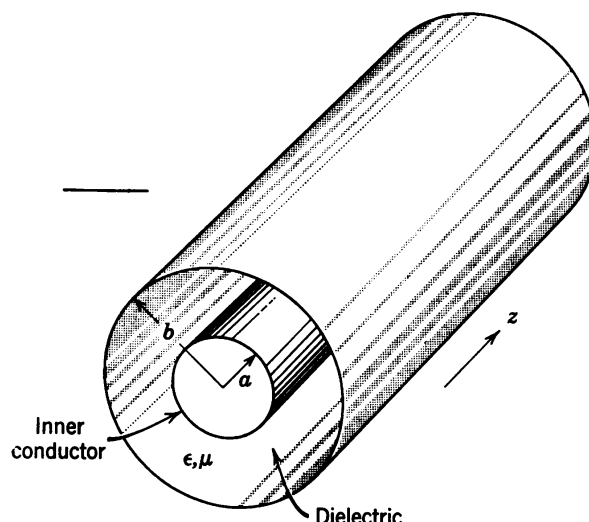


Figure A.1 Coaxial cable as a transmission line.

For a *TEM*-wave, by definition, the  $z$ -components of the electric and magnetic fields are zero. The length of the cable is parallel to the

$z$ -axis, which is the direction of propagation. Furthermore, only the lowest order mode (which is independent of the azimuthal angle  $\phi$ ) is considered. Thus all field quantities are independent of  $\phi$  so that  $\partial/\partial\phi = 0$  everywhere. Further, the wave is assumed to have an  $e^{j\omega t}$  time dependence and to vary as  $e^{\gamma z}$ . The dielectric constant and permeability of the medium between the two conductors are  $\epsilon$  and  $\mu$ , respectively. In this case Maxwell's equations in the dielectric (see Reference 9, Chapter 1) are easily seen to reduce to

$$\frac{1}{r} \frac{\partial}{\partial r} (r H_\phi') = 0 \quad (\text{A.1})$$

$$E_r' = -j \frac{\gamma}{\omega \epsilon} H_\phi' \quad (\text{A.2})$$

$$E_r' = j \frac{\omega \mu}{\gamma} H_\phi' \quad (\text{A.3})$$

where  $e^{j\omega t - \gamma z}$  has been factored out. From the last two equations it is seen that

$$\gamma^2 = -\omega^2 \mu \epsilon \quad (\text{A.4})$$

or

$$\gamma = \pm j\omega \sqrt{\mu \epsilon} \equiv \pm j\beta \quad (\text{A.5})$$

where the plus sign gives the forward and the minus sign the backward mode. Thus, by Eqs. A.3 and A.5,

$$E_r' = \sqrt{\frac{\mu}{\epsilon}} H_\phi' \quad (\text{A.6})$$

Further, by Eq. A.1

$$H_\phi' = \frac{c_1}{r} \quad (\text{A.7})$$

where  $c_1$  is a constant of integration.

The constant  $c_1$  is evaluated from Ampère's law. The current carried by the wire is obtained by the line integral of  $H_\phi'$  around the surface of the inner conductor of radius  $a$ . Thus

$$\begin{aligned} I' &= \oint \mathbf{H}' \cdot d\mathbf{s} = \int_0^{2\pi} H_\phi' a d\phi = 2\pi a H_\phi' \\ &= 2\pi c_1 \end{aligned} \quad (\text{A.8})$$

by Eq. A.7. Thus the magnetic field is given by

$$H_\phi = \frac{I'}{2\pi r} e^{j(\omega t - \beta z)} = \frac{I}{2\pi r} \quad (\text{A.9})$$

and by Eq. A.6 the electric field is

$$E_r = \sqrt{\frac{\mu}{\epsilon}} \frac{I'}{2\pi r} e^{j(\omega t - \beta z)} = \frac{I}{2\pi r} \sqrt{\frac{\mu}{\epsilon}} \quad (\text{A.10})$$

The potential difference between the inner and outer conductor is given by

$$V = \int_a^b E_r dr = \frac{I}{2\pi} \sqrt{\frac{\mu}{\epsilon}} \ln \frac{b}{a} \quad (\text{A.11})$$

and the characteristic impedance is defined by

$$Z_0 = \frac{V}{I} = \frac{1}{2\pi} \sqrt{\frac{\mu}{\epsilon}} \ln \frac{b}{a} \quad (\text{A.12})$$

Put Eq. A.11 in the form of the transmission-line equations. Differentiate Eq. A.11 with respect to  $z$ . Thus

$$\frac{\partial V}{\partial z} = Z_0 \frac{\partial I}{\partial z} \quad (\text{A.13})$$

But, by Eq. A.9,  $I = I' e^{j(\omega t - \beta z)}$ , where  $\beta = \omega \sqrt{\mu \epsilon}$  by Eq. A.5. Thus

$$\frac{\partial I}{\partial z} = -j\beta I = -j\omega \sqrt{\mu \epsilon} I \quad (\text{A.14})$$

By using this in Eq. A.13 and using Eq. A.12,

$$\frac{\partial V}{\partial z} = -j \frac{\omega \mu}{2\pi} \ln \frac{b}{a} I \quad (\text{A.15})$$

Similarly, it is found that

$$\frac{\partial I}{\partial z} = -j \frac{2\pi \omega \epsilon}{\ln b/a} V \quad (\text{A.16})$$

However, Eqs. A.15 and A.16 are just the lossless transmission-line equations (1.45) of the text, so that by comparison it is seen that

$$L = \frac{\mu}{2\pi} \ln \frac{b}{a} \text{ (henrys/meter)} \quad (\text{A.17})$$

$$C = \frac{2\pi \epsilon}{\ln b/a} \text{ (farads/meter)} \quad (\text{A.18})$$

Finally, consider the power flow in the  $z$ -directions. By Poynting's theorem,

$$P_z = \int_0^{2\pi} \int_a^b \frac{1}{2} \operatorname{Re} (E_r H_\phi^*) r dr d\phi \quad (\text{A.19})$$

By using Eqs. A.9 and A.10, this becomes

$$\begin{aligned} P_z &= \frac{I'^2}{4\pi} \sqrt{\frac{\mu}{\epsilon}} \ln \frac{b}{a} = \frac{1}{2} \operatorname{Re} (VI^*) \\ &\equiv \overline{VI} \end{aligned} \quad (\text{A.20})$$

where Eq. A.11 has been used and the bar represents a time average.

## Appendix B

# Space-charge waves in a cylindrical beam\*

In region I ( $0 \leq r \leq b$ ) of Figure 2.3c, Eqs. 2.21, 2.23, 2.25, 2.27, and 2.29 of the text must be solved. Assuming an  $e^{-j\beta z}$  dependence, the continuity Eq. 2.25 results in

$$\beta J_1 = \omega \rho_1 \quad (\text{B.1})$$

and the equation of motion (2.27) reduces to

$$\frac{e}{m} E_{1z} = j(\omega - \beta v_0) u_1 \quad (\text{B.2})$$

where  $v_0$  is constant, whereas by Eq. B.1 and Eq. 2.29 it is seen that

$$u_1 = \frac{(\omega - \beta v_0)}{\omega \rho_0} J_1 \quad (\text{B.3})$$

Combine Eqs. B.2 and B.3 to obtain

$$E_{1z} = j \frac{(\omega - \beta v_0)^2}{\epsilon_0 \omega \omega_p^2} J_1 = j \frac{(\beta_e - \beta)^2}{\beta_e} \frac{2V_0}{|J_0|} J_1 \quad (\text{B.4})$$

This relation should be compared with Eq. 2.38 of the text for an infinite beam.

A current that flows in only the  $z$ -direction can have no magnetic field in the  $z$ -direction. Thus it is clear that only  $TM$  waves will interact with the beam so that  $H_{1z} = 0$ . Further, it will turn out that the  $\phi$  dependence must vary as  $e^{jn\phi}$  and  $n$  must be an integer in order that

\* S. Ramo, "Space-Charge and Field Waves in an Electron Beam," *Phys. Rev.*, **56**, 276–283, August 1939.

the fields be single valued in  $\phi$ . Thus by factoring out this  $\phi$  dependence, Eq. 2.21 in cylindrical coordinates reduces to

$$H_{1\phi} = \frac{\omega\epsilon_0}{\beta} E_{1r} \quad (\text{B.5})$$

$$H_{1r} = -\frac{\omega\epsilon_0}{\beta} E_{1\phi} \quad (\text{B.6})$$

$$\frac{1}{r} \frac{d}{dr} (rH_{1\phi}) - j \frac{n}{r} H_{1r} = j\omega\epsilon_0 \left(1 - \frac{\omega_p^2}{(\omega - \beta v_0)^2}\right) E_{1z} \quad (\text{B.7})$$

(where Eq. B.4 has been used). Equation 2.23 reduces to

$$\frac{n}{r} E_{1z} + \beta E_{1\phi} = -\omega\mu_0 H_{1r} \quad (\text{B.8})$$

$$\frac{dE_{1z}}{dr} + j\beta E_{1r} = j\omega\mu_0 H_{1\phi} \quad (\text{B.9})$$

$$\frac{d}{dr} (rE_{1\phi}) = jnE_{1r} \quad (\text{B.10})$$

When Eqs. B.5 and B.9 are combined, it is seen that

$$E_{1r} = -\frac{j\beta}{\left[\left(\frac{\omega}{c}\right)^2 - \beta^2\right]} \left(\frac{dE_{1z}}{dr}\right) = \frac{\beta}{\omega\epsilon_0} H_{1\phi} \quad (\text{B.11})$$

Further, by Eqs. B.6 and B.8

$$E_{1\phi} = \frac{n\beta}{\left[\left(\frac{\omega}{c}\right)^2 - \beta^2\right]} E_{1z} = -\frac{\beta}{\omega\epsilon_0} H_{1r} \quad (\text{B.12})$$

By utilizing Eqs. B.5, B.6, B.7, B.11 and B.12,

$$\frac{d^2E_{1z}}{dr^2} + \frac{1}{r} \frac{dE_{1z}}{dr} + \left(T^2 - \frac{n^2}{r^2}\right) E_{1z} = 0 \quad (\text{B.13})$$

which is just Bessel's equation, in which

$$T = + \left[\left(\frac{\omega}{c}\right)^2 - \beta^2\right]^{\frac{1}{2}} \left(1 - \frac{\beta_p^2}{(\beta_e - \beta)^2}\right)^{\frac{1}{2}} \quad (\text{B.14})$$

Thus the general solution is given by

$$E_{1z} = AJ_n(Tr) + BY_n(Tr) \quad (\text{B.15})$$

where  $J_n$  and  $Y_n$  are Bessel functions of the first and second kind. Now, at  $r = 0$ ,  $E_{1z}$  is finite, and  $B = 0$  in region I, since  $Y_n(0) \rightarrow \infty$ . Thus

$$E_{1zI} = AJ_n(Tr) \exp [j(\omega t - \beta z + n\phi)] \quad (\text{B.16})$$

In region II there is no space charge, so that  $\rho_0 \rightarrow 0$  and  $\omega_p^2 \rightarrow 0$  and

$$T \rightarrow j\tau \equiv j \left[ \beta^2 - \left( \frac{\omega}{c} \right)^2 \right]^{\frac{1}{2}} \quad (\text{B.17})$$

Thus in region II (outside the beam)

$$E_{zII} = [CI_n(\tau r) + DK_n(\tau r)] \exp [j(\omega t - \beta z + n\phi)] \quad (\text{B.18})$$

where  $I_n$  and  $K_n$  are the modified Bessel functions.

The next step consists of matching boundary conditions at the beam boundary,  $r = b$ , and at the cylinder boundary,  $r = a$ . These boundary conditions are (1)  $E_{zII} = 0$  at  $r = a$ , (2)  $E_{zI} = E_{zII}$  at  $r = b$ , and (3)  $H_{\phi I} = H_{\phi II}$  at  $r = b$ . This results in the following transcendental equation, which must be solved:

$$(Tb) \frac{J_n'(Tb)}{J_n(Tb)} = (\tau b) \frac{I_n'(\tau b) + D_n K_n'(\tau b)}{I_n(\tau b) + D_n K_n(\tau b)} \quad (\text{B.19})$$

where

$$D_n = - \frac{I_n(\tau a)}{K_n(\tau a)} \quad (\text{B.20})$$

Since space-charge waves are slow waves (phase velocity approximately equal to the d-c beam velocity) and since  $v_0 \ll c$ , it follows that

$$\beta^2 \cong \beta_e^2 = \left( \frac{\omega}{v_0} \right)^2 \gg \left( \frac{\omega}{c} \right)^2 \quad (\text{B.21})$$

and Eqs. B.14 and B.17 reduce to

$$T \cong \beta \sqrt{\left( \frac{\beta_p}{\beta_e - \beta} \right)^2 - 1} \equiv \beta \sqrt{\frac{1}{\mathfrak{R}^2} - 1} \quad (\text{B.22})$$

where the last expression defines  $\mathfrak{R}$ , which is called the space-charge reduction factor, and

$$\tau \cong \beta \quad (\text{B.23})$$

Equation B.19 must be solved for the propagation constant  $\beta$ , when  $\beta_e$  and  $a/b$  are given. In principle, this equation can be reduced to the form

$$|\mathcal{R}| = F\left(\beta_e b, \frac{a}{b}\right) \quad (\text{B.24})$$

If  $a/b$  and  $\beta_e b$  are chosen,  $\mathcal{R}$  can be found, and since

$$\mathcal{R} \equiv \frac{\beta_e - \beta}{\beta_p} \equiv \frac{\beta_q}{\beta_p} \quad (\text{B.25})$$

$\beta$  is determined when  $\beta_p$  is specified.  $\beta_q$  is called the reduced plasma propagation constant and is defined by this relation. This symbolic algebra is not to be construed as implying that the solution of the transcendental equation is easy.

Once the reduction factor is known (see Reference 4, Chapter 2), it follows that Eq. B.4 can be written

$$E_{1z} = j \frac{\mathcal{R}^2 \beta_p^2}{\beta_e} \frac{2V_0}{|J_0|} J_1 \equiv j \frac{\beta_q^2}{\beta_e} \frac{2V_0}{|J_0|} J_1 \quad (\text{B.26})$$

which is the equation for the infinite beam (Eq. 2.38) if  $\mathcal{R} = 1$ , and it shows, since  $\mathcal{R} < 1$  for a finite beam, that the field inside the beam is reduced.

An infinite number of solutions applies to the transcendental equation; therefore, an infinite number of space-charge modes can propagate on a finite beam. Only the lowest order modes, for which  $n = 0$ , are considered in the text.

## Appendix C

# General method of finding the normal mode form

Consider a set of  $n$ -coupled first-order ordinary linear differential equations with constant coefficients. These can be written

$$\frac{dw_i}{dz} = \sum_{j=1}^n c_{ij}w_j \quad (i = 1, 2, \dots, n) \quad (\text{C.1})$$

This is a more general case of the transmission-line equations. The  $c_{ij}$ 's are constants.

In order to proceed most easily, write these equations in matrix form. Let

$$W = \begin{bmatrix} w_1 \\ w_2 \\ \vdots \\ w_n \end{bmatrix} \quad C = \begin{bmatrix} c_{11} & c_{12} & \cdots & c_{1n} \\ c_{21} & c_{22} & \cdots & c_{2n} \\ \vdots & \vdots & & \vdots \\ \vdots & \vdots & & \vdots \\ c_{n1} & c_{n2} & \cdots & c_{nn} \end{bmatrix} \quad (\text{C.2})$$

Equations C.1 in matrix form become

$$\frac{dW}{dz} = CW \quad (\text{C.3})$$

**Theorem.** In general, there exists a linear transformation of the  $W = (w_1, w_2, \dots, w_n)$  to another set of variables  $A = (a_1, a_2, \dots, a_n)$  of the form

$$W = SA \quad (\text{C.4})$$

where  $S$  is a constant matrix of the same general form as  $C$  which will transform Eq. C.3 to the form

$$\frac{dA}{dz} = \Lambda A \quad (C.5)$$

where  $\Lambda$  is a diagonal matrix. The equations involving  $a_i$  (Eq. C.5) are completely decoupled, and this is the *normal mode form* of Eqs. C.1. [In ordinary notation Eq. C.5 is

$$\frac{da_i}{dz} = \lambda_{(i)} a_i \quad (i = 1, 2, \dots, n) \quad (C.6)$$

The  $a_i$ 's, which are linear combinations of the  $w_i$ 's, are called the normal mode amplitudes.  $\Lambda = \text{diag}(\lambda_1, \lambda_2, \dots, \lambda_n)$ .]

The theorem is proved by showing how the linear combinations of Eq. C.4 can be found, and this shows the existence of the  $s_{ij}$  elements of  $S$ . In finding the  $s_{ij}$ 's, the  $\lambda_{(i)}$ 's are found and the theorem is proved.

Put Eq. C.4 in C.3 and multiply both sides of the equation from the left by  $S^{-1}$ , the inverse of  $S$ . Then

$$\frac{dA}{dz} = S^{-1}CSA \quad (C.7)$$

Now the  $S$  is arbitrary. Choose it so that

$$S^{-1}CS = \Lambda \quad (C.8)$$

where  $\Lambda$  is a diagonal matrix whose elements are still unknown. Multiply both sides of Eq. C.8 from the left by  $S$ . It follows that

$$CS = S\Lambda \quad (C.9a)$$

or, in terms of the matrix elements,

$$\sum_{\rho=1}^n c_{ip} s_{\rho j} = \sum_{\rho=1}^n s_{ip} \lambda_{(\rho)} \delta_{\rho j} \quad (i, j = 1, 2, \dots, n) \quad (C.9b)$$

where the  $\lambda_{(i)}$ 's are the diagonal elements of  $\Lambda$  and  $\delta_{ij}$  is the Kronecker delta defined by

$$\begin{aligned} \delta_{ij} &= 1 & i = j \\ &= 0 & i \neq j \end{aligned} \quad (C.10)$$

By using Eq. C.10, the right side of Eq. C.9b can be reduced to

$$s_{ij} \lambda_{(j)} = \sum_{\rho=1}^n \delta_{ip} s_{\rho j} \lambda_{(j)} \quad (C.11)$$

Combine this equation with the left-hand side of Eq. C.9b. Then

$$\sum_{\rho=1}^n (c_{i\rho} - \lambda_{(j)} \delta_{i\rho}) s_{\rho j} = 0 \quad (\text{C.12})$$

The  $c_{ij}$ 's are known, and this represents a set of homogeneous algebraic equations that must be solved for the  $s_{ij}$ . From the well-known results of algebra, in order that such a set of equations have nontrivial (non-zero) solutions, the determinant of the coefficients must vanish, i.e.,

$$\| c_{ij} - \lambda \delta_{ij} \| = 0 \quad (\text{C.13})$$

This determinant is of the  $n$ th order in  $\lambda$ , and there are  $n$  solutions, or  $n$  values of  $\lambda$  in terms of the  $c_{ij}$ 's, that will make this determinant zero. For simplicity, it will be assumed that all  $n$  of the  $\lambda$ 's are different. These, then, are the desired  $n$  values of  $\lambda$  in Eq. C.6 and the normal mode propagation constants. To find the  $s_{ij}$ 's, take these  $n$  values of  $\lambda$  and put them into Eq. C.12 and solve these equations  $n$  times.

All the  $s_{ij}$ 's cannot be found this way. Recall that, for each  $\lambda$ ,  $n - 1$  of the  $s_{ij}$ 's can be expressed only in terms of the  $n$ th one. Therefore, there will still be  $n$  undetermined  $s_{ij}$ 's (there are  $n^2 s_{ij}$  elements altogether). This arbitrariness leaves some latitude of choice in the particular linear combination of the  $w$ 's that make up the normal mode amplitude. The arbitrariness can be removed by requiring that power be conserved and that the normal mode amplitudes squared represent the power carried by the mode.

## Appendix D

# Normal mode form for the synchronous modes

Write Eq. 2.59 of the text as

$$\left( \frac{d}{dz} + j(\beta_e - \beta_c) \right) a_{1+} = 0 \quad (\text{D.1})$$

$$\left( \frac{d}{dz} + j(\beta_e + \beta_c) \right) a_{1-} = 0 \quad (\text{D.2})$$

where  $a_{1\pm}$  are defined by Eq. 2.58. Further, define

$$r_{\pm} = k(\xi_{1x} \pm j\xi_{1y}) \quad (\text{D.3})$$

Use this definition and write Eq. 2.61 as

$$\left( \frac{d}{dz} + j\beta_e \right) r_+ = \frac{1}{v_0} a_{1+} \quad (\text{D.4})$$

$$\left( \frac{d}{dz} + j\beta_e \right) r_- = \frac{1}{v_0} a_{1-} \quad (\text{D.5})$$

Although Eqs. D.1 and D.2 are decoupled and are therefore in normal mode form to yield the cyclotron modes, Eqs. D.4 and D.5 are still coupled to them. In order to decouple, the same technique is used as in Eq. 1.3 of Chapter 1. Accordingly, multiply both sides of Eq. D.4 by  $g$  and add to Eq. D.1 and both sides of Eq. D.5 by  $h$  and add to Eq. D.2;  $g$  and  $h$  are the arbitrary constants chosen to decouple the

equations. Then

$$\begin{aligned} \left( \frac{d}{dz} + j\beta_e \right) (a_{1+} + gr_+) &= \frac{1}{v_0} (j\omega_c + g)a_{1+} \\ \left( \frac{d}{dz} + j\beta_e \right) (a_{1-} + hr_-) &= \frac{1}{v_0} (-j\omega_c + h)a_{1-} \end{aligned} \quad (\text{D.6})$$

Now choose

$$\begin{aligned} g &= -j\omega_c \\ h &= +j\omega_c \end{aligned} \quad (\text{D.7})$$

and

$$a_{2\pm} = a_{1\pm} \mp j\omega_c r_\pm \quad (\text{D.8})$$

and the equations will be decoupled.

## Appendix E

# Coupled mode form of beam-circuit equations

In order to put the beam circuit equations in coupled mode form, the same technique is used as in Eq. 1.3 of Chapter 1. Multiply Eq. 3.3b by  $\pm Z_c$ , and add to Eq. 3.3a, and Eq. 3.3d by  $\pm Z_b$ , and add to Eq. 3.3c. This results in

$$\begin{aligned} \left( \frac{d}{dz} \pm j\beta_c \right) a_{1\pm} &= \pm \frac{1}{4} \sqrt{Z_c} \frac{d}{dz} (-i_1) \\ \left( \frac{d}{dz} + j(\beta_e \mp \beta_q) \right) a_{2\pm} &= \frac{1}{4\sqrt{Z_b}} \frac{dV_c}{dz} \end{aligned} \quad (\text{E.1})$$

where  $\beta_c = \omega\sqrt{LC}$ ,  $\beta_q = \omega_q/v_0$ , and Eqs. 3.4 have been used. Solve Eqs. 3.4 for  $V_c$  and  $-i_1$  in terms of the mode amplitudes:

$$\begin{aligned} V_c &= 2\sqrt{Z_c} (a_{1+} + a_{1-}) \\ -i_1 &= \frac{2}{\sqrt{Z_b}} (a_{2+} - a_{2-}) \end{aligned} \quad (\text{E.2})$$

Substitute Eq. E.2 in the right side of Eq. E.1, and Eqs. 3.6 of the text result.

## Appendix F

# The Chu kinetic power theorem

The small signal Poynting theorem is given in Eq. 2.19:

$$\nabla \cdot (\mathbf{E}_1 \times \mathbf{H}_1^*) = -\mathbf{J}_1^* \cdot \mathbf{E}_1 - j\omega(\mu_0|H_1|^2 - \epsilon_0|E_1|^2) \quad (\text{F.1})$$

From Eqs. 2.25, 2.27, and 2.29 of the text it follows that

$$J_{1z}^* E_{1z} = j \frac{m}{e} \omega \rho_0 |u_{1z}|^2 - \frac{\partial}{\partial z} (V_1 J_{1z}^*) \quad (\text{F.2})$$

where

$$V_1 = \frac{m}{|e|} v_{0z} u_{1z} \quad (\text{F.3})$$

For confined flow  $\mathbf{J}_1 = J_{1z} \mathbf{e}_3$ , so that

$$J_{1z}^* E_{1z} = j \frac{m}{e} \omega \rho_0 |u_{1z}|^2 + \nabla \cdot [V_1 (-\mathbf{J}_1^*)] \quad (\text{F.4})$$

Consider now a cylindrical beam surrounded by a circuit, as shown in Figure F.1. Integrate Eq. F.1 over the dotted volume between planes  $z$  and  $z + dz$  which encloses the beam. Then, by Eqs. F.1 and F.4,

$$\frac{1}{2} \operatorname{Re} \iiint \nabla \cdot [\mathbf{E}_1 \times \mathbf{H}_1^* + V_1 (-\mathbf{J}_1^*)] d\tau = 0 \quad (\text{F.5})$$

By Gauss's theorem, transform these volume integrals to surface integrals over the surface enclosing the volume. The normal to the surface of integration in the direction  $d\sigma$  is outward from the surface. Then

$$\operatorname{Re} \iint [\frac{1}{2} \mathbf{E}_1 \times \mathbf{H}_1^* + \frac{1}{2} V_1 (-\mathbf{J}_1^*)] \cdot d\sigma = 0 \quad (\text{F.6})$$

This is the Chu kinetic power theorem.

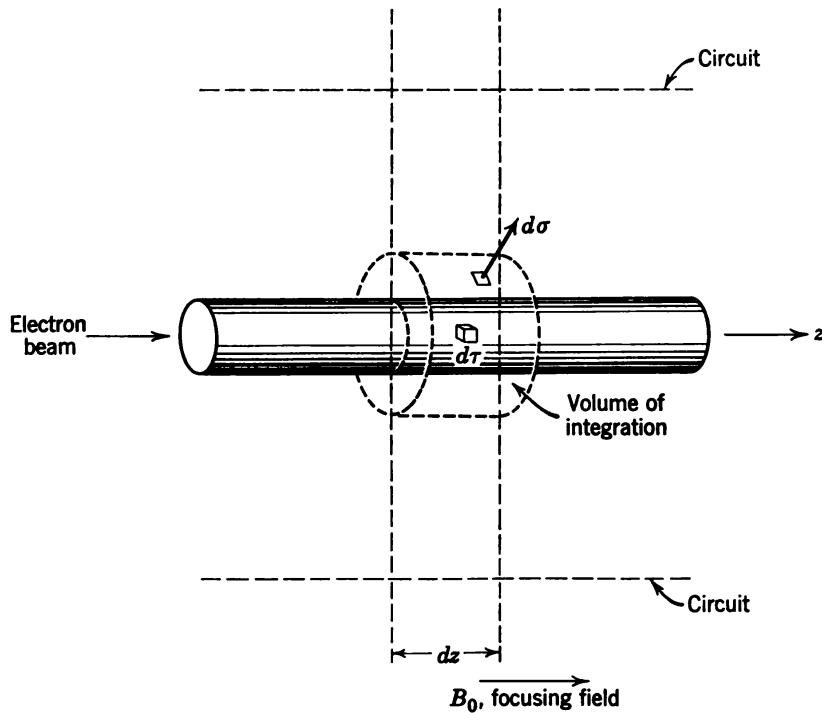


**Figure F.1** Cylindrical electron beam surrounded by a circuit. (From Reference 9, Chapter 3.)

Consider now the special case of a very thin beam. Let the cylindrical surface move out to infinity so that the volume over which the integration is being carried out is between the two infinite planes at  $z$  and  $z + dz$ . The fields and current are zero at infinity, and the only contribution to the integrals in Eq. F.6 will be from the integration over the surfaces of the two planes.

The thin beam carries almost no electromagnetic power, since the space-charge magnetic field is nearly zero in the beam. Further, for the thin beam,  $J_{1z}$  and  $V_1$  are almost constant across the beam. Now let

$$i_1 = \iint J_{1z} dx dy \cong J_{1z}\sigma \quad (\text{F.7})$$

represent the beam current, where  $\sigma$  is the beam area. The second integral in Eq. F.6 can be written approximately as

$$\frac{1}{2}V_1(-i_1)|_{z+dz} - \frac{1}{2}V_1(-i_1)|_z = \Delta \frac{1}{2}V_1(-i_1) \quad (\text{F.8})$$

which is the change in the kinetic beam power between the two planes.

Consider next the first integral in Eq. F.6. The fields of the circuits decay rapidly away from the circuit. The main contribution is in the immediate circuit vicinity. Thus

$$\begin{aligned} \operatorname{Re} \left( \iint_{z+dz} \frac{1}{2} \mathbf{E}_1 \times \mathbf{H}_1^* \cdot d\sigma - \iint_z \frac{1}{2} \mathbf{E}_1 \times \mathbf{H}_1^* \cdot d\sigma \right) \\ = \operatorname{Re} \left( \frac{1}{2} V_c I_c^*|_{z+dz} - \frac{1}{2} V_c I_c^*|_z \right) \quad (\text{F.9}) \end{aligned}$$

where  $V_c$  is the circuit voltage and  $I_c$  is the circuit current. Combine Eqs. F.8 and F.9 to obtain the approximate Chu power theorem for a thin beam, viz.,

$$\frac{1}{2} \operatorname{Re} [V_c I_c^* + V_1(-i_1^*)] = \text{constant} \quad (\text{F.10})$$

## Appendix G

# Matrix representation of TWT power series solutions

In order to put the TWT equations (3.24) in matrix form, let

$$\begin{bmatrix} a_{1+} \\ a_{2+} \\ a_{2-} \end{bmatrix} = \begin{bmatrix} a_{1+}' \\ a_{2+}' \\ a_{2-}' \end{bmatrix} e^{-j\beta_e z} \quad (\text{G.1})$$

Further let

$$\begin{aligned} \beta_e C z &= \xi \\ q &= \sqrt{4QC} \end{aligned} \quad (\text{G.2})$$

Then, in matrix form, Eqs. 3.24 become

$$j \frac{d\Psi}{dz} = \mathcal{K}\Psi \quad (\text{G.3})$$

where  $\Psi$  and  $\mathcal{K}$  are matrices defined by

$$\Psi = \begin{bmatrix} a_{1+}' \\ a_{2+}' \\ a_{2-}' \end{bmatrix} \quad \mathcal{K} = \begin{bmatrix} b & (2q)^{-\frac{1}{2}} - (2q)^{\frac{1}{2}} \\ (2q)^{-\frac{1}{2}} & -q & 0 \\ (2q)^{\frac{1}{2}} & 0 & q \end{bmatrix} \quad (\text{G.4})$$

If  $[A]$  is a square matrix, define the matrix  $[B] = e^{[A]}$  by

$$[B] = e^{[A]} = \sum_{n=0}^{\infty} \frac{[A]^n}{n!} \quad (\text{G.5})$$

Use this definition and write the solution of Eq. G.3 as

$$\begin{aligned}\Psi(\xi) &= e^{-j[\mathcal{H}]\xi} \Psi(0) \\ &\equiv \sum_{n=0}^{\infty} \frac{(-j\xi)^n}{n!} [\mathcal{H}]^n \Psi(0)\end{aligned}\quad (\text{G.6})$$

This is a matrix representation of a power series solution of the TWT equations. The coefficient of  $\Psi(0)$  is a matrix  $[M(\xi)]$

$$[M(\xi)] = e^{-j[\mathcal{H}]\xi} \quad (\text{G.7})$$

In order to obtain the matrix elements of  $M$ , the matrix  $\mathcal{H}$  must be multiplied by itself in accordance with Eq. G.6.

## Appendix H

# Evaluation of mutual coupling coefficients

The mutual coupling coefficients for two oscillators that are parametrically coupled will be evaluated by the general coupled mode approach of Chapter 1.

The normal mode amplitudes, given in Eqs. 4.30 of the text, are

$$\begin{aligned} a_1(t) &= \frac{1}{2}\sqrt{L_1}(I_1 + j\omega_1 C_{11}V_1) \\ a_2^*(t) &= \frac{1}{2}\sqrt{L_2}(I_2 - j\omega_2 C_{22}V_2) \end{aligned} \quad (\text{H.1})$$

In line with the transformation given in Eq. 4.9, let

$$\begin{aligned} a_1(t) &= A_1(t)e^{j\omega_1 t} \\ a_2^*(t) &= A_2^*(t)e^{-j\omega_2 t} \end{aligned} \quad (\text{H.2})$$

where  $A_1$  and  $A_2^*$  are slowly varying functions of time when weak coupling is assumed.

Substitute the transformation given in Eqs. H.2 into the coupled mode equations (4.23) in the text and find that

$$\begin{aligned} \frac{dA_1}{dt} &= c_{12}A_2^* \\ \frac{dA_2^*}{dt} &= c_{21}A_1 \end{aligned} \quad (\text{H.3})$$

The current that flows through the variable capacitance at frequency  $-\omega_2$ , due to the voltage variation at frequency  $\omega_1$  across the variable

capacitance in Figure 4.4, is

$$\begin{aligned} I(\omega_2) &= \frac{d}{dt} C_p(t) V_1(t) \\ &= -\frac{j}{\sqrt{C_{11}}} \frac{d}{dt} \left[ \frac{\Delta C}{2} (e^{j(\omega t + \phi)} + e^{-j(\omega t + \phi)}) (A_1 e^{j\omega_1 t} - A_1^* e^{-j\omega_1 t}) \right] \end{aligned} \quad (\text{H.4})$$

since  $C_p = \Delta C \cos(\omega t + \phi)$ .  $V_1$  has been expressed in terms of  $A_1$  and  $A_1^*$ , using Eqs. H.1 and H.2. Since  $\omega = \omega_1 + \omega_2$ ,  $A_1$  is a slowly varying function of time and only frequency  $\omega_2$  can be sustained in circuit 2 because of the ideal filter. It follows from Eq. H.4 that

$$I(\omega_2) \cong -\omega_2 \frac{\Delta C}{2\sqrt{C_{11}}} (e^{-j\phi} A_1 e^{-j\omega_2 t} + e^{j\phi} A_1^* e^{j\omega_2 t}) \quad (\text{H.5})$$

The voltage across  $C(t)$  at frequency  $\omega_2$  is found by solving Eqs. H.1 for  $V_2$  in terms of  $a_2$  and  $a_2^*$  and using Eqs. H.2. Therefore,

$$V_2 = -\frac{j}{\sqrt{C_{22}}} [A_2(t) e^{j\omega_2 t} - A_2^*(t) e^{-j\omega_2 t}] \quad (\text{H.6})$$

The power supplied by the variable capacitance at frequency  $\omega_2$  is given by

$$P_2 = -\overline{V_2 I(\omega_2)} = -\frac{j\omega_2 \Delta C}{2\sqrt{C_{11} C_{22}}} (A_1 A_2 e^{-j\phi} - A_1^* A_2^* e^{j\phi}) \quad (\text{H.7})$$

where the bar denotes a time average.

From the definition of normal mode amplitudes this must equal the total power supplied to circuit 2, which is

$$P_2 = \frac{d}{dt} 2|a_2^*|^2 \equiv \frac{d}{dt} 2|A_2^*(t)|^2 \quad (\text{H.8})$$

If Eqs. H.3 are utilized, it follows that Eq. H.8 can be rewritten

$$P_2 = 2(c_{21} A_1 A_2 + c_{21}^* A_1^* A_2^*) \quad (\text{H.9})$$

Compare Eqs. H.7 and H.9; it follows that

$$c_{21} = -\frac{j\omega_2 \Delta C}{4\sqrt{C_{11} C_{22}}} e^{-j\phi} = \frac{\omega_2}{\omega_1} c_{12}^* \quad (\text{H.10})$$

in which the last equality follows from the Manley-Rowe relations of Chapter 4. It could also be derived by considering the power supplied to circuit 1. This is the desired relation for the coupling coefficients given in Eq. 4.31 of the text.

## Appendix I

# Effect of loss on coupled mode theory

Consider the resonant circuit shown in Figure I.1 where a conductance  $G$  is shunted across the inductance and capacitance. It is easy to see that the coupled equations relating the current and voltage are given by

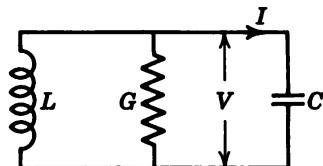


Figure I.1 Resonant circuit with loss.

$$\frac{dI}{dt} + G \frac{dV}{dt} = -\frac{V}{L} \quad (a)$$

$$\frac{dV}{dt} = +\frac{I}{C} \quad (b)$$

The presence of the conductance will obviously change the character of the normal modes. In order to find the effect of  $G$  on the normal modes, Eqs. I.1 will be put in normal mode form. To do this, use the procedure in Chapter 1, Eq. 1.3. The result is

$$\frac{da}{dt} = +j\omega_1' a \quad (I.2)$$

$$\frac{da^*}{dt} = -j\omega_1'^* a^*$$

where

$$\omega_1' = \omega_0 \left[ \sqrt{1 - \left( \frac{1}{2Q} \right)^2} + j \frac{1}{2Q} \right] \quad (I.3)$$

$\omega_0 = (CL)^{-\frac{1}{2}}$ ,  $Q = \omega_0 C/G$ , the circuit quality factor, and the mode amplitudes are

$$a = \frac{1}{2}\sqrt{L}(I + j\omega_1' * CV) \quad (\text{I.4})$$

In most cases the loss will be small, so that  $Q \gg 1$ . Then

$$\omega_1' \cong \omega_0 \left( 1 + j \frac{1}{2Q} \right) \quad (\text{I.5})$$

Now solve Eqs. I.2 and

$$\begin{aligned} a(t) &= a(0)e^{j\omega_1't} \rightarrow a(0)e^{-(\omega_0 t/2Q)}e^{j\omega_0 t} \\ a^*(t) &= a^*(0)e^{-j\omega_1'*t} \rightarrow a^*(0)e^{-(\omega_0 t/2Q)}e^{-j\omega_0 t} \end{aligned} \quad (\text{I.6})$$

That is, as should be expected, both mode amplitudes decay with time because of the circuit loss.

Thus, by replacing  $+\omega_1$  by  $+\omega_0[1 + j(1/2Q)]$  and  $-\omega_1$  by  $-\omega_0[1 - j(1/2Q)]$  in the equations and the opposite way round in the mode amplitudes (compare Eqs. 4.3 and 4.5 of the text) loss can be taken into account.

## Appendix J

# Evaluation of space-charge mutual coupling coefficients

It is a very difficult problem to treat the space-charge wave parametric amplifier rigorously from the fundamental equations (2.1–2.7) of Chapter 2 due to their nonlinear nature. Instead of the exact treatment, the thin beam approximations will be made in which the plasma frequency is replaced by the reduced plasma frequency.

To begin, assume an infinite d-c axial magnetic focusing field. There will then be only velocity and current components in the axial direction. The equation of motion (2.6) then reduces to

$$\frac{\partial v}{\partial t} + v \frac{\partial v}{\partial z} = -\frac{e}{m} E_z \quad (\text{J.1})$$

For a thin beam it was shown that  $E_r \cong 0$  across the beam. For the lowest order modes  $\partial/\partial\phi = 0$ , so that Eq. 2.3 becomes approximately

$$\frac{\partial E_z}{\partial z} = \frac{1}{\epsilon_0} \rho \quad (\text{J.2})$$

Further, since  $\mathbf{J} = J \mathbf{e}_3 = \rho v \mathbf{e}_3$ , the continuity equation (2.5) becomes

$$\frac{\partial J}{\partial z} = -\frac{\partial \rho}{\partial t} \quad (\text{J.3})$$

Now differentiate Eq. J.2 partially with respect to  $t$  and combine with Eq. J.3. Then

$$\frac{\partial}{\partial z} \left( \frac{\partial E_z}{\partial t} + \frac{1}{\epsilon_0} J \right) = 0 \quad (\text{J.4})$$

and since  $\omega_p^2 = e\rho_0/m\epsilon_0$ , it follows from Eq. J.4 that

$$J = - \frac{e\rho_0}{m\omega_p^2} \frac{\partial E_z}{\partial t} \rightarrow - \frac{|J_0|v_0}{2V_0\omega_q^2} \frac{\partial E_z}{\partial t} \quad (\text{J.5})$$

where in the thin approximation  $\omega_p$  is replaced by  $\omega_q$ ,  $J_0 = \rho_0 v_0$ , and  $2|e|V_0 = mv_0^2$ . This is in agreement with Eq. 2.51a of the text.

Differentiate Eq. J.1 with respect to  $t$  and use Eq. J.5. The equation of motion then is

$$\frac{\partial^2 v}{\partial t^2} + \frac{\partial^2}{\partial z \partial t} \frac{v^2}{2} = -\omega_q^2 v_0 \frac{i}{|I_0|} \quad (\text{J.6})$$

where  $J/|J_0|$  is replaced by  $i/|I_0|$ , the beam current.

Further, by Eq. 2.7,  $\rho = J/v$  so that the equation of continuity (J.3) can be written

$$v^2 \frac{\partial i}{\partial z} + v \frac{\partial i}{\partial t} - i \frac{\partial v}{\partial t} = 0 \quad (\text{J.7})$$

Equations J.6 and J.7 are taken as the nonlinear equations governing the thin beam SCWPA. It can easily be shown that they reduce to Eqs. 2.51 of the text when a single SCW is excited at one frequency only.

Now assume that the beam is excited by a fast SCW at frequency  $\omega$  whose amplitude is small compared with d-c quantities so that small signal theory can be used. Further assume that a signal and idler wave at frequencies  $\omega_1$  and  $\omega_2$ , respectively, propagate on the beam. Assume that the amplitudes of the signal and idler waves are small enough compared with the pump wave amplitude that they will not perturb the pump wave. This is consistent with the treatment of the transmission line of Chapter 5 in which the signal and idler waves were assumed tacitly not to affect the pump wave capacitance variation down the line. However, the pump wave will weakly couple the signal and idler waves.

The velocity and current are assumed to be given by

$$i(z, t) = -|I_0| + \operatorname{Re} [m|I_0|e^{j(\omega t - \beta z)} + i_1(z)e^{j\omega_1 t} + i_2(z)e^{j\omega_2 t}] \quad (a)$$

$$v(z, t) = v_0 + \operatorname{Re} \left[ -\frac{\omega_q}{\omega} m v_0 e^{j(\omega t - \beta z)} + v_1(z)e^{j\omega_1 t} + v_2(z)e^{j\omega_2 t} \right] \quad (b) \quad (\text{J.8})$$

where

$$m = \frac{i_{\text{pump}}}{|I_0|} \quad (\text{J.9})$$

and is the depth of current modulation at the pump frequency. Further,

$$\beta = \frac{\omega}{v_0} - \frac{\omega_q}{v_0} \quad (\text{J.10})$$

Also  $\omega_q$  is frequency-dependent, as may be seen in Figure 2.4. It is evaluated at  $\omega$ . Since the pump wave is a fast SCW, the current and velocity are related by

$$\frac{v_{\text{pump}}}{v_0} = \frac{\omega_q}{\omega} \frac{(-i_{\text{pump}})}{|I_0|} \equiv -\frac{\omega_q}{\omega} m \quad (\text{J.11})$$

This follows from Eqs. 2.33 and 2.50 when  $a_- = 0$ .

Now substitute Eqs. J.8 into Eqs. J.6 and J.7. Drop products of signal and idler terms. The coefficients of  $e^{j\omega_1 t}$  and  $e^{-j\omega_2 t}$  in these equations then are seen to be

$$\begin{aligned} \left( \frac{d}{dz} + j \frac{\omega_1}{v_0} \right) \frac{i_1}{|I_0|} + j \frac{\omega_1}{v_0} \frac{V_1}{2V_0} \\ = j \frac{\omega_1 m}{v_0 2} e^{-j\beta z} \left( \frac{V_2^*}{2V_0} - \frac{\omega_q}{\omega} \frac{i_2^*}{|I_0|} \right) \quad (a) \end{aligned}$$

$$\begin{aligned} \left( \frac{d}{dz} - j \frac{\omega_2}{v_0} \right) \frac{i_2^*}{|I_0|} - j \frac{\omega_2}{v_0} \frac{V_2^*}{2V_0} \\ = -j \frac{\omega_2 m^*}{v_0 2} e^{j\beta z} \left( \frac{V_1}{2V_0} - \frac{\omega_q}{\omega} \frac{i_1}{|I_0|} \right) \quad (b) \end{aligned}$$

$$\begin{aligned} \left( \frac{d}{dz} + j \frac{\omega_1}{v_0} \right) \frac{V_1}{2V_0} + j \frac{\omega_1}{v_0} \left( \frac{\omega_{q1}}{\omega_1} \right)^2 \frac{i_1}{|I_0|} \\ = -j \frac{\omega_1 m}{v_0 2} e^{-j\beta z} \frac{\omega_q}{\omega} \frac{V_2^*}{2V_0} \quad (c) \end{aligned}$$

$$\begin{aligned} \left( \frac{d}{dz} - j \frac{\omega_2}{v_0} \right) \frac{V_2^*}{2V_0} - j \frac{\omega_2}{v_0} \left( \frac{\omega_{q2}}{\omega_2} \right)^2 \frac{i_2^*}{|I_0|} \\ = j \frac{\omega_2 m^*}{v_0 2} e^{j\beta z} \frac{\omega_q}{\omega} \frac{V_1}{2V_0} \quad (d) \end{aligned}$$

where the  $\omega_{q1,2}$  are evaluated at  $\omega_1$  and  $\omega_2$ , respectively,  $V_1 = mv_0v_1/|e|$ ,  $V_2^* = mv_0v_2^*/|e|$ , and  $\omega = \omega_1 + \omega_2$ .

It is straightforward to put these equations in coupled mode form by the standard procedure. Define the mode amplitudes by

$$a_{1\pm} = \frac{1}{4\sqrt{Z_{01}}} [V_1 \pm Z_{01}(-i_1)] \quad (\text{J.13})$$

where

$$Z_{01} = \frac{2V_0}{|I_0|} \frac{\omega_{q_1}}{\omega_1} \quad (\text{J.14})$$

with similar expressions for  $\omega_2$ . Then the coupled mode form of Eqs. J.12 is

$$\left[ \frac{d}{dz} + j \left( \frac{\omega_1}{v_0} - \frac{\omega_{q_1}}{v_0} \right) \right] a_{1+} = -j \frac{\omega_1 m}{v_0 4} e^{-j\beta z} \sqrt{\alpha_1 \alpha_2} \left[ \left( 1 + \frac{\alpha}{\alpha_1} + \frac{\alpha}{\alpha_2} \right) a_{2+}^* + \left( 1 + \frac{\alpha}{\alpha_1} - \frac{\alpha}{\alpha_2} \right) a_{2-}^* \right] \quad (a)$$

$$\left[ \frac{d}{dz} + j \left( \frac{\omega_1}{v_0} + \frac{\omega_{q_1}}{v_0} \right) \right] a_{1-} = j \frac{\omega_1 m}{v_0 4} e^{-j\beta z} \sqrt{\alpha_1 \alpha_2} \left[ \left( 1 - \frac{\alpha}{\alpha_1} + \frac{\alpha}{\alpha_2} \right) a_{2+}^* + \left( 1 - \frac{\alpha}{\alpha_1} - \frac{\alpha}{\alpha_2} \right) a_{2-}^* \right] \quad (b)$$

$$\left[ \frac{d}{dz} - j \left( \frac{\omega_2}{v_0} - \frac{\omega_{q_2}}{v_0} \right) \right] a_{2+}^* = j \frac{\omega_2 m^*}{v_0 4} e^{j\beta z} \sqrt{\alpha_1 \alpha_2} \left[ \left( 1 + \frac{\alpha}{\alpha_1} + \frac{\alpha}{\alpha_2} \right) a_{1+} + \left( 1 - \frac{\alpha}{\alpha_1} + \frac{\alpha}{\alpha_2} \right) a_{1-} \right] \quad (c)$$

$$\left[ \frac{d}{dz} - j \left( \frac{\omega_2}{v_0} + \frac{\omega_{q_2}}{v_0} \right) \right] a_{2-}^* = -j \frac{\omega_2 m^*}{v_0 4} e^{j\beta z} \sqrt{\alpha_1 \alpha_2} \left[ \left( 1 + \frac{\alpha}{\alpha_1} - \frac{\alpha}{\alpha_2} \right) a_{1+} + \left( 1 - \frac{\alpha}{\alpha_1} - \frac{\alpha}{\alpha_2} \right) a_{1-} \right] \quad (d)$$

where  $\alpha = \omega_q/\omega$ ,  $\alpha_{1,2} = \omega_{q_{1,2}}/\omega_{1,2}$ .

This is the form of the coupled mode equations when only three frequencies are present. When the pump goes to zero ( $m \rightarrow 0$ ), these equations reduce to the standard SCW normal mode form (Eqs. 2.44) at  $\omega_1$  and  $\omega_2$ .

The coupling coefficient between the  $a_{1+}$ -mode and the  $a_{2+}^*$ -mode is found by inspection of Eq. J.15a, viz.,

$$\begin{aligned} c_{1+,2+} &= -j \frac{\omega_1}{v_0} \frac{m}{4} \sqrt{\alpha_1 \alpha_2} \left( 1 + \frac{\alpha}{\alpha_1} + \frac{\alpha}{\alpha_2} \right) \\ &= -\frac{j}{4} \sqrt{\frac{\omega_1}{\omega_2}} m \sqrt{\beta_{q1} \beta_{q2}} \left( 1 + \frac{\alpha}{\alpha_1} + \frac{\alpha}{\alpha_2} \right) \\ &= +\frac{\omega_1}{\omega_2} (c_{2+,1+})^* \end{aligned} \quad (\text{J.16})$$

where the latter equality follows from Eq. J.15c by inspection. The + sign shows that the modes are actively coupled.

It will now be shown by computing the transfer factors that coupling between the fast and slow modes may be neglected.

In order to use transfer factors, the  $z$ -dependence of the coupling coefficients must be removed. This can be done (see Eq. 5.19) by making transformations of the type

$$\begin{aligned} a_{1\pm} &= A_{1\pm} \exp \left[ -j \left( \beta_1 + \frac{\Delta\beta}{2} \right) z \right] \\ a_{2\pm}^* &= A_{2\pm}^* \exp \left[ +j \left( \beta_2 + \frac{\Delta\beta}{2} \right) z \right] \end{aligned} \quad (\text{J.17})$$

in Eqs. J.15 where

$$\begin{aligned} \Delta\beta &= \beta - \beta_1 - \beta_2 = -(\beta_q - \beta_{q1} - \beta_{q2}) \\ \beta_{1,2} &= \frac{\omega_1}{v_0} - \frac{\omega_{q2}}{v_0} \quad \beta = \frac{\omega}{v_0} - \frac{\omega_q}{v_0} \end{aligned} \quad (\text{J.18})$$

Equations J.15 then reduce to

$$\begin{aligned} \left( \frac{d}{dz} - j \frac{\Delta\beta}{2} \right) A_{1+} &= c_{1+,2+} A_{2+}^* + c_{1+,2-} A_{2-}^* \\ \left( \frac{d}{dz} - j \frac{\Delta\beta}{2} + j2\beta_{q1} \right) A_{1-} &= c_{1-,2+} A_{2+}^* + c_{1-,2-} A_{2-}^* \\ \left( \frac{d}{dz} + j \frac{\Delta\beta}{2} \right) A_{2+}^* &= c_{2+,1+} A_{1+} + c_{2+,1-} A_{1-} \\ \left( \frac{d}{dz} + j \frac{\Delta\beta}{2} - j2\beta_{q2} \right) A_{2-}^* &= c_{2-,1+} A_{1+} + c_{2-,1-} A_{1-} \end{aligned} \quad (\text{J.19})$$

where  $c_{1+,2+}$  and  $c_{2+,1+}$  are given in Eqs. J.16,

$$c_{1+,2-} = -j \frac{m}{4} \sqrt{\frac{\omega_1}{\omega_2}} \sqrt{\beta_{q1}\beta_{q2}} \left( 1 + \frac{\alpha}{\alpha_1} - \frac{\alpha}{\alpha_2} \right) = - \left( \frac{\omega_1}{\omega_2} \right) (c_{2-,1+})^* \quad (\text{J.20a})$$

and

$$c_{1-,2+} = j \frac{m}{4} \sqrt{\frac{\omega_1}{\omega_2}} \sqrt{\beta_{q1}\beta_{q2}} \left( 1 - \frac{\alpha}{\alpha_1} + \frac{\alpha}{\alpha_2} \right) = - \left( \frac{\omega_1}{\omega_2} \right) (c_{2+,1-})^* \quad (\text{J.20b})$$

These modes are passively coupled.

The mode transfer factors, as defined in Chapter 1, must now be found for Eqs. J.19 rather than Eqs. J.15. They are given by

$$\begin{aligned} F_{1+,2+} &= \left[ 1 - \left( \frac{\Delta\beta}{2} \right)^2 \frac{1}{|c_{1+,2+}|^2} \frac{\omega_1}{\omega_2} \right]^{-1} \\ F_{1+,2-} &= \left[ 1 + \left( \frac{\Delta\beta}{2} - \beta_{q2} \right)^2 \frac{1}{|c_{1+,2-}|^2} \frac{\omega_1}{\omega_2} \right]^{-1} \\ F_{2+,1-} &= \left[ 1 + \left( \frac{\Delta\beta}{2} - \beta_{q1} \right)^2 \frac{1}{|c_{1-,2+}|^2} \frac{\omega_1}{\omega_2} \right]^{-1} \end{aligned}$$

It now follows that if  $|F_{1+,2-}| \ll 1$  and  $|F_{2+,1-}| \ll 1$ , coupling to the slow modes may be neglected. For a given pump modulation, the gain will be a maximum when  $\Delta\beta$  is a minimum. If the beam is very thin,  $\Delta\beta \approx 0$  and  $\alpha \approx \alpha_1 \approx \alpha_2$ , and it follows directly that the transfer factors are given approximately by

$$F_{1+,2-} \approx \frac{1}{1 + \frac{16}{|m|^2}} \approx F_{2+,1-}$$

and it is certainly justified to neglect the slow modes. Even for thick beams, if  $|m|$  is sufficiently small, coupling may be neglected since

$$F_{1+,2-} \sim \frac{1}{1 + \frac{\lambda}{|m|^2}}$$

where  $\lambda$  is a constant. However, the gain is decreased as  $|m|$  is decreased.

Physically, if  $\Delta\beta = 0$ , optimum gain will be realized, since the pump, signal, and idler waves travel in exact synchronism. The slow modes are out of synchronism and may be neglected.

## Appendix K

# Coupled mode equations for circuit-cyclotron system

### The Beam Equations

Under the assumptions of Chapter 2, Section 2.6, the beam is described by the equations of motion (2.56). The coupling to the circuit is accounted for by adding the electric field of the circuit at the position of the beam (Eq. 2.6). Therefore, Eq. 2.56a has an additional term added,  $eE_x(z)/mv_0$ , and Eq. 2.56b has a coupling term,  $eE_y(z)/mv_0$ , since  $\mathbf{E}(z, t) = \text{Re}[\mathbf{E}(z)e^{j\omega_1 t}]$ . The equations of motion with the coupling term (compare with Eq. 2.59) can then be written

$$\left( \frac{d}{dz} + j(\beta_e \mp \beta_c) \right) a_{1\pm} = \frac{ek}{mv_0} E_{\pm} \quad (\text{K.1})$$

where  $\beta_e = \omega_1/v_0$ ,  $\beta_c = \omega_c/v_0 = |e|B_0/mv_0$ , where the fast and slow cyclotron mode amplitudes are defined by

$$a_{1\pm} = k(u_{1x} \pm ju_{1y})$$
$$E_{\pm} = E_x \pm jE_y \quad (\text{K.2})$$

$$k = \frac{1}{4} \sqrt{m \frac{|I_0|}{|e|} \frac{\omega_1}{\omega_c}}$$

$E_{\pm}$  are the circularly polarized components of the electric field. This shows that the  $E_+$  circuit field couples only to the fast cyclotron wave, which is left-hand circularly polarized;  $E_-$  couples only to the slow cyclotron wave, which is right-hand circularly polarized.

In addition, the position and velocity are related by Eq. 2.61, viz.,

$$\left( \frac{d}{dz} + j\beta_e \right) r_{\pm} = \frac{1}{v_0} a_{1\pm} \quad (\text{K.3})$$

where

$$r_{\pm} = k(\xi_{1x} \pm j\xi_{1y}) \quad (\text{K.4})$$

A combination of Eqs. K.1 and K.3, as in Appendix D, results in

$$\left( \frac{d}{dz} + j\beta_e \right) a_{2\pm} = \frac{ek}{mv_0} E_{\pm} \quad (\text{K.5})$$

where

$$a_{2\pm} = a_{1\pm} \mp j\omega_c r_{\pm} \quad (\text{K.6})$$

(Compare with Eq. 2.76.) Again, it is seen that the  $E_+$  circuit field couples only to the left-hand circularly polarized synchronous mode,  $a_{2+}$ , whereas the  $E_-$  circuit field couples only to the right-hand circularly polarized synchronous mode,  $a_{2-}$ .

Thus Eqs. K.1 and K.5 describe the effect of the circuit field coupling on the beam. Space-charge has been neglected so that the space-charge electric field is omitted, and the electrons therefore act independently of one another. As a result, only a thin beam need be considered.

### The Circuit Model and Equations <sup>1</sup>

The fields,  $E_{\pm}$ , are the transverse electric fields of a circuit that will be taken as a slow wave circuit in the present analysis. It was shown in Chapter 3 that a transmission line can be used as an equivalent circuit for a slow wave structure. Let  $V(z)$  represent the complex voltage on the equivalent transmission line, and let  $I(z)$  be the complex current.

It is clear from the beam equations and the treatment of the cyclotron and synchronous modes on a beam in a drift region of Chapter 3 that these modes are circularly polarized. Accordingly, if it is desired to excite, for example, the fast cyclotron wave, the circuit field should have a left-hand circularly polarized component. This field would also excite the left-hand synchronous mode,  $a_{2+}$ , as shown in Eq. K.5.

The transmission line can be used to represent an actual circuit that provides an arbitrary state of polarization. This can be accomplished by letting the line voltage <sup>1</sup>  $V$  be related to the *actual* circuit fields by

$$E_{\pm} = -f_{\pm} \frac{V}{D} = E_x \pm jE_y \quad (\text{K.7})$$

where  $D$  is a normalizing characteristic distance on the equivalent transmission line and  $f_{\pm}$  are dimensionless complex parameters which give the type of polarization the circuit has. For example, if  $f_- = 0$  and  $f_+ = 1$ , the circuit field is left-hand circularly polarized, whereas, if  $f_+ = 0$  and  $f_- = 1$ , the circuit field is right-hand polarized. If  $f_+ = f_-$ , the field is linearly polarized. The field polarization parameters,  $f_{\pm}$ , are normalized so that

$$|E_x|^2 + |E_y|^2 = \frac{|V|^2}{2D^2} \quad (\text{K.8})$$

where

$$|f_+|^2 + |f_-|^2 = 1$$

From Eq. K.7 it follows that

$$E_x = -\frac{1}{2}(f_+ + f_-) \frac{V}{D} \quad E_y = -\frac{j}{2}(f_+ - f_-) \frac{V}{D} \quad (\text{K.9})$$

Actual slow-wave circuits, which will provide linear or circularly polarized waves, are available.

The circuit is represented by the transmission-line equations, and the effect of the beam on the circuit is given by the current the beam induces in the circuit. Therefore, by Eqs. 3.3, the circuit beam equations are

$$\begin{aligned} \frac{dV}{dz} &= -j\beta_0 Z_0 I \\ \frac{dI}{dz} &= -j \frac{\beta_0}{Z_0} V - \frac{di_1}{dz} \end{aligned} \quad (\text{K.10})$$

where  $\beta_0$  is the uncoupled circuit propagation constant and  $Z_0$  is the uncoupled circuit characteristic impedance. As shown in Chapter 3, a field analysis would have to be carried out in order to determine these quantities in terms of the actual circuit parameters, such as dimensions and dielectric constants.

Before proceeding, it is necessary to find the current induced in the circuit,  $di_1/dz$ , in terms of the d-c beam current, velocity, and position. Only an approximate derivation will be given. The justification is given by Siegman<sup>1</sup> and Klüver.<sup>2</sup> The results have also been noted by Adler,<sup>3</sup> Wade,<sup>4</sup> Fank,<sup>5</sup> and Johnson.<sup>6</sup>

The rate of change of total power (real  $P$  plus reactive  $Q$ ) with dis-

tance on the transmission line is given by

$$\begin{aligned} \frac{\partial}{\partial z} (P + jQ) \Big|_{\text{circuit}} &= \frac{1}{2} \frac{\partial}{\partial z} (VI^*) \\ &= j \frac{1}{2} \left( \frac{\beta_0}{Z_0} V^* V - \beta_0 Z_0 I^* I \right) - \frac{1}{2} V \frac{di_1^*}{dz} \quad (\text{K.11}) \end{aligned}$$

where the last equality follows from Eqs. K.10. The terms proportional to  $V^*V$  and  $I^*I$  represent the reactive energy stored in the passive elements of the transmission line. The term  $-\frac{1}{2}V \frac{di_1^*}{dz}$  represents the total power (real plus reactive) delivered by the beam to the circuit.

From the small signal power theorem of Eq. 2.19 it follows that the power delivered to the circuit field per unit length by the beam is

$$\frac{\partial}{\partial z} (P + jQ) \Big|_{\text{from beam}} = \frac{1}{2} \mathbf{E} \cdot \mathbf{J}_1^* \quad (\text{K.12})$$

where in the present instance  $\mathbf{E}$  represents the transverse circuit field and  $\mathbf{J}_1^*$  represents the transverse beam current.

It is argued that the induced current is caused by the motion of the beam as a whole rather than by the transverse velocity of an individual electron.<sup>1-6</sup> Therefore,

$$\mathbf{J}_1 = \rho_0 j \omega_1 \xi_1 \quad (\text{K.13})$$

where  $\rho_0$  is the d-c charge per unit length of beam and  $d/dt$  is replaced by  $\partial/\partial t$ , since the current moves transverse to the circuit at a fixed  $z$ . Use Eqs. K.4, K.7, and K.13, and Eq. K.12 can be written

$$\frac{\partial}{\partial z} (P + jQ) \Big|_{\text{from beam}} = +j \frac{\omega_1 \rho_0}{4k} \frac{V}{D} (f_+ r_+^* + f_- r_-^*) \quad (\text{K.14})$$

By comparing Eqs. K.11 and K.14, it follows that

$$\frac{di_1}{dz} = j \frac{\omega_1 \rho_0}{2kD} (f_+^* r_+ + f_-^* r_-) \quad (\text{K.15})$$

From Eqs. K.15 and K.10, it follows that

$$\left( \frac{d}{dz} \pm j\beta_0 \right) a_{\pm} = \mp j \frac{\omega_1 \rho_0}{8kD} \sqrt{Z_0} (f_+^* r_+ + f_-^* r_-) \quad (\text{K.16})$$

where the circuit mode amplitudes are

$$a_{\pm} = \frac{1}{4\sqrt{Z_0}} (V \pm Z_0 I) \quad (\text{K.17})$$

Now use Eqs. K.2, K.7, and K.17, and Eqs. K.1 and K.5 can be written

$$\left( \frac{d}{dz} + j(\beta_e \mp \beta_c) \right) a_{1\pm} = f_{\pm} c_{12}(a_+ + a_-) \quad (a)$$
(K.18)

$$\left( \frac{d}{dz} + j\beta_e \right) a_{2\pm} = f_{\pm} c_{12}(a_+ + a_-) \quad (b)$$

where

$$c_{12} = \frac{1}{2D} \sqrt{\frac{Z_0 |I_0| \omega_1}{2V_0 \omega_c}} \quad (K.19)$$

and  $2|e|V_0 = mv_0^2$ . Further, by Eqs. K.2 and K.6, Eq. K.16 becomes ( $I_0 = \rho_0 v_0$ ).

$$\left( \frac{d}{dz} \pm j\beta_0 \right) a_{\pm} = \pm c_{12}[f_+^*(a_{2+} - a_{1+}) - f_-^*(a_{2-} - a_{1-})] \quad (K.18c)$$

Equations K.18 are the required coupled mode form of the beam-circuit equations.

## BIBLIOGRAPHY

1. A. E. Siegman, "The Waves on a Filamentary Electron Beam in a Transverse-Field Slow Wave Circuit," *J. Appl. Phys.*, **31**, 17-26 (January 1960).
2. J. W. Klüver, "Transverse-Field Interaction at Low Space-Charge Densities," *Bell Labs. Internal Memorandum 59-124-24* (July 9, 1959).
3. R. Adler, "An Equivalence Principle in High Frequency Tubes," *Conv. Rec. IRE*, Part 6, 54 (1953).
4. G. Wade, see Reference 1.
5. B. Fank, "Investigation of the Transverse-Field Klystron," *Tech. Rept. No. 905-1*, Stanford Electronics Lab., Stanford, California, March 10, 1958.
6. C. C. Johnson, "Theory of Fast-Wave Parametric Amplification," *Technical Memorandum No. 540*, Research Labs., Hughes Aircraft Co., Culver City, California (February 1959). Appendix by R. W. Gould.

## Appendix L

# Equations of motion for beam in quadrupolar pump field

The equations of motion for the beam in the pump region (Eq. 2.6) are given by

$$\frac{d\mathbf{v}}{dt} = \frac{e}{m} (\mathbf{E}_p + \mathbf{v} \times \mathbf{B}) \quad (L.1)$$

where  $\mathbf{v}$  is a function of  $\mathbf{r}$  and  $t$ . Further, the position and velocity are related by

$$\frac{d\mathbf{r}}{dt} = \mathbf{v} \quad (L.2)$$

Now let  $\mathbf{r}_0$  be the position of an electron under the action of the d-c fields and  $\mathbf{R}_1(\mathbf{r}_0, t)$  the small a-c displacement of the same electron from its unperturbed position. Then

$$\mathbf{r}(\mathbf{r}_0, t) = \mathbf{r}_0 + \mathbf{R}_1(\mathbf{r}_0, t) \quad (L.3)$$

The velocity of the electron at  $\mathbf{r}$  is given by

$$\mathbf{v}(\mathbf{r}, t) = \mathbf{v}_0(\mathbf{r}_0) + \mathbf{V}_1(\mathbf{r}_0, t) \quad (L.4)$$

where  $\mathbf{V}_1$  is the first order a-c velocity and  $\mathbf{v}_0 = d\mathbf{r}_0/dt$ .

Now use Eqs. L.3 and L.4, and the left sides of Eqs. L.1 and L.2 reduce to

$$\left( \frac{\partial}{\partial t} + \mathbf{v}_0 \cdot \nabla \right) \mathbf{V}_1(\mathbf{r}_0, t) = \frac{d\mathbf{V}_1}{dt} \quad (L.5)$$

and

$$\left( \frac{\partial}{\partial t} + \mathbf{v}_0 \cdot \nabla \right) \mathbf{R}_1(\mathbf{r}_0, t) = \frac{d\mathbf{R}_1}{dt} \quad (L.6)$$

Now  $\mathbf{E}_p(\mathbf{r}, t)$  must be expanded in a Taylor series about  $\mathbf{r}_0$ , since the electron will see the field at  $\mathbf{r}_0 + \mathbf{R}_1$  rather than  $\mathbf{r}_0$ . Therefore, Eq. L.1 reduces to

$$\left( \frac{\partial}{\partial t} + \mathbf{v}_0 \cdot \nabla \right) \mathbf{V}_1(\mathbf{r}_0, t) = \frac{e}{m} [\mathbf{E}_p(\mathbf{r}_0) + (\mathbf{R}_1 \cdot \nabla) \mathbf{E}_p|_{\mathbf{r}_0} + \mathbf{V}_1 \times \mathbf{B}_0] \quad (\text{L.7})$$

where Eq. L.5 was used.

Similarly, Eq. L.2 reduces to

$$\left( \frac{\partial}{\partial t} + \mathbf{v}_0 \cdot \nabla \right) \mathbf{R}_1 = \mathbf{V}_1 \quad (\text{L.8})$$

The effect of the beam on the circuit fields is neglected, since the pump field amplitude is assumed large compared with signal quantities. The pump field is a driving term in the equations of motion. If mixing between signal and idler modes is to take place, it is seen that the pump field must have a nonzero gradient, since the only nonlinear term in these equations (L.7 and L.8) is  $(\mathbf{R}_1 \cdot \nabla) \mathbf{E}_p$ .

Now assume that the d-c velocity is entirely  $z$ -directed and that the pump field is purely transverse of the form  $\frac{1}{2} \mathbf{E}_p(x, y) e^{j(\omega t - \beta z)} + \text{c.c.}$  Also assume that the transverse position and velocity can be expanded as a signal and idler wave of the form

$$\begin{aligned} \mathbf{R}_1 &= \xi_1(z) e^{j\omega_1 t} + \xi_2^*(z) e^{-j\omega_2 t} + \text{c.c.} \\ \mathbf{V}_1 &= \mathbf{u}_1(z) e^{j\omega_1 t} + \mathbf{u}_2^*(z) e^{-j\omega_2 t} + \text{c.c.} \end{aligned} \quad (\text{L.9})$$

since  $\mathbf{r}_0 = (0, 0, z)$ . Also, the usual parametric frequency requirement is

$$\omega = \omega_1 + \omega_2 \quad (\text{L.10})$$

Substitute these expansions in Eqs. L.7 and L.8, and it will be seen that the coefficients of  $e^{j\omega_1 t}$  and  $e^{-j\omega_2 t}$  are

$$\begin{aligned} \left( \frac{d}{dz} + j\beta_1 \right) \mathbf{u}_1 + \frac{1}{v_0} \mathbf{u}_1 \times \boldsymbol{\omega}_c &= - \frac{|e|}{mv_0} (\xi_2^* \cdot \nabla) \mathbf{E}_p(x, y) e^{-j\beta z} \\ \left( \frac{d}{dz} - j\beta_2 \right) \mathbf{u}_2^* + \frac{1}{v_0} \mathbf{u}_2^* \times \boldsymbol{\omega}_c &= - \frac{|e|}{mv_0} (\xi_1 \cdot \nabla) \mathbf{E}_p^*(x, y) e^{j\beta z} \\ \left( \frac{d}{dz} + j\beta_1 \right) \xi_1 &= \frac{1}{v_0} \mathbf{u}_1 \\ \left( \frac{d}{dz} - j\beta_2 \right) \xi_2^* &= \frac{1}{v_0} \mathbf{u}_2^* \end{aligned} \quad (\text{L.11})$$

where  $\beta_{1,2} = \omega_{1,2}/v_0$  and  $\boldsymbol{\omega}_c = |e| \mathbf{B}_0/m$ .

## EQUATIONS OF MOTION FOR BEAM IN QUADRUPOLAR PUMP FIELD 263

Let the fast and slow cyclotron mode amplitudes at  $\omega_1$  and  $\omega_2$  be

$$\begin{aligned} A_{1\pm} &= k_1(u_{1x} \pm ju_{1y}) & (a) \\ A_{2\pm}^* &= k_2(u_{2x}^* \mp ju_{2y}^*) & (b) \end{aligned} \quad (\text{L.12})$$

where

$$k_{1,2} = \frac{1}{4} \sqrt{m \frac{|I_0|}{|e|} \frac{\omega_{1,2}}{\omega_c}} \quad (\text{L.13})$$

and let the synchronous mode amplitudes at  $\omega_1$  and  $\omega_2$  be

$$\begin{aligned} S_{1\pm} &= A_{1\pm} \mp j\omega_c r_{1\pm} & (c) \\ S_{2\pm}^* &= A_{2\pm}^* \pm j\omega_c r_{2\pm}^* & (d) \end{aligned} \quad (\text{L.12})$$

where

$$\begin{aligned} r_{1\pm} &= k_1(\xi_{1x} \pm j\xi_{1y}) & (L.14) \\ r_{2\pm}^* &= k_2(\xi_{2x}^* \mp j\xi_{2y}^*) \end{aligned}$$

Then, by the usual procedure, the coupled mode form of Eqs. L.11 are

$$\begin{aligned} \left( \frac{d}{dz} + j(\beta_1 \mp \beta_c) \right) A_{1\pm} &= j\alpha_1[(S_{2+}^* - A_{2+}^*)\nabla_T - (S_{2-}^* - A_{2-}^*) \\ &\quad \times \nabla_T^*]E_{p\pm}e^{-j\beta_z} \\ &= \left( \frac{d}{dz} + j\beta_1 \right) S_{1\pm} \\ \left( \frac{d}{dz} - j(\beta_2 \mp \beta_c) \right) A_{2\pm}^* &= -j\alpha_2[(S_{1+} - A_{1+})\nabla_T^* - (S_{1-} - A_{1-}) \\ &\quad \times \nabla_T]E_{p\pm}^*e^{j\beta_z} \\ &= \left( \frac{d}{dz} - j\beta_2 \right) S_{2\pm}^* \end{aligned} \quad (\text{L.15})$$

where

$$\alpha_1 = \frac{|e|}{2mv_0\omega_c} \sqrt{\frac{\omega_1}{\omega_2}} = \frac{\omega_1}{\omega_2} \alpha_2 \quad (\text{L.16})$$

$$\nabla_T = \frac{\partial}{\partial x} + j \frac{\partial}{\partial y} \quad \nabla_T^* = \frac{\partial}{\partial x} - j \frac{\partial}{\partial y} \quad (\text{L.17})$$

and

$$E_{p\pm} = E_{px} \pm jE_{py} \quad (\text{L.18})$$

This is the coupled mode form of the equations. For the quadrupolar field of the text (Eqs. 8.15)

$$E_{p\pm} = (-y \mp jx) \frac{V_p}{D^2} \quad (\text{L.19})$$

In this case Eqs. L.15 reduce to

$$\begin{aligned} \left( \frac{d}{dz} + j(\beta_1 - \beta_c) \right) A_{1+} &= c_{12}(S_{2+}^* - A_{2+}^*)e^{-j\beta z} \\ &= \left( \frac{d}{dz} + j\beta_1 \right) S_{1+} \\ \left( \frac{d}{dz} - j(\beta_2 - \beta_c) \right) A_{2+}^* &= c_{21}^*(S_{1+} - A_{1+})e^{j\beta z} \\ &= \left( \frac{d}{dz} - j\beta_2 \right) S_{2+}^* \end{aligned} \quad (\text{L.20})$$

where

$$c_{12} = \frac{V_p}{D^2 v_0 B_0} \sqrt{\frac{\omega_1}{\omega_2}} = \frac{\omega_1}{\omega_2} c_{21}^* \quad (\text{L.21})$$

with similar equations for the waves of opposite polarization that are not coupled to these modes.

# Index

- Active mode coupling, 26, 30, 193, 199  
contradirectional coupler, 30  
distributed parametric amplifier, 134  
four-frequency parametric amplifier,  
140  
parametric oscillator, 98, 101  
parity, 139, 140
- Backward wave amplifier and oscillator,  
84  
circuit model, 86  
start oscillation condition, 88
- Boundary conditions, coupled oscillators,  
13  
cyclotron wave amplifier, 198  
parametric oscillator, 98, 103  
transmission-line, 23
- Characteristic impedance, backward  
wave amplifier circuit, 87  
space-charge waves, 42, 50, 72  
transmission line, 21
- Chu kinetic power theorem, 44, 74
- Converter (*see* Frequency converter)
- Coupled mode amplitudes (*see also*  
Normal mode amplitudes)  
backward wave amplifier, 87  
coupled modes of propagation, 25  
coupled oscillators, 9  
cyclotron modes, 191  
parametric amplifier, 96, 112, 133  
space-charge modes, 72  
synchronous modes, 191
- Coupled mode amplitudes, traveling wave  
tube, 72
- Coupled mode approximation (*see* Weak  
coupling approximation)
- Coupled mode equations, backward wave  
amplifier, 86  
coupled modes, 12, 16, 25  
coupled oscillators, 9  
cyclotron modes, 192  
frequency converter, 119  
parametric amplifier, 97, 100, 112,  
133  
synchronous modes, 192  
traveling wave tube, 73
- Coupled modes, direct approach, 12  
general approach, 15, 18, 25  
parametric oscillator and amplifier,  
93, 100, 132  
of propagation, 18, 25  
of vibration, 3  
time-invariant systems, 138  
time-varying systems, 139  
theory of, 1
- Coupling coefficients, backward wave  
amplifier, 87  
coupled oscillators, 9  
directional coupler for cyclotron  
waves, 192  
and energy conservation, 16  
evaluation of, 17  
parametric amplifiers, 97, 102, 112,  
134, 141, 171, 198  
and power conservation, 26

- Coupling coefficients, relations between, 26  
 time-invariant systems, 138  
 time-varying systems, 139  
 traveling wave tubes, 73
- Cyclotron wave parametric amplifier, 190
- Cyclotron waves, 51
- Diode parametric amplifier (*see also* Junction diode), 148
- Directional coupler, codirectional, 27  
 contradirectional, 30  
 cyclotron wave, 194  
 Kompfner dip helix, 80
- Distributed frequency converter, 137
- Distributed parametric amplifier, 131
- Double sideband operation, 116
- Double stream amplifier, 90
- Easitron, 90
- Electron beams, 35, 168, 190
- Energy conservation, effect on coupling coefficients, 16
- Energy considerations, parametric amplifier, 99
- Energy stored, coupled oscillators, 10  
 oscillator (simple), 6
- Equations of motion, coupled oscillators, 8  
 electron beam, 36  
 ferrite magnetization, 205, 214, 217  
 oscillator, 4, 5, 6
- Excess noise temperature (*see also* Noise figure)  
 definition, 116  
 parametric amplifiers, 116, 117, 118, 144, 146, 160
- Experimental results, cyclotron wave parametric amplifier, 200  
 diode parametric amplifier, 148, 163  
 ferrite frequency converter, 225  
 ferrite parametric amplifier, 220  
 space-charge parametric amplifier, 176
- Ferrite parametric amplifier, 203  
 modes of operation, 212  
 theory of, 213  
 uniform precession mode, 207
- Filling factors, 219
- Frequency converter, diode, 154  
 distributed, 137  
 ferrite, 223  
 lumped circuit, 118  
 space-charge wave, 175
- Gain, backward wave amplifier, 88  
 cyclotron wave parametric amplifier, 199  
 diode parametric amplifier, 154  
 distributed parametric amplifier, 135  
 ferrite parametric amplifier, 221  
 lumped circuit parametric amplifier, 114  
 space-charge wave parametric amplifier, 173  
 threshold, 137, 171, 219  
 traveling wave tube, 77
- Gain parameter, traveling wave tube, 73
- Group velocity, backward wave circuit, 86  
 space-charge waves, 43, 50  
 transmission-line, 23
- Gyromagnetic resonance, 208
- Helix, 67, 68
- Junction diode, 149  
 capacitance of, 151
- Kinetic power flow (*see also* Power flow)  
 space-charge waves, 44
- Kinetic voltage, 41
- Klystron, 90
- Kompfner dip conditions, cyclotron wave coupler, 194  
 helix, 81, 82
- Landau-Lifshitz equations, 214
- Magnetic energy, 205
- Magnetization vector, 203
- Manley-Rowe relations, Derivation of, 104  
 frequency converter, 119  
 parametric amplifier, 99, 101, 134, 171, 199  
 time-varying systems, 139
- Mavar (*see* Parametric amplifier and oscillator)
- Maxwell equations, 35, 37, 39

- Noise in diodes, 154  
Noise figure (*see also* Excess noise temperature)  
definition, 115  
minimum, 169  
parametric amplifier, 142, 146, 159  
Normal mode amplitudes (*see also* Coupled mode amplitudes)  
cyclotron waves, 53  
oscillator, 6  
parametric oscillator, 96  
space-charge waves, 43, 50  
synchronous waves, 61  
transmission line, 22  
Normal mode form of equations,  
    cyclotron waves, 53  
oscillator, 6  
space-charge waves, 43  
synchronous waves, 61  
transmission line, 21  
  
Parametric amplifier and oscillator, brief  
    history, 121  
crossed field version, 202  
cyclotron wave, 190  
    pump field, 196  
diode, 148, 163  
    equivalent circuit, 153, 156, 157  
distributed, 131  
ferrite, 203, 221  
four-frequency, 140  
lumped circuit, 93, 109  
oscillation threshold, 113  
space-charge wave, 168  
Parity, 138, 139  
Passive mode coupling, 26, 119, 137, 141, 175, 199  
    and parity, 139, 140  
Phase sensitivity of parametric oscillator, 99, 103  
Phase velocity, backward wave amplifier circuit, 86  
    cyclotron waves, 54, 58  
helix, 69  
space-charge waves, 43, 50, 172  
synchronous waves, 61  
transmission line, 23  
Plasma frequency, 41  
Plasma propagation constant, 41  
Plasma reduction factor, 49  
  
Power conservation, 24, 25  
Power flow, backward wave amplifier, 87  
    directional couplers, 28, 31, 81  
    parametric amplifier, 135, 172  
    transmission line, 23  
    traveling wave tube, 74  
Power theorem (*see also* Chu kinetic power theorem)  
    cyclotron, synchronous, and circuit modes, 193  
    time-invariant systems, 138  
Poynting's vector, 19  
Poynting theorem, small signal, 38  
Propagation constant, backward wave amplifier, 86  
coupled modes, 26  
directional coupler, 27, 30  
parametric amplifier, 170  
slow wave circuit, 72  
transmission line, 22  
traveling wave tube, 77, 79  
  
Reactance amplifier (*see* Parametric amplifier)  
Reduced plasma frequency, 49  
Reflection-type cavity, 111, 115, 156  
Resistive wall amplifier, 90  
  
Semiconductor diode (*see also* Diode), 149  
Single sideband operation, 116  
Slow wave circuits, 67, 70, 86, 190  
Space-charge parameter, 73  
Space-charge waves, coupled to slow wave circuit, 70  
    finite beam, 47  
    infinite beam, 39  
    normal mode representation, 43  
    parametric amplifier, 168  
Synchronous waves, 60  
  
Transfer factors, backward wave amplifier, 87  
coupled modes, 15  
coupled oscillators, 14  
definition, 13  
directional couplers, 30, 31, 80, 194  
parametric amplifier, 172  
traveling wave tube, 75  
Transmission line, 19

Transmission-type cavity, 110, 114  
Traveling wave tube theory, 76, 78

Variable capacitance (*see* Semiconductor diode; Parametric amplifier and oscillator)

Weak coupling approximation, coupled modes of propagation, 25  
coupled oscillators, 11, 12  
parametric oscillator and amplifier, 96,  
    176  
traveling wave tube, 75

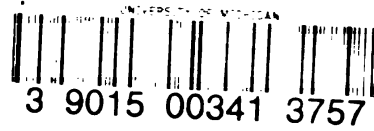












3 9015 00341 3757



